

https://dspace.org/

Three dimensional geometry of the bushveld complex derived from potential field modelling

Cole, Janine

2018

https://hdl.handle.net/10539/27082

Cole, Janine, (2018) Three dimensional geometry of the Bushveld Complex derived from potential field modelling, University of the Witwatersrand, Johannesburg, https://hdl.handle.net/10539/27082

Downloaded from a DSpace repository. https://dspace.org/

Three dimensional geometry of the Bushveld Complex derived from potential field modelling

Janine Cole

A Thesis submitted to the Faculty of Science, University of the Witwatersrand, Johannesburg, in fulfilment of the requirements for the degree of Doctor of Philosophy

Johannesburg, 2018

DECLARATION

I declare that this Thesis is my own, unaided work. It is being submitted for the Degree of Doctor of Philosophy at the University of the Witwatersrand, Johannesburg. It has not been submitted before for any degree or examination at any other University.



(Signature of candidate)

22nd day of June 2018 in Pretoria

ABSTRACT

The three dimensional geometry of the Bushveld Complex has been a source of controversy for over 50 years.

Two dimensional gravity models and a few magnetic models limited to short profiles in the eastern sections of the BC have been used to propose conflicting geometries for the Rustenburg Layered Suite (RLS), especially between the western and eastern lobes; one school argued for completely separate intrusions, while the other proposed that the outcropping lobes are connected at depth. These competing models suggest different emplacement models. They provide a valuable starting point, but, 2.5D potential field modelling is not well suited to modelling complex three dimensional geology. Also, in previous work the magnetics or only the gravity data were modelled independently. Here I present the first full three dimensional potential field forward modelling of the central and southern Bushveld Complex (BC) which has been used to test the geometry of the Bushveld Complex in areas obscured by younger geological cover. Both gravity and magnetic data have been used to develop a geological model that is consistent with both data sets. Joint 3D modelling of regional gravity and magnetic data combined with published crustal thickness models derived from broadband seismic tomography studies were used to create a 3D model of the central and southeastern sections of the BC, as well as the southern part of the northern lobe. Eight downhole logs with more than 730 000 new density and magnetic susceptibility measurements from the RLS were combined with existing data to determine values for Bushveld Complex lithologies that were used in the model. The 3D model has a complex geometry with thick continuous RLS in most of the western lobe, thinner RLS in the south-eastern lobe, but a disrupted RLS in the eastern lobe. Large domes of Transvaal dolomite or thicker granites and granophyre in the eastern lobe interrupt the continuity of the RLS. The western and eastern lobes are therefore broadly connected, with major disruptions largely in the eastern lobe. However, they are not separate intrusions, but represent a single magma chamber affected by pre-existing and syn-magmatic updoming. The model includes the whole thickness of the crust and requires dense material at the crust mantle boundary. Thus, for the first time, I have imaged the remnants of magma staging chambers. The chambers, constrained by the extent of the diffuse crust-mantle transition as determined from teleseismic data, underlie the whole Bushveld Complex, but is thickest under the northern, south-eastern and western parts of the complex. I propose feeders that correlate with the chambers in the northern lobe near the large gravity high near Polokwane and in the south-eastern lobe.

ACKNOWLEDGEMENTS

- The Council for Geoscience, for providing me with the opportunity, funding and data for this study.
- Anglo Platinum for wireline logging data
- My supervisors Susan Webb and Carol Finn. Thank you for all the guidance, patience, skype and other conversations. I hope that one day I can come close to being a scientist of your calibre
- My colleague, Patrick Cole, for programming the PyGMI 3D modelling software. Without this software I would still have been busy with my first model…
- All my family, friends and colleagues for support, interest and encouragement
- Stephanie Scheiber-Enslin for all her kindness and help
- My mom, the most amazing woman who gave her children opportunities she never had. I am sorry I couldn't finish in time.
- My husband, Patrick Cole. I have no words that can describe your support, encouragement, counselling, advice and patience. Thank you best friend Bug

To my mom Wena Prinsloo, a true academic in her own right

1938 - 2017

TABLE OF CONTENTS

DECLARATION ..... **ii**

ABSTRACT ..... **iii**

ACKNOWLEDGEMENTS ..... **iv**

TABLE OF CONTENTS ..... **vi**

LIST OF FIGURES ..... **x**

LIST OF TABLES ..... **xxi**

NOMENCLATURE ..... **xxiii**

CHAPTER 1 INTRODUCTION **1**

1.1 Thesis organisation 1

1.1.1 Chapter 2: Physical properties of the Bushveld Complex 1

1.1.2 Chapter 3: The importance of 3D modelling and taking crustal thickness into account 2

1.1.3 Chapter 4: Importance of magnetic data 2

1.1.4 Chapter 5: Geometry of the Bushveld Complex 2

1.1.5 Chapter 6: A possible magma staging chamber under the Bushveld Complex 3

1.2 Contributions 3

CHAPTER 2 PHYSICAL PROPERTIES OF THE BUSHVELD COMPLEX **6**

2.1 Abstract 7

2.2 Introduction 8

2.3 Data 9

2.3.1 Density 9

2.3.2 Magnetic Properties 10

2.4 Lithology-based physical property estimation 12

2.4.1 Results 18

2.5 Petrography-based physical property estimation 25

2.6 Discussion and conclusions 28

2.7 Acknowledgements 29

CHAPTER 3 THE IMPORTANCE OF 3D MODELLING AND TAKING CRUSTAL THICKNESS INTO ACCOUNT 30

3.1 Abstract 31

3.2 Introduction 32

2. Geological Overview 36

3.3 Gravity Data 37

3.4 Model Constraints 38

3.4.1 Crustal Thickness Data 38

3.4.2 Physical Properties 41

3.4.3 Bushveld Complex Occurrences 42

3.5 Model Reassessment 46

3.5.1 2.5D vs 3D Gravity Modelling 46

3.5.2 Effect of variable crustal thickness 54

3.5.3 Dipping sheets vs. connected lobes models 58

3.6 Discussion 61

3.7 Conclusions 64

3.8 Acknowledgments 66

CHAPTER 4 IMPORTANCE OF THE MAGNETIC DATA 67

4.1 Abstract 68

4.2 Introduction 69

4.3 Airborne Magnetic Data Specifications 69

4.4 Geological and Rock Property Overview 71

4.5 Magnetic Signatures 74

4.5.1 Upper Zone 80

4.5.2 Main Zone 90

4.5.3 Critical and Lower Zones 94

4.5.4 Non-Bushveld Complex Rocks 94

4.5.5 Faults and IRUPs 96

4.6 Central Bushveld Geometry 99

4.7 Summary and Discussion 101

4.8 Conclusions 103

CHAPTER 5 GEOMETRY OF THE BUSHVELD COMPLEX 105

5.1 Abstract 106

5.2 Introduction 107

5.3 Geology 108

5.4 Data 111

5.4.1 Gravity Data 111

5.4.2 Magnetic Data 111

5.4.3 Crustal Thickness Models 114

5.5 Modelling constraints 118

5.5.1 Geological maps 118

5.5.2 Physical properties 118

5.5.3 Deep seismic reflection 120

5.5.4 Boreholes 121

5.5.5 Combined gravity and magnetic modelling 122

5.5.6 Self-demagnetisation 123

5.6 Modelling Results 124

5.6.1 Deeper-seated dense material 124

5.6.2 Thickness and depth 125

5.6.3 Domes and diapirs 130

5.6.4 Gravity lows in the eastern lobe 133

5.6.5 Feeders 135

5.6.6 Faulting 136

5.7 Discussion 138

5.7.1 Deep-seated dense material 138

5.7.2 Domes and diapirs 139

5.7.3 Gravity low in the eastern lobe 143

5.7.4 Feeders 145

5.7.5 Faulting 147

5.7.6 Connectivity between the different lobes 148

5.8 Summary and Conclusions 149

CHAPTER 6 A POSSIBLE MAGMA STAGING CHAMBER UNDER THE BUSHVELD COMPLEX 151

6.1 Abstract 152

6.2 Introduction 152

6.3 Methods 155

6.3.1 Gravity data 155

6.3.2 Broadband Seismic Data (SASE) 156

6.3.3 Gravity modelling 156

6.4 Crust-mantle transition 156

6.5 Gravity model with staging chamber 160

6.6 Discussion 165

CHAPTER 7 CONCLUSIONS AND FUTURE WORK 169

7.1 Future work 170

CHAPTER 8 REFERENCES 171

APPENDIX ADDITIONAL PAPER 187

LIST OF FIGURES

Figure 2.1. Distribution of sampling sites and boreholes for which physical properties information were available. Table 2.1 summarises specifications of the physical property measurements in each borehole 10

Figure 2.2. Comparison between the (a) density log and (b) magnetic susceptibility log with the corresponding lithology log determined by visual geological logging by a geologist for borehole AP3 from the western lobe. The lithologies all form part of the Main Zone. An 11-point moving average filter was applied to original data (grey) in (a) and (b) for visualisation purposes (dark line). The question marks indicate density anomalies which were not identified as lithological variations on the visually determined geological log; (c) The visually logged lithology defined the depth range for which the physical property (density in this case) was extracted. The median for the selected values was then calculated 13

Figure 2.3. Magnetic susceptibility versus density coloured according to lithology for borehole AP3. FV – Feldspar vein; LAMP – Lamprophyre; GN – Gabbronorite; AN – Anorthosite; MGN – Melagabbronorite; LGN – Leucogabbronorite; MN – Melanorite; LN – Leuconorite; N – Norite; PYX – Pyroxenite; FPYX – Feldspathic pyroxenite; POIKFPYX – Poikilitic feldspathic pyroxenite; POIKAN– Poikilitic anorthosite; VTAN – Vari-textured anorthosite; PYXAN – Pyroxene anorthosite; CR – Chromitite; PEG – Pegmatite; FPEG - Feldspathic pegmatite. The plot displays 12 404 data points 14

Figure 2.4. (a) to (h) Density distributions for anorthosite in the Main Zone. The red line indicates the median density for anorthosite in the borehole. (i) All the medians in (a) to (h) shown on one graph to illustrate the variability in the calculated medians. The medians are (from left to right) from AP1a, AP1b, AP3, AP4, MO1_lab, BV1, MO1 and AP2 15

Figure 2.5. (a) to (e) Density distributions for norite in the Critical Zone. The red line indicates the median density for norite in the borehole. (f) All the medians in (a) to (e) shown on one graph to illustrate the variability in the calculated medians. The medians are (from left to right) from AP1b, AP1a, AP4, AP3, AP2. BV1, MO-1, RUS1, RUS1A, FF1-85 and AP5 do not contain CZ 16

Figure 2.6. Wire-line logging and laboratory measurements of density (a) and magnetic susceptibility (b) measured in the MO1 borehole 18

Figure 2.7. Observed densities for samples with petrographic analysis from the Upper Zone in the BV1 borehole. (a) Samples with plagioclase (Plag), ortho (OPX)- and clinopyroxene (CPX) (and inverted pigeonite (InvPig) and opaques. (b) Samples with plagioclase, ortho- and clinopyroxene (and inverted pigeonite), olivine and opaques. 26

Figure 2.8. Observed densities for samples with petrographic analysis from the Main Zone in borehole BV1. (a) Samples with plagioclase, orthopyroxene and clinopyroxene and inverted pigeonite. (b) Samples with plagioclase, ortho- and clinopyroxene (and inverted pigeonite), and olivine 27

Figure 2.9. Densities calculated for samples with petrographic analysis from the (a) Upper and (b) Main Zones in borehole BV1. Densities were calculated from the modal abundances and published densities for the minerals (Table 2.10) 28

Figure 2.10. Progression in representation of densities. (a) Traditional approach showing the range of values for magnetite gabbro in BV1 in blue and the median value in red; (b) Histogram representation of the same data; (c) Ternary plot of modal abundance for petrographically analysed samples in the Upper Zone 29

Figure 3.1 Simplified geological map of the Bushveld Complex. CRF – Crocodile River Fragment; DD – Dennilton Dome; MHF – Marble Hall Fragment; EC – Elandskraal Complex; PK – Palmietgat Kimberlite; FF – Fairfield borehole; CDM – Cullinan Diamond Mine. 33

Figure 3.2 Historic conceptual models of the Bushveld Igneous Complex proposed by (a) G.A.F Molengraaff, (b) A.L. du Toit and (c) A.L. Hall (from Hall, 1932)..... 34

Figure 3.3 Two dimensional gravity models through the centre of the Bushveld Complex in a west-east direction. The position of each profile is shown overlain on the Bouguer Anomaly data next to each model. (a) Model of Cousins (1959). Dotted area – TVL Supergroup; ^ ^ - Bushveld Group; + + - Granite; (b) Dipping sheet gravity model of Meyer and De Beer (1987). (Reprinted by permission from Macmillan Publishers Ltd: NATURE, Meyer, R. and De Beer, J.H. (1987), © 1987); (c) Connected Bushveld model (Webb et al., 2004). 35

Figure 3.4 Bouguer anomaly map of the Bushveld area. The outlines of the Rustenburg Layered Suite as they appear on the 1:250 000 geological maps are indicated in black and alkaline complexes are outlined in white. Grey points represent the gravity measuring point 38

Figure 3.5 (a) Topography of the Bushveld Complex area; (b) Crustal thickness estimated from the topography using Airy-Heiskanen isostatic compensation (reference crustal thickness = 38 km, density contrast across the Moho = 400 kg/m^3; (c) SASE stations overlain on Precambrian terrains for Southern Africa (adapted from Kgaswane et al., 2009). The Bushveld Complex is indicated and the green box outlines the area shown in (a), (b) and (d) to (h). ; (d) Crustal thicknesses (Nguuri et al., 2001) for the area around the Bushveld Complex; (e) Gravity field calculated for the Moho model of Nguuri et al (2001); (f) Crustal thicknesses (Nair et al., 2006) for the area around the Bushveld Complex; (g) Gravity field calculated for the Moho model of Nair et al (2006); (h) Crustal thicknesses (Kgaswane et al., 2012) for the area around the Bushveld Complex. The value below the station number is the thickness of the layer with Vs≥4.0 km/s; (i) Gravity field calculated for the Moho model of Kgaswane et al (2012). Black dots indicate the localities of seismic stations with the thickness at each station indicated in km. In (a), (b), (d), (f) and (h) the station number is shown below the black dot. In (e), (g) and (i) estimated crustal thicknesses are shown above the black dot. The outline of the Rustenburg Layered Suite is shown in all images. 40

Figure 3.6 Borehole logs for (a) FF drilled on the farm Fairfield FF1-85 (Walraven, 1987; Moen, 1989) and (b) CDM located at the Cullinan Diamond Mine (Cawthorn and McKenna, 2006). The localities of the boreholes are indicated in Figure 3.1 and Figure 3.4 43

Figure 3.7 Comparison between gravity fields calculated along a profile using 2.5D and 3D modelling for progressively more complex models. Indicated body dimensions are in kilometres. (a) North-south striking body with a density of 2750 kg/m^3. The body extends 2.5 km either side of the profile; (b) Similar to body in (a) but northern extension curves to the east. The body starts to curve at roughly 1.7 km north of the profile and at its northeastern end is 2.4 km north of the profile. (c) Body in (b) cut by a southeast dipping body with a density of 2950 kg/m^3. At its shallowest (300 m) it is located 800 m to the south of the profile. At its deepest (3.6 km) it is located 2 km to the south of the profile 47

Figure 3.8(a) Recreation of Cousins' (1959) model in 2.5 dimensions along the profile shown in Figure 3(a); (b) Model and calculated gravity field extracted from the three dimensional model and field along Cousins' profile; (c) Perspective views of the three dimensional model (vertical axis exaggerated) 49

Figure 3.9 (a) Recreation of Meyer and De Beer's (1987) model in 2.5 dimensions along the profile shown in Figure 3(b); (b) Model and calculated gravity field extracted from

the three dimensional model and field along Meyer and De Beer's' profile; (c) Perspective views of the three dimensional model (vertical axis exaggerated) 51

Figure 3.10 (a) Recreation of Webb et al's (2004) 2.5D model of the Bushveld Complex along the white dashed part of the profile shown in Figure 3(c); (b) Model and calculated gravity field extracted from the three dimensional model along Webb et al's profile; (c) Perspective views of the 3D model (vertical axis exaggerated)..... 53

Figure 3.11 Model and calculated gravity field extracted from Meyer and De Beer's (1987) model extended into 3 dimensions and with the thickened crust included; (a) Results when using the crustal thickness model of Nguuri et al. (2001); (b) Results when using the crustal thickness model of Nair et al. (2006); (c) Results when using the crustal thickness model of Kgaswane et al. (2012). The orange line indicates the Airy-Heiskanen Moho..... 55

Figure 3.12 Model and calculated gravity field extracted from Webb et al.'s (2004) model extended into 3 dimensions and with the thickened crust included; (a) Results when using the crustal thickness model of Nguuri et al. (2001); (b) Results when using the crustal thickness model of Nair et al. (2006); (c) Results when using the crustal thickness model of Kgaswane et al. (2012). The orange line indicates the Airy-Heiskanen Moho 57

Figure 3.13 Testing the dipping sheet model using updated density information (Table 3.2) and including continuous Transvaal Supergroup underneath the whole Complex. (a) Results when using the crustal thickness model of Nguuri et al. (2001); (b) Results when using the crustal thickness model of Nair et al. (2006); (c) Results when using the crustal thickness model of Kgaswane et al. (2012). 59

Figure 3.14 Testing the connected-lobe model using updated density information (Table 3.2). (a) Results when using the crustal thickness model of Nguuri et al. (2001); (b) Results when using the crustal thickness model of Nair et al. (2006); (c) Results when using the crustal thickness model of Kgaswane et al. (2012) 60

Figure 3.15 Modified version of the model shown in Figure 3.14(a) using Nguuri et al's (2001) crustal thickness model and incorporating variations in the mantle density. (a) Model along the WE profile; (b) Model along the NW-SE profile; (c) Model along the SW-NE profile. The localities of the profiles are shown in Figure 3.1 62

Figure 3.16 Modified version of the model shown in Figure 3.14b) using Nair et al's (2006) crustal thickness model and incorporating magma underplating. (a) Model

along the WE profile; (b) Model along the NW-SE profile; (c) Model along the SW-NE profile. The localities of the profiles are shown in Figure 3.1 63

Figure 3.17 Modified version of the model shown in Figure 3.14(c) using Kgaswane et al's (2012) crustal thickness model and including the dense, high velocity layer above the Moho. (a) Model along the WE profile; (b) Model along the NW-SE profile; (c) Model along the SW-NE profile. The localities of the profiles are shown in Figure 3.1 65

Figure 4.1 Outlines of survey blocks for regional (linear hatching) and higher resolution (dotted hatching) data overlain on the geology of the Bushveld Igneous Complex (Council for Geoscience, 1997) 70

Figure 4.2 Gridded image of the merged higher resolution magnetic data sets overlain on the regional magnetic data collected over the Bushveld Complex. Small blocks labelled I to VI outline anomaly type areas shown in Figure 4.6 72

Figure 4.3 Geological map of the Bushveld Igneous Complex compiled from the published 1:1 000 000 geological map of South Africa (Council for Geoscience, 1997). CRF – Crocodile River Fragment; PC – Pilanesberg Complex. Small blocks labelled I to VI outline anomaly type areas shown in Figure 4.6 73

Figure 4.4 Synthetic two dimensional models showing the effect of changes in depths and dips of magnetic bodies on the magnetic field in the northern part of South Africa. (a) Increasing the depth of a vertical dyke results in progressively smaller amplitudes and wider anomalies; (b) Increasing the depth of a body with an irregularly shaped top surface results in a smoother anomaly; (c) to (f) Decreasing the dip of a body substantially changes the shape of the magnetic anomaly 75

Figure 4.5 Synthetic two dimensional models showing the anomaly shapes expected for the Upper and Main Zones of the Bushveld Complex. Average remanent magnetisation parameters are from Letts et al. (2009). (a) Magnetic field for rocks in the Upper Zone; (b) Magnetic field of the remanently magnetised Main Zone rocks; (c) Combined magnetic anomaly calculated for adjoining steeply dipping Upper and Main Zone material; (d) Individual magnetic anomalies calculated for the Upper and Main Zones in (c) shown separately; (e) Combined magnetic anomaly calculated for adjoining shallower dipping Upper and Main Zone material; (f) Individual magnetic anomalies calculated for the Upper and Main Zones in (e) shown separately 77

Figure 4.6 Anomaly types typically encountered in the Rustenburg Layered Suite based on correlation with detailed geologic mapping (Geological Survey of South Africa, 1974, 1978, 1981), rock properties (Hattingh, 1986, 1989; Letts et al., 2009) and

modelling (Figure 4.4, 5.5 and 5.12). White dots indicate localities of palaeomagnetic samples with reversed magnetisation 79

Figure 4.7 Magnetic field calculated along north-south directed lines spaced 200 m apart crossing different simulated configurations of magnetite layers (white lines). Data calculated along the lines were gridded using a cell size of 50 m, similar to the higher resolution observed magnetic data 80

Figure 4.8 Mapped Rustenburg Layered Suite from the 1:250 000 Geological map overlain on the magnetic data for the western lobe of the Bushveld Complex, north of Pilanesberg. Outlines and faults inferred from the magnetic data are also indicated. A – mottled anomalies of the Upper Zone; B – layering in Upper Zone in mottled anomalies; C – high amplitude positive anomaly in Upper Zone; D – deeper-seated Upper Zone; E – syenite dykes; F – interaction between Upper and Main Zone anomalies; G – diabase 82

Figure 4.9 Mapped Rustenburg Layered Suite from the 1:250 000 Geological map overlain on the magnetic data for the western lobe of the Bushveld Complex, south of Pilanesberg. Outlines and faults inferred from the magnetic data are also indicated. a – mottled anomalies of the Upper Zone; b, c, d – inferred faults; e – Upper Zone anomaly splits into positive northern part and negative part in south; f – interaction between Upper and Main Zone anomalies; g – negative linear anomalies within Main Zone; h – anomaly close to Main Zone – Critical Zone boundary; i – reversely polarised magnetic body, possibly in Main Zone; j – possible continuation of Rustenburg Layered Suite rocks; k – Middelwater Sill 84

Figure 4.10 Mapped Rustenburg Layered Suite from the 1:250 000 Geological map overlain on the magnetic data for the eastern lobe of the Bushveld Complex, south of the Steelpoort Fault. Outlines and faults inferred from the magnetic data are also indicated. SF - Steelpoort Fault; LF - Laersdrif Fault. 1 – mottled anomalies of the Upper Zone; 2,3 – negative anomaly at eastern and southern boundaries of Upper Zone; 4 – deeper-seated Upper Zone; 5 – dykes; 6 – deep-seated remanently magnetised body; 7 – possible iron-rich pegmatoids; 8 – reversely polarised magnetic body, possibly in Main Zone 85

Figure 4.11 Mapped Rustenburg Layered Suite from the 1:250 000 Geological map overlain on the magnetic data for the eastern lobe of the Bushveld Complex, north of the Steelpoort Fault. Outlines and faults inferred from the magnetic data are also indicated. The inset shows an enlarged image of the Main Zone west of the Wonderkop Fault. SF - Steelpoort Fault; WF - Wonderkop Fault; SfF – Stofpoort

Fault. i – shallow-dipping Upper Zone; ii – low magnetic intensities due to Transvaal Supergroup updoming; iii - deeper-seated Upper Zone; iv – steeply dipping Upper Zone with layering visible; v – layers within Main Zone; vi – interaction between Upper and Main Zone anomalies..... 87

Figure 4.12 Mapped Rustenburg Layered Suite from the 1:250 000 Geological map overlain on the magnetic data for the northern lobe of the Bushveld Complex. Outlines and faults inferred from the magnetic data are also indicated. α,β, γ –Upper Zone; δ, ε – possible edges of a graben; ζ – magnetite layers in the Upper Zone; η, θ, ι – interaction between Upper and Main Zone anomalies ; κ – Lower Zone; λ – negative anomaly correlating with Lower Zone); μ – BIF; ν, ξ – dolerite sills..... 89

Figure 4.13 Synthetic magnetic fields calculated for (a) a vertical body, (b) a body dipping 70º to the south, (c) three adjacent southward dipping bodies, showing their individual contributions to the field, and (d) three adjacent southward dipping bodies, showing their combined response. All of the bodies are remanently magnetised, with an inclination of 58º and a declination of 19º..... 93

Figure 4.14 (a) Linear features and IRUPS inferred from the magnetic data for the western lobe. Figure 4.15 shows data in the area marked by the black box; (b) Linear features and IRUPS inferred from the magnetic data for the eastern lobe. 97

Figure 4.15 (a) High resolution magnetic data shown by Campbell (2006) for the area marked in Figure 4.14. Data were collected at 50 m line spacing, 30-40 m terrain clearance using a helicopter. (Colour bar labels were enlarged for legibility); (b) Lower resolution data for the same area collected with a fixed-wing aircraft at 200 m line spacing and 80 m terrain clearance..... 98

Figure 4.16 Simple 2.5 dimensional models calculated along a profile running from east to west through the Bushveld Complex (see Figure 4.2 for locality). (a) Mafic rocks continuous between the western and eastern lobes at a constant level; (b) Mafic rocks modelled as separate dipping sheets; (c) Continuous mafic rocks, but with more complex geometry. For all cases the vertical:horizontal exaggeration is 10:1100

Figure 5.1. Geological map of the Bushveld Complex. The dashed line indicates the outline of the modelling area. CRF – Crocodile River Fragment; RF – Rooiberg Fragment; DD – Dennilton Dome; MHF – Marble Hall Fragment; SF – Stavoren Fragment; JHBD – Johannesburg Dome; DC – Dwarsfontein Complex; EC – Elandskraal Complex; PC – Pilanesberg Complex; RC – Roodeplaat Complex; SC – Spitskop Complex; TML – Thabazimbi-Murchison Lineament; UF1 and UF2 – unnamed faults. The hatched area indicates the TML zone 110

Figure 5.2. Diapirs in the northeastern Bushveld Complex (see Figure 5.1 for locality) 111

Figure 5.3. (a) Regional gravity and (b) magnetic data. Dashed lines indicate profiles extracted from the 3D model and shown in Figure 5.9, Figure 5.11, Figure 5.12 and Figure 5.14. Borehole localities, large faults and pre-BC inliers, and deep reflection seismic lines are shown. Diapirs from Figure 5.2 are outlined in white. 113

Figure 5.4. Depth to Moho derived by (a) Nguuri et al. 2001, (c) Nair et al. 2006, (e) Kgaswane et al. 2012 and gravity fields calculated for the models using a crustal density of 2700 kg/m^3 and an upper mantle density of 3380 kg/m^3 (b, d and f). Black dots are SASE stations with the station number above and Moho depth underneath the dot. Major structural features and the outline of the RLS are shown. Models extracted from simple 3D gravity models along the WE profile (blue line) are shown in Figure 5.6 115

Figure 5.5. Depth to Moho derived by (a) Youssof et al. (2013), (c) Delph and Porter (2015), (e) average of the five crustal thickness models and gravity fields calculated for the models using a crustal density of 2700 kg/m^3 and an upper mantle density of 3380 kg/m^3 (b, d and f). Black dots are SASE stations with the station number above and Moho depth underneath the dot. Major structural features and the outline of the RLS are shown. Models extracted from simple 3D gravity models along the WE profile (blue line) are shown in Figure 5.6..... 116

Figure 5.6. Models extracted from simple 3D gravity models along the profile shown in Figure 5.4 and Figure 5.5. The models include crustal thickness from different studies (a - Nguuri et al., 2001; b - Nair et al., 2006; c - Kgaswane et al., 2009, 2012; d - Youssof et al. 2013; e - Delph and Porter, 2015; f – the average crustal thickness model) and show that changes in the crustal thicknesses affect the RLS thickness, but the overall geometry remains relatively similar..... 117

Figure 5.7. Deep seismic reflection lines with positions of profiles indicated. (a) P1-86 line (Odgers, Hinds and Von Gruenewaldt, 1993); (b) Sekukhuneland line (Odgers and Du Plessis 1993) 121

Figure 5.8. Logs for boreholes of which the localities are shown in Figure 5.1 and in the models in Figure 5.9, Figure 5.11and Figure 5.12. (a) (Teigler and Eales, 1996); (b) from (Tegner, Cawthorn and Kruger, 2006); (c) from Hartzer (2000); (d) Donated to the Council for Geoscience by Goldfields (Pty) Ltd; (e) from Moen (1989) ; (f) from Wilson (2015); (g) Drilled by the Council for Geoscience in 1963 (h) Drilled by the Council for Geoscience in 2006; (i) Donated to the Council for Geoscience Transvaal Consolidated Land and Exploration Company (j) and (k) from Buchanan (1975)... 122

Figure 5.9(a) Magnetic field calculated for a tabular body representing the Upper Zone; (b) Magnetic field of the same tabular body after the effect of self-demagnetisation has been taken into account following the approach of Clark and Emerson (1999) 124

Figure 5.10. Models along profiles extracted from the 3D model. (a) and (b) Two different ways of modelling the eastern gravity low along Profile C; (c) Model along Profile W, with the locality of borehole KK1 shown (log in Figure 5.8c); (d) Profiles CW with the P1-86 deep seismic reflection line shown (Figure 5.7a). Figure 5.3 shows the profile localities. CRF – Crocodile River Fragment; CRFt – Crocodile River Fault; DD – Dennilton Dome; DT – Droogekloof Thrust; EC - Elandskraal Complex; JHBD – Johannesburg Dome; StFt – Steelpoort Fault. Localities of crossing profiles are indicated above the model (eg. Pr-W). Table 5.1 shows the densities and magnetic properties used in the model 126

Figure 5.11. Thickness of the modelled RLS for two models. (a) Model with updoming in the east; (b) Model with thick granite-granophyre in the east. Pink triangles indicate areas where the two models differ the most. DC – Dwarsfontein Complex; DD – Dennilton Dome; FF1-85 is a borehole (log in Figure 5.8e) 127

Figure 5.12. (a) Model extracted from the 3D model along profile N; (b) Model extracted from the 3D model along profile S. Figure 5.3 shows the profile localities. The position of the deep seismic reflection line Sek (Figure 5.7b) is indicated in (a). CH6 and BN1 are boreholes (logs in Figure 5.8f, g). DC – Dwarsfontein Complex; IF1 – Inferred Fault 1; JHBD – Johannesburg Dome; StFt – Steelpoort Fault; WFt – Wonderkop Fault. Localities of crossing profiles are indicated above the model (eg. Pr-W). Table 5.1 shows the densities and magnetic properties used in the model 128

Figure 5.13. Model extracted from the 3D model along profile E. Figure 5.3 shows the profile locality. The position where the profile crosses the deep seismic reflection line Sek (Figure 5.7b) is indicated. ONZ1 and PD are boreholes (logs in Figure 5.8j, k). DD – Dennilton Dome; SbFt – Sugarbush Fault; TML – Thabazimbi-Murchison Lineament; WFt – Wonderkop Fault. Localities of crossing profiles are indicated above the model (eg. Pr-S). Table 5.1 shows the densities and magnetic properties used in the model..... 129

Figure 5.14. Synthetic potential field models of (a) a dome surrounded by dense material; (b) and (c) a diapir at different stages of development; (d) a diapir that has been completely disconnected from its base. Physical properties of the individual layers are indicated in the model. In (d) magnetic remanence properties are shown where

applicable. The ambient magnetic field has an inclination of -63º, a declination of -17º, and an intensity of 28 500 nT 131

Figure 5.15. Two models along profile CE extracted from the 3D model. (a) Gravity lows in the southern half modelled as domes; (b) Gravity lows in the southern half modelled as a dome and thick granite-granophyre. Figure 5.3 shows the profile locality. DC – Dwarsfontein Complex; UF1 – Unnamed Fault 1; TML – Thabazimbi-Murchison Lineament. Localities of crossing profiles are indicated above the model (eg. Pr-S). Table 5.1 shows the densities and magnetic properties used in the model 134

Figure 5.16. (a) Modelled depth to the Upper Zone; (b) to (d) Models extracted from the 3D model along three profiles where normal faults were modelled.; DC – Dwarsfontein Complex; DD – Dennilton Dome; DT – Droogekloof Thrust; JHBD – Johannesburg Dome. Localities of crossing profiles are indicated above the model (eg. Pr-S). Table 5.1 shows the densities and magnetic properties used in the model 137

Figure 5.17. (a) Interpreted down-faulted TVL Supergroup rocks south of the TML in the northeast of the BC; (b) Gravity data with the interpretation overlain; (c) Magnetic data with the interpretation overlain. IF1 – Inferred fault 1; UF2 – Unnamed fault 2 138

Figure 5.18. Some of the main findings shown on the observed gravity data set 139

Figure 5.19. Perspective views of the CRF looking from the (a) south and (b) north showing the modelled diapiric shape. From left to right, images show additions of the various components of the model 140

Figure 5.20. One possible development sequence for the Dennilton and Marble Hall pre-BC inliers. (a) Updoming starts due to the heat of the RLS. The floor may have been already undulating prior to the intrusion; (b) Diaprism brings deeper material closer to the surface; (c) Current situation 143

Figure 5.21. Modelled thickness of the granite-granophyre for the model with a possible feeder for these rocks in the east. DC – Dwarsfontein Complex; DD – Dennilton Dome. Localities of crossing profiles are indicated above the model (eg. Pr-W) 145

Figure 5.22. (a) Synthetic model with a single BIF layer; (b) Calculated gravity field (100 m cell size) for model in (a). Black dots are gravity stations; (c) Regridded gravity field of data extracted at gravity stations (1 km cell size); (d) Synthetic model with a

BIF layer and a deeper seated dense body; (e) Calculated gravity field (100 m cell size) for model in (d); (f) Regridded gravity field of data extracted at gravity stations (1 km cell size). 146

Figure 6.1. Simplified geological map of the Bushveld Complex. The dashed black line shows the extent inferred from geophysical data. Blue ellipses indicate feeders inferred from gravity data. The hachured area is the Thabazimbi Murchison Lineament. PK – Palmietgat kimberlite; FF – Fairfield borehole; CDM – Cullinan diamond mine. Lower left inset: NL – Northern lobe, EL – Eastern lobe, SEL – South-eastern lobe, WL – Western lobe, FWL – Far western lobe..... 155

Figure 6.2. Results from seismic receiver function studies. The Northern Marginal Zone (NMZ), Central Zone (CZ) and Southern Marginal Zone (SMZ) of the Limpopo Belt are outlined (Kgaswane et al., 2009). (a) Apparent V_p/V_s (Delph and Porter, 2015); (b) Moho sharpness (Youssof et al., 2013). The Moho sharpness quantifies the quality of the P to S conversions. Higher values indicate sharper Moho; (c) Quality of P to S conversions (Delph and Porter, 2015). (d) Thickness of the high Vs layer in the lower crust overlain on the depth to this layer (Kgaswane et al., 2009, 2012); (e) Ternary image combining normalised values of Vp/Vs (Delph and Porter, 2015), Moho sharpness (Youssof et al., 2013) and the thickness of the high Vs lower crustal layer (Kgaswane et al., 2009, 2012); (f) Distribution of the Karoo Large Igneous Province in South Africa overlain on the ternary image..... 159

Figure 6.3. (a) Inferred extent and thickness estimates for a magma staging chamber with a density of 3250 kg/m^3 underneath the BC. Thick blue lines are known faults. The cross-hatched area indicates the TML; (b) to (e) Profiles extracted from the 3D gravity model along the profiles indicated in (a). PSZ – Palala Shear Zone; SBF – Sugarbush Fault; TML – Thabazimbi-Murchison Lineament; Table 6.1 lists the densities used in the model 163

Figure 6.4. Simple diagram showing the possible stages of development of a staging chamber remnant under parts of the BC. (a) Situation prior to the intrusion of the RLS. The TML was already present at this time (Good and De Wit, 1997); (b) A magma chamber forms at the lower curst-mantle interface; (c) Magma flows upwards in the TML and Mokopane feeder and intrudes into the volcano-sedimentary Transvaal Supergroup; (d) The RLS and magma chamber solidifies and isostatic adjustment due to the dense thick RLS in the upper crust results in thicker crust underneath the BC..... 168

LIST OF TABLES

Table 2.1. Summary information for the boreholes displayed in Figure 2.1 11

Table 2.2. Median values estimated for lithologies of the RLS encountered in boreholes and published in the Physical Properties database (PPdb) and by Letts et al. (2009). Magnetic susceptibilities were only estimated from laboratory measurements (BV1, MO1_Lab, RUS1, RUS1A, PPdb, Letts et al. 2009)..... 19

Table 2.3. Calculation of the representative density and magnetic susceptibility for the Upper Zone 21

Table 2.4. Calculation of the representative density and magnetic susceptibility for the Main Zone 22

Table 2.5. Calculation of the representative density and magnetic susceptibility for the Critical Zone based on the contribution of lithologies observed in the western lobe (Teigler et al., 1992)..... 23

Table 2.6. Calculation of the representative density and magnetic susceptibility for the Critical Zone based on the contribution of lithologies observed in the eastern lobe (Cameron, 1978, 1982)..... 23

Table 2.7. Calculation of the representative density for the Lower Zone 24

Table 2.8. Calculation of the representative density for the Marginal Zone 25

Table 2.9. Calculation of the representative density for the Basal Ultramafic Sequence. 25

Table 2.10. Published densities for minerals in the Main and Upper Zones 28

Table 3.1 Number of teleseismic events used in the crustal thickness models..... 39

Table 3.2 Densities for the Bushveld Complex and surrounding lithologies. The last column shows average densities for the zones in the RLS..... 44

Table 4.1 Summary of the typical magnetic anomalies associated with the Rustenburg Layered Suite as they appear on 1 km and 200 m line spacing magnetic data..... 102

Table 5.1. Geological units with the petrophysical properties used in the modelling (Table 2.3, Table 2.4 and palaeomagnetic data from Letts et al., 2009). 119

Table 6.1. Densities used in the gravity model 164

NOMENCLATURE

BC	**B**ushveld **C**omplex
Moho	**Moho**rovičić discontinuity
SASE	**S**outhern **A**frican **S**eismic **E**xperiment
RLS	**R**ustenburg **L**ayered **S**uite
UZ	**U**pper **Z**one
MZ	**M**ain **Z**one
CZ	**C**ritical **Z**one
LZ	**L**ower **Z**one
MgZ	**M**arginal **Z**one
BUS	**B**asal **U**ltramafic **S**equence
IRUP	**I**ron-**r**ich **U**ltramafic **P**egmatoid
TVL	Transvaal

CHAPTER 1 INTRODUCTION

The Bushveld Complex (BC) is the largest known layered igneous intrusion and hosts vast mineral resources including 80% of the world's platinum and chromium (Cawthorn, 2010). Yet, despite extensive studies since it was first described by Molengraaff (1901), there is still intense disagreement about emplacement, geometry, mineralization formation etc. in competing models which are hotly debated. Some of the main questions concern the 3D geometry of the Rustenburg Layered Suite (RLS) vis-à-vis continuity between the eastern and western lobes, the mechanism of emplacement of the RLS and location of possible feeders. Thick sedimentary and volcanic sequences and the absence of deep geophysical and borehole data over the central part of the Complex make answers to these questions elusive.

In this project I have assessed the details of the three dimensional geometry of the Bushveld Complex using potential field data constrained by broadband seismic tomography, geologic, geochemical, borehole and rock property data. Deriving robust consistent models lay the basis for making inferences about emplacement mechanisms and syn-and post emplacement evolution. Over the years two dimensional gravity models (Cousins, 1959; Du Plessis and Kleywegt, 1987; Meyer and De Beer, 1987; Cawthorn et al., 1998; Webb et al., 2004) have provided meaningful models to help further evaluate the overall geometry of the Bushveld Complex. The models incorporated additional geophysical data as it became available. Coupling the availability of new data with much improved computing power means that the creation of a full three dimensional geophysically-based model of the entire BC was possible.

1.1 Thesis organisation

1.1.1 Chapter 2: Physical properties of the Bushveld Complex

A fundamental aspect of geophysical models is the physical properties of the geological units used in developing the models. In Chapter 2 I collate density and magnetic properties for Bushveld Complex lithologies from published data and unpublished wireline logging data, and determine realistic densities and magnetic susceptibilities for the individual lithologies. I also calculated average values that can be used for the individual zones in the Rustenburg Layered Suite which constitutes the thick mafic-ultramafic succession of the intrusion. These physical property data were used in the subsequent

modelling of the BC. New visualisations of rock properties using modal abundances and ternary diagrams reveal how changes in the abundance of minerals affect the physical properties (Dentith, Webb, personal communication, 2017). It demonstrates that traditional presentation of physical properties of a lithology as a mean value with standard deviations is an oversimplification of the real situation. This ternary display helps link geological processes, such as alteration, directly to the physical properties. This type of information is invisible if the physical properties are only related to lithology. This method of display is more useful for detailed studies of geological features or mineral deposits, but not useful for large, more regional models of the BC developed here.

1.1.2 Chapter 3: The importance of 3D modelling and taking crustal thickness into account

Published 2D and 2.5D gravity models of the Bushveld Complex evolved from two separate lopoliths under the western and eastern lobes (Cousins, 1959), to a model of dipping sheets (Du Plessis and Kleywegt, 1987; Meyer and De Beer, 1987) and then to a continuous layer that incorporated crustal thickness (Webb et al., 2004). This chapter firstly shows the importance of modelling complex geological bodies in three dimensions and at scales appropriate for the lateral extent. It then goes on to test the effect of three crustal thickness models derived from different teleseismic receiver functions studies (Nguuri et al., 2001; Nair et al., 2006; Kgaswane et al., 2009, 2012) on gravity models of the Bushveld Complex. The results support the proposed continuity of mafic and ultramafic rocks of the Rustenburg Layered Suite between the eastern and western lobes.

1.1.3 Chapter 4: Importance of magnetic data

The magnetic data over the Bushveld Complex effectively maps the magnetite-rich Upper Zone of the RLS. However, even though the other zones are not highly magnetic, the Main Zone is strongly remanently magnetised. Interaction between the magnetic anomalies caused by variably magnetised sources adds a level of complexity to interpreting the magnetic data. In Chapter 4 I incorporate the palaeomagnetic results of Letts (2009) in the Bushveld Complex to clarify the sources of characteristic magnetic signatures expected in different parts of the intrusion.

1.1.4 Chapter 5: Geometry of the Bushveld Complex

Chapter 5 develops a significantly more detailed three dimensional model of the Bushveld Complex using potential field data. For this model the RLS was not modelled as a single unit as in Chapter 3, but it was divided into four zones comprising the mafic-ultramafic succession of the Upper Zone, Main Zone, Critical Zone and Lower Zone. This was done to account for the differences in physical properties of the different zones as determined

in Chapter 2. This more detailed modelling highlighted anomalies that are consistent with the interpretation of feeders. An essential part of these models is the crustal thickness derived from seismic tomography studies, and the average of five crustal thickness models were used to constrain the potential field model. The few available seismic reflection lines and a number of deep boreholes constrained the model in additional locations. This more detailed modelling has revealed that the RLS is significantly disrupted in the eastern lobe, revealing a complex geometry.

1.1.5 Chapter 6: A possible magma staging chamber under the Bushveld Complex

Chapter 6 focuses on gravity modelling incorporating lower crustal density variations of the BC based on constraints from seismic receiver function data (Nguuri et al., 2001; Nair et al., 2006; Kgaswane et al., 2009, 2012; Youssof et al. 2013; Delph and Porter, 2015). The models require additional dense material under parts of the BC to obtain a fit between the observed and calculated data. The thickness of this dense material varies beneath the BC and the gravity model is consistent with the width of the receiver functions. Chapter 6 develops a model for this material and how it could be explained by a magma staging chamber underneath the BC.

1.2 Contributions

In this section I discuss how the work in each chapter contributes to our understanding of the Bushveld Complex.

This study presents the first full 3D potential field model of the world's largest and most iconic layered mafic intrusion, the Bushveld Complex. Two-dimensional modelling does not adequately take the complexity of geology into account and results will be inherently flawed. For the upper crust, the contribution to the gravity and magnetic field from lithologies surrounding a profile will affect the extent and thickness of the modelled units. On a larger scale, deep-seated variations in crustal thickness add long wavelength anomalies to the gravity field that must be considered when modelling an entity as large as the Bushveld Complex. Previous work showed the importance of including this information in gravity modelling, but only in two dimensions along an east-west profile across the central Bushveld Complex (Cawthorn et al., 1998; Webb et al., 2004). The next logical step was to extend this important conceptual work into a full 3D model of the Bushveld Complex and this study does that.

Magnetic and density properties provide important constraints on modelling of geological units. Palaeomagnetic properties of the Bushveld Complex are widely available (Hattingh, 1986a, 1986b, 1989, 1990, 1991, Hattingh and Pauls, 1994, Letts et al., 2009) and

detailed densities and magnetic susceptibility data were obtained for the BV-1borehole in the northern lobe (Ashwal et al., 2005). This borehole penetrated through granite, the Upper and Main Zones of the Rustenburg Layered Suite. Very little has been published on density and magnetic properties for the Critical, Lower and Marginal Zones of the Rustenburg Layered Suite. It became clear that more measurements were required and that a single resource providing density and magnetic properties for the Bushveld Complex and host rocks was greatly needed. Anglo Platinum provided geophysical wireline logging data sets for a number of boreholes in the western and eastern lobes and ranges of densities and susceptibilities for the different zones in the Rustenburg Layered Suite (RLS) were determined from these. By accounting for the different measuring instruments used in wireline logging and laboratory measurements, a comprehensive set of densities and magnetic susceptibilities were assembled for the Bushveld Complex and surrounding units.

Before detailed magnetic modelling could commence, the plethora of sources for the magnetic anomalies needed to be characterized. Often the anomalies are considered as simply reflecting the presence of magnetite in the Upper Zone, but by carefully studying the anomalies in conjunction with information about the remanent magnetisation, a more complex picture emerged. Some of the anomalies are in fact caused by the interaction between fields of the highly magnetic magnetite in the Upper Zone, and the low magnetic intensity but strongly remanently magnetised Main Zone rocks. I also summarise typical anomalies look in different parts of the Bushveld Complex.

The largest contribution of this study to the knowledge and understanding of the Bushveld Complex is the detailed three dimensional potential field model, which incorporates information from all of the separate studies, leading to the first comprehensive and synoptic view of the Bushveld Complex. It revealed the truly complex nature of the deeper parts of the RLS. The model not only confirmed the continuity of the RLS between the eastern and western lobes, but it also showed areas where the RLS is possibly absent, or disrupted in the eastern part of the Complex. I showed that the data could be modelled in two very different ways in this area, but both models required that the RLS was absent. In one model the RLS tapered off over what I interpreted as pre-Bushveld Complex doming, while in the other more than 10 km thick granite and granophyre of the intrusion's acid phase, presenting a possible granite feeder, cut through the mafic rocks. I also modelled the pre-Bushveld Complex inliers that was previously described as domes and fragments as diapirs. Domes and fragments generally form due to tectonic stresses, whereas heating of the underlying layers by the intrusion causes diapirism.

The model corroborated the gravity anomaly near Mokopane as a feeder and supported the widely held view that the Thabazimbi Murchison Lineament is a feeder zone. I also

show for the first time that the gravity high defining the southern margin of the south-eastern lobe is best modelled as a feeder. This has implications for how the intrusion was emplaced as we now have evidence of multiple feeders throughout the BC. These feeders would have tapped a source or sources in the lower crust and upper mantle, but these have never been geophysically modelled. During the modelling I found that it was impossible to obtain a good fit between the observed gravity field and the field calculated for a geologically feasible model, without adding deeper seated dense material at the depth of the Moho. I modelled this material as remnants of a staging chamber located at the crust-mantle boundary, the first time evidence has been provided for this idea.

This thesis is presented as a series of published and prepared manuscripts. Two peer reviewed journal articles are presented as chapters 3 and 4 and, chapters 2, 5 and 6 will be submitted shortly. A paper I contributed to is attached in the Appendix. My co-supervisor Dr CA Finn was the main author.

CHAPTER 2 PHYSICAL PROPERTIES OF THE BUSHVELD COMPLEX

This chapter will be submitted as a paper to a peer reviewed journal. The work was conducted by me and I constructed the manuscript. My co-authors edited the manuscript and suggested improvements.

Cole – 70% (conducted the research and constructed the manuscript)

Webb – 20% (suggested ways of plotting physical properties, reviewed the manuscript and suggested improvements)

Finn - 10% (reviewed the manuscript and suggested improvements)

Densities and magnetic susceptibilities of the Bushveld Complex rocks from borehole measurements

Janine Cole

Geophysics Unit, Council for Geoscience, Private Bag X112, Pretoria, 0001, South Africa
School of Geosciences, University of the Witwatersrand, Private Bag 3, WITS, 2050, South Africa
email: jcole@geoscience.org.za

Susan J. Webb

School of Geosciences, University of the Witwatersrand, Private Bag 3, WITS, 2050, South Africa
email: susan.webb@wits.ac.za

Carol A. Finn

US Geological Survey, Denver, Colorado 80225, USA
email: cfinn@usgs.gov

2.1 Abstract

Reliable estimates of densities and magnetic susceptibilities are essential for creating potential field models. Densities and magnetic susceptibilities for the Bushveld Complex have been measured by laboratory measurements on borehole core and field samples, in situ field measurements and using wire-line logging. However, considering the size and extent of the Bushveld Complex, both laterally and vertically, only a small portion has been characterised. Here I present new physical property data for eight sites in the Bushveld Complex. The new data are combined with previously published data to reduce the uncertainty in the estimates. Laboratory magnetic susceptibility data were collected using a Digico Susceptibility Bridge and Fiskars Geoinstruments TH-15 susceptibility meter, and wire-line logging companies used Weatherford and Auslog magnetic susceptibility logging tools that work on the same principle as the laboratory instruments. In the laboratory, densities were measured using Archimedes' principle, whereas wireline logging instruments measure density as a function of gamma-ray scattering. Different measurement principles, calibration issues, inconsistent geological logging and natural

magnetic or density variations within a lithology contribute to discrepancies in the physical properties of a specific lithology across different boreholes. This was addressed by calculating the median density and susceptibility for each lithology within a borehole. For each zone in the Rustenburg Layered Suite (Upper, Main, Critical, Lower, Marginal Zones and Basal Ultramafic Sequence) a generalised lithostratigraphic section was established, and the percentage that each lithology constitutes of the total thickness of the zone calculated. Using these percentages to weigh the densities and magnetic susceptibilities of the lithologies in the zone, it was possible to calculate a representative density and magnetic susceptibility for the zone. Densities for the Upper, Main, Critical, Lower and Marginal Zones were 3135 kg/m^3, 2911 kg/m^3, 2924 kg/m^3, 2946 kg/m^3, 3142 kg/m^3 and 2959 kg/m^3 respectively. The Basal Ultramafic Sequence encountered in the eastern lobe of the Bushveld Complex has a density of 3033 kg/m^3. Magnetic susceptibilities could only be determined for the Upper (0.185 SI) and Main (0.0017 SI) Zones.

Physical property measurements are most commonly displayed and recorded associated with lithological units. Although the uncertainty of the physical property values can be quantified, the quality of the geological logging is difficult to quantify. Plots of susceptibility against density highlight geological logging errors making this a valuable quality control tool. Having access to petrographic analyses of the measured samples allows for quantitative comparison between modal abundances and physical properties. We plot density data from the Bellevue core in a novel ternary diagram, that highlights details in density variation that are lost when density is only associated with lithology. In the Bellevue borehole measured density variations correspond with the density values calculated from model abundances of rock forming minerals such as plagioclase, pyroxene and opaque minerals. Where the correlation is poor, alteration of the borehole core is likely to be the cause. Plotting density variation with modal abundances in this novel ternary diagram highlights the effects of mineralogical composition, presence of hydrothermal alteration, and metamorphism in the core.

2.2 Introduction

Rock physical properties provide significant constraints on geophysical models. Borehole cores provide a unique data set to comprehensively investigate the density and magnetic susceptibility properties of the Bushveld Complex (BC), a layered igneous intrusion renowned for its size and mineral wealth. Because thick sedimentary and volcanic sequences cover the central part of the Complex (Figure 2.1), well constrained potential field models are critical for understanding the geometry of the BC under this cover. An important constraint is reliable densities and magnetic properties for lithologies in the model. Magnetic and palaeomagnetic properties and a few densities of samples collected

from outcrops (Figure 2.1) appear in the literature (Hattingh, 1986a, 1986b, 1989, 1990, 1991, Hattingh and Pauls, 1994, Letts et al., 2009). Physical properties have also been measured in the laboratory on borehole cores of FF1/85 (Filmalter, 1986), BV1 (Ashwal et al., 2005) and MO1 (Maré and Loots, 2007) (Figure 2.1). These boreholes penetrated only the Upper and/or Main Zones of the intrusion's mafic and ultramafic component (Rustenburg Layered Suite), and not the Critical, Lower and Marginal Zones.

Anglo Platinum provided wire-line logging data sets for boreholes located in the western and eastern lobes of the BC (Figure 2.1, Table 2.1). The boreholes generally started in the Main Zone and ended in the Critical Zone and measured properties included densities and magnetic susceptibilities. The first aim is to determine representative densities and magnetic susceptibilities for lithologies in the BC that can be used in potential field modelling. However, this approach assumes that the lithologies were logged correctly, and that a logged lithology has a single representative density or magnetic susceptibility. We show that linking physical properties to proper petrographic analyses of the rocks reveals the correlation between mineral composition and physical property variations within a lithology. Unfortunately for most of the boreholes this information was absent and the simple lithological approach had to suffice.

2.3 Data

2.3.1 Density

Density measured in a laboratory is a function of mass and volume, whereas wire-line logging instruments measure density as a function of gamma-ray scattering. The electron density of the surrounding matter determines the amount of scattering (Serra, 1984). The relation between electron density (ρ_e) and bulk density (ρ_b) of a material is (Serra, 1984):

$$\rho_e = \rho_b \left(\frac{Z}{A}\right) N \qquad \mathbf{1}$$

where Z = atomic number, A = atomic mass and N = Avogadro's number (6.02 x 10^{23}). For most rock Z/A ≈ 0.5, and the density provided by the wire-line logging system is based on this assumption (Chatfield, 2009).

An advantage of wire-line logging is that the logging measures the density in situ. Laboratory measurements only determine the density of a small subsample of the actual rock formation and if the sample is altered, fragmented or dehydrated, it does not give the bulk density of the formation (Telford et al., 1976: 24).

2.3.2 Magnetic Properties

Laboratory-based magnetic susceptibility measurements generally use the principle that magnetically susceptible material will influence an oscillating electromagnetic field to varying degrees (Maré, 2010). Wire-line logging instruments also work on the principle of electromagnetic induction. An oscillating electromagnetic field will induce an oscillating secondary electromagnetic field in a zone around the borehole tool. The in-phase component of the secondary field is a measure of the magnetic susceptibility of the surrounding material (Chatfield, 2009).

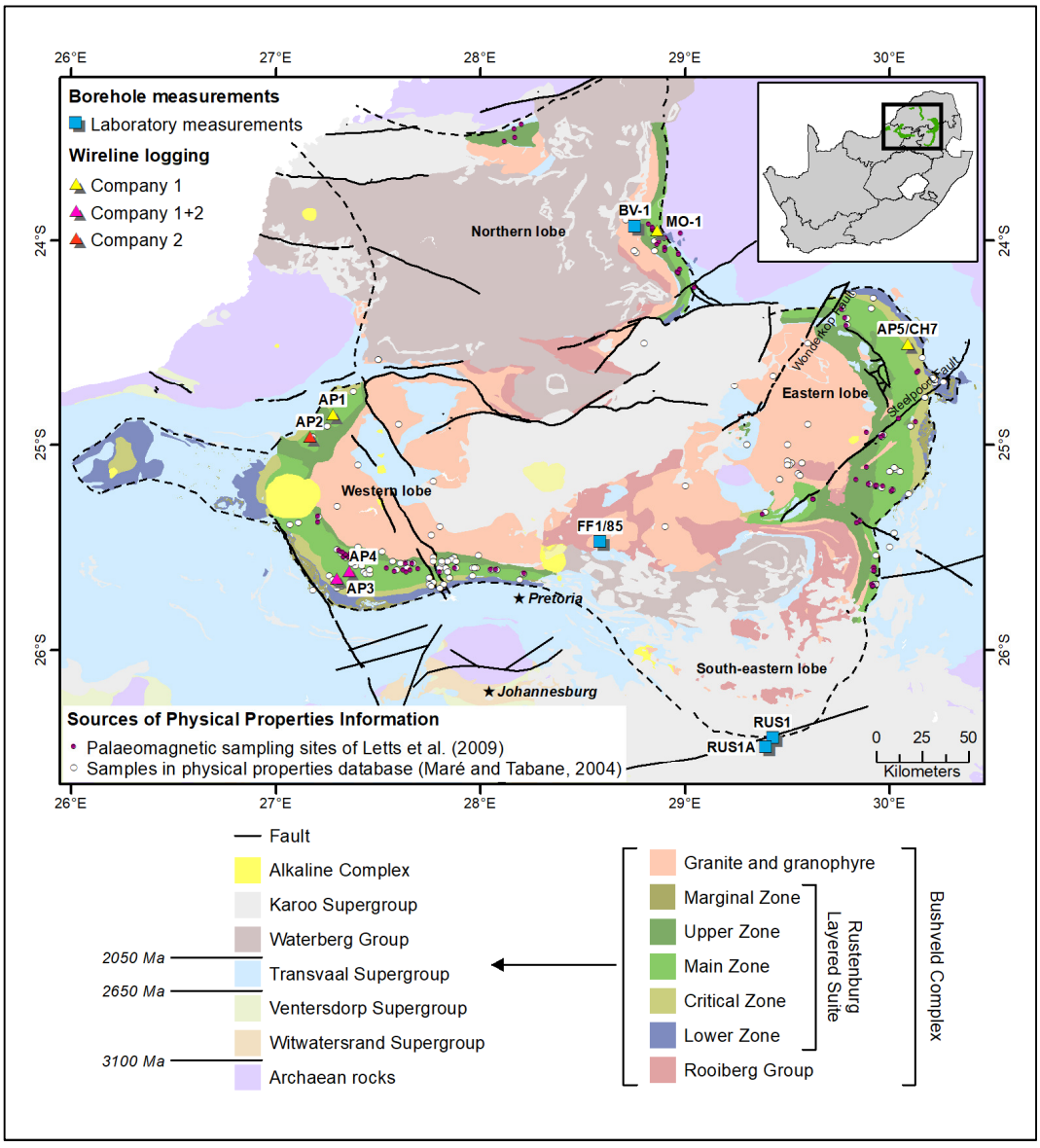


Figure 2.1. Distribution of sampling sites and boreholes for which physical properties information were available. Table 2.1 summarises specifications of the physical property measurements in each borehole

Table 2.1. Summary information for the boreholes displayed in Figure 2.1

Borehole	Longitude	Latitude	Logging length (m)	Method	Sampling interval (m)	Measured by
AP1a	27.281036º E	24.852386º S	1186.37	Wire-line (Quicklog)	0.01	Anglo Platinum
AP1b	27.281036º E	24.852386º S	1250.23	Wire-line (Weatherford)	0.01	Anglo Platinum
AP2	27.166416º E	24.961370º S	2324.00	Wire-line (Quicklog)	0.01	Anglo Platinum
AP3	27.300131º E	25.651871º S	1258.00	Wire-line (Weatherford/ Quicklog)	0.10	Anglo Platinum
AP4	27.361122º E	25.617107º S	2002.02	Wire-line (Weatherford/ Quicklog)	0.01	Anglo Platinum
AP5 (CH7)	30.087740º E	24.503659º S	1287.99	Wire-line (Quicklog)	0.01	Anglo Platinum
FF1/85	28.585278º E	25.470556º S	917.28	Laboratory	10.00	CGS
RUS1	29.428772º E	26.426103º S	155.00	Laboratory	Density: 1.50 Mag.sus: 0.50	Goldfields/ CGS
RUS1A	29.395508º E	26.472050º S	500.00	Laboratory	Density: 5.00 Mag.sus: 0.5	Goldfields/ CGS
BV-1	28.755646º E	23.926296º S	2949.50	Laboratory	Density: 1.70 Mag.sus: 0.02	CGS/Wits
MO1	28.864139º E	23.948986º S	1563.02	Wire-line (Quicklog)	0.01	Wits/Anglo Platinum
				Laboratory	Variable (average ~9 m)	CGS

2.4 Lithology-based physical property estimation

Densities and magnetic susceptibilities were estimated only for logs that had lithological information so that physical properties could be linked to lithology. These are BV1 and MO1 in the northern lobe, AP1 to AP4 in the western lobe, AP5 (Wilson's CH7 (2015)) in the eastern lobe, FF1/85 in the central part of the complex, and RUS1 and RUS1A in the south-eastern lobe (Figure 2.1). Only densities were measured for FF1/85.

Visually acquired geological logs provided with the wire-line logging data were marked on the density and susceptibility logs. The geological logs for the Main Zone of the RLS generally contained less detail than the geophysical logs. For example, in a section on the log for AP3 anomalous density values (question marks in Figure 2.2a) were not identified on the geological log.

The correlation between magnetic susceptibility and lithology for the same borehole (Figure 2.2b) is less clear, this is expected as magnetite is a minor mineral. For example, between depths of 300 m and 340 m, the anorthosite magnetic susceptibilities are higher than for the surrounding gabbronorites, but at 530 m the anorthosite cannot be distinguished from the surrounding material based on susceptibility (Figure 2.2b). In the case of density, the anorthosite is consistently less dense than the surrounding material. Also, only part of an anorthosite layer may have higher susceptibilities. The whole anorthosite layer between 375 m and 390 m has lower densities than the sections above and below, but only the upper part has higher susceptibilities. In the simple lithology-based approach, the median susceptibility for anorthosite will combine both the magnetic and nonmagnetic sections of anorthosite.

Densities and susceptibilities for a lithological unit were extracted and assigned to the corresponding lithological unit (Figure 2.2c). The starting and ending depths were chosen away from contacts so that sharp changes between high and low susceptibilities or densities associated with different lithologies did not affect the values. This methodology was followed for all the boreholes except BV1. Detailed petrographic studies on BV1 (Ashwal et al., 2005) ensured excellent geological control, and the density and susceptibility for each rock type was simply extracted from the data.

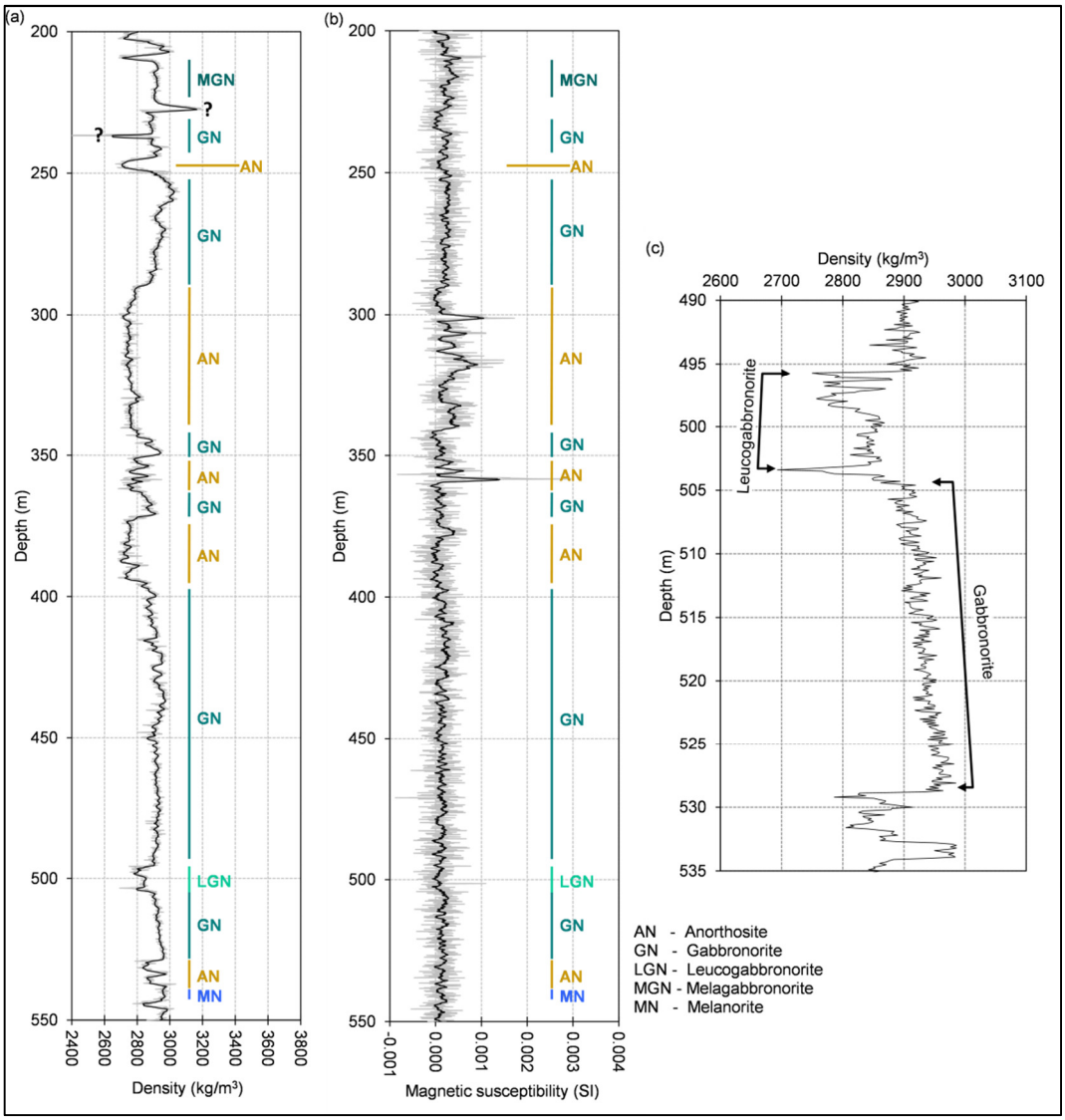


Figure 2.2. Comparison between the (a) density log and (b) magnetic susceptibility log with the corresponding lithology log determined by visual geological logging by a geologist for borehole AP3 from the western lobe. The lithologies all form part of the Main Zone. An 11-point moving average filter was applied to original data (grey) in (a) and (b) for visualisation purposes (dark line). The question marks indicate density anomalies which were not identified as lithological variations on the visually determined geological log; (c) The visually logged lithology defined the depth range for which the physical property (density in this case) was extracted. The median for the selected values was then calculated

An X-Y plot of magnetic susceptibility vs density for the identified lithologies shows large variations in the susceptibility, but better constrained densities (Figure 2.3). The susceptibilities in the Main and Critical Zones are generally very low, as it is mostly composed of norite and gabbronorite which are essentially non-magnetic. For the more

magnetic lithologies such as pegmatite and pyroxenite the susceptibilities ranges are smaller. Misclassification and oversimplification of the lithologies contribute to the large susceptibility and, to a lesser extent, density spreads as does variation in mineral composition, mineral abundances, alteration, etc.

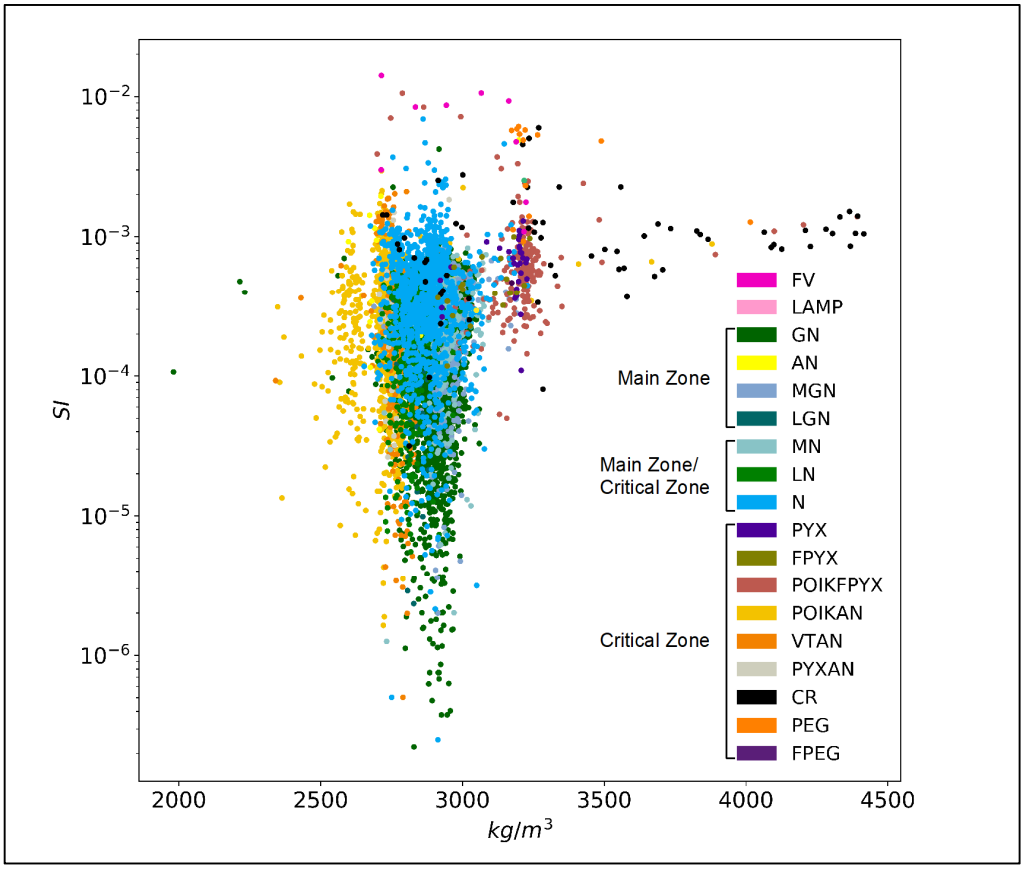


Figure 2.3. Magnetic susceptibility versus density coloured according to lithology for borehole AP3. FV – Feldspar vein; LAMP – Lamprophyre; GN – Gabbronorite; AN – Anorthosite; MGN – Melagabbronorite; LGN – Leucogabbronorite; MN – Melanorite; LN – Leuconorite; N – Norite; PYX – Pyroxenite; FPYX – Feldspathic pyroxenite; POIKFPYX – Poikilitic feldspathic pyroxenite; POIKAN– Poikilitic anorthosite; VTAN – Vari-textured anorthosite; PYXAN – Pyroxene anorthosite; CR – Chromitite; PEG – Pegmatite; FPEG - Feldspathic pegmatite. The plot displays 12 404 data points

The measured densities for a specific lithology in a borehole (e.g. anorthosite in the Main Zone, Figure 2.4; norite in the Critical Zone, Figure 2.5) were combined and plotted on a histogram. In many instances the density distribution is normal (Figure 2.4b, Figure 2.5b), while others are skewed (Figure 2.4f) or even bimodal (Figure 2.5c, e). The median density for each distribution was calculated. If we were to combine the densities of each

lithology from all boreholes and plot a histogram, before calculating the median, this would bias the result towards the borehole with the highest number of density measurements for that specific lithology. The abundance of the lithology in a borehole, and the sampling interval determines the count. A good example of this sampling bias is seen in the different mean density determined in MO1 wireline logging data (n=4471) (Figure 2.4g) and lab measurements (n=10) on the same core (Figure 2.4h).

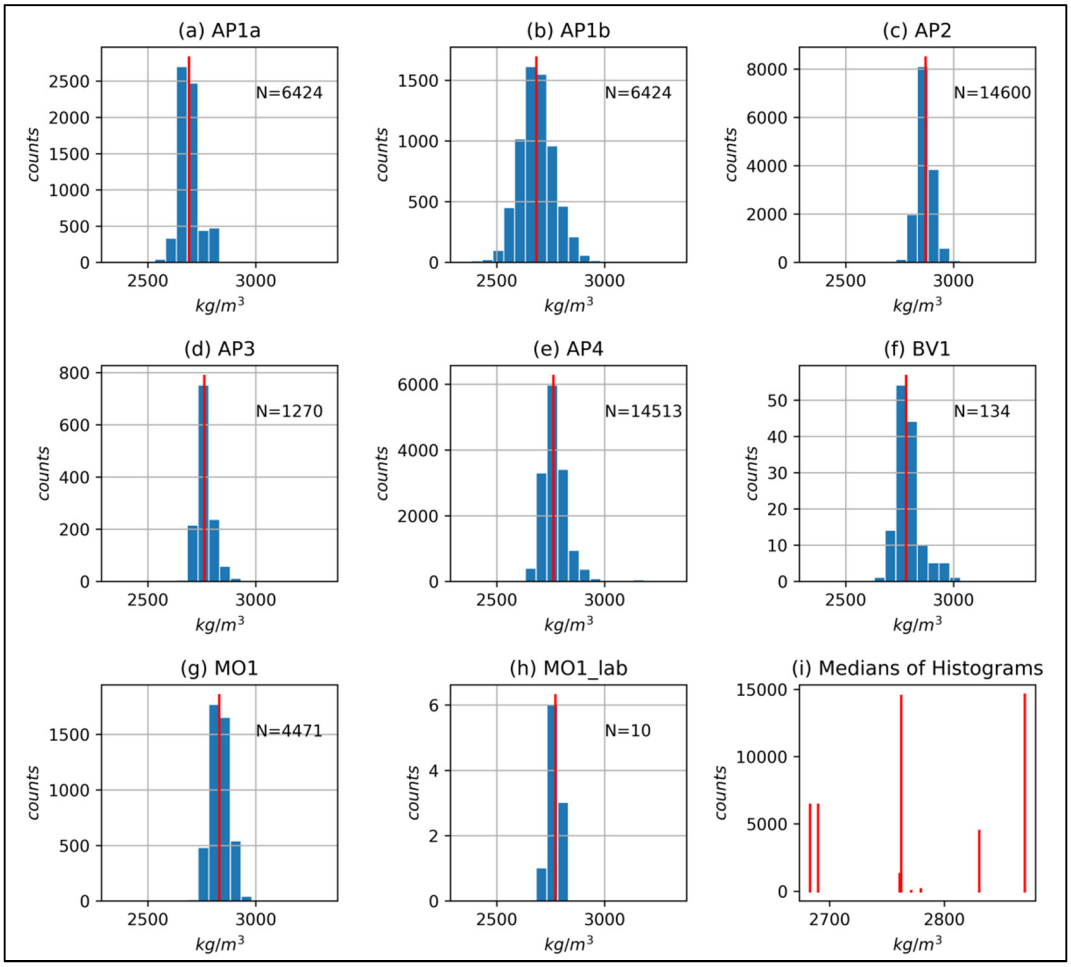


Figure 2.4. (a) to (h) Density distributions for anorthosite in the Main Zone. The red line indicates the median density for anorthosite in the borehole. (i) All the medians in (a) to (h) shown on one graph to illustrate the variability in the calculated medians. The medians are (from left to right) from AP1a, AP1b, AP3, AP4, MO1_lab, BV1, MO1 and AP2

The variations in the medians can result from calibration issues with the wire-line logging instruments, different measuring techniques in the laboratory and wire-line logging settings, or density variations of a within a lithology due to composition of the minerals or proportions in different parts of the BC. The large differences between the densities in

AP1a and AP1b, and the densities in AP2 cast doubt on the latter as they are all located in the north-western BC. Magnetic susceptibility measured in the laboratory are consistently higher than the wireline logging measurements.

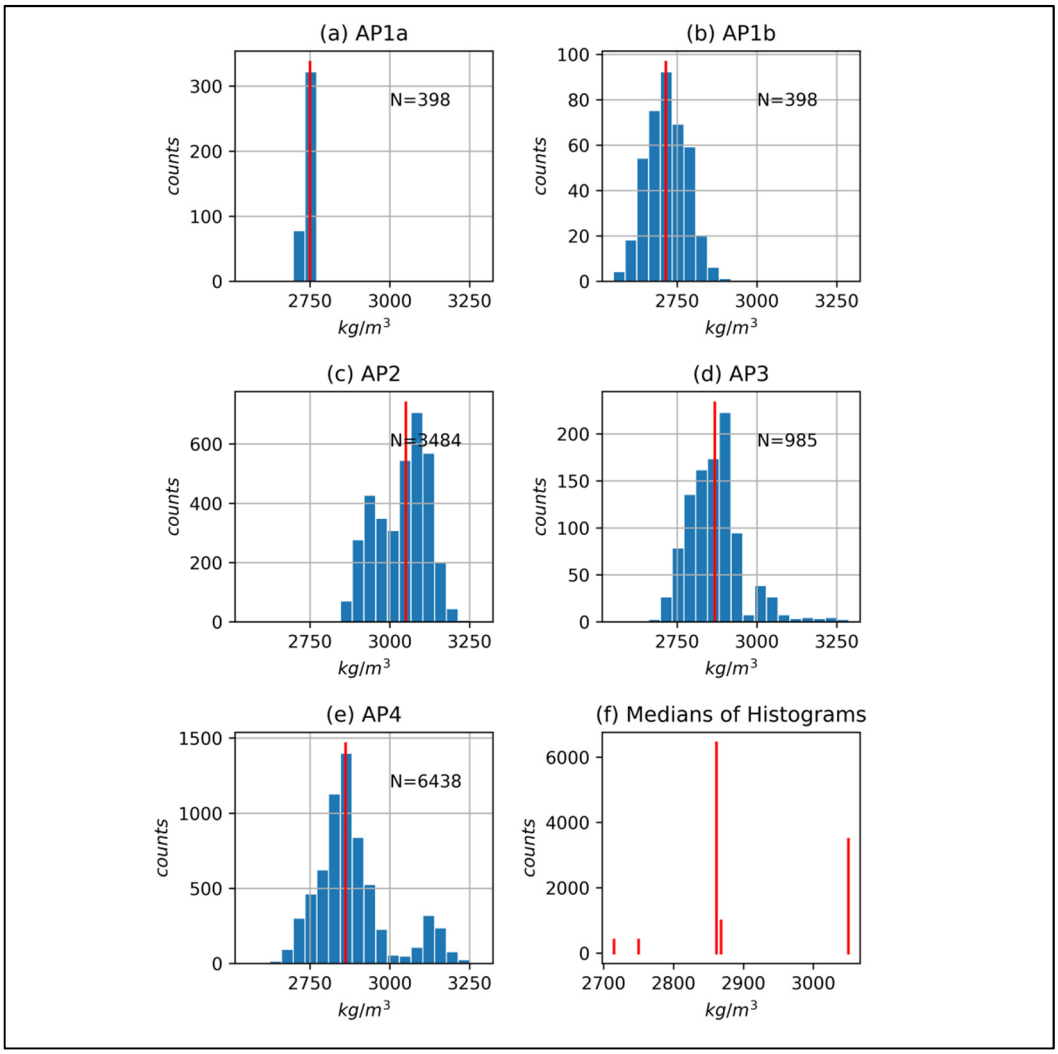


Figure 2.5. (a) to (e) Density distributions for norite in the Critical Zone. The red line indicates the median density for norite in the borehole. (f) All the medians in (a) to (e) shown on one graph to illustrate the variability in the calculated medians. The medians are (from left to right) from AP1b, AP1a, AP4, AP3, AP2. BV1, MO-1, RUS1, RUS1A, FF1-85 and AP5 do not contain CZ

For the MO1 hole and core, both wireline logging and laboratory measurements were available, thus allowing for direct comparison between results from the different types of measurement. The borehole logging data acquired a measurement every 1 cm, but the core measurement intervals generally ranged from 1 to 10 m, and a few higher than 40

m. The average interval is roughly 9 m (Maré and Loots, 2007). Unfortunately, there is a degree of uncertainty in the depths of the laboratory core measurements due to a limited number of useable depth-markers within the trays. Many of the markers were made of wood and deteriorated over the years. Furthermore, some of the core was lost, and possibly incorrectly replaced during transfer from wooden to metal trays (Roelofse, 2012).

The wire-line and laboratory densities for MO1 correlate relatively well (Figure 2.6a, b) although the difference in sampling interval and the noise in the wire-line logging data make the comparison difficult. Magnetic susceptibilities measured in the laboratory are substantially higher than the wire-line logging measurements (Figure 2.6c, d), especially in the upper part of the borehole (Figure 2.6c). Lower down in the borehole wire-line logging susceptibilities for highly magnetic material are higher than for laboratory measurements. There is an apparent depth offset between the two data sets, but it is difficult to determine the exact offset since it is unclear which anomalies to compare (Figure 2.6c).

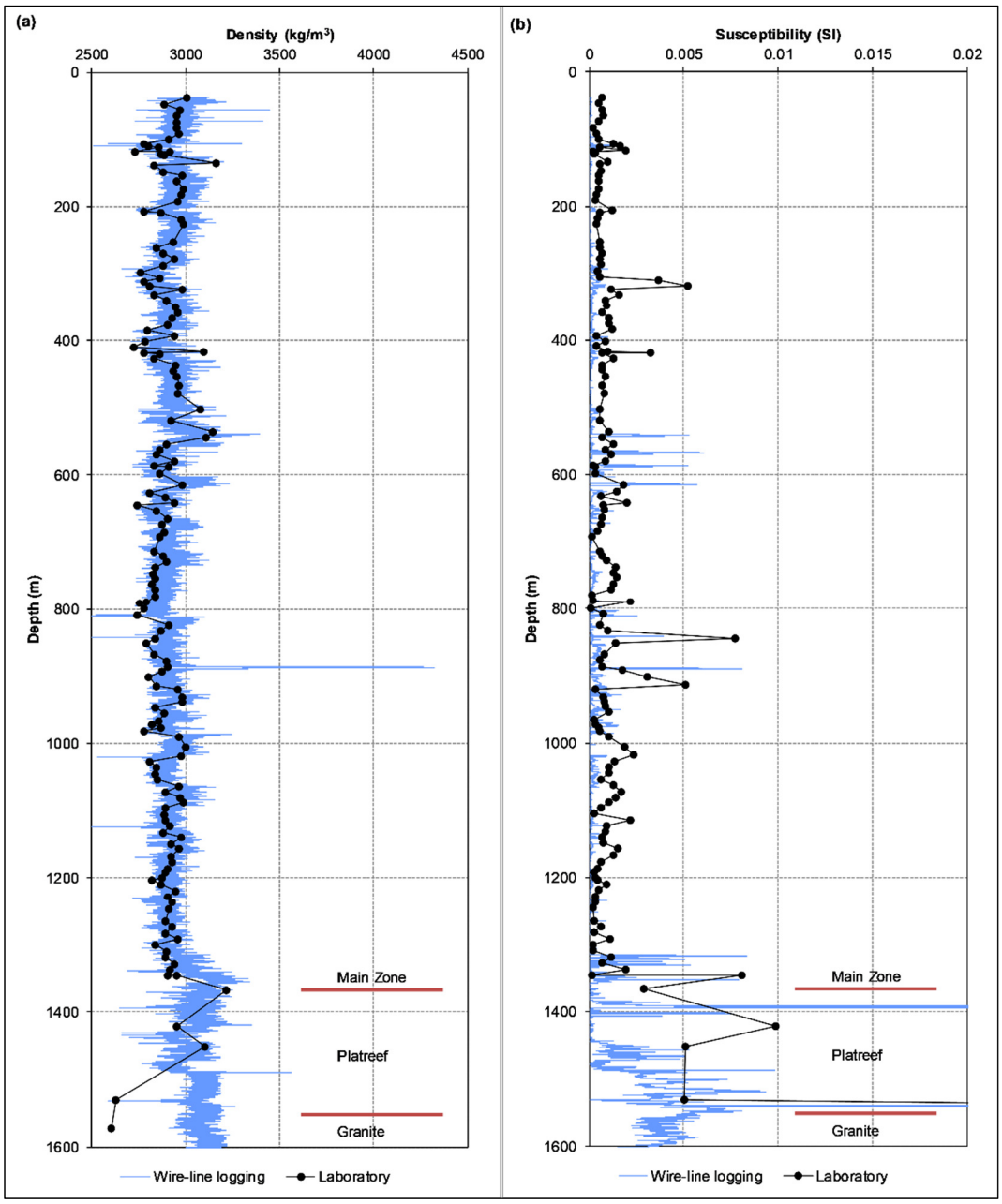


Figure 2.6. Wire-line logging and laboratory measurements of density (a) and magnetic susceptibility (b) measured in the MO1 borehole

2.4.1 Results

Median densities and susceptibilities were calculated for all the lithologies encountered in the boreholes (Table 2.2). The data were supplemented by data from the Council for Geoscience's physical properties database and by magnetic susceptibilities published by Letts et al. (2009). Median absolute deviations (MAD, Table 2.2) show the spread in the

data distribution. For lithologies with only one data sources, e.g. one borehole, the median absolute deviation could not be calculated.

Table 2.2. Median values estimated for lithologies of the RLS encountered in boreholes and published in the Physical Properties database (PPdb) and by Letts et al. (2009). Magnetic susceptibilities were only estimated from laboratory measurements (BV1, MO1_Lab, RUS1, RUS1A, PPdb, Letts et al. 2009)

Zone	Lithology	Density		Magnetic susceptibility		Sources
		Median (kg/m^3)	MAD (kg/m^3)	Median (SI)	MAD (SI)	
Upper	Anorthosite	2894	107	0.06612	0.03313	BV1, RUS1A
	Ferrodiorite	3156		0.130776		BV1
	Olivine gabbro	3248		-		FF1-85
	Leucogabbro	3155		0.321236		BV1
	Gabbronorite	2846	42	0.133313	0.003437	RUS1, RUS1A, PPdb
	Leucogabbronorite			0.001516		BV1
	Magnetite gabbro	3139	29	0.19086	0.021504	BV1, PPdb
	Magnetite	4305		1.376253		BV1
	Pegmatite	2862		0.095375		RUS1A
	Troctolite	3273		-		FF1_85
Main	Anorthosite	2771	59	0.00083	0.000032	AP1a, AP1b, AP2, AP3, AP4, BV1, MO1, MO1_lab, PPdb
	Iron replacement	3134	4			AP1a, AP1b
	Intermediate pegmatoid	3024				AP4
	Leucogabbro	2764	83	0.000662		AP1a, AP1b, AP2, MO1_lab
	Melagabbro	2960	64	0.002757		AP1a, AP1b, AP2, BV1
	Gabbro	2907	53	0.001706	0.000905	AP1a, AP1b, AP2, BV1, PPdb
	Leucogabbronorite	2821	83	0.000662		AP1a, AP1b, AP2, AP3, AP4, MO1_lab
	Melagabbronorite	2830	19			AP1a, AP1b, AP3
	Gabbronorite	2911	37	0.001080	0.00009	AP1a, AP1b, AP2, AP3, AP4, MO1, MO1_lab, PPdb, Letts (mag)
	Leuconorite	2843	9	0.001033	0.000444	AP3, MO1_lab
	Melanorite	2962				AP3
	Norite	2913	13			AP2, AP3, AP4
	Porphyritic gabbronorite	2990				AP2
	Pyroxenite	3054	114	0.006514		BV1, MO1

Zone	Lithology	Density		Magnetic susceptibility		Sources
		Median (kg/m^3)	MAD (kg/m^3)	Median (SI)	MAD (SI)	
	Troctolite	2932		0.006661		BV1
	Ultramafic pegmatoid	3330				AP2
Critical	Anorthosite	2765	36	0.002528		AP2, AP3, AP4,PPdb (grav), Letts (mag)
	Chromitite	3129	72	0.001162		AP1a, AP1b, AP3, AP4,PPdb
	Iron replacement	3274	216			AP1a, AP1b
	Harzburgite	3039	69			AP1a, AP1b
	Leuconorite	2768	21			AP1a, AP1b, AP3, AP4
	Melanorite	2944	65			AP1a, AP1b, AP2, AP3
	Norite	2865	88	0.000441		AP1a, AP1b, AP2, AP3, AP4,PPdb
	Pyroxenite	3140	67			AP1a, AP1b, AP2, AP3, AP4,PPdb
	Ultramafic pegmatoid	3790				AP2
Lower	Feldpsathic orthopyroxenite	3010				AP5/CH7
	Norite	2907		0.000195		PPdb
	Bronzitite	3244				PPdb
Marginal	Calcsilicate	2930				AP5/CH7
	Gabbro	3020				AP5/CH7
	Gabbronorite	2920				AP5/CH7
	Magnetite gabbro	3010				AP5/CH7
	Melanorite	2990				AP5/CH7
	Norite	3054				PPdb
Basal ultramafic Sequence	Dunite	3070				AP5/CH7
	Pyroxenite	3020				AP5/CH7

Regional models of the Bushveld Complex will conceivably not include individual lithologies, but is more likely to model the zones of the RLS as units. We calculated this by considering generalised lithostratigraphic sections for the zones, and determining the percentage each lithology constitutes of the total thickness of the zone. The densities and magnetic susceptibilities of the lithologies in the zone were then weighted by these percentages and summed to give a representative density and magnetic susceptibility for the zone.

Upper Zone

The upper part of the Rustenburg Layered Suite contains some of the densest and most magnetic material in the Bushveld Complex, including many magnetite layers. The BV1 borehole intersected the entire Upper Zone and, since the UZ is similar throughout the BC, the geology from this borehole was used to estimate an average density and magnetic susceptibility for the zone (Table 2.3). Ferrodiorite dominates the top third of the log while anorthosite and magnetite gabbro are prevalent in the lower two thirds. Magnetite layers are present throughout the log. The estimated density is 3135 kg/m^3 and the susceptibility is 0.1849 SI.

Table 2.3. Calculation of the representative density and magnetic susceptibility for the Upper Zone

Lithology	Thickness (m)	% of total thickness	Density (kg/m^3)			Magnetic susceptibility (SI)		
			Median	Min	Max	Median	Min	Max
Ferrodiorite	287	23	3156	3156	3156	0.1308	0.1308	0.1308
Magnetite	25	2	4305	4305	4305	1.3763	1.3763	1.3763
Magnetite gabbro	772	61.8	3139	3110	3168	0.1909	0.1694	0.2124
Anorthosite	162	13	2894	2787	3001	0.0661	0.0330	0.0993
Leucogabbro	3	0.2	3155	3155	3155	0.3212	0.3212	0.3212
Upper Zone	1249		3135	3103	3166	0.1849	0.1673	0.2025

Main Zone

The Main Zone is a thick succession of predominantly gabbronorite for most of the zone, and norite at the base (Cawthorn et al., 2006). Anorthosite and pyroxenite layers are also present throughout the Main Zone and troctolite were observed in the northern lobe (Ashwal et al., 2005). Although it has been subdivided into upper and lower sections based on changes in cumulus minerals (Tegner, Cawthorn and Kruger, 2006) we consider it as a whole in this study. Some of the borehole logs show mostly gabbronorite in the Main Zone while others show gabbro. Gabbro consists of clinopyroxene and plagioclase, and if more than 5% of orthopyroxene is also present, it becomes a gabbronorite. In terms of physical properties, gabbro and gabbronorite have very similar densities, but the leucocratic and melanocratic versions show differences of roughly 130 to 160 kg/m^3. Fortunately in most of the boreholes these variations form only about 10% of the gabbro and gabbronorite. (Table 2.4). Very low susceptibilities characterize all lithologies, but reversed magnetisation is important in this zone (Letts et al., 2009).

Table 2.4. Calculation of the representative density and magnetic susceptibility for the Main Zone

Lithology	Thickness (m)	% of total thickness	Density (kg/m^3)			Magnetic susceptibility (SI)		
			Median	Min	Max	Median	Min	Max
Gabbronorite	2400	75	2911	2874	2948	0.0017	0.0008	0.0026
Anorthosite	150	5	2771	2712	2830	0.0008	0.0008	0.0009
Norite	500	15	2913	2900	2926	0.0002	0.0000	0.0004
Pyroxenite	150	5	3054	2940	3168	0.0065		
Main Zone	3200		2911	2874	2949	0.0017	0.0006	0.0021

Critical Zone

Wireline logging data of the Critical Zone (CZ) only intersect the upper section of the zone, while the physical properties database lists seven densities for pyroxenite, and three each for norite and anorthosite. Detailed descriptions of the Critical Zone and the western (Teigler, Eales and Scoon, 1992) and eastern (Cameron, 1980, 1982) lobes show the Upper Critical Zone (UCZ) to contain mostly norite with interlayered anorthosite, pyroxenite and thin layers of chromitite, and the Lower Critical Zone (LCZ) to consist of pyroxenite with norite and chromitite layers. The total thickness of the chromitite layers in the west is 11 m (Teigler et al., 1992). The representative density for the Critical Zone in the western lobe range between 2852 and 2996 kg/m^3, with a median value of 2924 kg/m^3 (Table 2.5). In the eastern lobe the pyroxenite in the upper CZ is described as orthopyroxenite, and the LCZ as feldspathic orthopyroxenite (Cameron, 1980, 1982). The density for pyroxenite measured by wireline logging was assigned to the pyroxenite in the UCZ, but the density of feldspathic orthopyroxenite measured in AP5/CH7 in the Lower Zone was used for the same rocks in the LCZ (Table 2.6). The overall CZ density in the eastern lobe ranges between 2894 and 2999 kg/m^3. The median is 2946 kg/m^3. Using pyroxenite's density from the UCZ for the LCZ pyroxenites results in a median of 2974 kg/m^3 and ranging from 2907 kg/m^3 to 3041 kg/m^3 (not shown in Table 2.6). As no laboratory susceptibility measurements were available for pyroxenite it was not possible to estimate a representative magnetic susceptibility for the CZ.

Table 2.5. Calculation of the representative density and magnetic susceptibility for the Critical Zone based on the contribution of lithologies observed in the western lobe (Teigler et al., 1992)

Lithology	Thickness (m)	% of total thickness	Density (kg/m^3)			Magnetic susceptibility (SI)		
			Median	Min	Max	Median	Min	Max
Norite	485	64	2865	2785	2945	0.0004	0.0004	0.0004
Anorthosite	80	11	2765	2729	2801	0.0025	0.0025	0.0025
Pyroxenite	180	24	3140	3073	3207			
Chromitite	11	2	3129	3057	3201	0.0012	0.0012	0.0012
Critical Zone	756		2924	2852	2996			

Table 2.6. Calculation of the representative density and magnetic susceptibility for the Critical Zone based on the contribution of lithologies observed in the eastern lobe (Cameron, 1978, 1982)

Lithology	Thickness (m)	% of total thickness	Density (kg/m^3)			Magnetic susceptibility (SI)		
			Median	Min	Max	Median	Min	Max
Norite	635	52	2865	2785	2945	0.0004	0.0004	0.0004
Anorthosite	60	5	2765	2729	2801	0.0025	0.0025	0.0025
Orthopyroxenite	158	13	3140	3073	3207			
Feldspathic orthopyroxenite	265	22	3010	3010	3010			
Interlayered harzburgite, feldspathic orthopyroxenite, orthopyroxenite, dunite	95	8	3091	3091	3091			
Chromitite	5	<1	3129	3057	3201	0.0012	0.0012	0.0012
Critical Zone	1218		2946	2894	2998			

Lower Zone

The Lower Zone in general consists predominantly of harzburgite and orthopyroxenite with dunite in places (Wilson, 2015; Yudovskaya et al., 2013; Cameron, 1978). Analyses on three boreholes in the north-eastern lobe (CH1, CH6, CH7) subdivided the pyroxenite into orthopyroxenite, feldspathic orthopyroxenite and olivine pyroxenite (Wilson, 2015). Orthopyroxenite is the most abundant in the upper part of the Lower Zone, and feldspathic orthopyroxenite increasing in the lower section. Borehole AP5/CH7

intersected only feldspathic orthopyroxenite (3010 kg/m^3) in the lowest part of the Lower Zone. Cameron (1978) divided the lower part of the zone into the basal feldspathic orthopyroxenite and lower orthopyroxenite sections. Three density measurements for Lower Zone orthopyroxenite in the Physical Properties database gave a median value of 3244 kg/m^3. No measurements were available for the harzburgite and dunite that form the central section in the Lower Zone, but in other zones these rocks have densities of 3039 kg/m^3 and 3070 kg/m^3 respectively. To obtain a single representative density of the Lower Zone we combined the SACS (1980) stratigraphy (orthopyroxenite-harzburgite-orthopyroxenite succession with equal thicknesses) with the information from Cameron (1978) and Wilson (2015), namely the presence of dunite in the central section and the subdivision of the lower section (Table 2.7). Magnetic susceptibilities measured in the laboratory were not available for the Lower Zone, but are known to be low (Hattingh, 1991).

Table 2.7. Calculation of the representative density for the Lower Zone

Lithology	Thickness (m)	% of total thickness	Density (kg/m^3)
Upper orthopyroxenite	500	33	3244
Harzburgite dunite, orthopyroxenite	500	33	3055
Lower orthopyroxenite	250	17	3244
Basal subzone: orthopyroxenite	250	17	3010
Lower Zone	1500		3142

Marginal Zone

Only borehole AP5/CH7 intersects the Marginal Zone (Wilson, 2015). Norite and gabbronorite make up most of the Marginal Zone, with some feldspathic orthopyroxenite also present. The geological log provided in Supplement 3 of Wilson (2015) was used to estimate the representative physical properties (Table 2.8). No laboratory measurements of magnetic susceptibilities were available for this zone.

Table 2.8. Calculation of the representative density for the Marginal Zone

Lithology	Thickness (m)	% of total thickness	Density (kg/m^3)
Melanorite	32.5	8	2990
Gabbronorite	211.5	51	2920
Calcsilicate	24.5	6	2930
Gabbro	65	16	3020
Magnetite gabbro	80	19	3010
Marginal Zone	413.5		2959

Basal Ultramafic Sequence

Below the Marginal Zone, AP5/CH7 encountered a 700 m thick ultramafic sequence of dunite and pyroxenite called the Basal Ultramafic Sequence (Wilson, 2015). The feldspathic orthopyroxenite makes up three quarters of the sequence (Table 2.9). As expected, the ultramafic sequence is very dense.

Table 2.9. Calculation of the representative density for the Basal Ultramafic Sequence

Lithology	Thickness (m)	% of total thickness	Density (kg/m^3)
Dunite	178	25	3070
Pyroxenite	520	75	3020
Basal Ultramafic Sequence	698		3033

2.5 Petrography-based physical property estimation

The certainty of physical property estimation with the traditional lithology-based approach depends greatly on the accuracy of the geological information, and the assumption that a lithology has uniform physical properties. The variations in the magnetic susceptibilities measured for anorthosite in borehole AP3 are good examples of the latter (Figure 2.2b), although it must be said that the geological log was not very detailed. The combined petrographic and petrophysical study of the BV1 borehole enabled us to investigate the

impact of modal abundances of rock forming minerals on physical properties and the veracity of the lithological identification.

The petrographic data allowed for the creation of ternary diagrams showing the modal abundances of the constituent minerals. For each sample the observed density was extracted from the density log and the points plotted on the ternary plot according to density (Figure 2.7). For the Upper Zone samples with opaque minerals, pyroxenes (clino (CPX) and ortho (OPX)), plagioclase and olivine were chosen. Inverted pigeonite (InvPig) is a low-calcium version of clinopyroxene and was also combined with the pyroxenes. To create ternary plots the percentages were normalised to 100%. The ternary plot for plagioclase, pyroxene and opaque minerals (Figure 2.7a) show that plagioclase is the most abundant minerals in the Upper Zone, and that the most plagioclase-rich samples have the lowest densities (roughly 2750 – 3000 kg/m^3). As the percentage pyroxene increases the density increases to between approximately 3000 and 3300 kg/m^3. As expected an increase in the percentage of opaque minerals generally corresponds to increasing density. There are some points where these simple correlations do not hold true. For example two samples with densities greater than 4500 kg/m^3 contain 54% and 65% opaque minerals, whereas a few samples with more than 90% opaque minerals only have densities of 3200 kg/m^3. This clearly shows a difference in composition between the opaque minerals, and we can assume that those with the highest densities are most probably magnetite. Including olivine in the ternary plot (Figure 2.7b) resulted in a few more high density samples (> 3750 kg/m^3), where combined pyroxene and olivine constitute 5-25% of the sample.

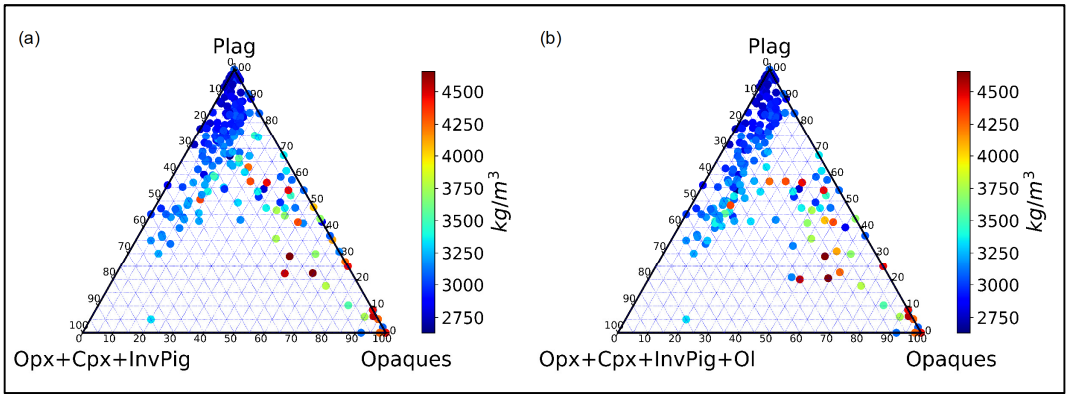


Figure 2.7. Observed densities for samples with petrographic analysis from the Upper Zone in the BV1 borehole. (a) Samples with plagioclase (Plag), ortho (OPX)- and clinopyroxene (CPX) (and inverted pigeonite (InvPig) and opaques. (b) Samples with plagioclase, ortho- and clinopyroxene (and inverted pigeonite), olivine and opaques.

Samples from the Main Zone show the correlation between plagioclase, ortho- and clinopyroxene (including inverted pigeonite) abundance and density (Figure 2.8a). Since opaque minerals are not prevalent in the Main Zone, they were excluded from the ternary plots. Similar to the Upper Zone (Figure 2.7a) plagioclase is the most abundant mineral. Orthopyroxene is considerably more prevalent than clinopyroxene, and increasing orthopyroxene generally correlates with increasing density. This may provide information about the mineral composition of the orthopyroxene. Olivine is not prevalent in the Main Zone, but combining all the pyroxenes shows a clear increase in density with pyroxene content.

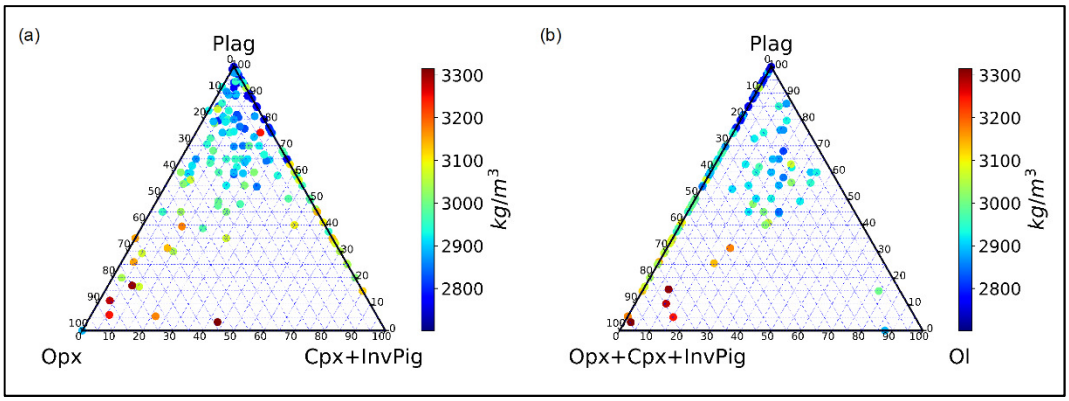


Figure 2.8. Observed densities for samples with petrographic analysis from the Main Zone in borehole BV1. (a) Samples with plagioclase, orthopyroxene and clinopyroxene and inverted pigeonite. (b) Samples with plagioclase, ortho- and clinopyroxene (and inverted pigeonite), and olivine

Because we know the modal abundances of the minerals forming the lithologies it is possible to calculate the expected published densities for the minerals (Table 2.10). The densities will depend on the exact mineral composition but for now, the average values were used. The ternary plots show density increasing gradually with increasing quantities of pyroxene in both zones, and opaque minerals in the Upper Zone (Figure 2.9). The observed densities do not increase quite as gradually but show similar trends (Figure 2.7, Figure 2.8).

Table 2.10. Published densities for minerals in the Main and Upper Zones

Mineral	Density (kg/m^3)	Source
Plagioclase (pure)	2670	Cawthorn and Spies (2003)
Orthopyroxene (pure)	3280	Cawthorn and Spies (2003)
Clinopyroxene (augite)	3392	Winchell (1961)
Pigeonite	3499	Winchell (1961)
Magnetite	5120 (4900-5200)	Telford et al. (1976: 28)
Ilmenite	4670 (4300-5000)	Telford et al. (1976: 28)
Titanium	3181	Temple (1966)

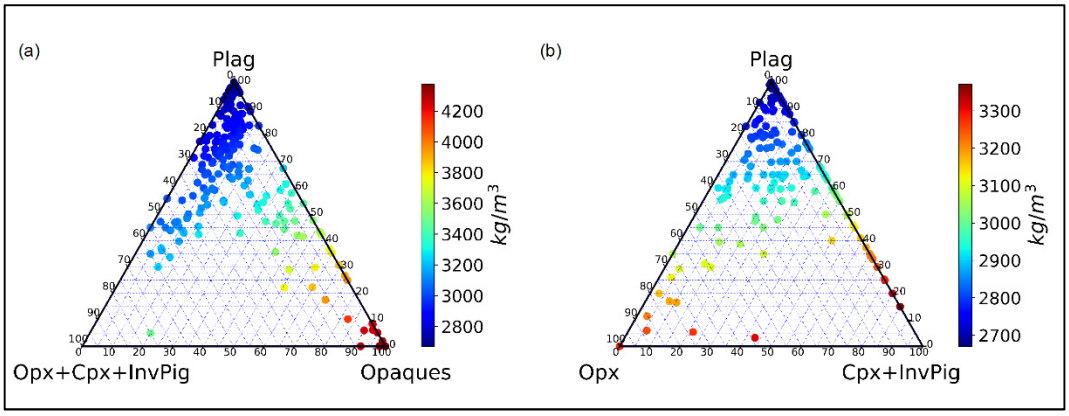


Figure 2.9. Densities calculated for samples with petrographic analysis from the (a) Upper and (b) Main Zones in borehole BV1. Densities were calculated from the modal abundances and published densities for the minerals (Table 2.10)

2.6 Discussion and conclusions

The progression of physical property representation (Figure 2.10) provides increasing information about the distribution of densities within a specific lithology. Traditionally the density range for a specific lithology is shown (Figure 2.10a). This provided very limited information about the lithology itself. The range is often large and could discourage people from using physical properties. Histograms provide more information in that it visually shows where most of the densities occur. For example, the histogram clearly shows that most of the densities fall between 2750 kg/m^3 and 3500 kg/m^3 (Figure 2.10b). In the traditional plot the range stretches from 2750 kg/m^3 to 4450 kg/m^3 without indication of which densities are more prevalent, although the median gives an idea of the

most common density. Having petrographic data available dramatically changes how we use petrophysical data. It can be used as an analytical tool giving information about the composition of rocks (Figure 2.10c). Where densities or susceptibilities are not consistent with the observed abundance of minerals, other factors can be considered, e.g. alteration and metamorphism. Even if only a limited number of petrographic analyses exist for a data set, it can form the basis of interpreting physical properties for the remainder of the data set without petrographic information. If very high resolution gravity or magnetic data are available over an area, having combined petrographic analyses and petrophysical properties will allow a modeller to model not only simple lithologies, but changes in mineral composition of a lithology. This can be useful when modelling changes due to mineralisation, metamorphism, alteration etc. Resulting geophysical models will add more to understanding the geological setting than lithology-based models already do.

The lack of petrographic data limits the ability to do such a detailed analysis of petrophysical properties. This was the case for most of the data in the Bushveld Complex available to this study, and for that reason the traditional approach was followed. The median densities derived for the zones in the RLS are adequate for regional potential field modelling.

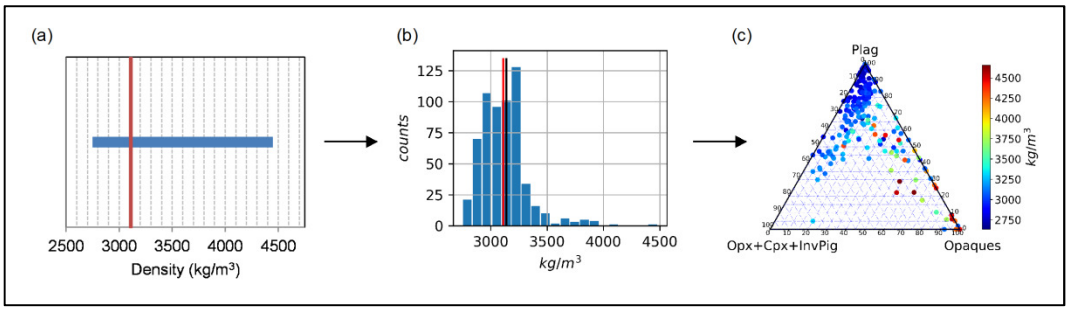


Figure 2.10. Progression in representation of densities. (a) Traditional approach showing the range of values for magnetite gabbro in BV1 in blue and the median value in red; (b) Histogram representation of the same data; (c) Ternary plot of modal abundance for petrographically analysed samples in the Upper Zone

2.7 Acknowledgements

Anglo Platinum for the wireline logging data. Prof L W Ashwal from the University of the Witwatersrand for the petrographic data.

CHAPTER 3 THE IMPORTANCE OF 3D MODELLING AND TAKING CRUSTAL THICKNESS INTO ACCOUNT

This chapter was published as a paper in the Journal of African Earth Sciences (2014, 92, pp. 97-118). I was invited to submit this paper after presentation of my work at the Annual Fall meeting of the American Geophysical Union in San Francisco in 2012. The manuscript was constructed by me with editing by my co-authors.

Cole – 80% (conducted the research and constructed the manuscript)

Webb – 15% (reviewed the manuscript and suggested improvements)

Finn - 5% (reviewed the manuscript and suggested improvements)

Gravity models of the Bushveld Complex - have we come full circle?

Janine Cole

Geophysics Unit, Council for Geoscience, Private Bag X112, Pretoria, 0001, South Africa
School of Geosciences, University of the Witwatersrand, Private Bag 3, WITS, 2050, South Africa
email: jcole@geoscience.org.za

Susan J. Webb

School of Geosciences, University of the Witwatersrand, Private Bag 3, WITS, 2050, South Africa
email: susan.webb@wits.ac.za

Carol A. Finn

US Geological Survey, Denver, Colorado 80225, USA
email: cfinn@usgs.gov

3.1 Abstract

Gravity models reveal the 3-D extent of the mafic component of the Bushveld Complex, critical for understanding the origin of the world's largest layered mafic intrusion and largest source of platinum-group elements (PGEs). New density information, broadband seismic data, borehole data and geological discoveries have improved the constraints on the gravity modelling. Furthermore, all of the models published up to now have been done in two or 2.5 dimensions which is not well suited to modelling the complex geometry of the Bushveld intrusion. Constrained three dimensional modelling takes into account effects of variations in geometry and geophysical properties of lithologies, providing better fits to the shape and amplitude of calculated fields. Gravity data reveal subsurface density contrasts to great depths and the significant density contrast between the mafic rocks of the Bushveld Complex and the surrounding granites and sediments, as well as contrasts across the crust-mantle boundary, make gravity modelling ideal for constraining the 3D geometry of the Bushveld Complex.

The aim of this paper is to demonstrate the effect of the new constraints and use of full three dimensional modelling on gravity models of the Bushveld intrusion. We remodel previously published models using full three dimensional potential field modelling software to test the existing conceptual models in an equally conceptual way. Including the measured thicker crust underneath the Bushveld Complex necessitates the presence of dense material in the central area between the eastern and western lobes. The simplest way to achieve this is to model the Rustenburg Layered Suite as a single connected intrusion. This is similar to the first geometries suggested for the Bushveld Complex. In addition to these findings, variations in the lower crust and mantle densities also contribute to models of this scale and have to be considered.

Keywords: Bushveld Complex; gravity modelling; seismic receiver function

3.2 Introduction

The Bushveld Complex is a large layered igneous intrusion located in the northern part of South Africa (Figure 3.1). It was discovered in the late 19th century and was first described in detail in 1901 (Molengraaff, 1901). The discovery of the host rocks of the major platinum deposits in 1924 (Cawthorn, 2006), moved the Bushveld Complex from being an interesting geological phenomenon to an economic resource of immense importance. During these earlier years the mafic rocks of the Bushveld Complex were considered to be a continuous intrusion that stretched all the way from the far western lobe to the eastern lobe, a distance of approximately 450 km (Figure 3.2) (Hall, 1932).

Gravity modelling has been widely used in constraining the geometry and emplacement of layered mafic intrusions around the world (Deemer and Hurich, 1997; Gupta and Sutcliffe, 1990; Karinen, 2010; Loncarevic et al., 1990). Regional gravity data collection by the then South African Geological Survey started in the 1930s and in 1958 were published on the 1:1 000 000 geological map (Geological Survey of South Africa, 1958). The mapped lobes of the Bushveld Complex were associated with prominent gravity highs while the area between the western and eastern lobes was characterised by gravity values equivalent to the background levels outside of the Bushveld Complex. The first two published gravity models of the whole Bushveld Complex (Cousins, 1959; Du Plessis and Kleywegt, 1987; Meyer and De Beer, 1987) explained the highs as two separate bodies of dense mafic material, disconnected in the middle (Figure 3.3(a) and (b)). Both of these models only considered the distribution of dense material in the upper crust. In the third class of gravity model (Cawthorn et al., 1998; Cawthorn and Webb, 2001; Webb et al., 2004), the Bushveld Complex is modelled as a continuous sheet if isostatic compensation at the crust-mantle boundary is taken into account (Figure 3.3(c)). Subsequent results from the Southern African Seismic Experiment (SASE) showing the

crust to be 5 – 6 km thicker underneath the Bushveld Complex than under the surrounding areas (Nguuri et al., 2001)) were used to refine the connected Bushveld model (Webb et al., 2004).

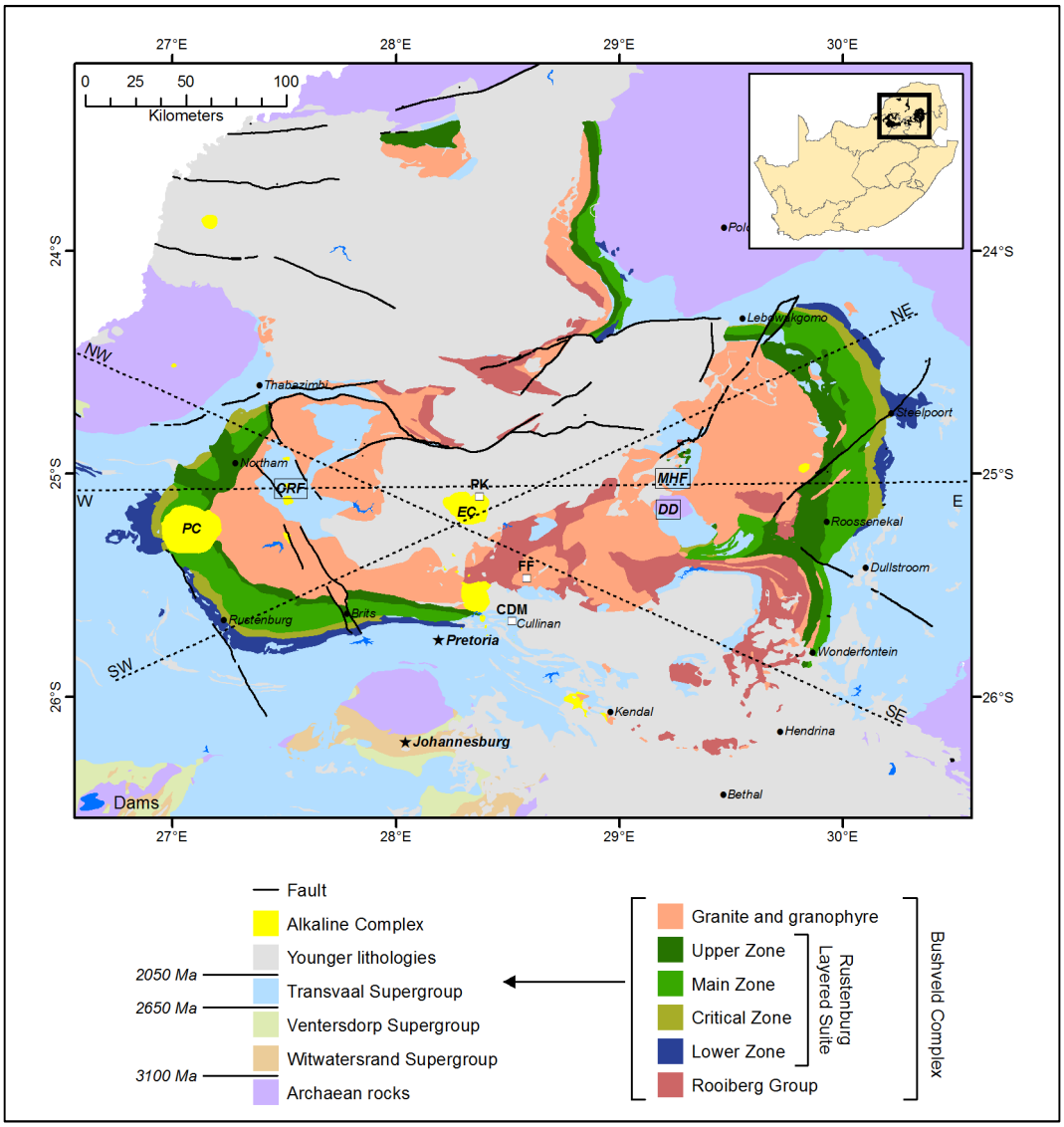


Figure 3.1 Simplified geological map of the Bushveld Complex. CRF – Crocodile River Fragment; DD – Dennilton Dome; MHF – Marble Hall Fragment; EC – Elandskraal Complex; PK – Palmietgat Kimberlite; FF – Fairfield borehole; CDM – Cullinan Diamond Mine.

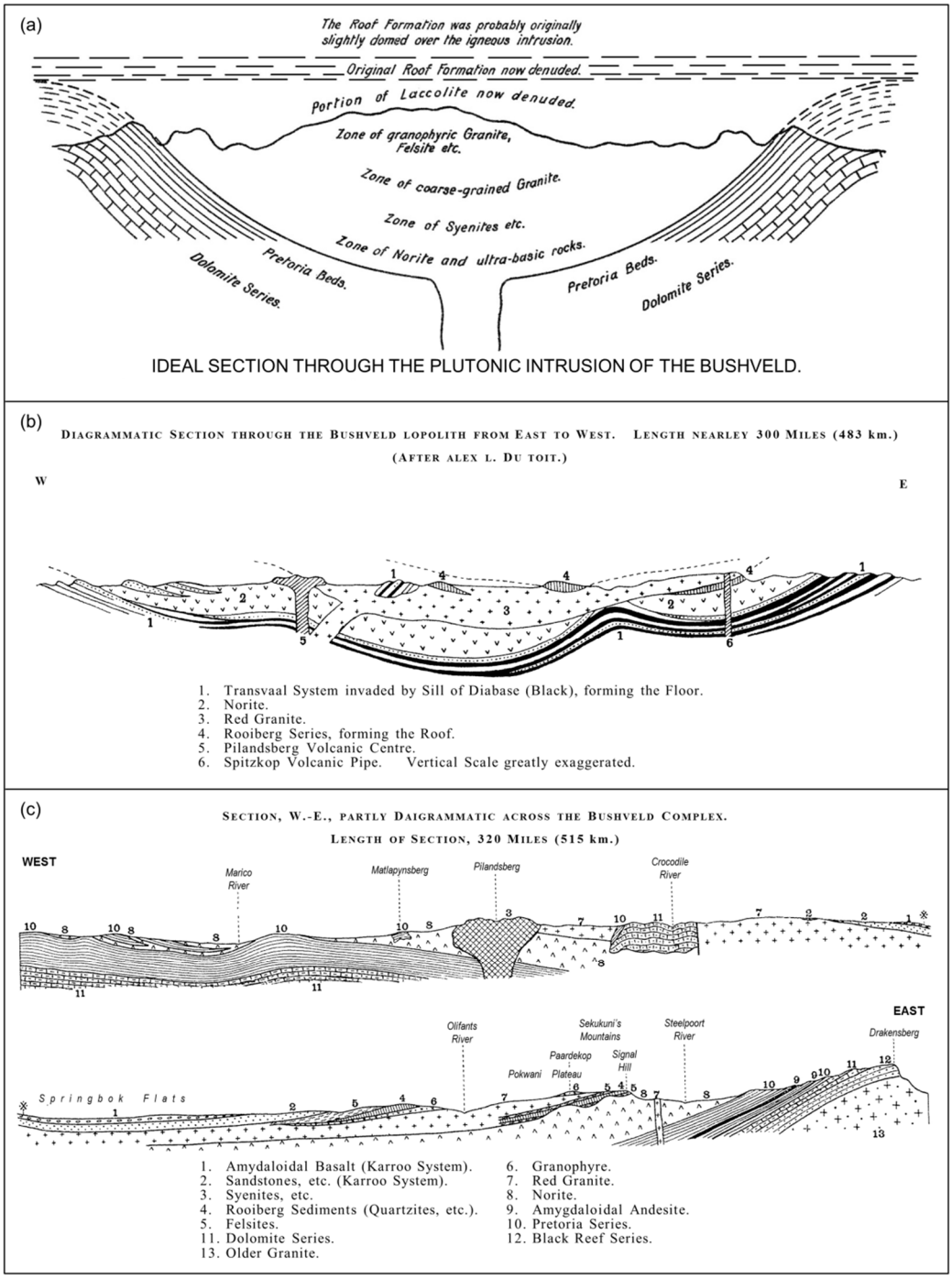


Figure 3.2 Historic conceptual models of the Bushveld Igneous Complex proposed by (a) G.A.F Molengraaff, (b) A.L. du Toit and (c) A.L. Hall (from Hall, 1932).

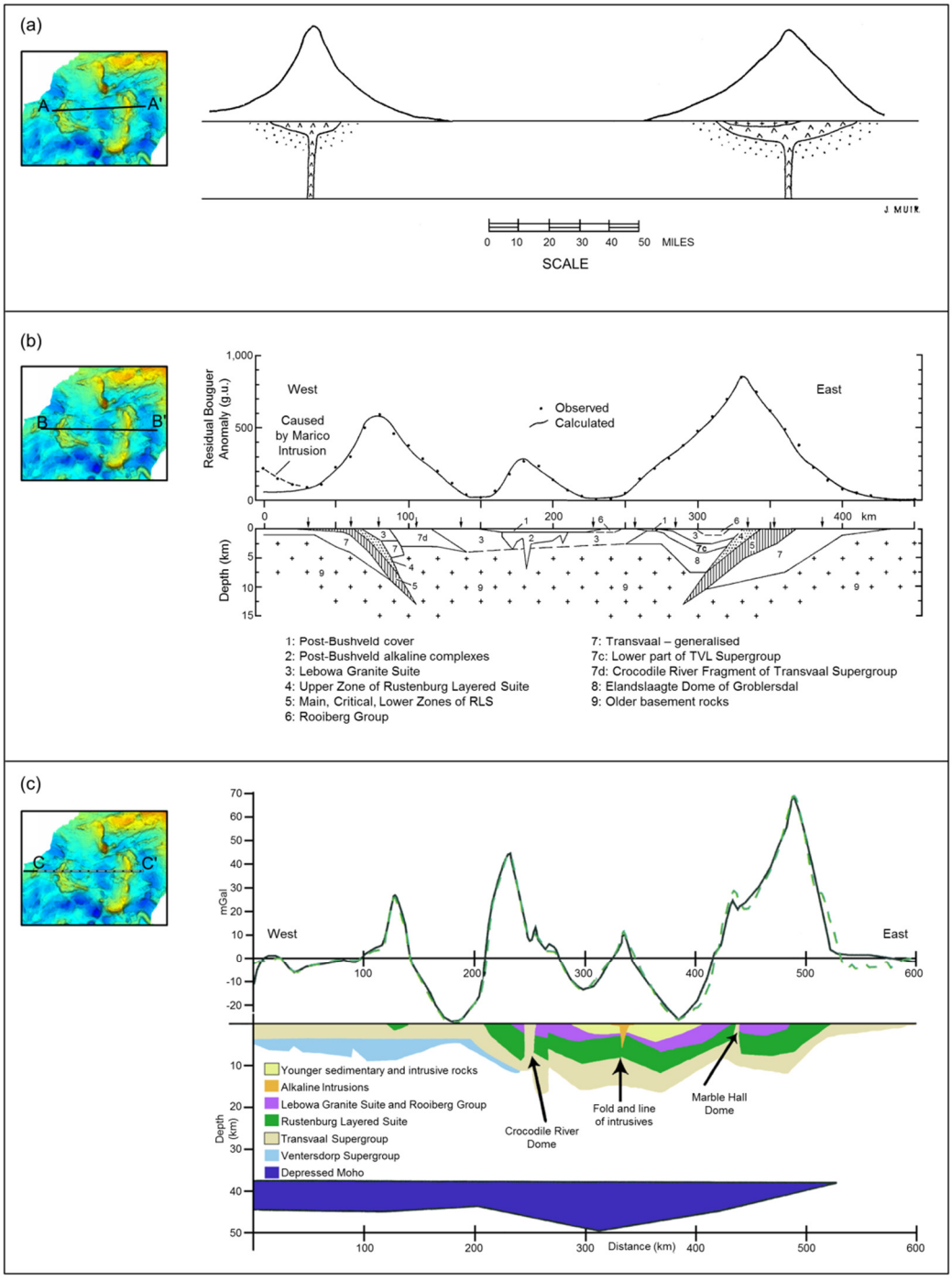


Figure 3.3 Two dimensional gravity models through the centre of the Bushveld Complex in a west-east direction. The position of each profile is shown overlain on the Bouguer Anomaly data next to each model. (a) Model of Cousins (1959). Dotted area – TVL Supergroup; ^ ^ - Bushveld Group; + + - Granite; (b) Dipping sheet gravity model of Meyer and De Beer (1987). (Reprinted by permission from Macmillan Publishers Ltd: NATURE, Meyer, R. and De Beer, J.H. (1987), © 1987); (c) Connected Bushveld model (Webb et al., 2004).

Many of the emplacement mechanisms for the mafic component of the Bushveld Complex that have been published since Cousins' (1959) gravity model consider the mafic rocks to be absent in the central part of the Bushveld Complex. These mechanisms include intrusion of a horizontal sill into a gently folded basin (Von Gruenewaldt, 1976), multiple feeders for various magma chambers located on a cone fracture that developed above a mantle diapir (Sharpe, Bahat and Von Gruenewaldt, 1981), and vertical feeders from the edges of a mantle diapir that penetrated into the crust, resulting in separate lobes (Hatton and Schweitzer, 1995). In an emplacement model where the mafic rocks intruded along a regional unconformity in the Transvaal Supergroup (Cheney and Twist, 1991), a gravity model showing the lobes of the Bushveld Complex as dipping sheets (Du Plessis and Kleywegt, 1987) was mentioned as proof that the mafic rocks of the Bushveld Complex are absent in the centre. The interconnected Bushveld model (Webb et al., 2004) suggests a sill-like structure for the mafic rocks (eg. Clarke et al., 2009; Kruger, 2005).

The few published gravity models have been deemed important in substantiating various emplacement models. Unfortunately all of these models were created in two or 2.5 dimensions along profiles crossing the Bushveld Complex in an east-west direction. However, the gravity field along a profile is not only influenced by density variations directly underneath the profile, but by variations in an area around the profile. Although 2.5 dimensional (2.5D) modelling seeks to address this issue by allowing adjustments of strike length, it is still not as accurate as creating a full three dimensional (3D) model that takes into account contributions to the gravity field from all directions. This is especially true in the case of the Bushveld Complex, where the geometry is complex and the density variations are relatively large. Additionally information about the crustal thickness beneath the Bushveld Complex and density values from drill core and samples were not available when the first two gravity models were published, and it is important to study the effect of this new knowledge on the older models.

The objectives are to extend the existing 2.5D gravity models into very simple 3D models and include the Moho, and see how it affects the calculated gravity field and our understanding of the Bushveld Complex geometry.

2. Geological Overview

The Bushveld Complex is a layered igneous complex that intruded volcano-sedimentary sequences of the Transvaal Supergroup. The northern lobe transgresses onto Archaean granite-gneisses. The preserved outcrop is estimated to cover an area of more than 65 000 km^2 (Cawthorn et al., 2006).

The Bushveld Complex comprises an earlier mafic phase, known as the Rustenburg Layered Suite, and a later granitic phase consisting of granite and granophyre. The Rustenburg Layered Suite was emplaced between 2059 and 2061 Ma (Buick, Maas and Gibson, 2001). It is generally divided into five zones based on changes in composition (Cawthorn et al., 2006) (Figure 3.1). The Upper Zone consists of gabbronorites and anorthosites with cumulus Fe-rich pyroxenes and olivine, magnetite and apatite also present (Cawthorn et al., 2006). The most conspicuous features of this zone are numerous magnetitite layers which occur in four groups consisting of up to seven layers each (Eales and Cawthorn, 1995) which contain vanadium (Cawthorn et al., 2006).

The Main Zone is a thick succession of norite and gabbronorite (Cawthorn et al., 2006). The Critical Zone comprising repeated layers of chromitite, pyroxenite, norite and anorthosite, contains vast resources of chromitite and platinum group elements (Cawthorn et al., 2006). The Lower Zone is composed of pyroxenite and harzburgite.

3.3 Gravity Data

During the last few decades of the twentieth century, gravity data were collected over the whole of South Africa (Council for Geoscience, 1997), with 19,214 gravity measurement points in the 260,000 km^2 Bushveld Complex (Figure 3.4), amounting to one measurement roughly every 14 km^2. Even though the coverage is regional in nature, it still provides useful information with regards to the distribution of lithological units and is ideal for this large scale investigation of the Bushveld Complex.

Measurements were carried out with LaCoste and Romberg gravimeters and elevations determined using micro-barometers. Bouguer anomaly values were calculated assuming a mean density of 2670 kg/m^3. The measurements were tied to the International Gravity Standardisation Net values (Morelli et al., 1974) and referred to the gravity formula based on the 1980 geodetic reference system (Moritz, 1992). The maximum error in the Bouguer anomaly value was estimated to be within 2 mgal (Stettler et al., 2000). This includes a reading accuracy of 0.1 mgal, positional inaccuracies of up to 100 m that adds an error of 0.05 mgal, elevation errors of up to 5 m and the cumulative influence of inaccurate base stations.

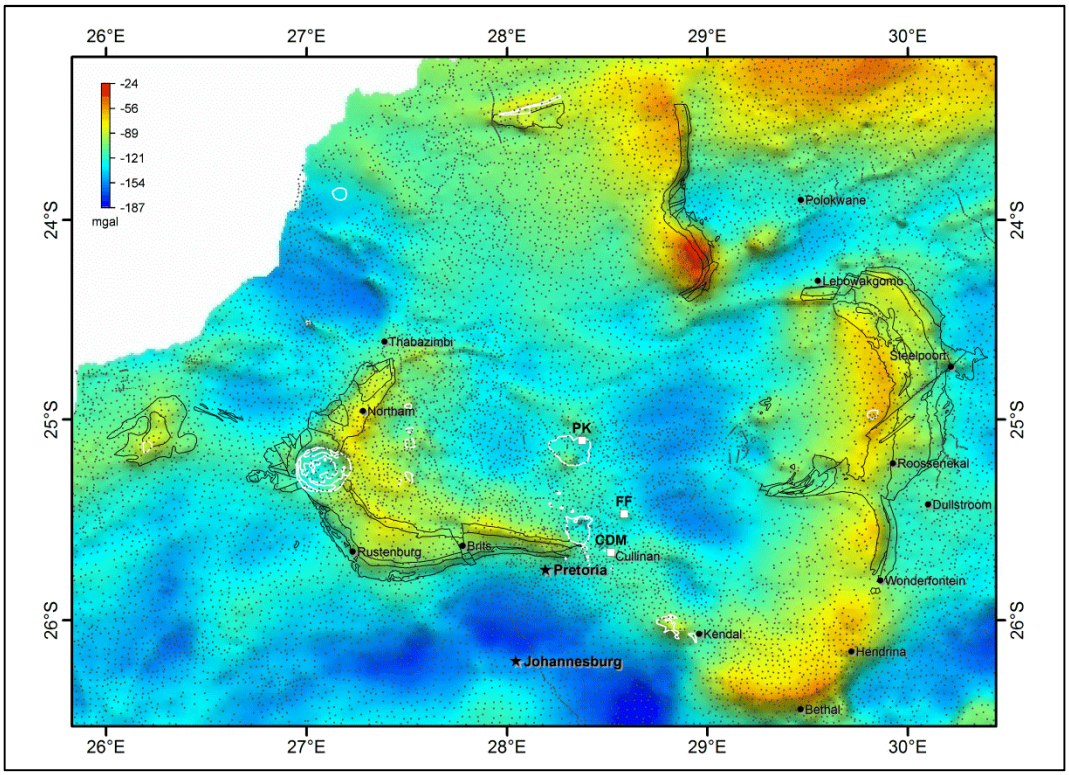


Figure 3.4 Bouguer anomaly map of the Bushveld area. The outlines of the Rustenburg Layered Suite as they appear on the 1:250 000 geological maps are indicated in black and alkaline complexes are outlined in white. Grey points represent the gravity measuring point

3.4 Model Constraints

Since the publication of the first models, more information that puts constraints on the model has become available. These include crustal thickness estimates from a broadband seismograph deployment across Southern Africa, physical property measurements of Bushveld Complex and surrounding rocks and the detection of Bushveld Complex rocks in boreholes in areas where older models precluded the presence of the layered intrusion. Each of these will be discussed in more detail.

3.4.1 Crustal Thickness Data

Crustal thicknesses derived from the topography (Figure 3.5(a)) assuming Airy-Heiskanen isostatic compensation shows a thick crust around the Bushveld Complex and 3 – 5 km thinner crust underneath it (Figure 3.5(b)). The calculation was done using 'LithoFLEX' software (Braitenberg et al., 2007) with a reference crustal thickness of 38 km and a 400 kg/m^3 density contrast across the Moho. Flexural rigidity was not taken into account.

In contrast receiver functions from the Southern African Seismic Experiment (Figure 3.5(c)) showed the crust underneath the Bushveld Complex to be 44 - 48 km thick, compared to an average crustal thickness of 38 km under undisturbed Kaapvaal Craton in Southern Africa (Nguuri et al., 2001; Nair et al., 2006; Kgaswane et al., 2009, 2012). Nguuri et al. (2001), Nair et al., (2006) and Kgaswane et al. (2009) used different processing approaches and number of teleseismic events (Table 3.1) and achieved different results (Figure 3.5(d),(f) and (h)). Kgaswane et al. (2012) refined their results for the Bushveld Complex area and it is these refined crustal thicknesses that are shown in Figure 3.5(h).

Table 3.1 Number of teleseismic events used in the crustal thickness models

Station	Nguuri et al. (2001)	Nair et al. (2006)	Kgaswane et al. (2009)
sa45	30	26	13
sa46	30	34	8
sa47	20	25	13
sa48	10	10	10
sa49	5	9	5
sa51	31	27	9
sa53	4	4	5

Crustal thickness variations underneath and around the Bushveld Complex will directly impact the gravity field and the resulting gravity model. All of the receiver function models show increased crustal thickness in the centre of the Bushveld Complex and to the west of the northern lobe. In the newest model (Kgaswane et al., 2012) the crust is 3-5 km thinner relative to the previous models, but Kgaswane et al. (2012) reported an uncertainty ~2-3 km in the estimated depths. Combined with uncertainties of 3 km by Nair et al. (2006) for their results, we can say with certainty that the crust underneath the central Bushveld Complex is roughly 6 to 10 km thicker than for the surrounding undisturbed Kaapvaal Craton. Significantly different depths were determined for station ‘sa49’ located immediately to the east of the eastern lobe outcrop (Figure 3.5(d), (f) and (h)). Nguuri et al (2001) and Kgaswane et al. (2012) show a thickness of 38 km, whereas Nair et al. (2006) give a depth of 52 km. At this station phase conversions from primary to secondary waves were very weak (Nair et al., 2006) and a low number of teleseismic events were recorded (Table 1) resulting in great uncertainty in estimated depths for all three models. Whereas Nguuri et al. (2001) attributed low phase conversion amplitudes underneath the Bushveld Complex to disturbance of the Moho by the intrusion of the Bushveld Complex, Nair et al. (2006) suggested that the smaller amplitudes may be due to less coherent stacking of events that originated from a deeper Moho.

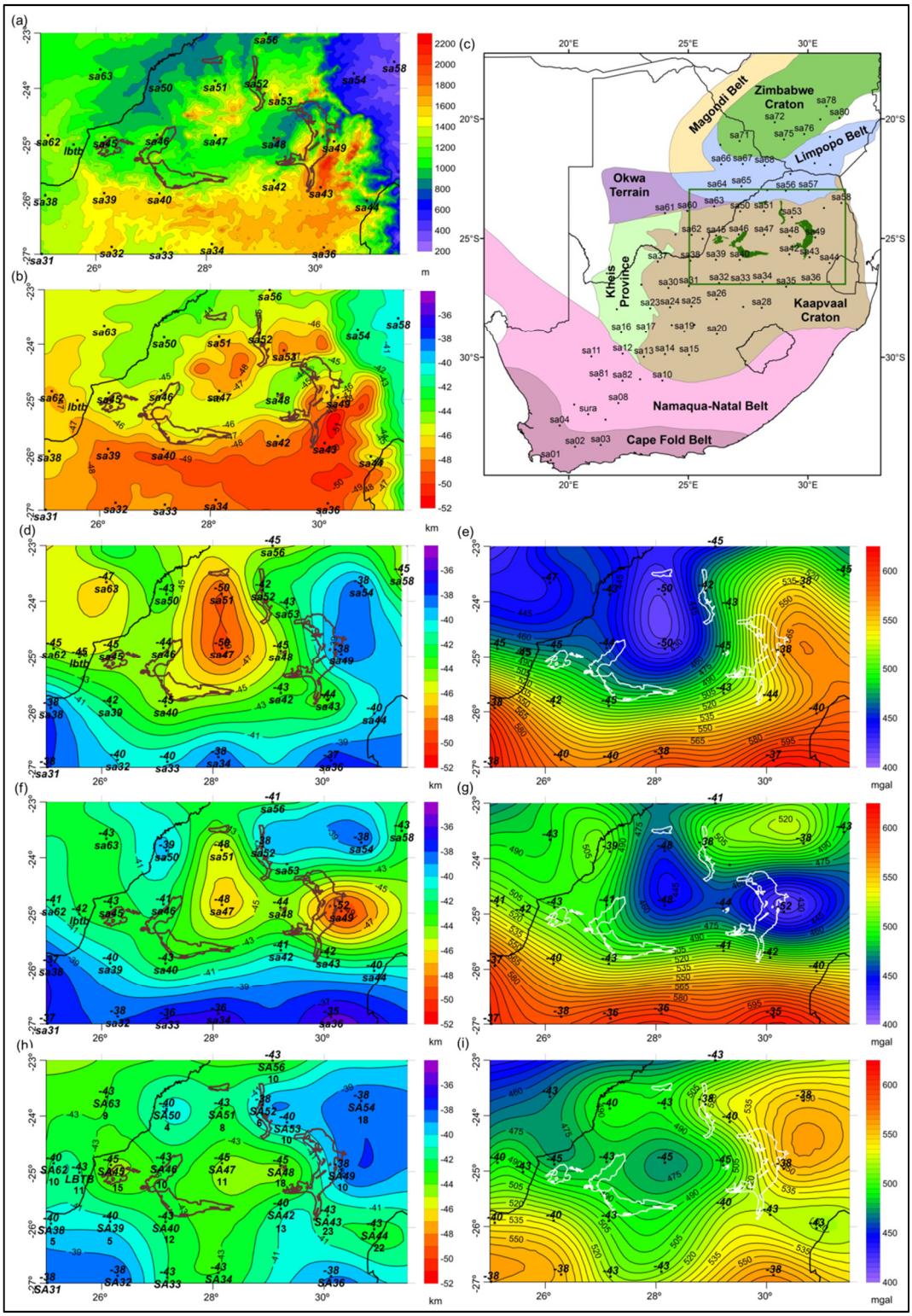


Figure 3.5 (a) Topography of the Bushveld Complex area; (b) Crustal thickness estimated from the topography using Airy-Heiskanen isostatic compensation (reference crustal thickness = 38 km, density contrast across the Moho = 400 kg/m^3; (c) SASE stations overlain on Precambrian terrains for Southern Africa (adapted from Kgaswane et al., 2009). The Bushveld Complex is indicated and the green box outlines the area shown in (a), (b) and (d) to (h). ; (d) Crustal thicknesses (Nguuri et al., 2001) for the area around the Bushveld

Complex; (e) Gravity field calculated for the Moho model of Nguuri et al (2001); (f) Crustal thicknesses (Nair et al., 2006) for the area around the Bushveld Complex; (g) Gravity field calculated for the Moho model of Nair et al (2006); (h) Crustal thicknesses (Kgaswane et al., 2012) for the area around the Bushveld Complex. The value below the station number is the thickness of the layer with Vs≥4.0 km/s; (i) Gravity field calculated for the Moho model of Kgaswane et al (2012). Black dots indicate the localities of seismic stations with the thickness at each station indicated in km. In (a), (b), (d), (f) and (h) the station number is shown below the black dot. In (e), (g) and (i) estimated crustal thicknesses are shown above the black dot. The outline of the Rustenburg Layered Suite is shown in all images.

The differences in the Moho models derived from the receiver functions have a significant effect on the calculated gravity fields, as illustrated in Figure 3.5(e), (g) and (i) where the constant density mantle was extended to a depth of 65 km and the gravity field calculated. The field east of the Bushveld Complex differs by 120 to 135 mgal between the three models. Considering that the gravity anomalies associated with the Rustenburg Layered Suite are in the order of 60 to 80 mgal, it is clear that the selection of a crustal thickness model will heavily impact on the geometry of the final three dimensional potential field model. It also places extra doubt on the previous models that did not include crustal thicknesses.

3.4.2 Physical Properties

Physical property measurements, and more specifically density measurements, have become more readily available as more exploration and research have been done on the Bushveld Complex. Published density values (eg. Hall, 1932; Hattingh, 1980) and density measurements conducted by staff of the Petrophysical Laboratory of the Council for Geoscience have been collated in a 'Density Atlas' (Maré, 2011). Detailed measurements of a borehole core located in the northern lobe provided a valuable database of densities for the Upper Zone and part of the Main Zone (Ashwal, Webb and Knoper, 2005). Densities measured down a number of boreholes using wire-line logging were also made available to this study. The methods for determining densities in the laboratory and using wire line logging are based on different principles. In the laboratory, density is measured as a function of a sample's mass and volume, whereas with wire-line logging density is measured as a function of gamma-ray scattering. In high density environments, measurements from detectors located 15 cm above the radioactive source is normally used to determine the density in a bore hole. Varying sample sizes are normally measured in the laboratory. Before data sets from the various sources could be combined, they had to be related to each other. Fortunately, one of the boreholes was logged geophysically using wire-line logging techniques, and later physical properties of

the core itself were measured in the laboratory. This provided an ideal opportunity to establish a relationship between wire-line and laboratory data sets. Differences were observed between densities measured in the two environments for the same lithologies. For these coincident lithologies, the average difference was determined between wire-line logging densities and laboratory measurements reported by Ashwal et al. (2005) for which the measurements and geological log were deemed very reliable (Table 3.2) The average difference was then used to calibrate the wire-line logging densities to the laboratory measurements by shifting the whole wire-line logging density data set by this amount.

3.4.3 Bushveld Complex Occurrences

Occurrences of the Rustenburg Layered Suite in areas precluded by the dipping sheet model strengthen the case for the connected-lobes concept. Mafic rocks of the Bushveld Complex have been encountered in a few boreholes in areas covered by sediments and granites of the Bushveld Complex. A borehole drilled on the farm Fairfield (FF in Figure 3.1 and Figure 3.4) intersected olivine gabbro at a depth of 587 m below the surface and ended at 917 m still in gabbro (Figure 3.6(a)) (Moen, 1989; Walraven, 1987). The gabbro is magnetite rich and exhibit Upper Zone characteristics such as an initial Sr^{87}/Sr^{86} ratio that is similar to that of the Upper Zone (Walraven, 1987). Approximately 22 km to the south-south-west of this borehole, rocks from the upper part of the Critical Zone occur in a borehole drilled at the Cullinan Diamond Mine (Cawthorn and McKenna, 2006) (CDM in Figure 3.1 and Figure 3.4). A 260 m thick succession of norite and pyroxenite was encountered 530 m below the surface and a metamorphic aureole was observed in the floor rocks (Pretoria Group Sediments) suggesting the absence of Lower Zone in this area (Figure 3.6(b)).

Xenoliths comprising chromite-bearing feldspathic pyroxenites were found at the Palmietgat Kimberlite (Webb, Ashwal and Cawthorn, 2011), located in the central part of the Bushveld Complex (PK in Figure 3.1 and Figure 3.4). Careful analyses of the xenoliths indicate lithologies similar to the upper part of the Critical Zone (Webb, Ashwal and Cawthorn, 2011).

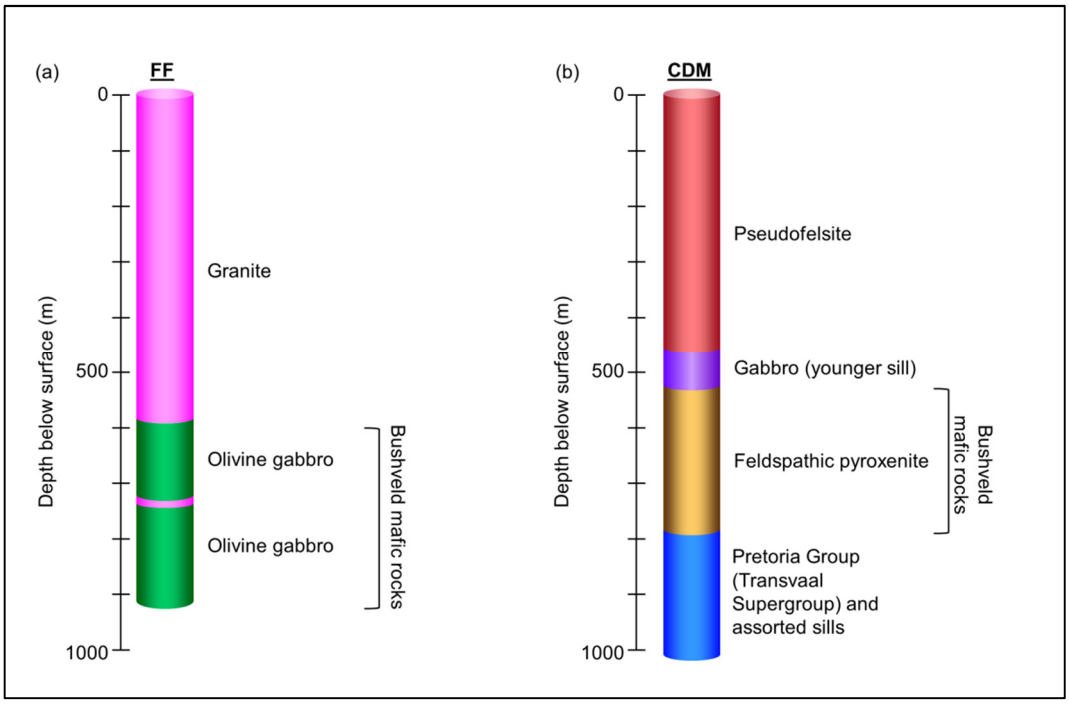


Figure 3.6 Borehole logs for (a) FF drilled on the farm Fairfield FF1-85 (Walraven, 1987; Moen, 1989) and (b) CDM located at the Cullinan Diamond Mine (Cawthorn and McKenna, 2006). The localities of the boreholes are indicated in Figure 3.1 and Figure 3.4

Table 3.2 Densities for the Bushveld Complex and surrounding lithologies. The last column shows average densities for the zones in the RLS

	Lithostratigraphy	Lithology	Physical Properties Atlas[a]			BV-1 Borehole[b]			Wireline logging[c]	
			Number of samples	Mean Density (kg/m³)	σ (kg/m³)	Number of samples	Mean Density (kg/m³)	σ (kg/m³)	Density (kg/m³)	Average density (kg/m³)
	Alkaline Complexes	Syenite, Nepheline syenite	21	2624	78					
		Unspecified lava	3	2740	147					
Bushveld Igneous Complex	Lebowa Granite Suite	Granite	9	2622	17	119	2636	68		
	Rashoop Granophyre	Granophyre	5	2617	35					
	RLS: Upper Zone	Magnetite gabbro	4	3098	108	605	3118	205		3110
		Magnetite	1	4481		27	4227	339		
		Ferrodiorite				177	3186	206		
		Leucogabbro				2	3528	374		
		Anorthosite				129	2807	71		
	RLS: Main Zone	Gabbronorite	45	2940	50				2943	2920
		Norite-Anorthosite	4	2985	166					
		Anorthosite				134	2790	58	2801	
		Gabbro				744	2935	80	2938	
		Melanogabbro				62	3070	95	2991	
		Pyroxenite				20	3159	136		
		Troctolite				100	2938	56		
	RLS: Critical Zone	Norite-Anorthosite	3	2970	394					3090
		Chromitite	12	3261	621				3729	
		Pyroxenite (chromitite-rich)	6	3338	200				3816	
		Leuconorite							2831	
		Norite							2937	
	RLS: Lower Zone	Bronzitite	3	3196	132					3196

	RLS: Marginal Zone	Norite	2	3054	100	3054
	Rooiberg Group	Felsite	2	2677	31	
TVL Supergroup	Pretoria Group	Quartzite,shale,lava	37	2720	110	
	Chuniespoort Group	Dolomite, chert, shale, BIF	23	2820	270	
Ventersdorp Supergroup	Klipriviersberg Group	Lava	3	2833	11	

[a] Maré (2011)
[b] Ashwal et al. (2005)
[c] Anglo American Platinum Limited

3.5 Model Reassessment

The first step in reassessing the existing models was to recreate the published models in 2.5D modelling software and ensuring that the calculated gravity fields were the same as those published. Only after this step could the further complexities such as 3D calculations and new crustal thickness knowledge be incorporated in the models.

3.5.1 2.5D vs 3D Gravity Modelling

Since the first gravity model (Cousins, 1959), continuous advances have been made in modelling software and algorithms for modelling in three dimensions (3D) have become more accessible. To illustrate the importance of modelling complex geometries in 3D, the gravity responses of a progressively more complex model were calculated using a 2.5D modelling algorithm (Talwani, Worzel and Landisman, 1959) and a 3D algorithm ('gbox' from Blakely, 1996:377). The first model contains only one rectangular source and as expected, the 2.5D and 3D gravity responses are exactly the same (Figure 3.7(a)). Adding an east-west striking section to the north causes a bigger difference between the 2.5D and 3D modelling results (Figure 3.7(b)). The maximum amplitude of the 3D calculation is 0.19 mgal higher, ~7%, than for the 2.5D calculation. In the final model (Figure 3.7(c)) a south-eastward dipping body was added 800 m to the south of profile AB. It cuts through the original body and is 200 kg/m^3 denser than the original body. There is a big difference between the calculated fields that reaches a maximum of 0.68 mgal, ~25%, north of the second body. These simple examples illustrate that simple 2.5D models are not adequate when creating a more complex and geologically reasonable model.

Intrusion of separate sill-like mafic bodies (Cousins, 1959)

In the first published gravity model of the Bushveld Complex, highs over the outcrops of mafic rocks in the eastern and western lobes were modelled as "sill-like bodies" with deep dyke-like fissures representing feeders to the sills (Cousins, 1959, Figure 3.3(a)). The gravity low over the covered region between the outcrops, combined with the presence of the Crocodile River and Marble Hall Fragments and the Dennilton Dome (referred to as the Moos River Fragment in Figure 3.1) towards the centre of the western and eastern lobes lead to the conclusion that the mafic rocks of the Bushveld Complex were not present in the central part of the intrusive complex (Cousins, 1959). It is unclear whether the outcropping floor rocks are the result of folding, doming or diapirism. More recently diapirism was proposed to have taken place in the northeast of the Bushveld Complex by Uken and Watkeys (1997).

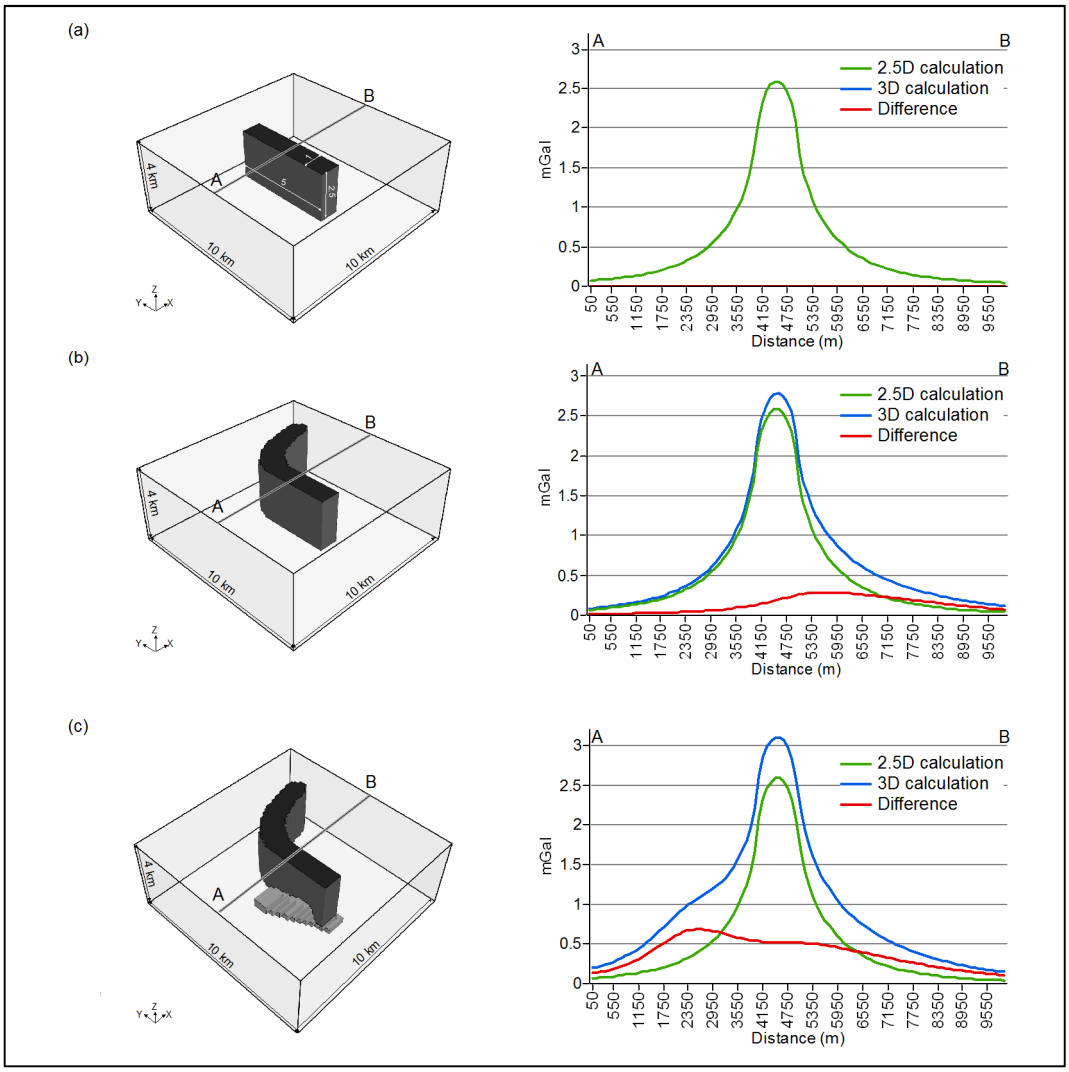


Figure 3.7 Comparison between gravity fields calculated along a profile using 2.5D and 3D modelling for progressively more complex models. Indicated body dimensions are in kilometres. (a) North-south striking body with a density of 2750 kg/m^3. The body extends 2.5 km either side of the profile; (b) Similar to body in (a) but northern extension curves to the east. The body starts to curve at roughly 1.7 km north of the profile and at its northeastern end is 2.4 km north of the profile. (c) Body in (b) cut by a southeast dipping body with a density of 2950 kg/m^3. At its shallowest (300 m) it is located 800 m to the south of the profile. At its deepest (3.6 km) it is located 2 km to the south of the profile

In order to recreate this early model (Cousins, 1959), the profile location was georeferenced and digitised and data were extracted along this profile from the Bouguer Anomaly data set. Densities of the bodies in the model were not specified (Cousins, 1959), and these had to be estimated based on current knowledge and a process of trial and error. 2.5D bodies were extended 120 km perpendicular to the profile and densities of 2900 kg/m^3 for the mafic rocks of the Bushveld Complex, 2680 kg/m^3 for the Bushveld

Complex granite and 2750 kg/m^3 for the Transvaal Supergroup rocks were used. These parameters reproduced the major features of the published model of Cousins (1959) (Figure 3.8(a)).

The 2.5D model was then extended into three dimensions (Figure 3.8(b) and (c)) by following the curvature of the gravity anomalies at the surface but keeping the depth information from the 2D model (Cousins, 1959). The feeder dyke was extended to follow the curvature of the modelled lobes. The gravity highs over the eastern lobe is much broader in the case of the 3D model (Figure 3.8(b)) than for the 2.5D model (Figure 3.8(a)), and the amplitude of the calculated field over this lobe is 20 to 40 mgal larger. These differences can be explained by the dense material to the side of the profile, properly taken into account by 3D modelling. The large increase in the gravity values over the eastern lobe may be related to deeper-seated density variations eg. an uneven Moho that Cousins (1959) did not include in his model. Since this model is not considered valid any longer, and essentially evolved into the dipping sheets model it will not be included in further discussions.

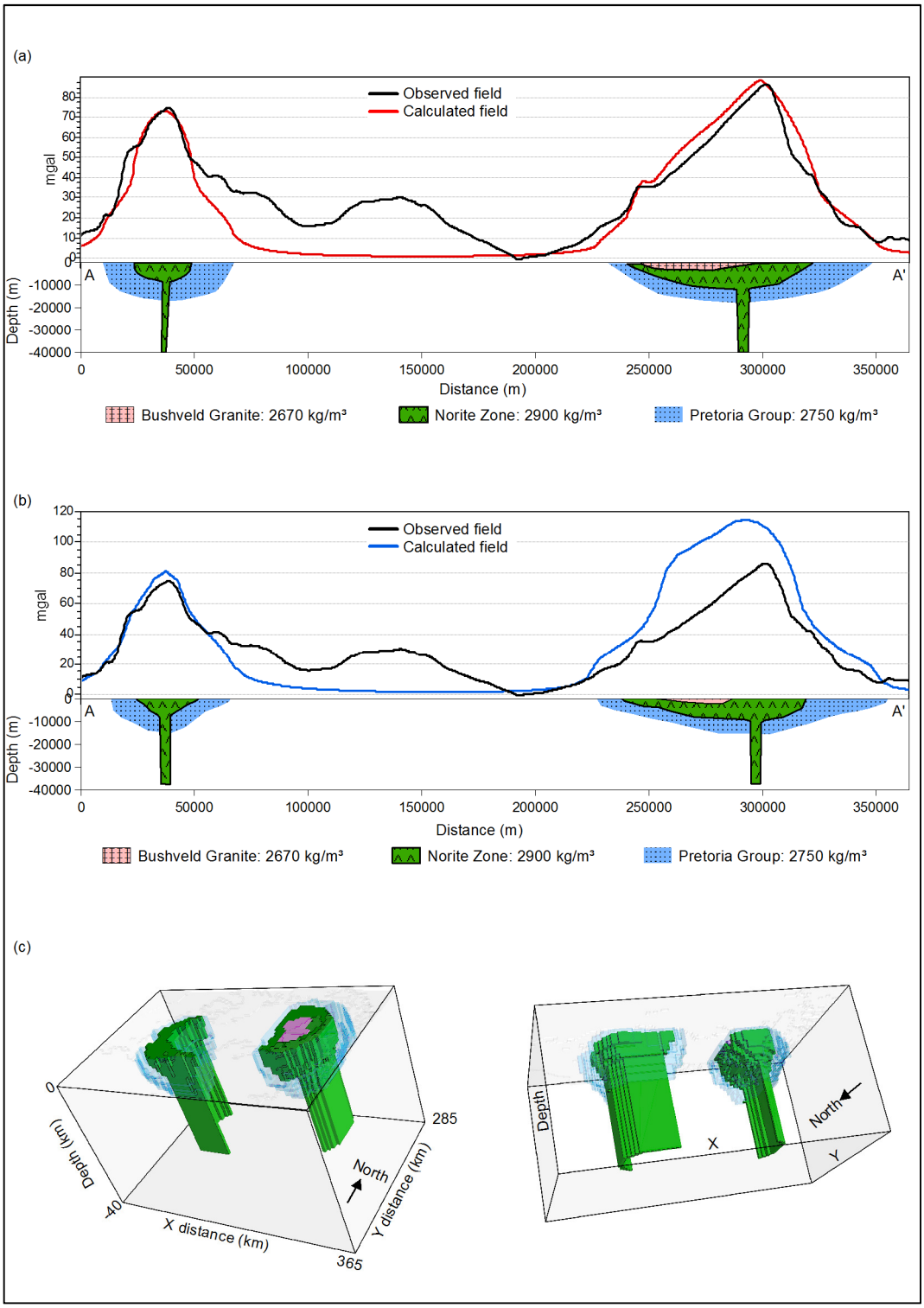


Figure 3.8(a) Recreation of Cousins' (1959) model in 2.5 dimensions along the profile shown in Figure 3(a); (b) Model and calculated gravity field extracted from the three dimensional model and field along Cousins' profile; (c) Perspective views of the three dimensional model (vertical axis exaggerated)

Dipping sheets model (Du Plessis and Kleywegt, 1987; Meyer and De Beer, 1987)

For many years the separated sill model (Cousins,1959) was the only geophysical model published. As magnetic and more gravity data became available, a few two dimensional models appeared in the literature (Hattingh, 1980; Molyneux and Klinkert, 1978). These models also used a trough shape, but without the vertical dyke-like feeders. Two very similar models were published in 1987, one based on gravity data (Du Plessis and Kleywegt, 1987), and the other derived from electrical resistivity work but also incorporating a gravity model (Meyer and De Beer, 1987). In both of these models, the eastern and western lobes are sheets dipping towards the centre of the Bushveld Complex (Figure 3.3(b)).

Du Plessis and Kleywegt (1987) modelled the mafic rocks as a shallow dipping sheet that simply extends down-dip from the surface geology. It thins downwards and the dip steepens with increasing depth until it becomes a vertical dyke-like feeder. In the resulting gravity model, the mafic rocks cut across different levels in the Transvaal Supergroup stratigraphy and reach depths of approximately 9 km in the western lobe and 12 km in the eastern lobe and separated by ~100 km in the centre. Another dipping sheet model showed an alternative relation between the Bushveld Complex rocks and lithologies it intruded into based on deep electrical resistivity measurements (Meyer and De Beer, 1987). In this model, the acid phase of the Bushveld Complex overlies mafic rocks of the Bushveld Complex only locally close to the shallowest parts of the lobes. Moving toward the centre of the Bushveld Complex, the granites of the Bushveld Complex are in contact with the Transvaal Supergroup, and in the central part of the Bushveld Complex, corresponding to the lowest gravity values, it is directly underlain by Archaean granites. These dipping sheets reach down to 12.5 km.

Because Meyer and De Beer (1987) provided a complete profile crossing the Bushveld Complex from west to east, their model was used as the basis for the dipping sheet models. We recreated their 2.5D model by estimating the densities that they assigned to the bodies, and the regional they subtracted from the data. The observed gravity data used in this study contain more detail than the data shown in Meyer and De Beer (1987) (Figure 3.3(b)), and the gravity values over the western lobe is roughly 10 mgal higher than on the published model (Figure 3.9(a)). The discrepancy can be attributed to inaccuracies in digitising the profile from the publication, and newer data used in our modelling.

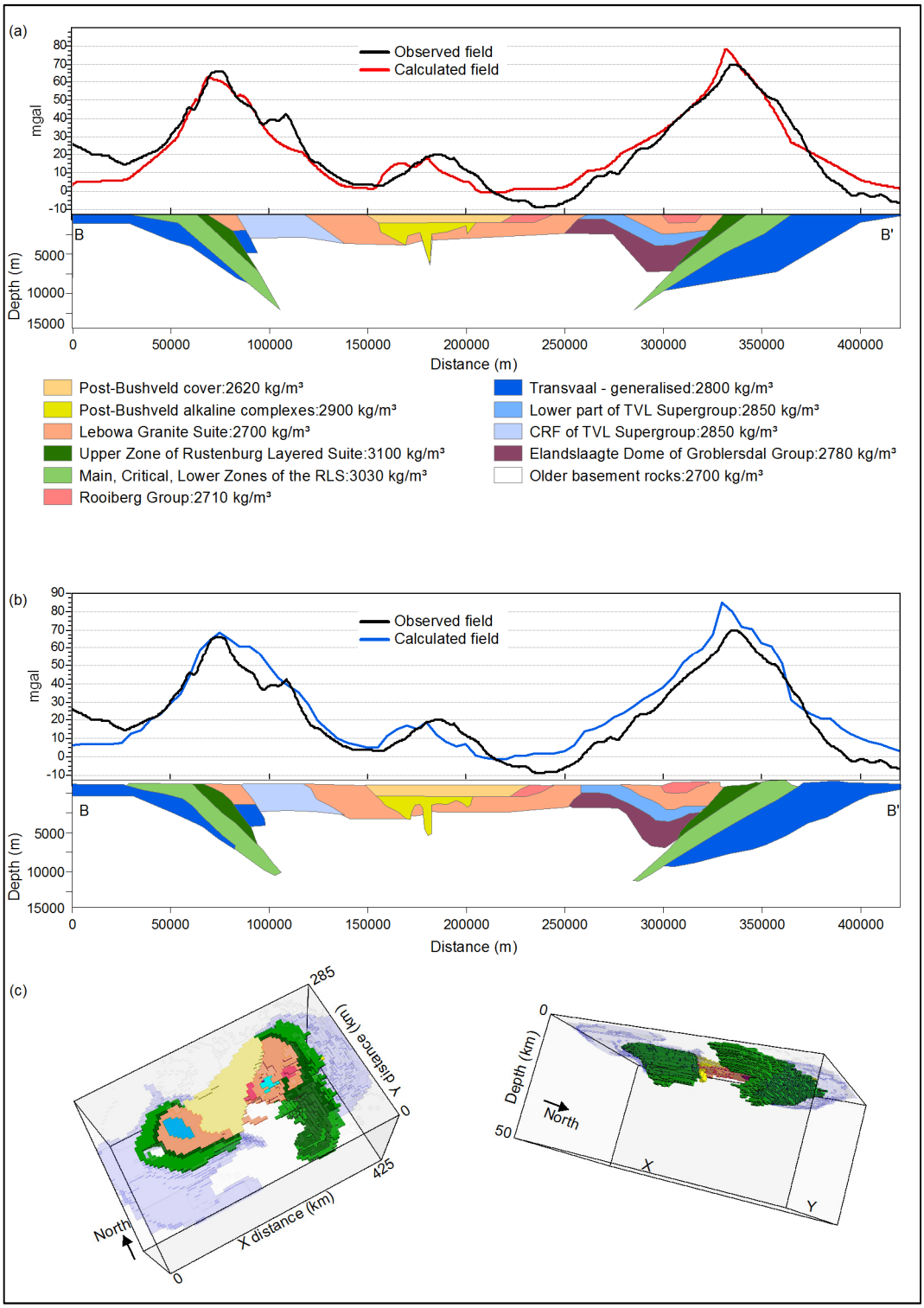


Figure 3.9 (a) Recreation of Meyer and De Beer's (1987) model in 2.5 dimensions along the profile shown in Figure 3(b); (b) Model and calculated gravity field extracted from the three dimensional model and field along Meyer and De Beer's' profile; (c) Perspective views of the three dimensional model (vertical axis exaggerated)

The 2.5D model was extended into three dimensions (Figure 3.9(b) and (c)) by following the geological map and the curve of the gravity anomalies associated with the two zones. The calculated field (Figure 3.9(b)) has a broader gravity high over the eastern and western lobes than for the 2.5D calculation (Figure 3.9(a)). This can be explained by the dense Rustenburg Layered Suite material that curves around on either side of the profile. In the 2.5D case the simple extension of bodies perpendicular to the profile is not a true reflection of the geometry of the Bushveld Complex, and as a result the widths and/or depth extents and/or densities (if these are unknown) are overestimated.

Connected-lobes model (Cawthorn et al., 1998; Cawthorn and Webb, 2001; Webb et al., 2004)

For many years the gravity low in the central part of the Bushveld Complex was attributed to the lack of mafic material in this area, supporting separate intrusions for the eastern and western lobes as discussed in the preceding sections. However, Cawthorn et al. (1998) and Cawthorn and Webb (2001) postulated that if the western and eastern lobes were connected, the 6-8 km of mafic material in the central part of the Bushveld Complex would cause an isostatic response at the crust-mantle boundary. The less dense crust would be thicker in this area resulting in lower gravity values. They illustrated the feasibility of this hypothesis by constructing a simple 2.5 dimensional gravity model incorporating the connected mafic rocks and isostatic adjustment of the crust. The model showed a 6 km depression of the crust into the mantle underneath the Bushveld Complex. When the seismic results became available (Nguuri et al., 2001), they showed that the crust underneath the Bushveld Complex was 6 – 8 km thicker than the surrounding craton, supporting the modelling (Cawthorn and Webb, 2001)) and Webb et al. (2004) incorporated this information into an updated model (Figure 3.3(c), recreated in Figure 3.10(a)). When the model is extended into three dimensions (Figure 3.10(b) and (c)) the calculated field over the central and eastern parts of the Bushveld Complex significantly exceeds the observed data (Figure 3.10(b)). Thinner crust underneath the eastern part of the Bushveld Complex (Figure 3.5(b)) partly explains this, but thickness variations of the Rustenburg Layered Suite that were not properly modelled will contribute.

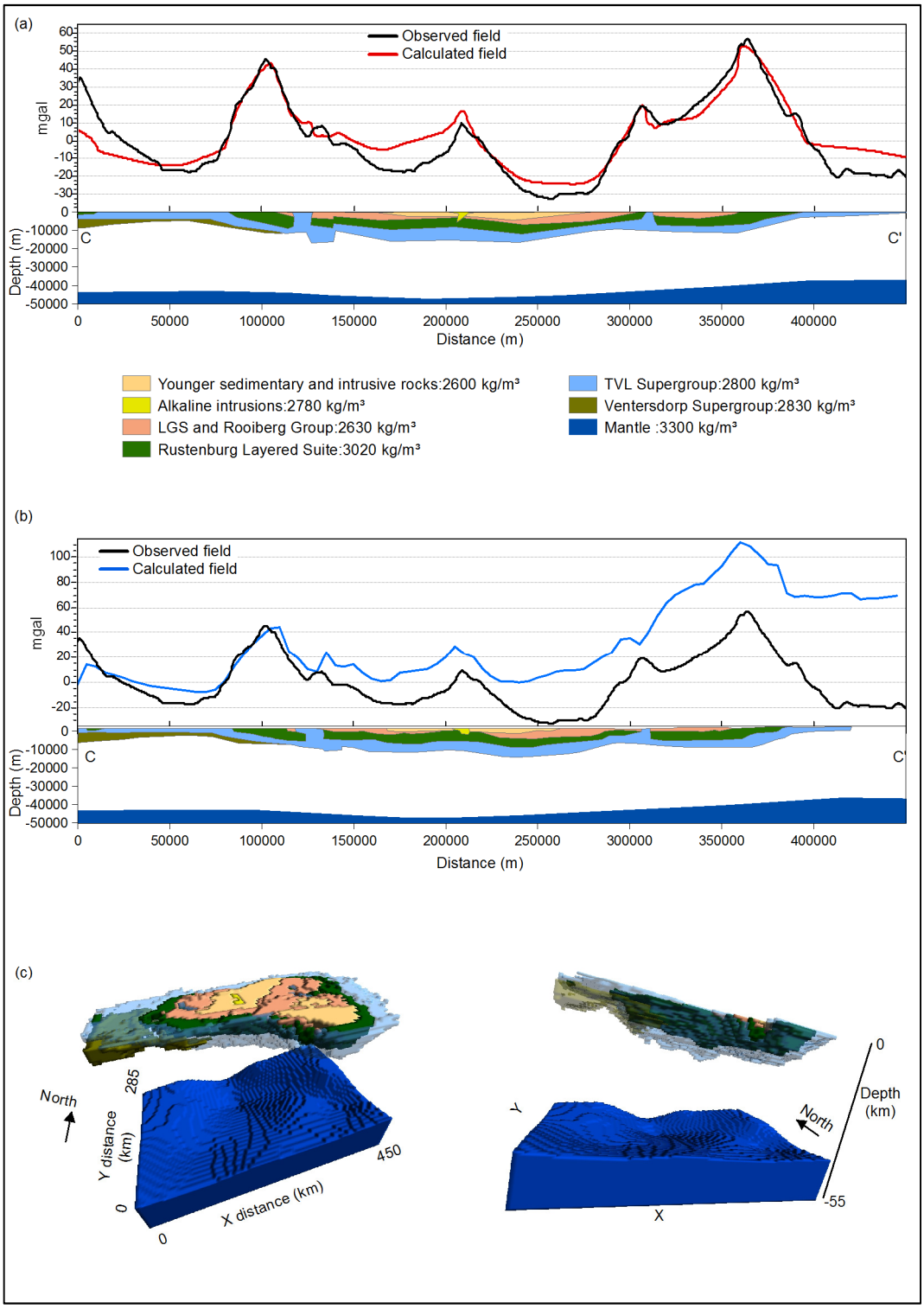


Figure 3.10 (a) Recreation of Webb et al's (2004) 2.5D model of the Bushveld Complex along the white dashed part of the profile shown in Figure 3(c); (b) Model and calculated gravity field extracted from the three dimensional model along Webb et al's profile; (c) Perspective views of the 3D model (vertical axis exaggerated).

3.5.2 Effect of variable crustal thickness

The next step was to add the seismically determined crustal thicknesses (Nguuri et al, 2001; Nair et al., 2006; Kgaswane et al., 2012) to the models. A density of 3300 kg/m^3 was used for the mantle (Webb et al., 2004). To enable direct comparison between the fields calculated for the three crustal thickness models, a constant regional was subtracted that resulted in a good fit over the western lobe between the observed field and the field calculated using Nguuri et al.'s, (2001) model. External effects such as the escarpment close to the eastern lobe make calibration to the western lobe preferable. This same regional was subsequently removed from the calculated fields for the other crustal thickness models which allowed for a direct comparison between the impacts of the different crustal thickness models. It is important to note that we are only interested in relative amplitude differences between gravity highs and lows at this stage.

Dipping sheets model (Du Plessis and Kleywegt, 1987)**; Meyer and De Beer, 1987)**

The gravity lows in the centre of the Bushveld Complex for the 3D dipping sheet model are different for the three crustal thickness models. For the models that include Nguuri et al. (2001) and Kgaswane et al. (2012) crustal thicknesses the calculated fields in the centre are lower than the observed field (Figure 3.11(a) and (c)), but for the Nair et al. (2006) crustal thickness model the two fields are more similar (Figure 3.11(b)). However, the Nair et al. (2006) crustal thickness model results in a higher calculated field over the western lobe than the first two models. Over the eastern lobe the calculated gravity values increase substantially when the crustal thickness models of Nguuri et al. (2001) and Kgaswane et al. (2012) are taken into account (50 to 70 mgal higher than the observed data). The eastward extension of thick crust in the Nair et al., (2006) model results in calculated gravity values that are similar to the observed field (Figure 3.11(b)).

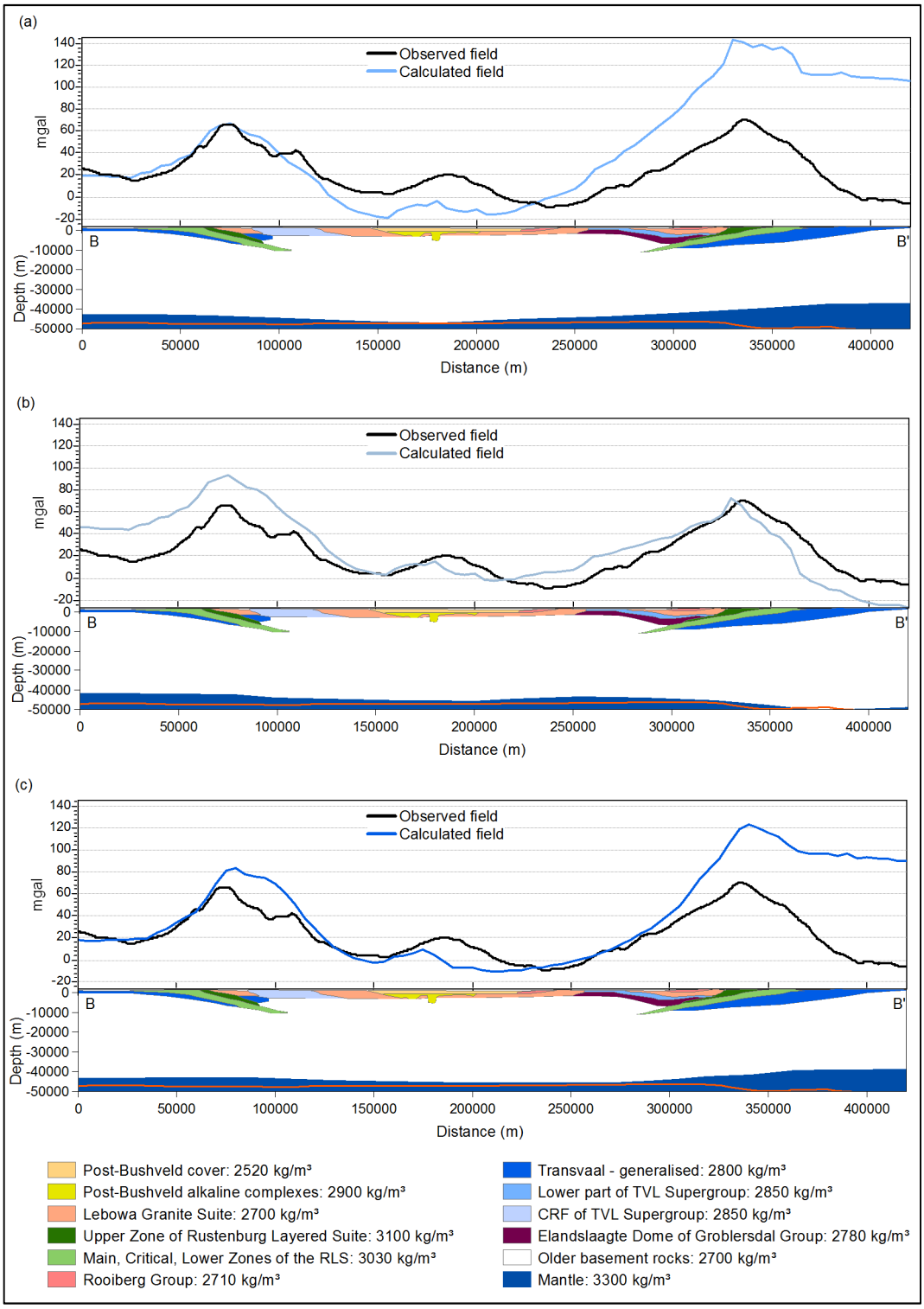


Figure 3.11 Model and calculated gravity field extracted from Meyer and De Beer's (1987) model extended into 3 dimensions and with the thickened crust included; (a) Results when using the crustal thickness model of Nguuri et al. (2001); (b) Results when using the crustal thickness model of Nair et al. (2006); (c) Results when using the crustal thickness model of Kgaswane et al. (2012). The orange line indicates the Airy-Heiskanen Moho

Connected lobes model (Cawthorn et al., 1998; Cawthorn and Webb, 2001; Webb et al., 2004)

Adding the various crustal thickness models to the 3D connected-lobes model results in bad fits between the observed and calculated gravity fields (Figure 3.12(a) to (c)). The calculated field over the central and eastern parts of the Bushveld Complex significantly exceeds the observed data for the Nguuri et al. (2001) crustal thickness model, whereas for the model of Nair et al. (2006) the calculated values over the western lobe are much lower than the observed data (Figure 3.12(b)). The crustal thickness model of Kgaswane et al. (2012) resulted in the best fit if the shapes of the fields are considered. It was mentioned previously that the same regional field was subtracted from all the models to allow for direct comparison between the calculated fields, but if a constant field is removed from the calculated field in Figure 3.12(c), the fit is much better. Calculated values in the centre of the Bushveld Complex is still too high which probably means the mafic rocks of the Bushveld Complex are thinner in this area or erroneous densities were used for some of the lithologies in the 3D model. The discrepancies resulting from the three different crustal thickness models enforce the importance of including the mantle in regional scale modelling as the deep scale variations affects the calculated gravity field in such a significant way.

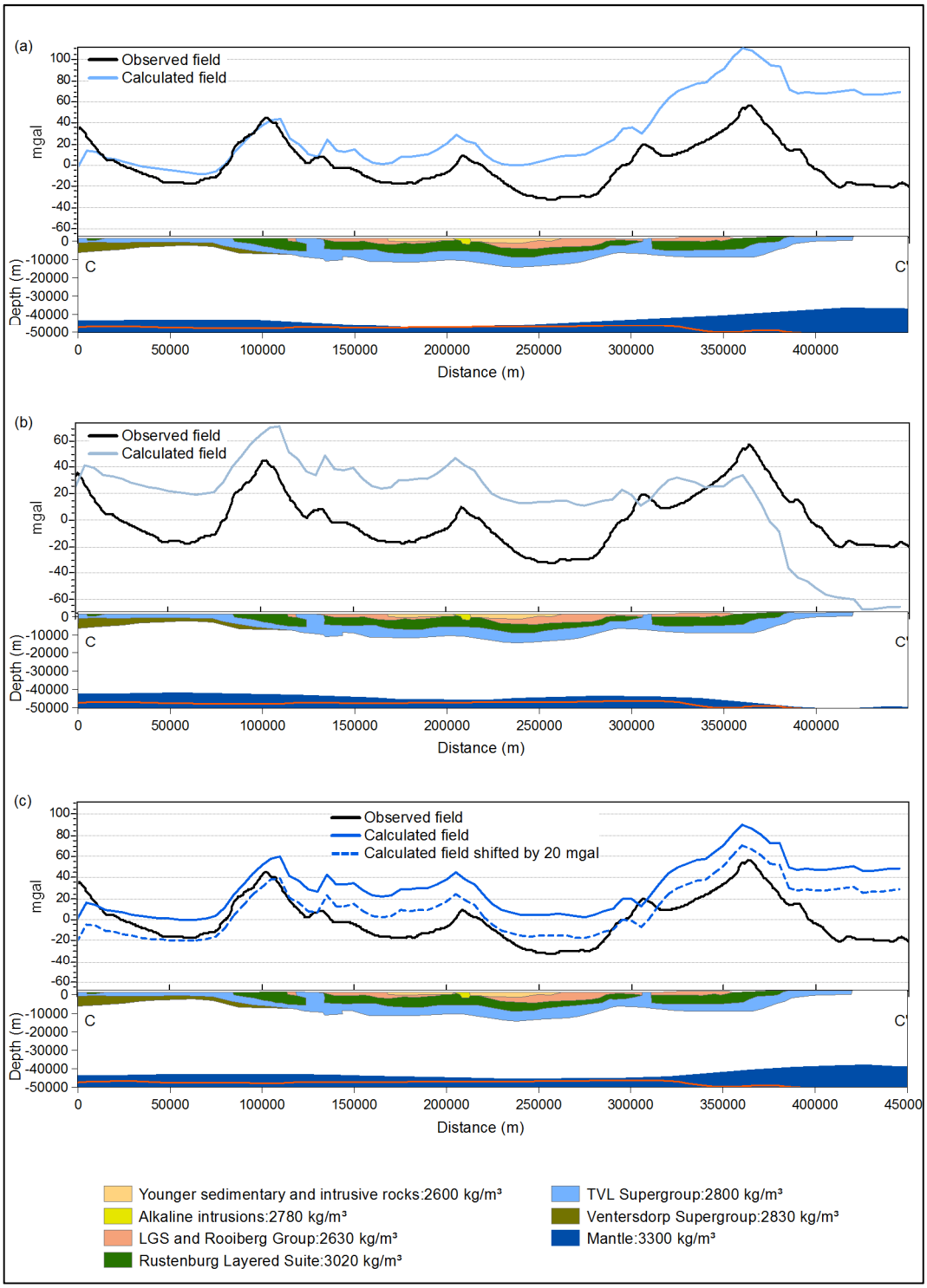


Figure 3.12 Model and calculated gravity field extracted from Webb et al.'s (2004) model extended into 3 dimensions and with the thickened crust included; (a) Results when using the crustal thickness model of Nguuri et al. (2001); (b) Results when using the crustal thickness model of Nair et al. (2006); (c) Results when using the crustal thickness model of Kgaswane et al. (2012). The orange line indicates the Airy-Heiskanen Moho

3.5.3 Dipping sheets vs. connected lobes models

The inclusion of crustal thickness information (Kgaswane et al., 2012; Nair et al., 2006; Nguuri et al., 2001) in the gravity models of the Bushveld Complex supports the concept of continuous bodies. However, new density information has become available since the publication of the three gravity models (Table 3.2) and it is necessary to test the 3D dipping sheets model and the connected-lobe model with this new information.

A critical aspect is the densities of the alkaline complexes that intruded in the central area of the Bushveld Complex (Figure 3.1). The alkaline complexes are located on a broad gravity high (Figure 3.4) which Webb et al. (2004) modelled as the Elandskraal Complex located above slightly folded mafic rocks of the Bushveld Complex (Figure 3.3(c)). Meyer and De Beer (1987) modelled the gravity high completely by alkaline complexes. To recreate the dipping sheet model (Meyer and De Beer, 1987) a density of 2900 kg/m^3 had to be assigned to these complexes, whereas Webb et al. (2004) obtained a density of 2780 kg/m^3 from major element analysis (Frick and Walraven, 1985) for the Elandskraal Complex (EC in Figure 3.1). Syenite and nepheline syenite (Harmer, 1985) make up most of the alkaline complexes, and the mean density of 2624 ± 78 kg/m^3 for these lithologies (Table 3.2) is substantially lower than densities used in the models. Higher densities have been measured for lavas of unspecified composition in the complexes (2740 ± 147 kg/m^3, Table 3.2). The Elandskraal Complex, consisting of tuff, trachytic and basaltic lavas (Frick and Walraven, 1985) has a similar density to the lava. Lowering the density of the alkaline complexes makes it impossible to model the gravity anomaly in the centre of the Bushveld Complex with the dipping sheet model as it is in Figure 3.11. Dense material is needed below the alkaline complexes. Adding the Transvaal Supergroup underneath the alkaline complexes is not sufficient on its own to cause the positive gravity anomaly (Figure 3.13). The inclusion of a varying Moho depth requires the presence of dense material in the centre of the Bushveld Complex to obtain a fit to the observed gravity data.

The connected-lobe model (Webb et al., 2004) still accounts for the positive anomaly in the centre even if a lower density is assigned to the alkaline complexes. The lower density actually improves the fit in the central part of the Bushveld Complex (Figure 3.14). Kgaswane et al.'s (2012) crustal thickness model provides the best fit between the calculated and observed gravity fields. Thinner crust at stations 'sa42', 'sa43', 'sa52' and 'sa53' (Figure 3.5h) compared to Nguuri et al.'s (2001) crustal thicknesses (Figure 3.5d) improves the fit for the eastern lobe even though the crustal thicknesses are very similar along the profile.

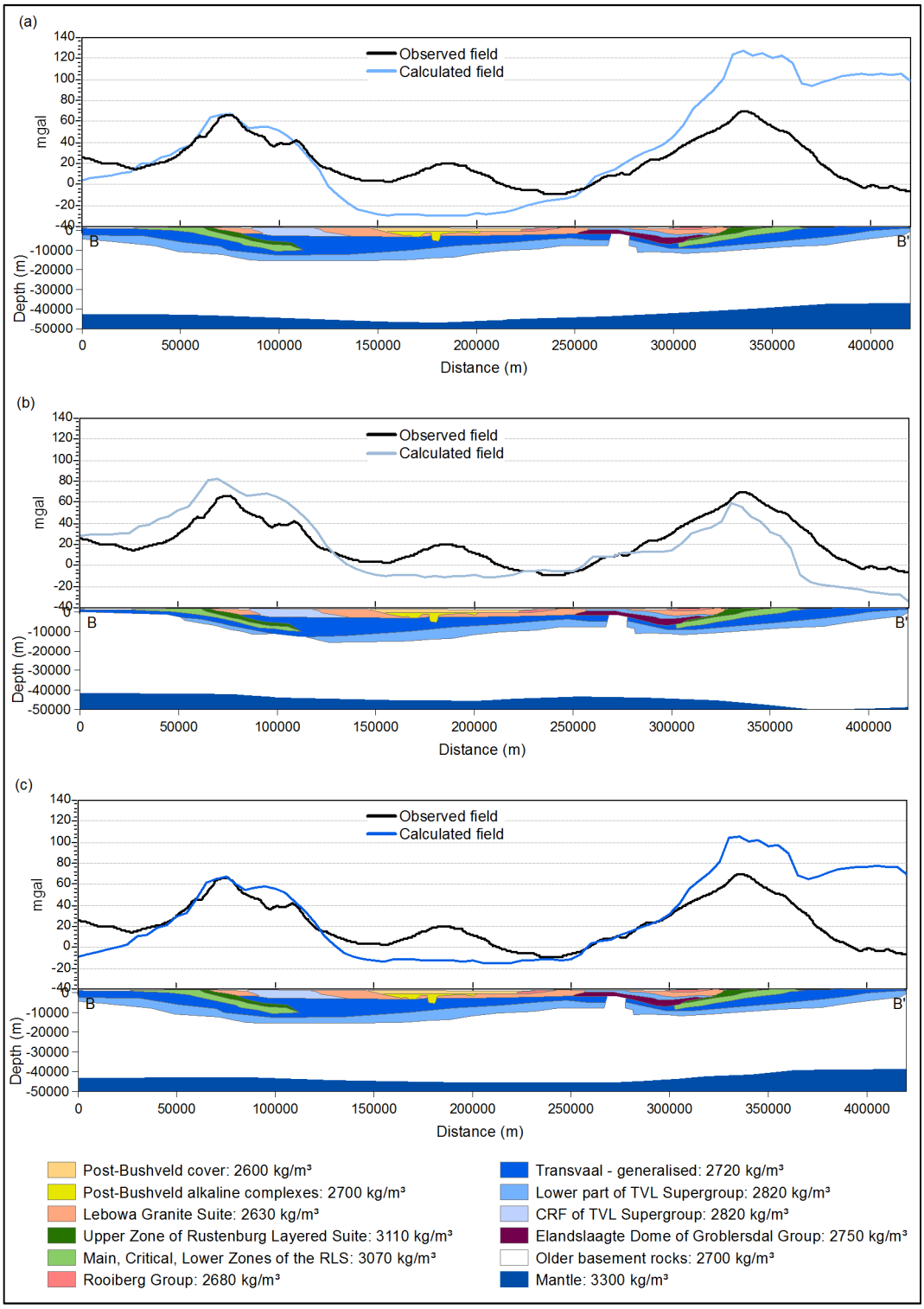


Figure 3.13 Testing the dipping sheet model using updated density information (Table 3.2) and including continuous Transvaal Supergroup underneath the whole Complex. (a) Results when using the crustal thickness model of Nguuri et al. (2001); (b) Results when using the crustal thickness model of Nair et al. (2006); (c) Results when using the crustal thickness model of Kgaswane et al. (2012).

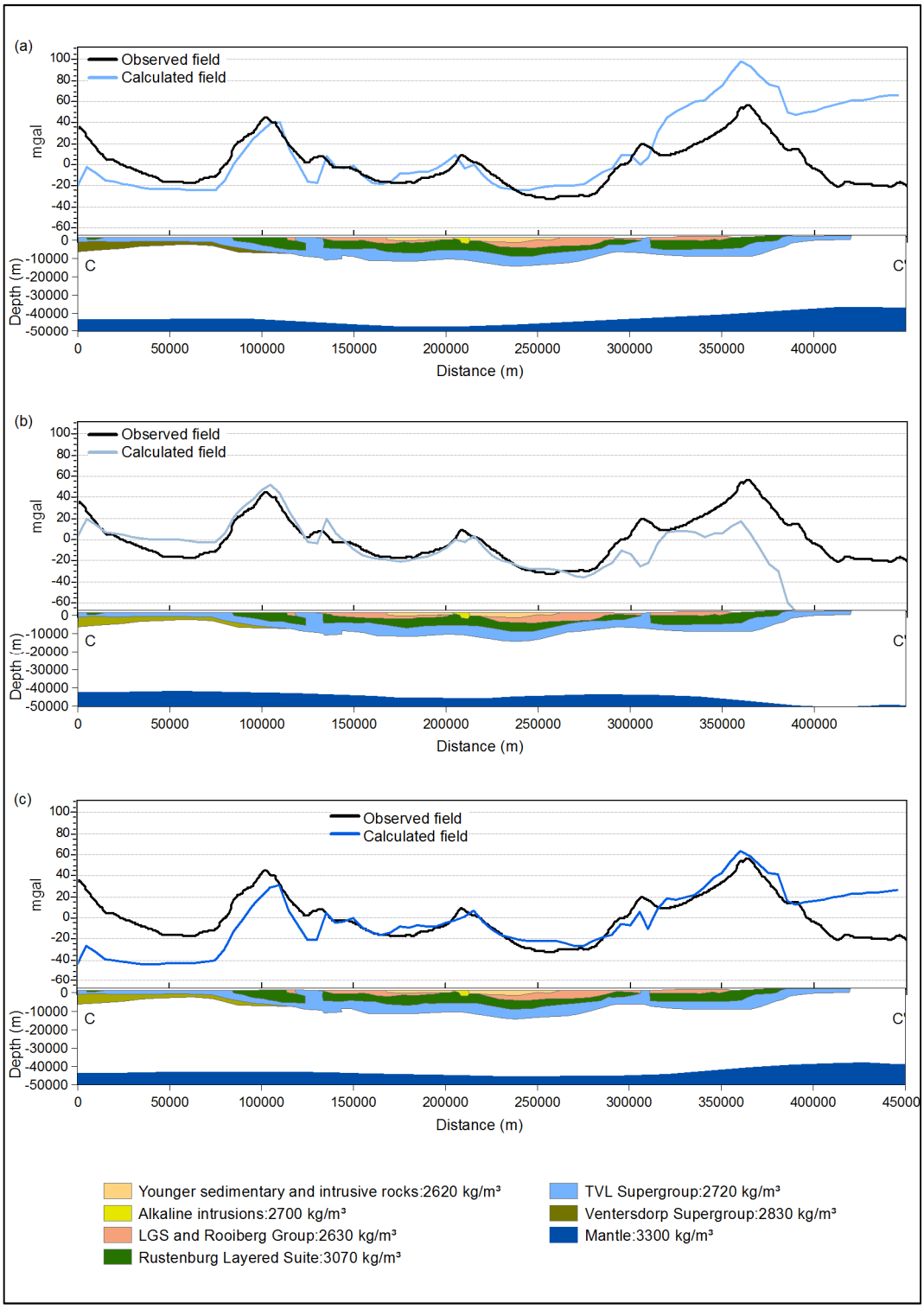


Figure 3.14 Testing the connected-lobe model using updated density information (Table 3.2). (a) Results when using the crustal thickness model of Nguuri et al. (2001); (b) Results when using the crustal thickness model of Nair et al. (2006); (c) Results when using the crustal thickness model of Kgaswane et al. (2012)

3.6 Discussion

Modelling in three dimensions and including new density and crustal thickness information corroborates the idea of a continuous Bushveld Complex first proposed by the early authors (Hall, 1932) and later by 2.5D gravity modelling (Cawthorn et al., 1998; Cawthorn and Webb, 2001; Webb et al., 2004). Although the three crustal thickness models discussed in this paper all allow for continuous mafic rocks in the centre of the Bushveld Complex, differences between the models underneath the eastern lobe result in bad fits between observed and calculated gravity data in the eastern part of the Bushveld Complex for the crustal thickness models of Nguuri et al. (2001) and Nair et al. (2006).

Variations in mantle density can be used to improve the model using the crustal thickness of Nguuri et al. (2001). Due to the Fe depletion of the mantle, the mantle keel under the Kaapvaal Craton has a density that is lower than expected for cold, high velocity material (Webb, 2009). In turn, slower mantle velocities observed under the Bushveld Complex may relate to metasomatism that decreased the Mg# resulting in an increase in density (relatively more Fe), or alternatively to increased temperature (Webb, 2009). A model with a mantle density of 3300 kg/m^3 underneath the Bushveld Complex and 3160 kg/m^3 under the Kaapvaal Craton was tested. Although these values are rough estimates only, it should be adequate for testing the mantle density variation concept. The model (Figure 3.15) does not include a separate lower crust. Lowering the density in the east successfully lowers the calculated gravity values over the eastern lobe and could be considered a feasible explanation. The lower mantle density under the Kaapvaal Craton causes the calculated gravity values over the western lobe to be too low. To fit the gravity lows in the center of the Bushveld Complex the mafic rocks had to be modelled thinner in the east around the Dennilton Dome (Figure 3.15(a)) and even peter out at the Marble Hall Fragment (Figure 3.15(b)). In effect the model is very similar to Du Toit's model (Hall, 1932) shown in Figure 3.2(b). The estimated values for the mantle densities clearly influence the results and more work is needed to refine this model.

A second model (Figure 3.16) was created using the crustal thicknesses determined by Nair et al. (2006). To improve the fit between the observed and calculated values in the eastern part of the Bushveld Complex, deeper-seated dense material was added below the eastern lobe of the Bushveld Complex at the base of the crust. This may reflect mafic material that intruded into the crust. Magma reservoirs associated with underplating result in wedge shaped mafic layered intrusions (Corriveau and Morin, 2000), similar to the shape of the body included in this model. In this model the mafic rocks are thicker near the Dennilton Dome (Figure 3.16(a)) and Marble Hall Fragment (Figure 3.16(b)) compared to the model shown in Figure 3.15.

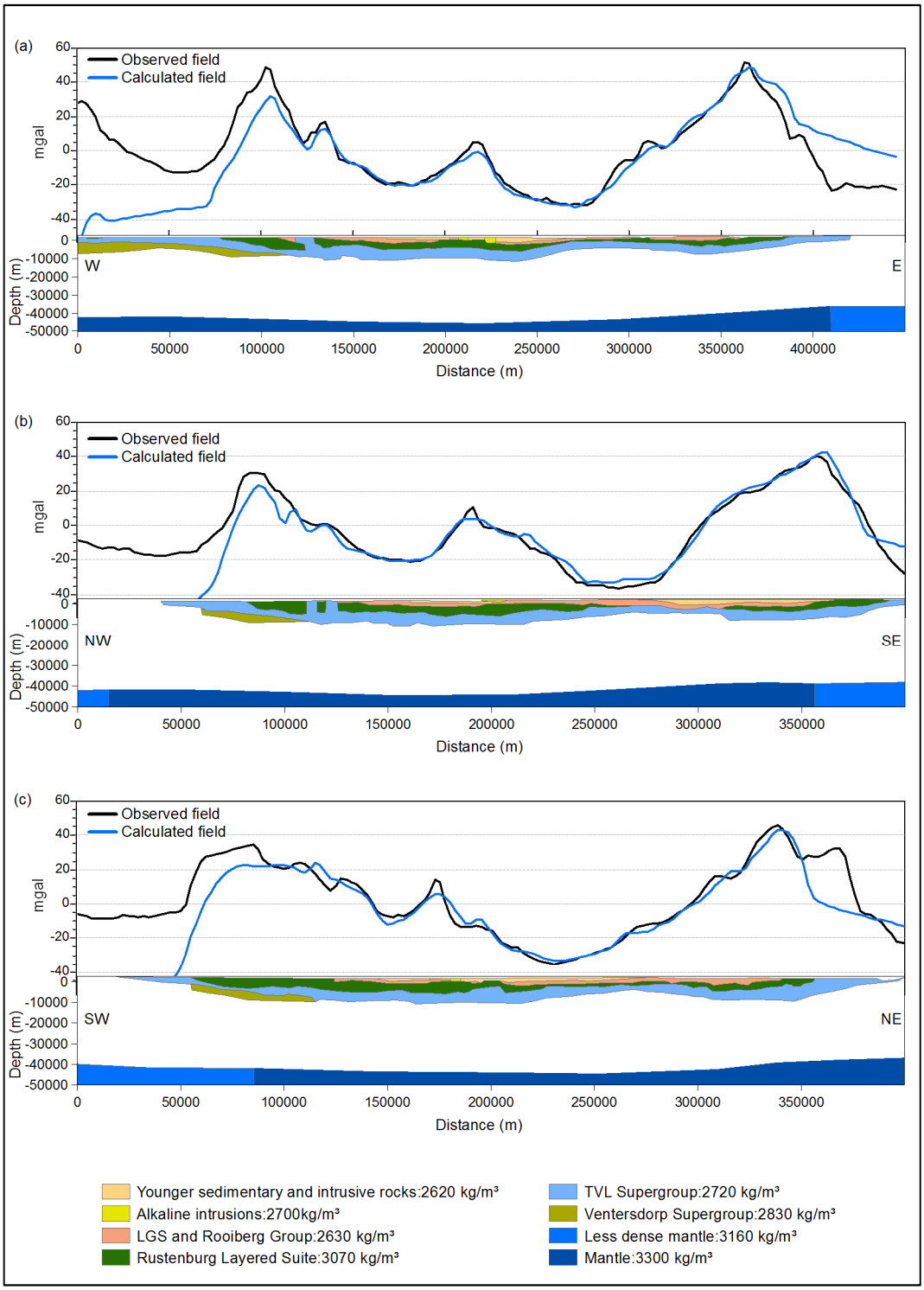


Figure 3.15 Modified version of the model shown in Figure 3.14(a) using Nguuri et al's (2001) crustal thickness model and incorporating variations in the mantle density. (a) Model along the WE profile; (b) Model along the NW-SE profile; (c) Model along the SW-NE profile. The localities of the profiles are shown in Figure 3.1

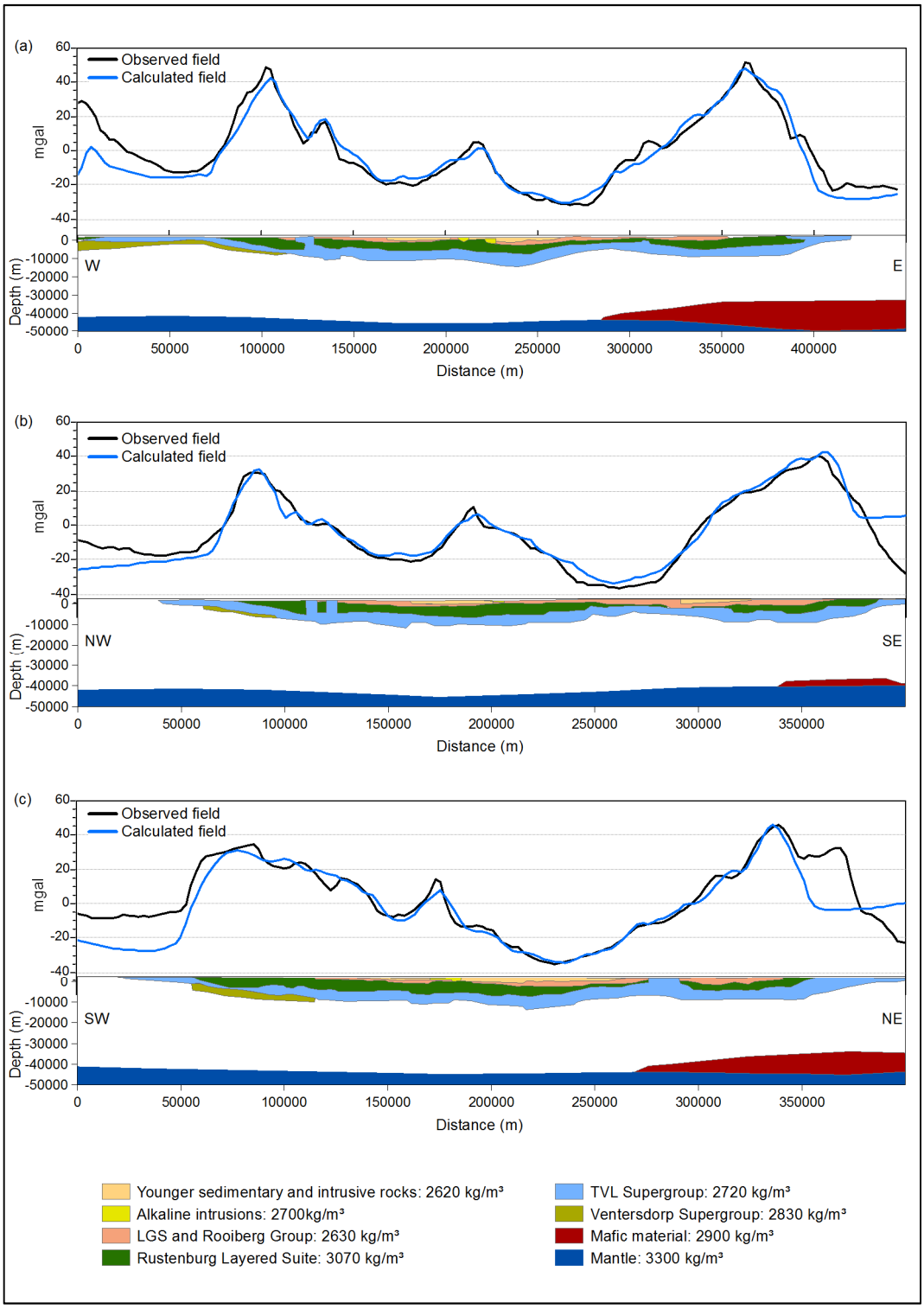


Figure 3.16 Modified version of the model shown in Figure 3.14b) using Nair et al's (2006) crustal thickness model and incorporating magma underplating. (a) Model along the WE profile; (b) Model along the NW-SE profile; (c) Model along the SW-NE profile. The localities of the profiles are shown in Figure 3.1

The previous two test models did not include a separate lower crust and in effect assumed a constant thickness lower crust. Kgaswane et al. (2012) observed an increase in shear-wave velocity above the Moho underneath the Bushveld Complex, with velocities exceeding 4.0 km/s. This high velocity layer thickens towards the east, reaching more than 20 km to the east and southeast of the Bushveld Complex (Figure 3.5(h)). Kgaswane et al. (2012) used an empirical equation (Christensen and Stanley, 2003) to convert from shear wave velocity to and average density of ~ 3200 kg/m^3 for this material. Including this in the model introduces an additional regional into the results (Figure 3.17) which cannot be accounted for by changes in the Bushveld Complex. There is clearly need for more detailed modelling of the lower and middle crust as the current models are oversimplified. This is outside the scope of this review paper.

3.7 Conclusions

Three dimensional gravity modelling that includes crustal thickness and incorporates new densities supports the concept of a connected Bushveld Complex. The first gravity models that showed this were restricted to 2.5D (Cawthorn et al., 1998, Cawthorn and Webb, 2001 and Webb et al, 2004) and was an oversimplification of the real situation as the thicker crust in the centre of the Bushveld Complex is simply extended north and south of the profile in 2.5D modelling. In reality the thicker crust is more localised (Figure 3.5) and varies. In addition, different crustal thickness models inferred from SASE data also result in variations in the calculated gravity fields for the 3D models. Gravity models using the different crustal thickness models and including various deep-seated bodies and density variations made it clear that uncertainty in the crustal thickness models has a large impact on the calculated gravity field for the Bushveld Complex, and affects the inferred thickness of and depth to the Rustenburg Layered Suite and in a substantial way. Most of these uncertainties affect the calculated gravity field over the eastern and western lobes, and is due to different results at one seismic station ('sa49'). The results over the central part of the Bushveld Complex are very similar for the three Moho models, and 3D modelling confirms that dense material is necessary between the eastern and western lobes to obtain a good fit.

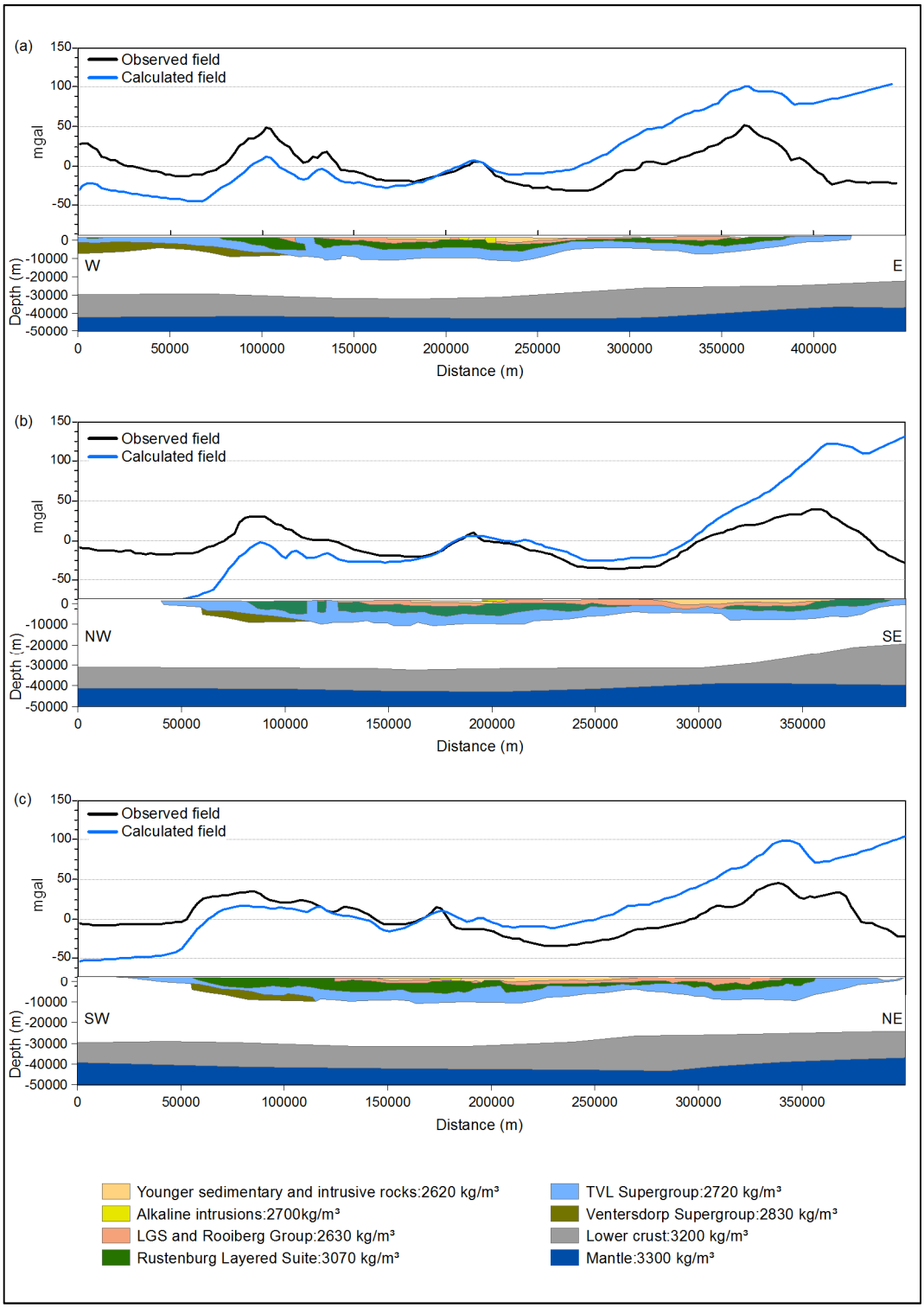


Figure 3.17 Modified version of the model shown in Figure 3.14(c) using Kgaswane et al's (2012) crustal thickness model and including the dense, high velocity layer above the Moho. (a) Model along the WE profile; (b) Model along the NW-SE profile; (c) Model along the SW-NE profile. The localities of the profiles are shown in Figure 3.1

Through the years, as new geophysical data became available, it impacted on the understanding of the Bushveld Complex geometry. Gravity data led to the original lopolithic concept being changed to separate intrusions for the western and eastern lobes. However, when new information about the crustal thicknesses became available, the model changed again to a more continuous geometry.

This study emphasises that to avoid flawed conclusions, modelling should be done in three dimensions, and that for models the size of the Bushveld Complex it is extremely important to take into account deep seated features and their varying lithological properties. For regional scale models, density variations in the lower crust and upper mantle cause long wavelength gravity anomalies that cannot be modelled by shallow crustal features alone.

3.8 Acknowledgments

The authors would like to thank Anglo American Platinum Limited for wire line logging data from a number of boreholes throughout the Bushveld Complex. We also appreciate the comments of VJS Grauch and an anonymous reviewer.

CHAPTER 4 IMPORTANCE OF THE MAGNETIC DATA

This chapter was published as a paper in Precambrian Research (2013, 236, pp. 193-213). The manuscript was constructed by me with editing and suggestions for improvements by my co-authors.

Cole – 80% (conducted the research and constructed the manuscript)

Finn – 15% (reviewed the manuscript and suggested improvements)

Webb - 5% (reviewed the manuscript and suggested improvements)

Overview of the magnetic signatures of the Palaeoproterozoic Rustenburg Layered Suite, Bushveld Complex, South Africa

Janine Cole

Geophysics Unit, Council for Geoscience, Private Bag X112, Pretoria, 0001, South Africa
School of Geosciences, University of the Witwatersrand, Private Bag 3, WITS, 2050, South Africa
email: jcole@geoscience.org.za

Carol A. Finn

US Geological Survey, Denver, Colorado 80225, USA
email: cfinn@usgs.gov

Susan J. Webb

School of Geosciences, University of the Witwatersrand, Private Bag 3, WITS, 2050, South Africa
email: susan.webb@wits.ac.za

4.1 Abstract

Aeromagnetic data clearly delineate the mafic rocks of the economically significant Bushveld Igneous Complex. This is mainly due to the abundance of magnetite in the Upper Zone of the Rustenburg Layered Suite of the Bushveld, but strongly remanently magnetised rocks in the Main Zone also contribute significantly in places. In addition to delineating the extent of the magnetic rocks in the Complex, the magnetic anomalies also provide information about the dip and depth of these units. The presence of varying degrees of remanent magnetisation in most of the magnetic lithologies of the Rustenburg Layered Suite complicates the interpretation of the data. The combination of available regional and high resolution airborne magnetic data with published palaeomagnetic data reveals characteristic magnetic signatures associated with the different magnetic lithologies in the Rustenburg Layered Suite. As expected, the ferrogabbros of the Upper Zone cause the highest amplitude magnetic anomalies, but in places subtle features within the Main Zone can also be detected. A marker with strong remanent magnetisation located in the Main Zone close to the contact with the Upper Zone is responsible for very

high amplitude negative anomalies in the southern parts of both the eastern and western lobes of the Bushveld Complex. Prominent anomalies are not necessarily related to a specific lithology, but can result from the interaction between anomalies caused by differently magnetised bodies.

The magnetic data provided substantial information at different levels of detail, ranging from contacts between zones, and layering within zones, to magnetite pipes dykes and faults that can have an impact on mine planning. Finally, simple modelling of the magnetic data supports the concept of continuous mafic rocks between the western and eastern lobes.

Keywords: Bushveld Complex; Rustenburg Layered Suite; Magnetic interpretation

4.2 Introduction

The importance of the Bushveld Igneous Complex, South Africa, from both an economic and research point of view has stimulated the continuous collection of large amounts of various data types including airborne magnetics which maps the presence of magnetic minerals, mostly magnetite, in the subsurface. Based on the characteristics of the magnetic anomalies associated with the presence of these minerals, deductions can be made about the size, dip, depth and even possible age of the host lithologies. Airborne magnetic data provides a synoptic view of the Complex at a single glance and information about various lithologies, as well as the distribution of lithologies throughout the Complex. However, the dipolar nature and the effect of remanent magnetisation (Hattingh, 1986, 1989; Letts et al., 2009) add complexity to magnetic data that make it difficult to simply infer features by inspection of the magnetic data without a priori information. A compilation of existing airborne magnetic data combined with measurements of remanent magnetisation parameters for the Rustenburg Layered Suite rocks from palaeomagnetic studies (Hattingh, 1986, 1989; Letts et al., 2009) allow delineation of the mafic rocks based on distinct magnetic signatures. The magnetic data were also compared to existing 1:50 000 scale geological maps, landsat imagery and regional geophysical data. This paper aims to provide an overview of the typical magnetic anomalies associated with magnetic lithologies within the Rustenburg Layered Suite of the Bushveld Complex to aid in identification of economically critical regions and identify layering, IRUPs and faults that interrupt the Bushveld.

4.3 Airborne Magnetic Data Specifications

The first of two data sets used in this study is regional magnetic data covering the whole Bushveld Complex that were collected between 1969 and 1978 in a number of separate

survey blocks (Figure 4.1) (Ledwaba et al., 2009). The flight line spacing was 1 km, and a flying height of 100 m to 150 m was maintained above the terrain. On average the tie line spacing was 15 km. The majority of the surveys were flown along north-south directed lines, but for the northern lobe and part of the eastern lobe the line direction was east-west. In most cases a Geometrics G803 proton magnetometer was used, although a few surveys were done with a Gulf Fluxgate Mark III magnetometer. The sampling rate of 1 Hz resulted in a magnetic reading roughly every 63 m along a flight line. The resolution of the regional 1 km magnetic data set is too low to detect marker horizons within the Main Zone but is suitable for regional scale study (Campbell, 2006, 2011).

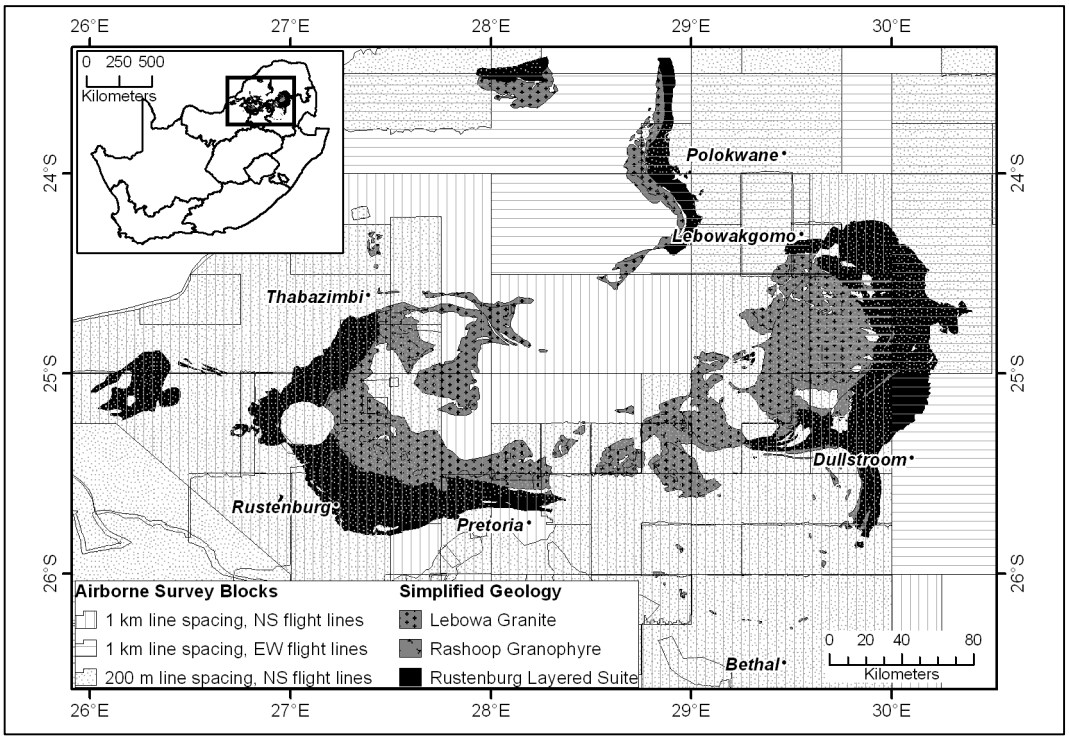


Figure 4.1 Outlines of survey blocks for regional (linear hatching) and higher resolution (dotted hatching) data overlain on the geology of the Bushveld Igneous Complex (Council for Geoscience, 1997)

Higher resolution data collection in South Africa started in the 1990s and is still continuing. Surveys north of Pretoria and around Thabazimbi were done by consultants in the early 1990's, but the remainder were conducted by the Council for Geoscience using its own airborne platform. Coverage includes large parts of the eastern and western lobes of the Bushveld Complex, but is incomplete (areas filled by dots in Figure 4.1). The line spacing was 200 m and a nominal flying height of 80 m was maintained where possible. In areas of rugged topography this terrain clearance could not be maintained in a fixed-

wing aircraft and the flying height was increased. Most of the surveys were conducted along north-south directed flight lines. The data sampling rate was 10 Hz, resulting in a reading roughly every 7 m along a flight line. Caesium vapour magnetometers were used for the surveys conducted by the Council for Geoscience. These magnetometers had an instrument resolution of 0.01 nT and the total noise envelope on collected data did not exceed 0.1 nT. Positioning was done by real-time differential GPS and accuracies of better than 2 m in the horizontal directions, and 3 m in the vertical were achieved. With the higher resolution data (200 m line spacing) it is possible to differentiate between the Upper and Main Zones, gain information about the dip of layering within the Upper Zone, and in certain instances to detect very subtle anomalies within the Main Zone.

Because both the regional and higher resolution data sets were collected in many different survey blocks, the data sets had to be merged (regional with regional and higher resolution with higher resolution, not regional with higher resolution). Before merging the data the appropriate International Geomagnetic Reference Field was removed from each data set. The data were gridded using a minimum curvature algorithm (Briggs, 1974). The gridding interval was 250 m for the regional data and 50 m for the higher resolution data. The image of the higher resolution data was overlain on the regional image (Figure 4.2). The limitation of the colour stretch to -1000 nT to 1000 nT enhanced subtle features in the magnetic data at the expense of clipping some of the largest anomalies. The effects of a high voltage power line that has been activated during the period of the higher resolution surveys can be seen running in a NNE sense through the eastern part of the Bushveld Complex.

Local, high resolution magnetic data (e.g. 20-50 m line spacing) collected for mining companies identify small-scale features of interest for PGE exploration that have been discussed elsewhere (Campbell, 2006; 2011).

4.4 Geological and Rock Property Overview

The Bushveld Complex is a vast layered igneous complex that intruded the volcano-sedimentary Pretoria Group of the late Archaean to early Proterozoic Transvaal Supergroup. The northern lobe transgresses onto Archaean granite-gneisses. The preserved outcrop is estimated to cover an area of more than 65 000 km^2 (Cawthorn et al., 2006).

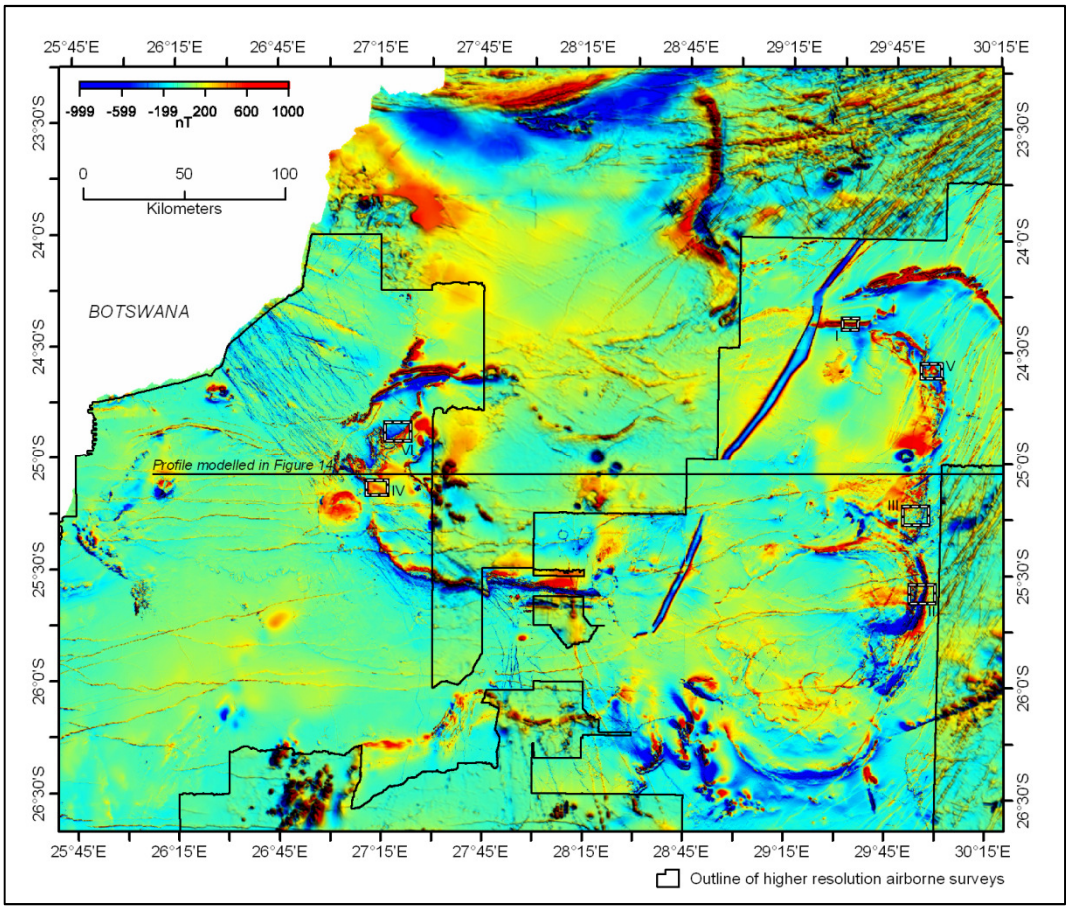


Figure 4.2 Gridded image of the merged higher resolution magnetic data sets overlain on the regional magnetic data collected over the Bushveld Complex. Small blocks labelled I to VI outline anomaly type areas shown in Figure 4.6

The Rustenburg Layered Suite, constituting the mafic component of the Bushveld Igneous Complex, was emplaced between 2059 and 2061 Ma (Buick et al., 2001). It is generally divided into five zones based on changes in composition (Cawthorn et al., 2006) (Figure 4.3). The Upper Zone consists of gabbronorites and anorthosites with cumulus Fe-rich pyroxenes and olivine, magnetite and apatite also present (Cawthorn et al., 2006). The most conspicuous features of this zone are numerous magnetitite layers which occur in four groups consisting of up to seven layers each (Eales and Cawthorn, 1995) which contain vanadium (Cawthorn et al., 2006). Their thicknesses range from a few centimetres to 2 m with the thickest reaching 6 m (Eales and Cawthorn, 1995). The high measured susceptibilities of Upper Zone magnetite layers (0.6 – 5 SI, Ashwal et al., 2005) produce very high amplitude positive anomalies (600-2400 nT). In places, layering in the Upper Zone is visible in the magnetic data.

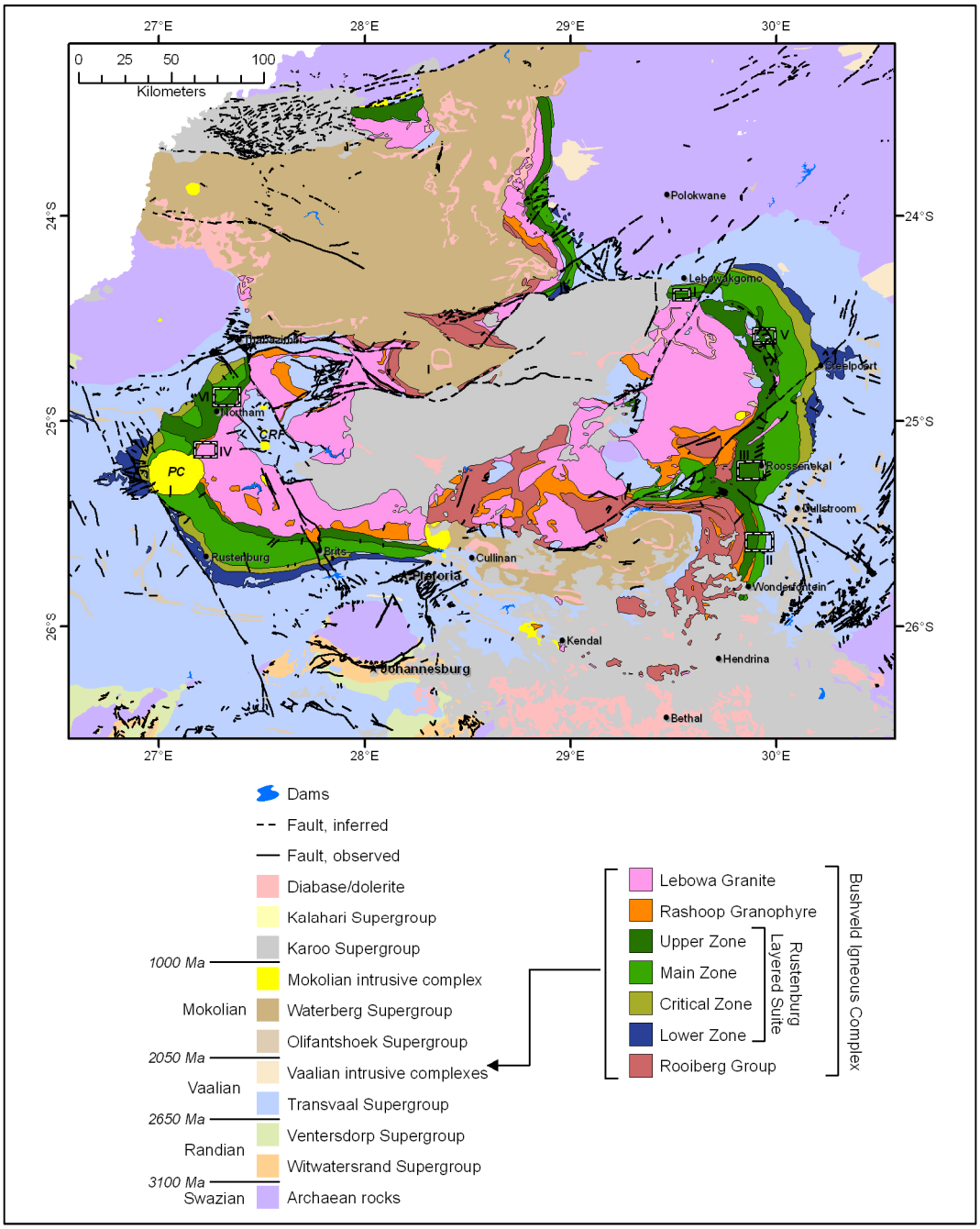


Figure 4.3 Geological map of the Bushveld Igneous Complex compiled from the published 1:1 000 000 geological map of South Africa (Council for Geoscience, 1997). CRF – Crocodile River Fragment; PC – Pilanesberg Complex. Small blocks labelled I to VI outline anomaly type areas shown in Figure 4.6

The Main Zone is a thick succession of norite and gabbronorite (Cawthorn et al., 2006) with susceptibilities of 0.00025 – 0.0089 SI and magnetizations of 0.02 – 28.87 A/m (Letts et al., 2009). Magnetite poor pyroxenite and anorthosite are rare, being confined to the

pyroxenite marker and the Main and Upper Mottled Anorthosites respectively (Eales and Cawthorn, 1995). Magnetic anomalies associated with the Main Zone range from -20 nT to -150 nT.

The Critical Zone comprising repeated layers of chromitite, pyroxenite, norite and anorthosite, contains vast resources of chromitite and platinum group elements (Cawthorn et al., 2006). Cawthorn (1999) reported inferred platinum and palladium resources of 939 and 711 million ounces respectively down to a depth of 2 km below the surface. This represents 75% and 50% of the world's platinum and palladium resources. These resources are hosted in chromitite layers that also hosts 45% of the world's chromium (Cawthorn et al., 2005). The Lower Zone is composed of pyroxenite and harzburgite. Susceptibilities in these zones are low, 0.0001 – 0.001 SI (Letts et al., 2009; Maré and Tabane, 2004) such that neither of these zones produce magnetic anomalies in the magnetic data.

The location of the Main Zone – Upper Zone boundary has been disputed to be either the first appearance of cumulus magnetite (SACS, 1980) or at the Pyroxenite Marker 200 – 800 m below this (Klemm et al., 1985; Kruger, 1990, 2005; Molyneux, 1974; Von Gruenewaldt,1973). We define the upper zone –Main zone boundary as the first appearance of cumulus magnetite based on the distinct magnetic signatures of the highly magnetic Upper Zone containing numerous magnetite zones compared with the more subdued magnetic signature of the Main Zone.

4.5 Magnetic Signatures

The shape of any magnetic anomaly is influenced by a combination of spatial, physical and magnetic parameters of the source body. Its location determines the intensity, inclination and declination of the inducing field. Physical parameters are width, depth and dip of the magnetic body and magnetic parameters comprise magnetic susceptibility and remanent magnetisation (defined by intensity, inclination and declination).

For the Bushveld region, the present-day magnetic field has an intensity of 28 834 nT, inclination of -62.12º and declination of -15.02º (IAGA, 2010). Generally, magnetic sources produce dipolar anomalies that are positive in the north and east with small negatives on the western and southern sides. Deviations from this signature can relate to the presence of remanence and/or changes in depth and dip of a body. Synthetic models illustrate the anomaly shapes that can be expected in South Africa, and how anomaly shapes change with variations in the geometry of magnetic bodies (Figure 4.4). For example, as a dyke increases in depth, the resulting magnetic anomaly broadens and its amplitude decreases (Figure 4.4a). The negative part of the anomaly decreases and can

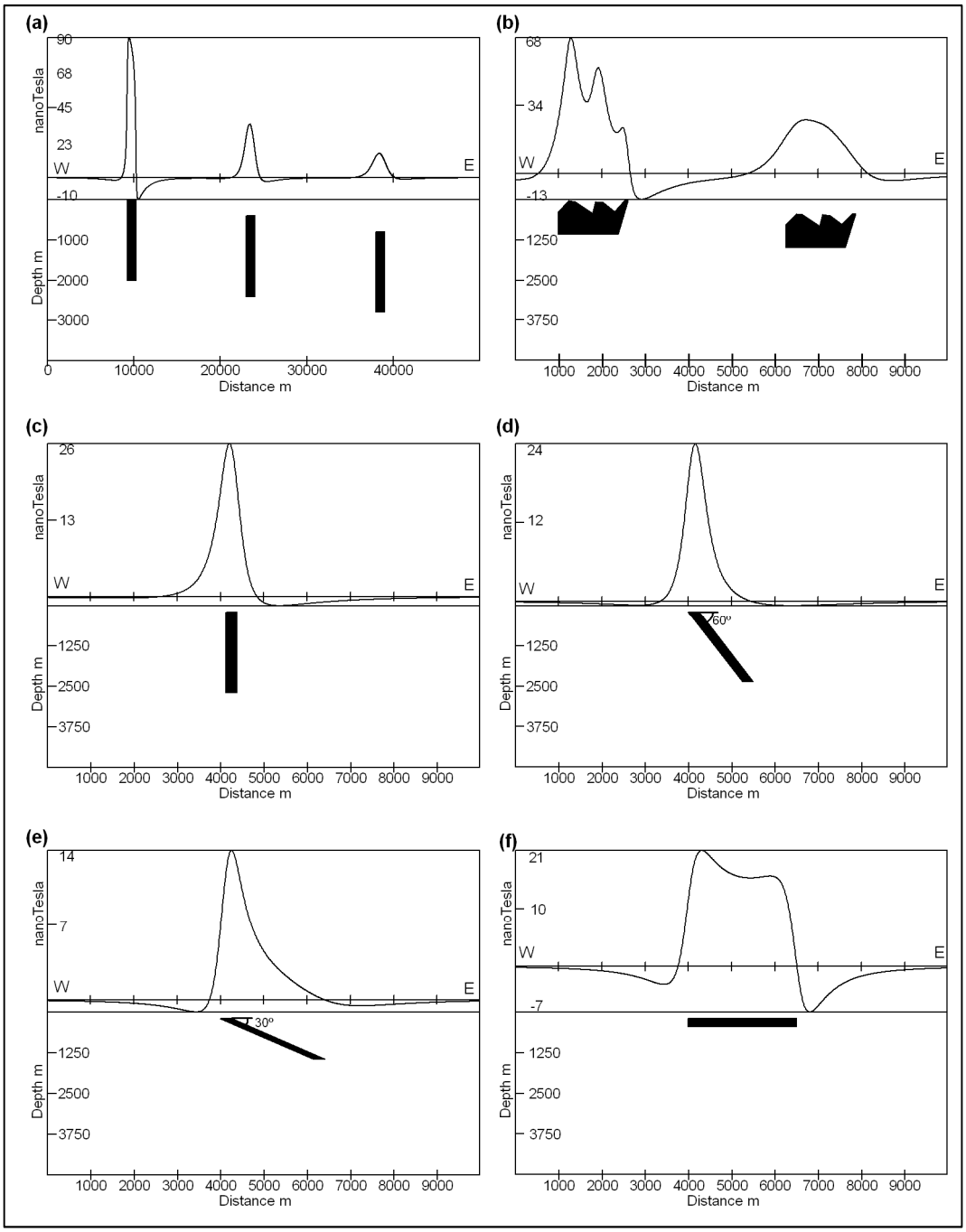


Figure 4.4 Synthetic two dimensional models showing the effect of changes in depths and dips of magnetic bodies on the magnetic field in the northern part of South Africa. (a) Increasing the depth of a vertical dyke results in progressively smaller amplitudes and wider anomalies; (b) Increasing the depth of a body with an irregularly shaped top surface results in a smoother anomaly; (c) to (f) Decreasing the dip of a body substantially changes the shape of the magnetic anomaly

be obscured by local anomalies associated with other geological features surrounding the dyke. In a magnetically quiet area the uncertainty in the presence of the negative anomaly is a function of the sampling rate and gridding algorithm. For an irregularly shaped body close to the surface, the calculated field contains anomaly peaks associated with the irregularities in the top surface (Figure 4.4b left). Moving the body 400 m deeper results in a smooth calculated field (Figure 4.4b right). If the dip of a dyke is steadily decreased from vertical to horizontal, the negative part of the dipolar anomaly becomes smaller with shallower dips (Figure 4.4c-e). For a sill (Figure 4.4(f)), a dipolar anomaly is visible at each end of the sill.

Remanence also affects anomaly shape. Palaeomagnetic studies have shown that the Upper Zone ferrogabbros contain remanent magnetisation with a similar inclination to the current magnetic field, but a different declination (Hattingh, 1986, 1989; Letts et al., 2009). The change in declination results in a predominantly strong positive anomaly (e.g. 1000 nT) with no clear negative (Figure 4.5a). In contrast, the Main Zone gabbros have a strong predominantly reversed remanent component (Q-ratios of 1 to 441 reported by Letts et al., 2009)) carried in small lamellae of titanium-poor titanomagnetites or nearly pure magnetite present in pyroxene and plagioclase that can cause negative anomalies (Letts et al., 2009) with amplitudes significantly lower than those for the Upper zone (Figure 4.5b). The presence of remanent magnetisation prevented the data from being reduced to the pole (MacLeod et al., 1993).

The interaction between separate anomalies can affect anomaly shapes. Synthetic two dimensional models, one in which the bodies dip steeply to the east (Figure 4.5c and d) and a second in which the dips are shallower (Figure 4.5e and f) illustrate how remanence in adjacent bodies influences the characteristics of a magnetic anomaly. For both the steeply and shallower dipping cases, the amplitude of the positive anomaly in the combined field has decreased by roughly 200 nT (Figure 4.5c, e, f) compared to the field calculated for the Upper Zone only (Figure 4.5a). The gradient of the positive anomaly's western flank is steeper in the combined anomaly. The amplitude of the negative part of the anomaly associated with the Main Zone also decreases and for both models the position of the negative peak has shifted towards the west by about 200 m.

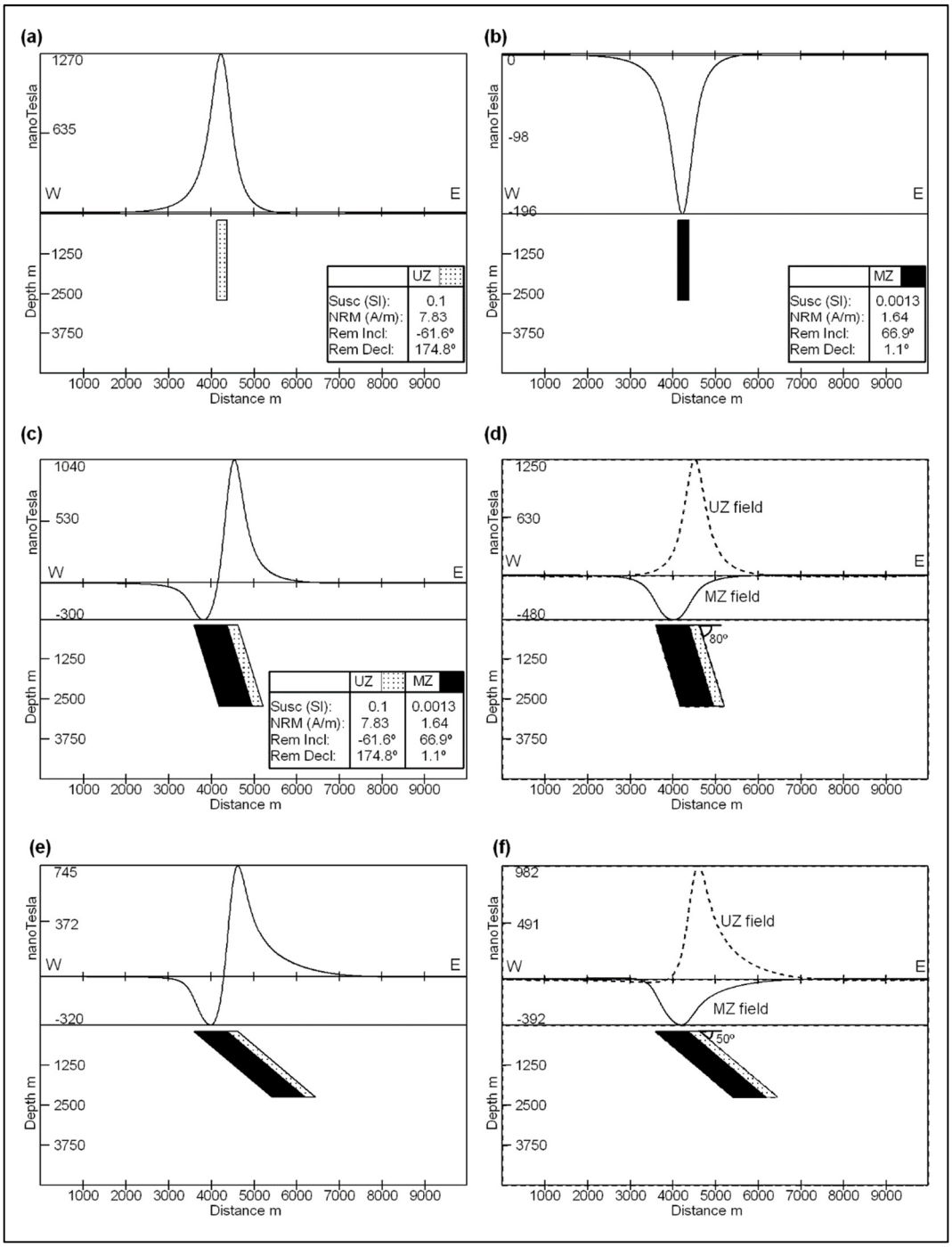


Figure 4.5 Synthetic two dimensional models showing the anomaly shapes expected for the Upper and Main Zones of the Bushveld Complex. Average remanent magnetisation parameters are from Letts et al. (2009). (a) Magnetic field for rocks in the Upper Zone; (b) Magnetic field of the remanently magnetised Main Zone rocks; (c) Combined magnetic anomaly calculated for adjoining steeply dipping Upper and Main Zone material; (d) Individual magnetic anomalies calculated for the Upper and Main Zones in (c) shown separately; (e) Combined magnetic anomaly calculated for adjoining shallower dipping Upper and Main Zone material; (f) Individual magnetic anomalies calculated for the Upper and Main Zones in (e) shown separately

Inspection of magnetic anomalies over the Rustenburg Layered Suite indicate characteristic signatures (here as Types I- VI) related to the depths, dips and shapes of their sources (Figure 4.6). Type I corresponds to Upper Zone rocks with mapped dips of 55º and 70º (Figure 4.6a) (Geological Survey of South Africa, 1978b). Type II (Figure 4.6b) corresponds very well to the shape of the reversely polarised magnetic anomaly calculated for the Main Zone (Figure 4.5b). An irregular or 'mottled' appearance caused by short wavelength anomalies characterises the Type III anomaly (Figure 4.6c). A number of factors can explain these anomalies, namely variations in composition, variable thicknesses of cover material and uneven terrain. The formation of magnetite in igneous rocks is sensitive to composition and crystallization temperature which is generally very heterogeneous, and can result in a mottled response on the magnetic data (Betts et al., 2003). Irregular topography can produce anomalies that are caused by lateral contrasts between magnetic materials underlying the topographic surface and nonmagnetic air (Grauch and Hudson, 2007). A further explanation may be the interaction between the strike direction of highly magnetic magnetite layers and flight line direction (Figure 4.7). Where the flight lines cross the magnetite layers perpendicularly the linear nature of the layers is clearly reflected in the magnetic field (Figure 4.7). If the flight lines cross a magnetite layer at an angle, the layered appearance degrades to a more circular shape (Figure 4.7). The large difference between the thickness of the magnetite layers (or packages of magnetite layers) and the flight line spacing means that layers can be easily missed or only partially crossed. The latter results in groups of localised anomalies that create a mottled appearance with circular, rather than linear anomalies.

Mafic rocks of the Rustenburg Layered suite are often buried beneath Bushveld granites. Type IV (Figure 4.6) represents smooth, broad anomalies typically associated with deeper-seated magnetic bodies, most probably Upper Zone magnetite-rich rocks (Figure 4.4b). The shape of the data extracted across anomaly Type V (Figure 4.6) is analogous to that of the horizontal slab (Figure 4.4f). Along a north-south striking profile the largest negative is located on the southern edge of the slab, and the largest positive on the northern edge. The geological map (Geological Survey of South Africa, 1978a) shows shallow-dipping magnetite layers coinciding with the positive anomalies. The magnetite layers dip shallowly (10º) to the centre of the anomaly, imitating a shallow sill. Type VI anomaly (Figure 4.6) is the result of the interaction between predominantly negative and predominantly positive magnetic anomalies (Figure 4.5c to f), and should not be interpreted as a negative anomaly caused by a separate remanently magnetised body.

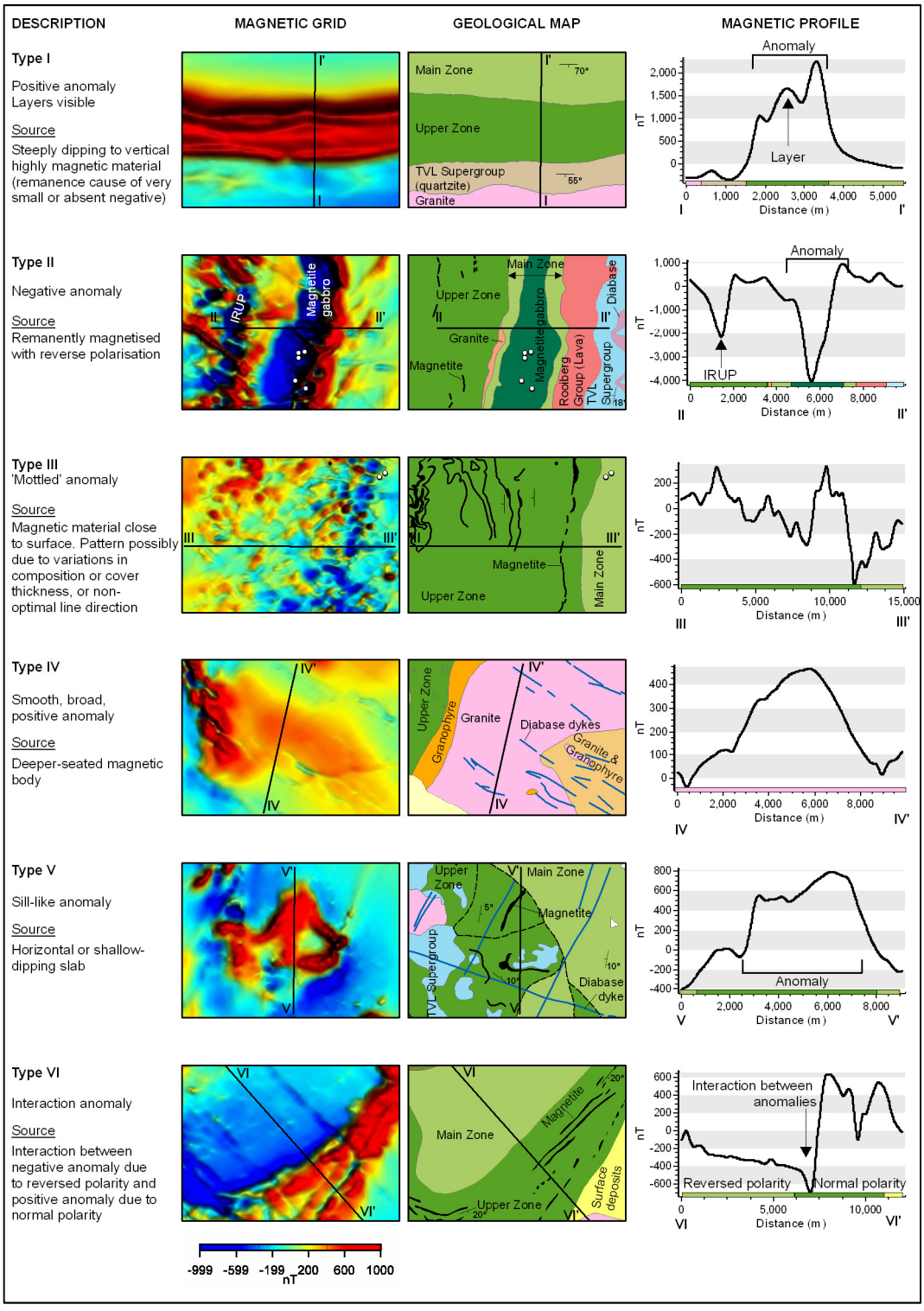


Figure 4.6 Anomaly types typically encountered in the Rustenburg Layered Suite based on correlation with detailed geologic mapping (Geological Survey of South Africa, 1974, 1978, 1981), rock properties (Hattingh, 1986, 1989; Letts et al., 2009) and modelling (Figure 4.4, 5.5 and 5.12). White dots indicate localities of palaeomagnetic samples with reversed magnetisation

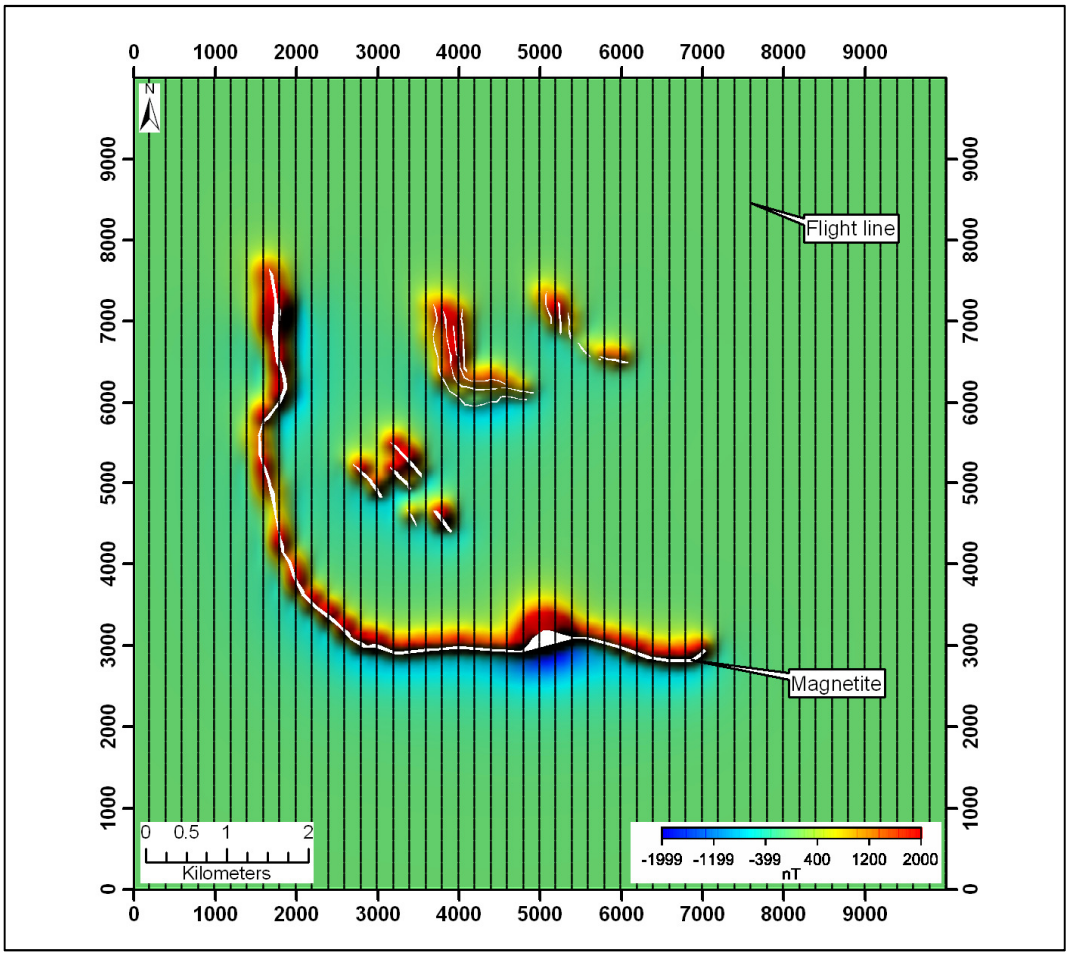


Figure 4.7 Magnetic field calculated along north-south directed lines spaced 200 m apart crossing different simulated configurations of magnetite layers (white lines). Data calculated along the lines were gridded using a cell size of 50 m, similar to the higher resolution observed magnetic data

4.5.1 Upper Zone

The magnetite-rich Upper Zone rocks are responsible for most of the very prominent positive magnetic anomalies (peak amplitudes ranging from 600 to 2400 nT) that outline the shape of the Rustenburg Layered Suite in the western (Figure 4.8 and Figure 4.9), eastern (Figure 4.10 and Figure 4.11) and northern lobes (Figure 4.12) of the Bushveld Complex. In places a series of adjacent, parallel linear anomalies is visible in the magnetic data, and although the height of the magnetometer above the ground precludes individual magnetite layers from being delineated, each linear anomaly probably represents the combined response of a number of magnetite layers. North of the Pilanesberg Complex the Upper Zone is characterised by a mottled appearance ('A', Figure 4.8) (similar to 'Type III', Figure 4.6). In many places layering is visible within the

mottled anomalies (‘B’ in Figure 4.8 point to a few examples). The Upper Zone rocks dip 20º to 35º away from the Main Zone outcrops in this area (Geological Survey of South Africa, 1974). Moving northwards, the positive magnetic anomalies become narrower and the amplitudes of the anomalies increase to almost 1500 nT above the background in places (‘C’ in Figure 4.8) and resemble ‘Type I’ (Figure 4.6). According to the geological map the dip remains shallow (20º to the east), but the magnetic data appear to refute this. The anomalies are more typical of steeper dipping magnetic bodies (Figure 4.4). The magnetic anomalies also show the Upper Zone to be narrower in this region than indicated on the geological map.

The magnetic data indicate that the ferrogabbros of the Upper Zone underlie the granites and granophyres (’Type IV’ in Figure 4.6) northeast of the Pilanesberg Complex (‘D’, Figure 4.8) The magnetic anomalies are smoother in this region than areas of outcrop, and the amplitudes decrease to roughly 400 nT above the background. Negative linear magnetic anomalies running through the area in a NW-SE direction are associated with syenite dykes of Pilanesberg age (~1.2 – 1.3 Ga) (‘E’, Figure 4.8).

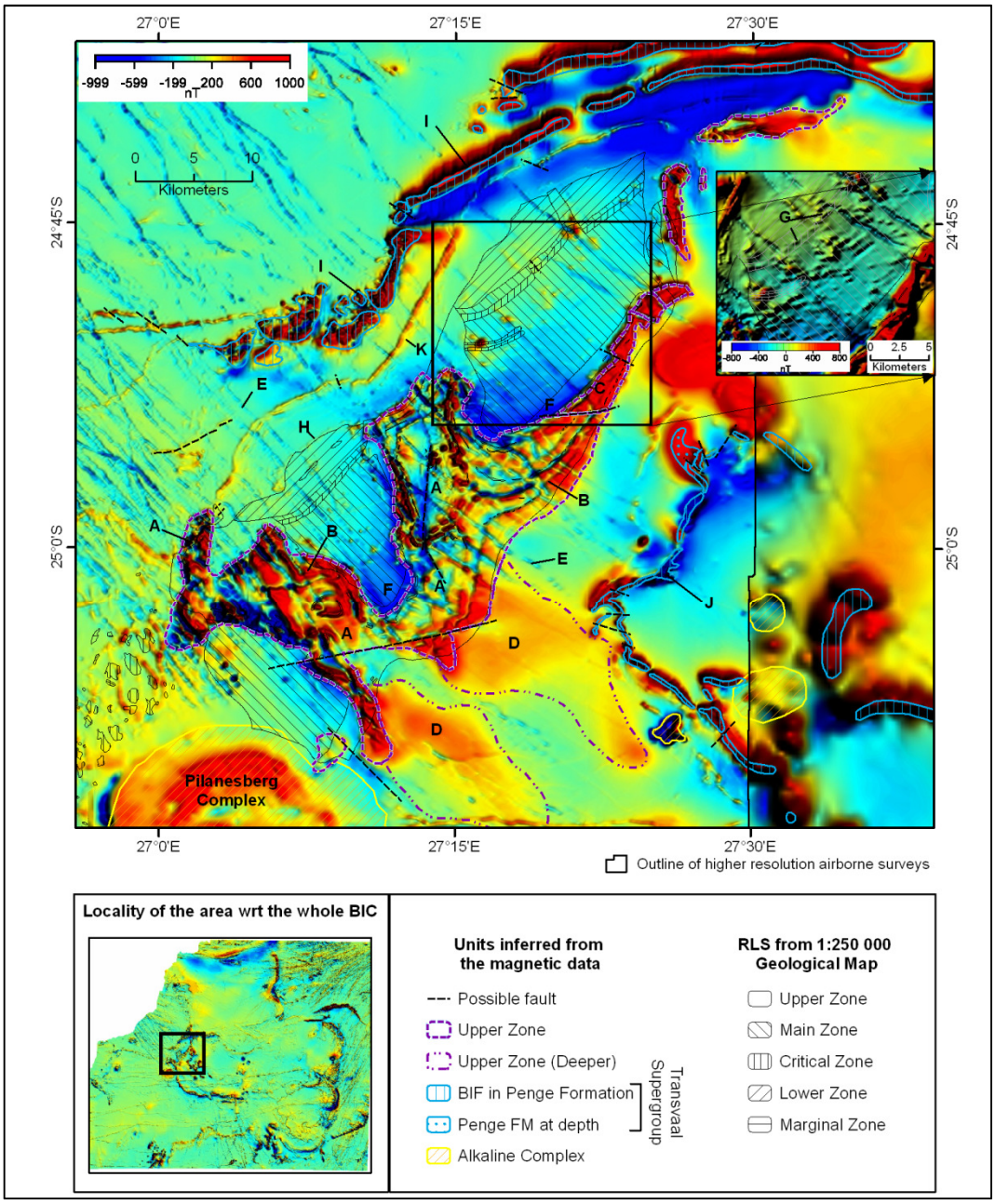


Figure 4.8 Mapped Rustenburg Layered Suite from the 1:250 000 Geological map overlain on the magnetic data for the western lobe of the Bushveld Complex, north of Pilanesberg. Outlines and faults inferred from the magnetic data are also indicated. A – mottled anomalies of the Upper Zone; B – layering in Upper Zone in mottled anomalies; C – high amplitude positive anomaly in Upper Zone; D – deeper-seated Upper Zone; E – syenite dykes; F – interaction between Upper and Main Zone anomalies; G – diabase

Southeast of the Pilanesberg Complex, the magnetic anomalies associated with the Upper Zone closest to the alkaline complex also appear 'mottled' ('a', amplitudes of 1300 nT, Figure 4.9). Changes in width of the Upper Zone anomalies correspond to locations of mapped faults (a-d, Figure 4.9) (Geological Survey of South Africa, 1981). East of an inferred fault (d, Figure 4.9) the Upper zone anomaly widens and more layering is visible. The anomaly package also has a more bimodal nature, with the northern part consisting of positive anomalies, whereas the values decrease significantly in amplitude to the south (-1200 nT, 'e', Figure 4.9). The first change can be observed to the south of a prominent layer within the larger anomaly package. Close to the southern margin of the Upper Zone rocks, negative lineaments coincide with mapped magnetite layers. For magnetic minerals to retain remanent magnetisation, the grains must be sufficiently small. This may indicate a change in the size of the magnetite grains in the area. If this is the case the magnetite layers may have recorded a reversal in the magnetic field. In this area the southern margin of the Upper Zone inferred from the magnetic data is located roughly 700 m to the south of the margin indicated on the geological map (Geological Survey of South Africa, 1981). In general the inferred Main Zone – Upper Zone contact corresponds well to that indicated on the geological map, with the largest differences ranging between 400 m and 700 m.

In the eastern lobe, south of the Steelpoort Fault (SF, Figure 4.10), magnetic anomalies caused by Upper Zone rocks also appear 'mottled' ('1', Figure 4.10). Mapped magnetite layers are not clearly visible, probably due to the flight line orientation being parallel to the trend of the layers (as in Figure 4.7). The eastern margin of the Upper Zone outcrop, or where the Upper Zone is close to the surface, is marked by a small negative anomaly (-400 nT, labelled '2' in Figure 4.10), similar to what can be expected along the eastern edge of a horizontal or shallow-dipping slab (Figure 4.4(f)). In places the negative anomaly is also visible along the southern margin of the magnetic rocks ('3', Figure 4.10). Granites and granophyres cover the western extension of the mafic rocks and in this area the amplitude of the magnetic anomalies are still high (400 nT), but very smooth ('4', Figure 4.10), resembling 'Type IV' anomalies (Figure 4.6). South of the Laersdrif Fault (LF, Figure 4.10) numerous dykes intruded into the Upper Zone rocks and create a NW-SE striking 'fabric' within the 700 nT magnetic anomalies ('5', Figure 4.10). Towards the southern extent of the mapped outcrop a large negative anomaly (reaching a peak amplitude of -2100 nT) obscures the anomalies associated with the Upper Zone ferrogabbros ('6', Figure 4.10). The negative anomaly is inferred to be caused by a deeper-seated body similar to the source of the Wanhoop anomaly, modeled as a westward dipping mafic sill located at about 1000 m below the surface (Blom, 1989). A borehole revealed mostly gabbronorite, pyroxenite and harzburgite (Schurmann, 1992). On the basis of the magnetic parameters used in the modelling, Blom (1989) stated that it

was tempting to consider this body as part of the Rustenburg Layered Suite, and that it cooled through the Curie temperature at the same time as the Main Zone. In the Mineral Range area very prominent negative anomalies (reaching -2500 nT) possibly related to reversely magnetized iron-rich ultramafic pegmatoids (IRUPS) are also visible further to the east ('7', Figure 4.10). IRUPs are generally concerned to be derived from Upper Zone magma during the development of the Upper Zone (Reid and Basson, 2002).

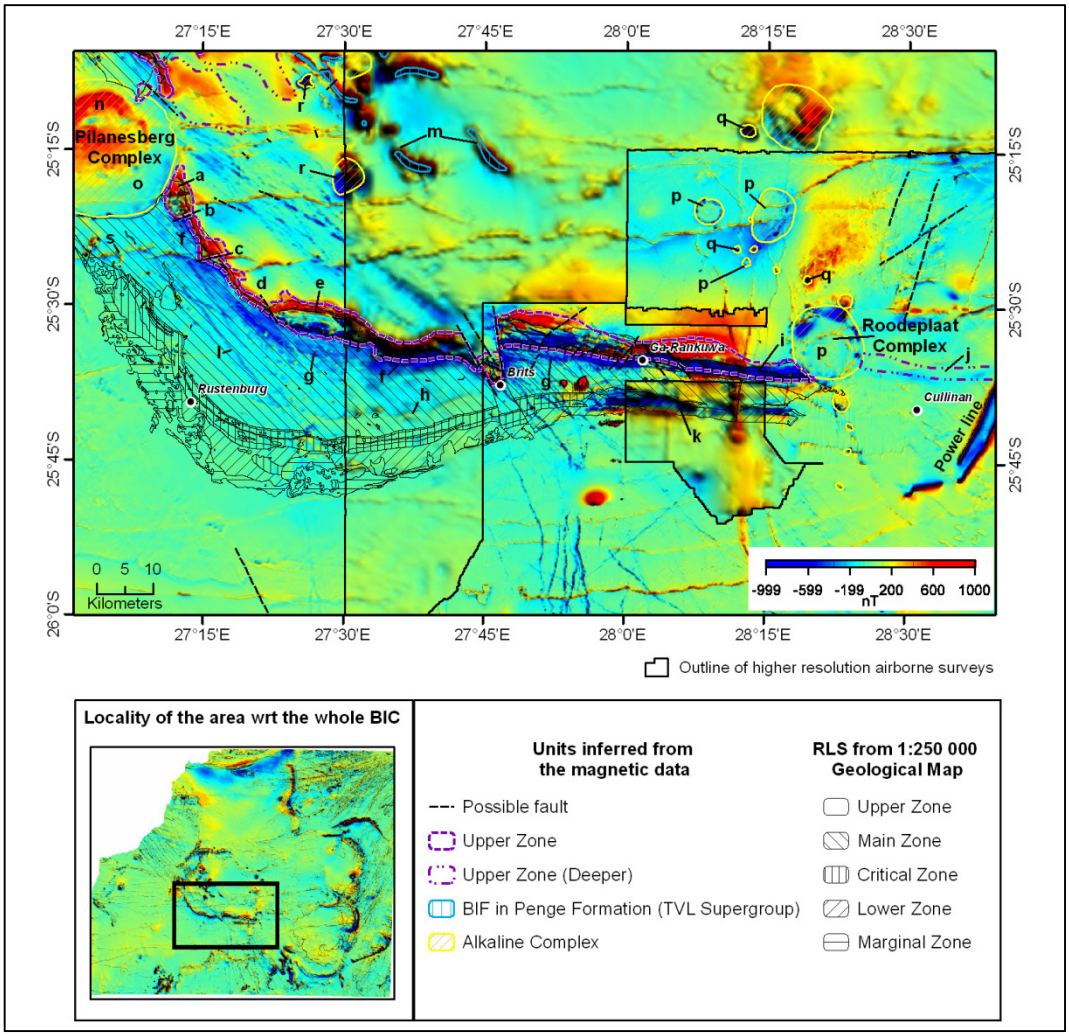


Figure 4.9 Mapped Rustenburg Layered Suite from the 1:250 000 Geological map overlain on the magnetic data for the western lobe of the Bushveld Complex, south of Pilanesberg. Outlines and faults inferred from the magnetic data are also indicated. a – mottled anomalies of the Upper Zone; b, c, d – inferred faults; e – Upper Zone anomaly splits into positive northern part and negative part in south; f – interaction between Upper and Main Zone anomalies; g – negative linear anomalies within Main Zone; h – anomaly close to Main Zone – Critical Zone boundary; i – reversely polarised magnetic body, possibly in Main Zone; j – possible continuation of Rustenburg Layered Suite rocks; k – Middelwater Sill

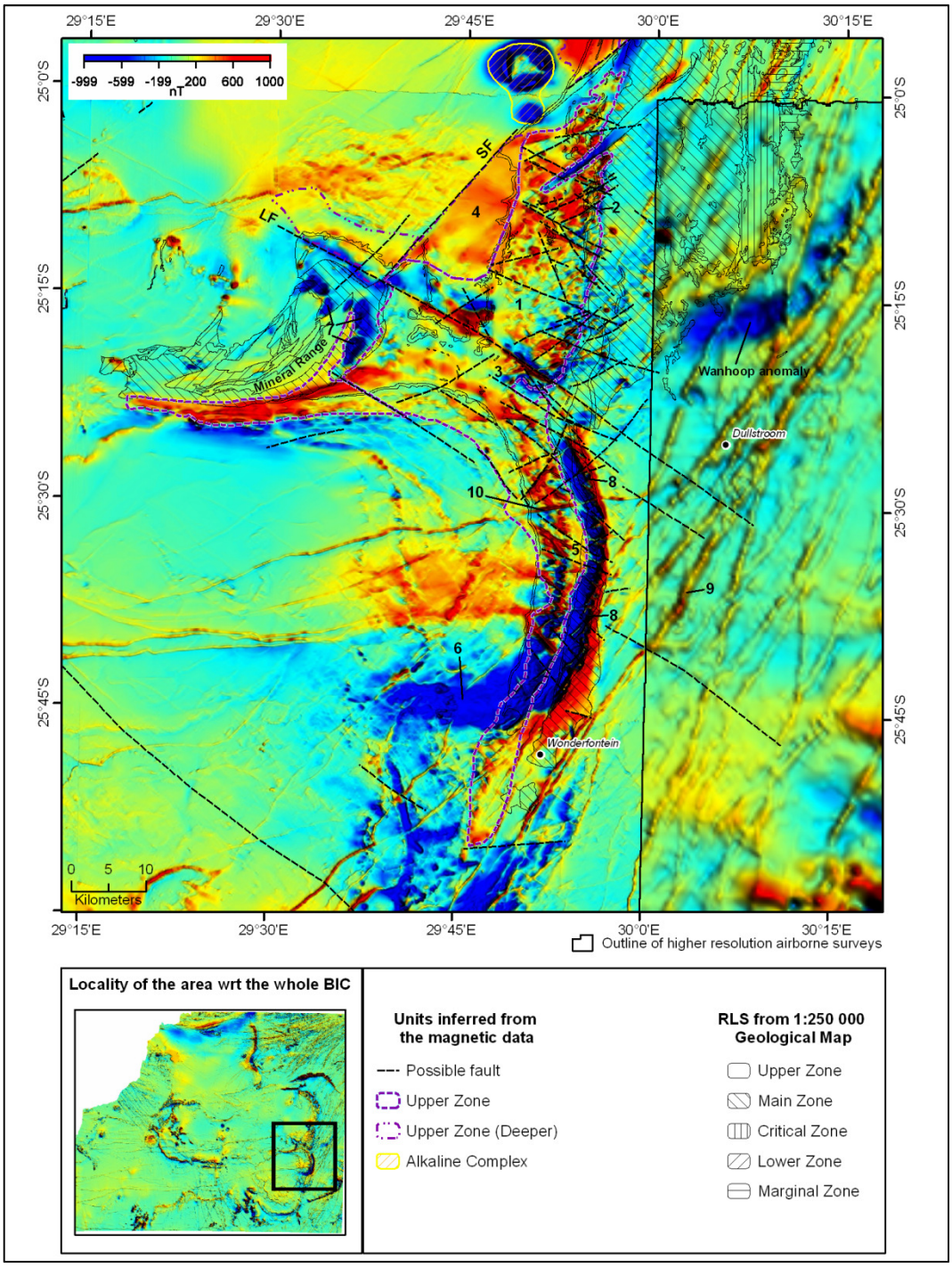


Figure 4.10 Mapped Rustenburg Layered Suite from the 1:250 000 Geological map overlain on the magnetic data for the eastern lobe of the Bushveld Complex, south of the Steelpoort Fault. Outlines and faults inferred from the magnetic data are also indicated. SF - Steelpoort Fault; LF - Laersdrif Fault. 1 – mottled anomalies of the Upper Zone; 2,3 – negative anomaly at eastern and southern boundaries of Upper Zone; 4 – deeper-seated Upper Zone; 5 – dykes; 6 – deep-seated remanently magnetised body; 7 – possible iron-rich pegmatoids; 8 – reversely polarised magnetic body, possibly in Main Zone

North of the Steelpoort Fault (SF, Figure 4.11), most Upper Zone anomalies reflect sill-like structures, with high amplitude anomalies (800 to 1200 nT) at the edges of the sill (anomaly 'Type V', Figure 4.6). This is consistent with the shallow 10º-15º dip of the mafic rocks in this area (Geological Survey of South Africa, 1978a). Northeast-trending linear magnetic lows within the main highs ('i', Figure 4.11) reflect magnetite layering within the Upper Zone. In places the magnetic values are very low (-500 nT) due to the presence of updomed Transvaal Supergroup rocks ('ii', Figure 4.11). Where the ferrograbbros lie at depth beneath granites and granophyres, the anomalies are attenuated (700 nT) ('iii' in Figure 4.11).

West of the Wonderkop Fault (WF, Figure 4.11) and Stofpoort Fault (StF, Figure 4.11), the Upper Zone is characterised by narrow, linear, east trending, very high amplitude anomalies (3500 nT above the background) with clear layering ('iv' in Figure 4.11). In this area the Bushveld rocks to dip 70º to the south (Figure 4.3). In the west, the upper zone disappears under the Karoo Supergroup sandstones and basalts on the geologic map (Figure 4.3), but the magnetic map shows it to continue for another roughly 11 kilometres ('vii,' Figure 4.11).

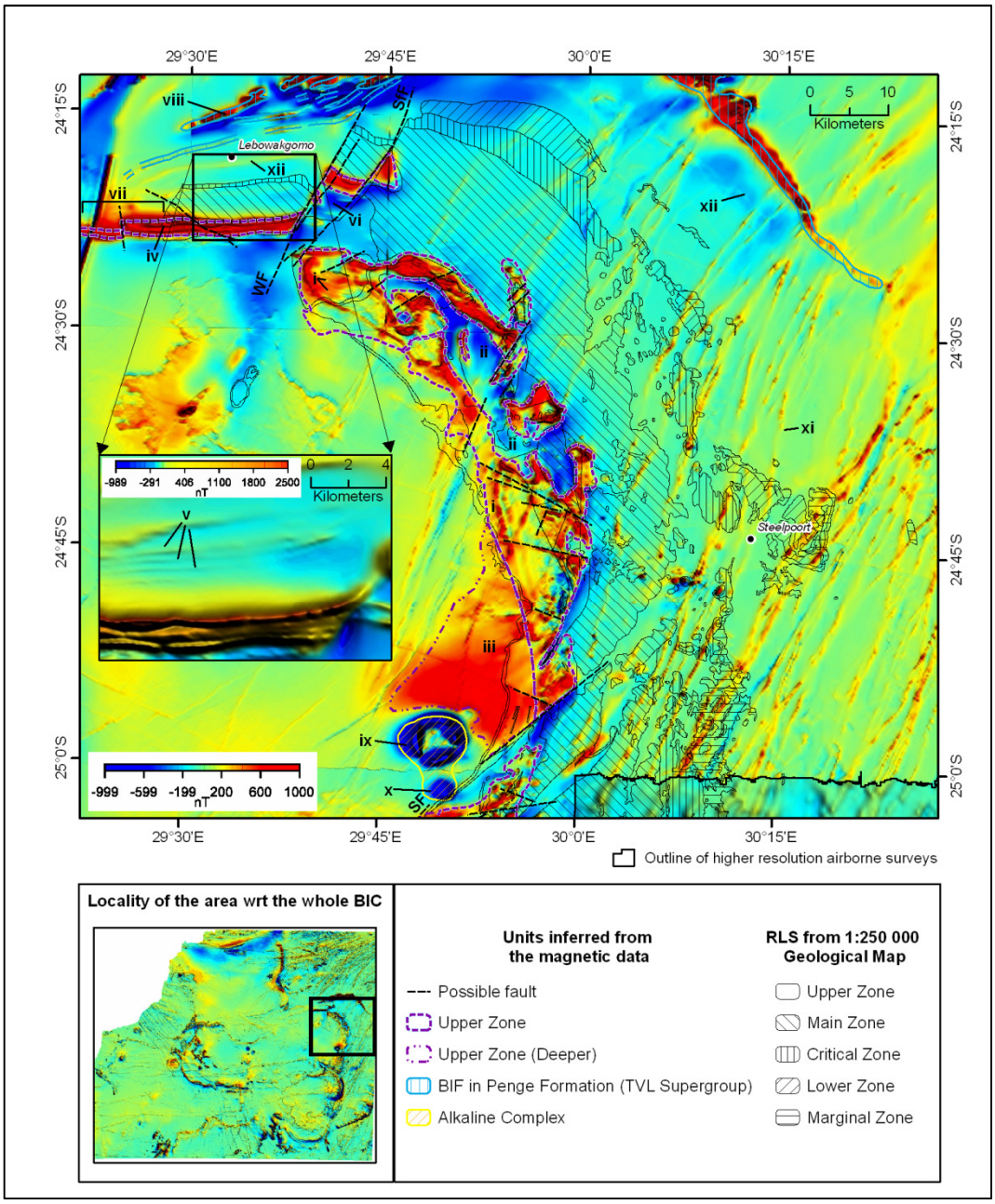


Figure 4.11 Mapped Rustenburg Layered Suite from the 1:250 000 Geological map overlain on the magnetic data for the eastern lobe of the Bushveld Complex, north of the Steelpoort Fault. Outlines and faults inferred from the magnetic data are also indicated. The inset shows an enlarged image of the Main Zone west of the Wonderkop Fault. SF - Steelpoort Fault; WF - Wonderkop Fault; SfF – Stofpoort Fault. i – shallow-dipping Upper Zone; ii – low magnetic intensities due to Transvaal Supergroup updoming; iii - deeper-seated Upper Zone; iv – steeply dipping Upper Zone with layering visible; v – layers within Main Zone; vi – interaction between Upper and Main Zone anomalies

The Upper Zone in the roughly north-south striking section of the northern lobe (Figure 4.12) is responsible for a very prominent mostly positive magnetic anomaly, with amplitudes changing from 1575 nT in the north to 150 nT near Mokopane in the south. Dips of between 15º and 20º to the west are indicated on the geological map (Geological Survey of South Africa, 1985). The magnetic data clearly shows the Upper Zone to extend at least 10 km further to the north than indicated on the geological map ('α', Figure 4.12). From the northern point of the anomaly down to about 23º45'S the anomaly resembles 'Type I' in Figure 4.6, but due to the numerous east-west striking dykes that cut through the area any possible layering is obscured. Exact ages for these dykes are unknown, but they are shown as Vaalian age on the Geological map (Geological Survey of South Africa, 1985), which puts them at roughly 2.2 Ga (Hartzer et al, 1998). South of 23º45'S the amplitude decreases to 650 nT and lower, and the anomaly becomes broader and smoother ('β', Figure 4.12), more representative of 'Type IV' (Figure 4.6). This change in magnetic signature coincides with the point where the Rustenburg Layered Suite starts to curve to the west. The Bellevue borehole (BV-1, Figure 4.12) encountered Upper Zone rocks at a depth of 85 m and extending down to 1580 m (Ashwal et al., 2005). The magnetic data shows the westward bulge of the mafic rocks to be more pronounced than drawn on the geological map. Mapped Upper Zone rocks in the bulge coincide with a very high amplitude (-2100 nT) negative anomaly. The positive anomaly associated with the Upper Zone continuing from the north runs almost completely to the west of the mapped Upper Zone rocks in the bulge. Magnetite layers close to the base of the Upper Zone cause positive anomalies within the negative anomaly ('γ', Figure 4.12), confirming that the Upper Zone rocks are indeed associated with the negative anomaly. In the rest of the Bushveld Complex the Upper Zone is characterised by predominantly positive magnetic anomalies. Reversed polarisations at the bottom of the Upper Zone have been measured in the eastern lobe. Magnetite exsolution lamellae were observed in pyroxene and plagioclase in the Upper Zone of the northern lobe which could be responsible for carrying the remanent magnetisation (Letts et al., 2009). The magnetite layers did not retain the reversely polarised magnetisation because of the large grain sizes of the magnetite minerals. It is not clear why the reversely polarised remanent magnetisation at the base of the Upper Zone is only present in this part of the north-south striking section (Figure 4.12).

Moving southward, the Rustenburg Layered Suite swings back to the east and the magnetic field abruptly decreases from more than 500 nT to 250 nT ('δ', Figure 4.12). Further to the south the anomaly amplitude increases equally abruptly from 220 nT to about 420 nT ('ε', Figure 4.12). Both of these sudden changes coincide with faults indicated on the geological map. The southern fault is known as the Ysterberg-Planknek fault and may form part of the Thabazimbi-Murchision Lineament (TML) that has been

reactivated at different times in its geological history (Good and De Wit, 1997). This section of the TML underwent reverse faulting and strike-slip movement in the Archaean with estimated vertical displacement of 10 km and dextral strike slip of 8-10 km (Good and De Wit, 1997). If the interpretation of a graben in this area is correct, this part of the TML may have been reactivated after the intrusion of the Bushveld Complex.

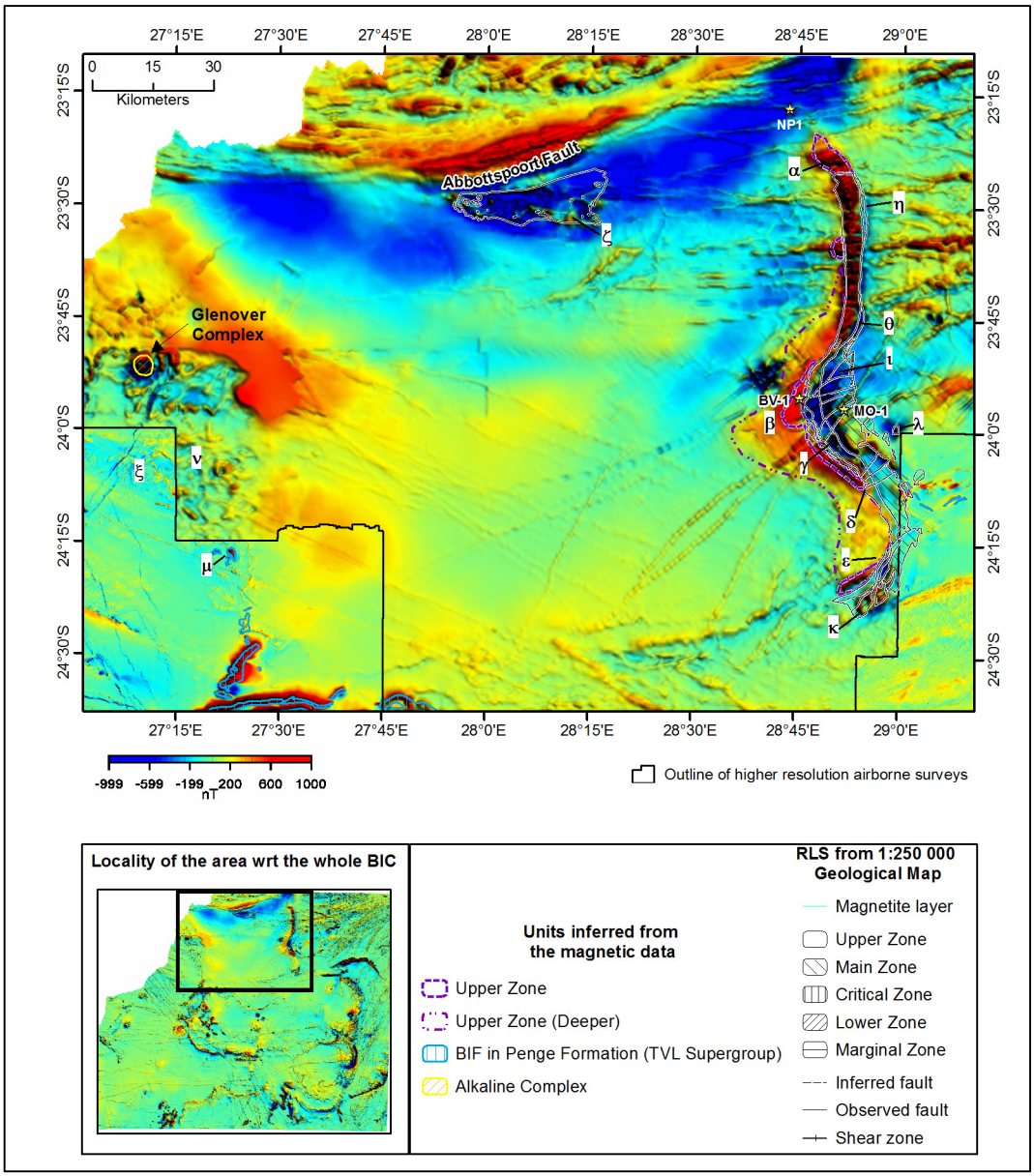


Figure 4.12 Mapped Rustenburg Layered Suite from the 1:250 000 Geological map overlain on the magnetic data for the northern lobe of the Bushveld Complex. Outlines and faults inferred from the magnetic data are also indicated. α,β, γ –Upper Zone; δ, ε – possible edges of a graben; ζ – magnetite layers in the Upper Zone; η, θ, ι – interaction between Upper and Main Zone anomalies ; κ – Lower Zone; λ – negative anomaly correlating with Lower Zone); μ – BIF; ν, ξ – dolerite sills

The Villa Nora section of the northern lobe consists of gabbro, anorthosite, ferrograbbro and norite that belong to the Upper Zone (Brandl, 1986). However, other authors show both the Main and Upper Zones to be present (Kruger, 2005; van der Walt, 1978). Narrow positive anomalies in the south of this section ('ζ' in Figure 4.12) correlate with mapped magnetite bands, but otherwise the magnetic field is predominantly negative in this area with maximum negative amplitudes of -1300 nT.

Sediments of the Waterberg Group cover the area between the north-south striking section and the Villa Nora section. Borehole NP1 (Figure 4.12) encountered olivine gabbros at depths beneath about 1300 m of sediments. Simple modelling shows that if the Upper Zone is present in this area, it is probably thinner than 100 m since it is not responsible for any clear anomalies on the regional magnetic data set.

4.5.2 Main Zone

With the exception of a few instances where 'Type II' anomalies are present low intensity magnetic values (-20 nT to -150 nT) characterise the Main Zone. The rocks of the Main Zone have very low magnetic susceptibilities (0.00025 – 0.0089 SI), but have a strong remanent magnetisation component (0.02 – 28.87 A/m) (Letts et al., 2009). The measured reversed magnetic inclinations for rocks in this zone range mostly between 60º and 80º and declinations between roughly 330º and 40º (Letts et al., 2009), and will therefore result in predominantly negative anomalies. Close to the contact with the Upper Zone, a narrow negative magnetic anomaly resembling 'Type VI' (Figure 4.6) is often visible as a result of the interaction between the magnetic fields caused by the highly magnetic Upper Zone, and the remanently magnetised Main Zone (eg. 'F', Figure 4.8 and 'f', Figure 4.9).

Along the southern part of the western lobe, negative magnetic lineaments express layering in the Main Zone. The layering is visible from close to the contact with the Upper Zone where it has an average amplitude of roughly -450 nT (e.g. 'g', Figure 4.9), down to the mapped contact with the Critical Zone where the amplitude is in the region of -200 nT. Layering is more visible where the RLS strikes east-west due to better sampling of the anomaly along the perpendicular north-south directed flight lines (Figure 4.7), and also in the curve where the strike changes to northwest-southeast. The anomalies are all negative indicating the possible presence of reversely magnetised needles of magnetite in plagioclase and pyroxene of the gabbronorite.

Rhythmic layering has been observed in the Main Zone (Nex et al., 1998) but is not as prolific as in the Critical and Upper Zones. Two of the most prominent units of layering in the Rustenburg area comprise interlayered anorthosite and gabbronorite, and interlayered gabbronorite and microgabbronorite. It is unknown whether this layering is

related to the negative lineaments observed on the magnetic data. These negative anomalies can be separated from the ubiquitous negative anomalies caused by syenite dykes ('l', Figure 4.9) on the basis that they follow the trend of the Bushveld rocks, whereas the dykes tend to be very linear and strike NW-SE. This also makes it more difficult to delineate layering where the Main Zone trends NW-SE as it is the same direction as the dykes. Two closely spaced relatively prominent anomalies are visible about 4 km to the north of the Main Zone-Critical Zone contact ('h', Figure 4.9). Campbell (2011) labelled these anomalies as 'mottled anorthosite stratigraphic markers'. East of the Brits graben (Figure 4.9) linear anomalies associated with layering within the RLS and those caused by syenite dykes are indistinguishable. This is due to a change in strike of the dykes to the WNW-ESE trend of the RLS.

Between Ga-Rankuwa and the Roodeplaat Complex, a very high amplitude negative ('Type II', Figure 4.6) anomaly (-1500 to -12 000 nT) with a positive peak on the southern side runs along the south of the inferred Upper Zone rocks ('i', Figure 4.9). This anomaly can be explained by a simple model with an inclination of 60º, declination of 40º, an NRM of 54.6 A/m and susceptibility of 0.012 SI of a 250 m thick layer located between the Upper and Main Zones. This direction and intensity is consistent with palaeomagnetic values measured in a magnetite gabbro in the Eastern Lobe ('8', Figure 4.10) (Letts et al., 2009). However, the maximum measured NRM was 28.87 A/m and the average for the ten samples was 16.383 A/m. This is much lower than the modelled value and may indicate a difference in the composition or magnetic grain size. Increasing the thickness of this layer and decreasing the NRM did not correctly model the steep gradients of the anomaly flanks. A lower amplitude anomaly (~-250 nT) inferred to be a continuation of this anomaly underneath younger cover material continues east of the Complex ('j', Figure 4.9) and can be followed to approximately 28º45'E. The modeled body needs to be at a depth of about 2.5 km to cause an anomaly of -250 nT. Mafic rocks similar to the Critical Zone of the Bushveld Complex are observed at a depth of ~520 m below the surface in a borehole at the Cullinan diamond mine (Figure 4.9) (Cawthorn and McKenna, 2006).

In the eastern lobe, south of the Steelpoort Fault only regional magnetic coverage exists for most of the mapped Main Zone rocks. South of the Laersdrif Fault a very high amplitude negative 'Type II' (Figure 4.6) anomaly (-2500 nT to -4000 nT) with positive values (1500 nT) along its eastern edge coincides with the mapped Main Zone rocks ('8', Figure 4.10). It coincides with the fine- to medium-grained magnetite gabbro located underneath the Pyroxenite Marker (Geological Survey of South Africa, 1978b; Van der Merwe, 2007). Measured susceptibilities are not very high, generally of the order of 0.004 SI, but the Koenigsberger ratios are very large indicating the presence of a very strong

remanent magnetisation component (Letts et al., 2009). Petrographic and palaeomagnetic analysis indicates that the carriers of remanence in the rocks sampled in this anomaly were single or pseudosingle domain magnetite grains that are present as lamellae in plagioclase and pyroxene (Letts et al., 2009). The inclination and declination of the remanent magnetisation are very similar to the values assigned to the layer in simple models created to examine the large negative anomaly observed in the southeastern part of the western lobe ('i' in Figure 4.9). This may suggest that a similar fine grained magnetite gabbro as observed here in the eastern lobe may be present close to the top of the Main Zone in the western lobe.

The magnetite gabbro continues north of the Laersdrif Fault (Geological Survey of South Africa, 1978b; Van der Merwe, 2007) with no clear negative magnetic expression. The NRM intensity for the samples in the northern area is much lower than the intensities in the southern area (Letts et al., 2009). The reason for this difference is unclear as neither a difference in magnetite grain size between the northern and southern samples, nor an increase in ilmenite from the north to the south was reported. In the northern part of the eastern lobe, the area that corresponds to mapped Main Zone rocks is once again characterised by quiet magnetic data. However, to the west of the Wonderkop Fault, a number of layers are visible ('v', inset Figure 4.11), consistent with reversely magnetized, steeply dipping layers (Figure 4.13).

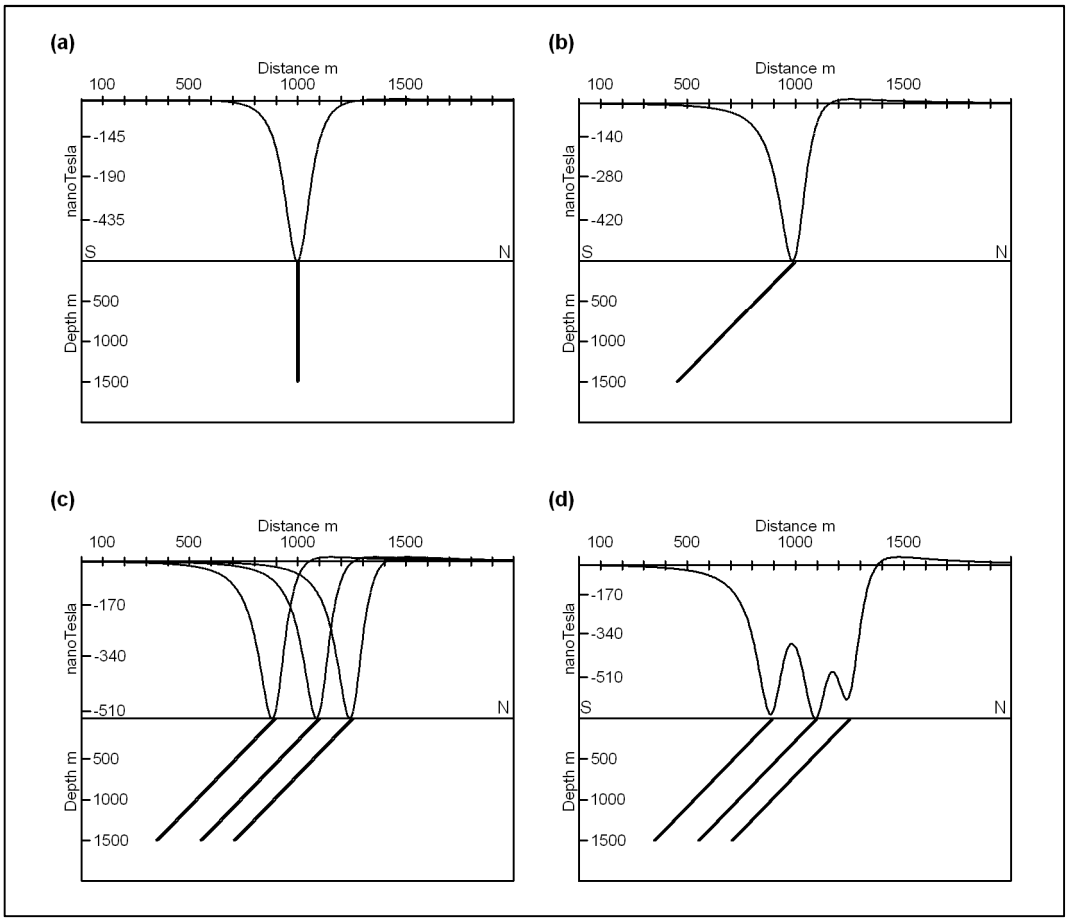


Figure 4.13 Synthetic magnetic fields calculated for (a) a vertical body, (b) a body dipping 70º to the south, (c) three adjacent southward dipping bodies, showing their individual contributions to the field, and (d) three adjacent southward dipping bodies, showing their combined response. All of the bodies are remanently magnetised, with an inclination of 58º and a declination of 19º.

South of the high amplitude positive Upper Zone magnetic anomalies between the Wonderkop and Stofpoort faults and also east of the Stofpoort Fault relatively strong negative anomalies (-550 nT) are present ('vi', Figure 4.11), likely due to reversely magnetised Main Zone rocks to the south of the Upper Zone in these areas. The interaction between the magnetic anomalies of the Main and Upper Zones will result in a negative along the southern margin of the Upper Zone ('Type VI', Figure 4.6). The interpretation of Main Zone rocks between the Transvaal Supergroup rocks (TVL, Figure 4.11) and the Upper Zone for the area between the two faults is similar to Scoon (2002), although the locality of the Upper Zone inferred from the magnetic data differs. The magnetic values to the east of the Stofpoort Fault and all the way down to the Steelpoort Fault have low intensities (-100 nT to -200 nT), with numerous NE-SW striking linear

anomalies associated with dykes that cut through the area. It is not possible to delineate the Critical Zone – Main Zone boundary from the magnetic data.

In the northern lobe (Figure 4.12) the Main Zone rocks are located to the east of the Upper Zone in the north-south striking section. In the north of this section ('η', Figure 4.12) the mapped Main Zone coincides with a -350 nT negative anomaly. Moving south the amplitude of this anomaly increases to -650 nT (θ', Figure 4.12). These anomalies correspond to 'Type VI' (Figure 4.6). In the westward bulge between borehole BV-1 and MO-1 ('ι', Figure 4.12) the anomaly widens to roughly 5.5 km from 1 km further to the north. Part of the negative anomaly is associated with the Upper Zone as discussed in the previous section.

4.5.3 Critical and Lower Zones

The Critical Zone does not have a clearly distinguishable magnetic expression on the 200 m line spacing data, but Campbell (2011) reported the detection of magnetic markers in the hanging wall of the Merensky Reef by helicopter aeromagnetic data collected at a line spacing of 50 m and a sensor height of 30 m. Even on the 200 m line spacing data linear features were visible in the western lobe ('G', Figure 4.8 inset). The northwestern edge of the mapped Lower Zone in the western lobe north of the Pilanesberg Complex coincides with small positive anomalies on the magnetic data ('H', Figure 4.8) associated with diabase that appears to have intruded into the Magaliesberg Quartzites and is located a little below the Magaliesberg Formation – Rustenburg Layered Suite contact. It is relatively persistent in the western lobe.

Lower Zone pyroxenites are present in the southern extreme of the north-south striking section of the Northern Lobe, and correlate with positive anomalies n the magnetic data ('κ', Figure 4.12). Occurrences north of Mokopane are not associated with clear magnetic anomalies, except at 'λ' (Figure 4.12) where it coincides with a circular negative anomaly.

4.5.4 Non-Bushveld Complex Rocks

Highly magnetic rocks that are not part of the Bushveld Complex cause a number of prominent anomalies in the proximity of, and sometimes intersecting the mafic layered rocks of the Bushveld Complex. The most obvious are very high amplitude anomalies (6500 nT – 8500 nT) associated with the banded iron-formation (BIF) of the Penge Formation located close to the base of the Transvaal (TVL) Supergroup. These anomalies are visible to the north of both the western and eastern lobes of the Bushveld Complex ('I', Figure 4.8, 'viii', Figure 4.11, 'μ', Figure 4.12). In the western lobe BIF also outcrops around the Crocodile River Fragment ('J', Figure 4.8 and 'm', Figure 4.9), a succession of Transvaal Supergroup rocks completely surrounded by Bushveld granites.

The biggest difference between the BIF and Upper Zone anomalies is the amplitude, but other than that it is very difficult to distinguish between them.

A very narrow positive anomaly of roughly 400 nT to 500 nT runs between the Penge Formation and the mapped mafic rocks of the BIC in the northwest ('K', Figure 4.8). It corresponds to mapped quartz arenites of the Daspoort Formation that occurs higher up in the Transvaal Supergroup than the Penge Formation (Geological Survey of South Africa, 1974). The magnetic anomaly associated with the Daspoort Formation can be attributed to subordinate ironstones that are present in places in this formation (Eriksson et al., 2006). Anomalies corresponding to the same formation are also visible in the northeast ('xii', Figure 4.11), but their amplitudes are much smaller, generally between 30 nT and 50 nT, reaching a maximum of 90 nT south of Lebowakgomo. If one is not careful, these anomalies may be erroneously interpreted as layering in the Critical or Main Zone of the Rustenburg Layered Suite.

An east trending linear negative anomaly ('k', Figure 4.9) is associated with the Middelwater Sill, a pre-Bushveld layered sill that has been mapped in this area (Roberts, 1992). Palaeomagnetic analysis provided an inclination of 84º, declination of 202º and intensity of 4.697 A/m for the remanent magnetisation component of the meta-quartz-dolerites of this sill.

Mottled anomalies visible on the magnetic data between Thabazimbi and the Glenover Complex ('v', Figure 4.12) correlate with Mokolian dolerite sills that are ubiquitous in this area and are not interpreted as 'Type III' (Figure 4.6) anomalies of the Bushveld Complex. The different character of these anomalies from the Bushveld anomalies is visible where higher resolution data are available ('ξ', Figure 4.12).

Between 1450 Ma and 1200 Ma alkaline volcanic and plutonic activity took place in the Kaapvaal Craton, giving rise to the Pilanesberg Alkaline Province located predominantly in the western part of the Bushveld Complex (Verwoerd, 2006). The most prominent is the Pilanesberg Complex that intruded into the western lobe of the Bushveld Complex. It is characterised by a circular positive anomaly ('n', Figure 4.9) with an average amplitude of roughly 500 nT, reaching 800 nT in places, ringed by a magnetically quiet area ('o', Figure 4.9). A number of complexes consist of a ring of negative magnetic values, including the Roodeplaat Complex ('p', Figure 4.9) and the Spitskop Complex ('ix', Figure 4.11). The negative values range from -200 nT for some complexes to -500 nT for others. For the Spitskop Complex the maximum is almost -4500 nT. Situated immediately to the south of the Spitskop Complex is a completely negative anomaly with a maximum amplitude of -1650 nT ('x', Figure 4.11). Similar anomalies are also visible to the north and northeast of the Roodeplaat Complex ('q', Figure 4.9). The final type is dipolar

anomalies with very strong negative components ('r', Figure 4.9 and the 'Glenover Complex' in Figure 4.12). The prevalence of negative magnetic anomalies attests to the presence of remanent magnetisation. Variations in anomaly shapes e.g. completely negative versus dipolar or even predominantly positive as in the case of the Pilanesberg Complex, may be due to shifts in magnetic polarisation, or simply differences in composition as certain magnetic minerals and grain sizes are better at retaining remanent magnetisation.

Three main sets of linear magnetic anomalies intersect the magnetic anomalies caused by the Bushveld mafic rocks. In the west a set of northwest-striking negative magnetic anomalies can be followed from the border with Botswana, continuing through the Bushveld Complex north and southeast of the Pilanesberg Complex (Figure 4.2). Anomaly amplitudes vary from -20 nT to -500 nT. These dykes constitute the Pilanesberg dyke swarm, which forms part of the Pilanesberg Alkaline Province. It cuts through the Bushveld Complex as can be seen in Figure 4.8 ('E') and Figure 4.9 ('l'). Northeast-striking positive lineaments (200 to 1000 nT amplitudes) in the east ('9', Figure 4.10 and 'xi', Figure 4.11) belong to the Olifants River dyke swarm (Uken and Watkeys, 1997). The dykes intruded into the Bushveld rock and are therefore younger than the Bushveld Igneous Complex. Palaeomagnetic data established that they are of Proterozoic age (~1.9 Ga) (Letts et al, 2005) and not Karoo age (~182 Ma, Uken and Watkeys, 1997) as originally thought. East-west trending dykes are the cause of the positive magnetic lineaments that can be followed through the whole Bushveld Complex (Figure 4.2) and in fact extend through the entire Kaapvaal Craton. They cut through the magnetic anomalies of the mafic Bushveld rocks ('s' in Figure 4.9 south of the Pilanesberg Complex, '10' in Figure 4.10) suggesting that they are younger than the Bushveld mafic rocks.

4.5.5 Faults and IRUPs

The Rustenburg Layered Suite is economically important, and features that may affect the continuation of economic reefs are as important as the reefs themselves. Campbell (2006, 2011) showed the delineation of these 'loss-of-ground' features from very high resolution magnetic data he had at his disposal, but the 200 m line spacing data collected at 80 m flying height can also be used to detect many of these features (Figure 4.14). Lineaments (positive and negative) and IRUPs were directly drawn in, while faults were inferred where magnetic anomalies were displaced, or where the amplitudes of anomalies suddenly changed. Figure 4.15 shows a comparison between the (a) data used by Campbell (2006) and (b) data collected for the same area at lower resolution. Features identified by Campbell (2006) on the high resolution data were pointed out on the lower resolution where they can be delineated. There is a clear difference in the detail visible on the two data sets, for example on the higher resolution data the two

stratigraphic marker horizons in the north can be followed continuously as separate anomalies up to the easternmost Pilanesberg dyke. On the lower resolution data the markers are visible but difficult to detect in places. All of the IRUPs indicated on the higher resolution data were visible on the lower resolution data. The smallest IRUPs detected on the 200 m line spacing data were roughly 100 m in diameter.

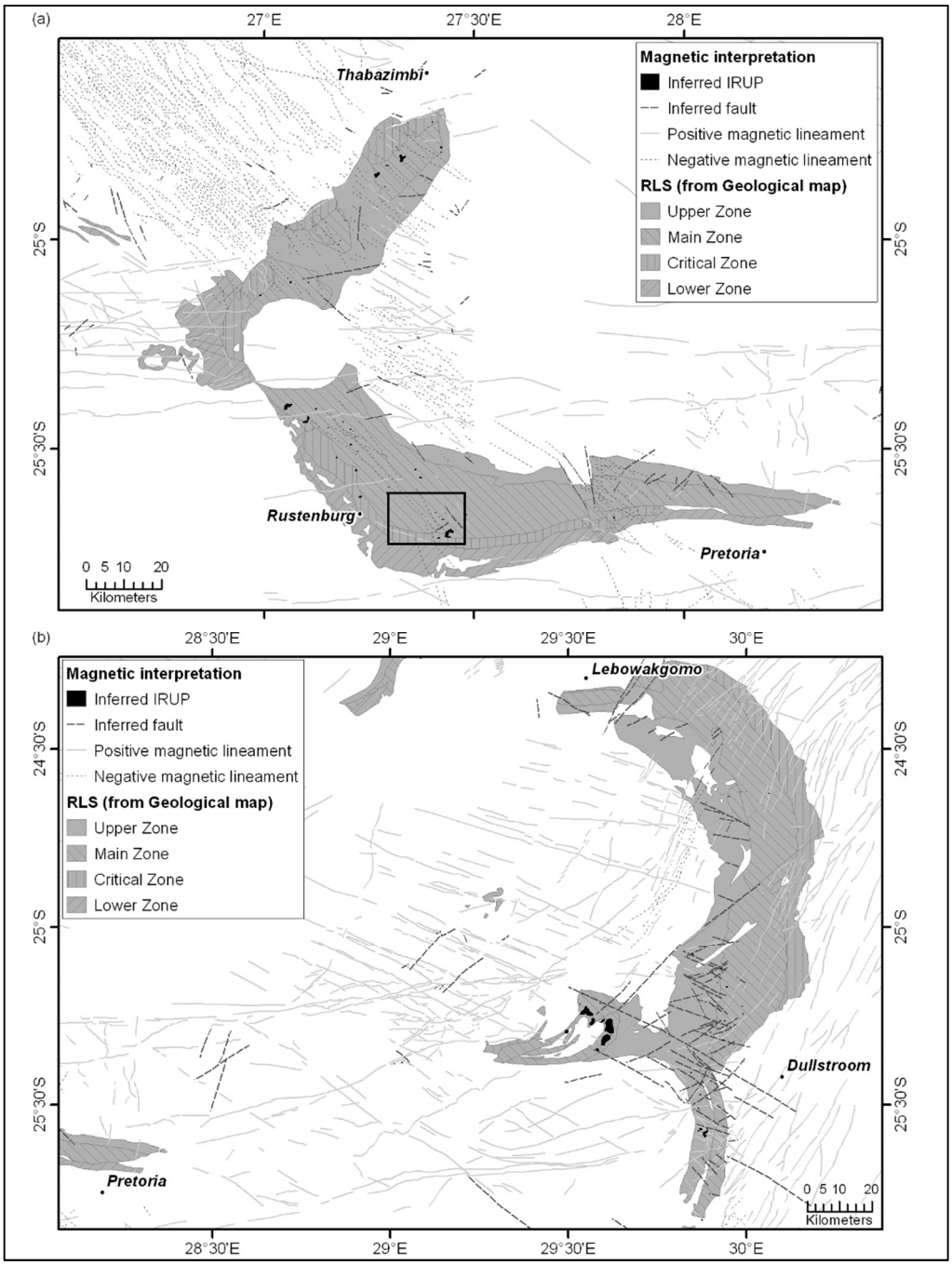


Figure 4.14 (a) Linear features and IRUPS inferred from the magnetic data for the western lobe. Figure 4.15 shows data in the area marked by the black box; (b) Linear features and IRUPS inferred from the magnetic data for the eastern lobe.

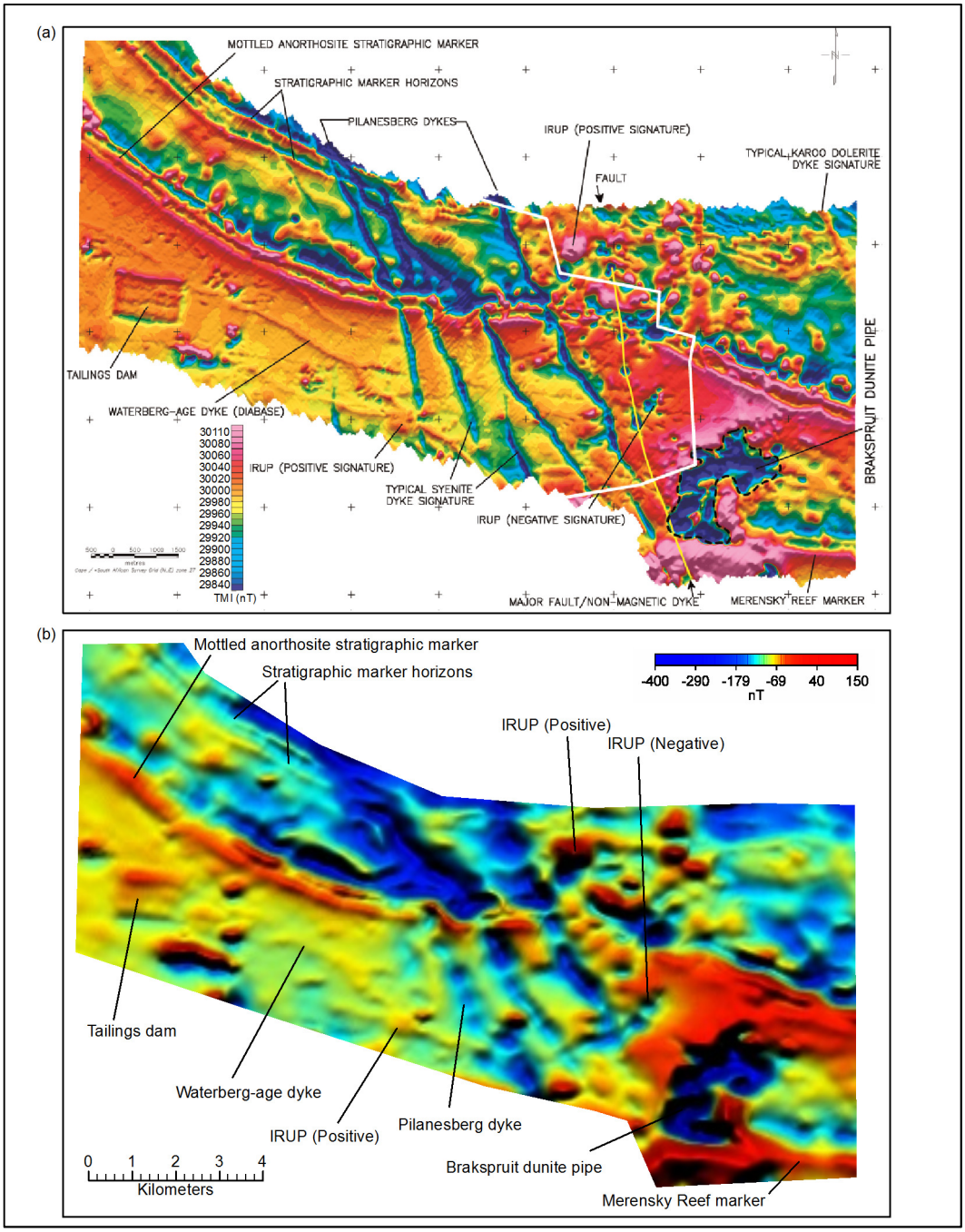


Figure 4.15 (a) High resolution magnetic data shown by Campbell (2006) for the area marked in Figure 4.14. Data were collected at 50 m line spacing, 30-40 m terrain clearance using a helicopter. (Colour bar labels were enlarged for legibility); (b) Lower resolution data for the same area collected with a fixed-wing aircraft at 200 m line spacing and 80 m terrain clearance.

4.6 Central Bushveld Geometry

Connectivity between the eastern and western lobes has been the subject of much debate. In the past gravity modelling has been used to propose various geometries, starting with separate intrusions with vertical feeders (Cousins, 1959), moving to separate dipping sheets (Du Plessis and Kleywegt, 1987; Meyer and De Beer, 1987) and finally showing the possibility that the lobes were connected at depth (Cawthorn et al., 1998; Cawthorn and Webb, 2001; Webb et al., 2004).

We constructed simple models along a central profile (Figure 4.12) to test whether the magnetic data requires continuity of the Bushveld Complex (Figure 4.16). Anomalies reaching amplitudes of almost 900 nT and 500 nT coincide with the western and eastern lobes respectively. In the centre of the Complex amplitudes reach -120 nT east of the western lobe and -220 nT west of the eastern lobe separated by a broad positive anomaly. In the first model (Figure 4.16a) the mafic rocks continue between the eastern and western lobe, roughly 4 km below the surface in the centre. The calculated magnetic field is flat at roughly 30 nT and clearly does not correspond to the negative anomalies on the insides of the two lobes. This is due to the fact that for a horizontal sill the largest anomalies are situated at the edges of the body, but over the central part the magnetic field is constant. The second model uses the separate dipping sheets concept (Figure 4.16b)). The dipping Upper Zone magnetic rocks cause positive magnetic anomalies extending towards the centre of the Complex, and in the area where mafic rocks are absent the calculated field is approximately 0 nT. The negative parts of the dipolar anomalies at the edges of the dipping sheets reach about -30 nT but does not account for the low magnetic values visible on the observed data.

If one considers a more complex geometry in the central part of the Complex, for example including domes and possible folding, it is possible to obtain a better fit between the observed and calculated fields (Figure 4.16c). The profile crosses the southern part of the Marble Hall Dome, an Archaean dome in the east considered by Hartzer (2000) to have formed prior to the deposition of the Transvaal Supergroup. Including this dome resulted in a better fit for the negative anomaly on the western side of the eastern lobe. The Upper Zone had to be excluded from the domed area which may corroborate the existence of the dome prior to the intrusion of the mafic Bushveld rocks. Diapirism is also known to have occurred at various localities in the Bushveld Complex (eg. Scoon, 2002) and therefore it is conceivable that doming and subsequent folding of the mafic rocks could have taken place after intrusion of the Bushveld Complex. It is clear though that Main Zone rocks are required to be present in the central part of the Complex to account for the negative magnetic anomalies in this area. To obtain a reasonable fit between observed and calculated fields for the positive anomaly located at about 200 km along the

profile, the mafic rocks were modelled to come closer to the surface, but the Upper Zone remained intact across this dome. The large negative spike located within the positive magnetic anomaly is associated with Pilanesberg Alkaline Complex intrusions.

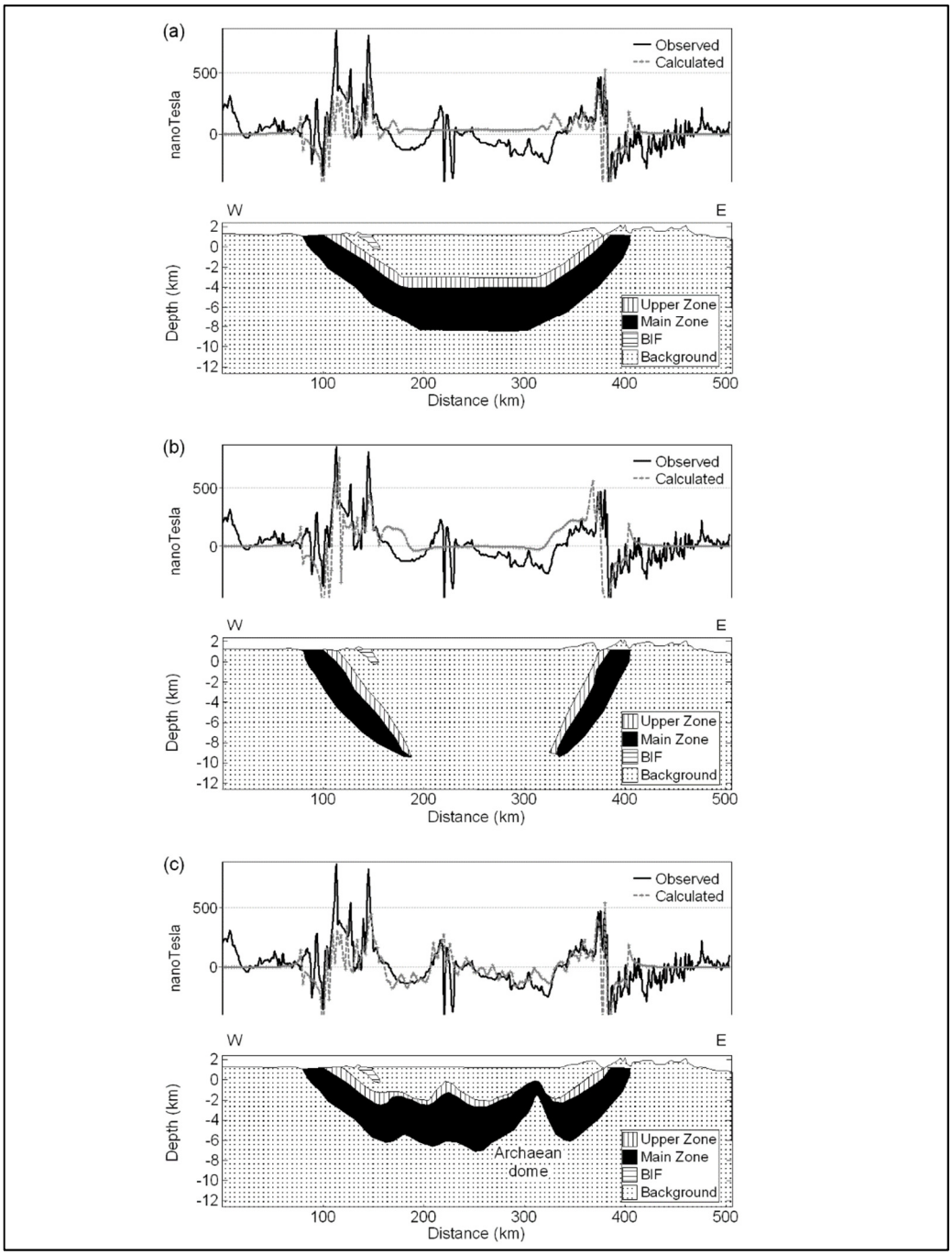


Figure 4.16 Simple 2.5 dimensional models calculated along a profile running from east to west through the Bushveld Complex (see Figure 4.2 for locality). (a) Mafic rocks continuous between the western and eastern lobes at a constant level; (b) Mafic rocks modelled as separate dipping sheets; (c) Continuous mafic rocks, but with more complex geometry. For all cases the vertical:horizontal exaggeration is 10:1

4.7 Summary and Discussion

Although variable, distinct magnetic signatures of the individual units of the Rustenburg Layered Zone can be recognised from the regional and higher resolution magnetic data sets (Table 4.1). The magnetic signature of the Upper Zone dominates the magnetic data collected over the Bushveld Complex. The abundance of magnetite results in large amplitude (400 nT-2400 nT), predominantly positive magnetic anomalies ('Type I', Figure 4.6). In areas where the Upper Zone rocks dip steeply and where the flight lines cross the layers perpendicularly, the anomalies are relatively narrow with clear linear layering visible. In other areas 'mottled' or irregular appearance on the magnetic data characterise the Upper Zone ('Type III', Figure 4.6). Where layering is parallel or semi-parallel to the flight lines, flight lines only intermittently cross the layers or parts of the layers, resulting in curved and divergent linear magnetic anomalies. Where the magnetic rocks disappear underneath younger material the anomalies become smoother but are still clearly visible ('Type IV' in Figure 4.6).

The contact between the Upper and Main Zones is almost always characterised by large negative anomalies. This is due to the interaction between the anomalies associated with the two zones ('Type VI' in Figure 4.6). Further away from the contact, the remanence of the Main Zone causes it to be vaguely visible on the magnetic data as slightly negative anomalies, but it is mostly associated with magnetically quiet areas. In two cases, namely in the north of the eastern lobe and in the south of the western lobe, it is possible to see some layering within the Main Zone on the magnetic data. This is probably helped by the better sampling of the EW-striking layers by the NS-directed flight lines in these two areas. In the eastern lobe the steep dip of the Main Zone caused the layer anomalies to be close together and resulted in what appeared to be predominantly positive anomalies. However, synthetic models showed this appearance to be due to the interaction between closely spaced, predominantly negative anomalies (Figure 4.13). The layer anomalies in the southern part of the western lobe are clearly negative.

The magnetic data used in this study were not very useful in delineating the Critical or Lower Zones of the Rustenburg Layered Suite since these zones lack significant magnetic minerals. The exception is magnetic layers within the Critical Zone in the northern part of the western lobe.

Table 4.1 Summary of the typical magnetic anomalies associated with the Rustenburg Layered Suite as they appear on 1 km and 200 m line spacing magnetic data

Zone	Description of typical anomalies	Anomaly type (cf. Figure 4.6)
Upper	• Predominantly positive anomalies (400 nT to 2400 nT range) caused by steeply dipping magnetite-rich material close to the surface. Layering, probably due to packages of magnetite layers, can be visible	I
	• Sill-like anomalies associated with shallow-dipping ferrogabbros close to the surface. Layering visible	V
	• Mottled anomalies caused by shallow magnetite-rich material with variable cover/irregular distribution of magnetic material	III
	• Smooth, broad positive anomaly originating from deeper-seated ferrogabbros	V
Main	• Mostly magnetically quiet with low amplitude (-20 nT to -200 nT) negative anomalies	
	• Linear negative anomalies with small amplitudes visible in the southwest and northeast where strike is perpendicular to flight line direction	
	• Very large amplitude negative anomalies (-4000 nT to -12 000 nT) with small positives along the southern and eastern sides visible in the southern parts of the western and eastern lobes	II
Critical and Lower	Magnetically quiet, not responsible for any visible anomalies on the available data	
Other	Negative anomalies along the contact between the Upper and Main Zones that are caused by the interaction between the predominantly positive anomalies of the Upper Zone and the negative anomalies of the Main Zone	VI

The magnetic character of the Upper Zone is consistent throughout the western and eastern lobes of the Bushveld Igneous Complex (Figure 4.2, Figure 4.8-Figure 4.11). This implies that the magnetic minerals in the ferrogabbros and magnetitite layers that constitute this zone are very similar throughout the Complex, suggesting a shared parental magma source. The magnetic rocks also intruded into the same palaeomagnetic environment. A marker at the contact between the Upper and Main Zones or close to the top of the latter, causes prominent remanently magnetised anomalies in the southern parts of the western and eastern lobes of the Bushveld Complex ('Type II' in Figure 4.6). This marker is not developed everywhere, but where it is present it is extremely prominent, even on regional magnetic data. The fact that it is only present in the southern parts of the western and eastern lobes may have significance for the intrusion style of the Rustenburg Layered Suite. It may represent a separate magma pulse that intruded only in the south, an idea refuted by Cawthorn and Webb (2013). Alternatively it could represent a difference in cooling period in the south that resulted in the formation of very fine grained minerals that are better at retaining remanent magnetisation. If the pseudosingle domain pure magnetite grains that carry the remanence (Letts et al., 2009) formed as the result of exsolution, it may imply a slower cooling rate in this part of the Complex (Butler, 1992). Contrary to this Cawthorn and Webb (2013) interpreted the reversed polarity observed in the southern part of the eastern lobe to faster cooling through the Curie temperature, and thus recording the oldest reversal. They noted that the same reversal was not recorded in palaeomagnetic samples collected in the southern part of the western lobe, and that this part of the Complex therefore may have cooled slower, but the large negative magnetic anomalies can only be explained by reversed polarity of the magnetic field. There is clearly scope for much more research in this area.

4.8 Conclusions

The magnetic data collected over the Rustenburg Layered Suite of the Bushveld Complex provide substantial information at different levels of detail. On a broad scale it sheds light on the geometry of the mafic intrusion. The high magnetic susceptibility of the Upper Zone and the remanent magnetisation of the Main Zone are important when considering the connectivity of the eastern and western lobes of the Bushveld Complex. In places where this zone is close to the surface, the amplitude of the magnetic field will definitely increase. This was illustrated in a simple model (Figure 4.16c) which gave the best result when the Upper and Main Zones were continuous between the eastern and western lobes.

Moving to a smaller scale, the data clearly shows the boundary between the Upper and Main Zones resulting from the difference in magnetite content between the zones. On an

even smaller scale magnetic layering could be detected in the Critical, Main and Upper Zones. Magnetic stratification in layered intrusion can reflect various magmatic processes such as, amongst others, the onset of crystallisation of a new magmatic phase, or the disruption of a crystallisation sequence due to the extraction or replenishment of the magma chamber (Ferré et al., 2009). In addition, geomagnetic reversals have been recorded in some of the layers, especially in the Main Zone, and therefore give insight into the rate of cooling and/or changes in composition.

Finally, magnetic data showed the presence of dykes, faults and IRUPs that have an impact on mine planning. Even though the ultra-high resolution data that are normally collected for exploration and mining purposes are not always available, lower resolution data are still extremely effective in gaining a better understanding of the Rustenburg Layered Suite.

CHAPTER 5 GEOMETRY OF THE BUSHVELD COMPLEX

This chapter will be submitted as a paper to a peer reviewed journal. The work was conducted by me and I constructed the manuscript. My co-authors edited the manuscript and suggested improvements.

Cole – 80% (conducted the research and constructed the manuscript)

Webb – 10% (reviewed the manuscript and suggested improvements)

Finn - 10% (reviewed the manuscript and suggested improvements)

3D potential field model of the Proterozoic Bushveld Complex, South Africa

Janine Cole

Geophysics Unit, Council for Geoscience, Private Bag X112, Pretoria, 0001, South Africa
School of Geosciences, University of the Witwatersrand, Private Bag 3, WITS, 2050, South Africa
email: jcole@geoscience.org.za

Susan J. Webb

School of Geosciences, University of the Witwatersrand, Private Bag 3, WITS, 2050, South Africa
email: susan.webb@wits.ac.za

Carol A. Finn

US Geological Survey, Denver, Colorado 80225, USA
email: cfinn@usgs.gov

5.1 Abstract

A full three dimensional potential field model of the central and southern Bushveld Complex (BC) reveals information about the Complex in areas obscured by younger geological cover. Two dimensional gravity models and a few magnetic models limited to certain sections of the BC have been used in the past to propose geometries for the Rustenburg Layered Suite (RLS), especially in the western and eastern lobes. These models were often used to support different emplacement models. Although these models provided valuable information, 2.5D potential field modelling is not well suited to modelling complex three dimensional geology. Also, in most cases only the magnetics or only the gravity data were modelled, but jointly modelling both data sets better constrains the results, as was shown recently for a 3D model of the northern lobe. Joint 3D modelling of regional gravity and magnetic data combined with published crustal thickness models derived from broadband seismic tomography studies and constrained by density and susceptibility data (e.g. Chapter 2), geologic mapping, boreholes and seismic reflection data were used to create a 3D model of the central and south-eastern

sections of the BC, as well as the southern part of the northern lobe. The model showed a complex geometry with thick continuous RLS in most of the western and south-eastern lobes, but less continuous RLS in the eastern lobe. Large domes or thick granites and granophyre in the latter interrupted the continuity of the RLS and the western and eastern lobes are strictly speaking only partially connected in places. However, they are not separate intrusions, but represent a single magma chamber affected by pre-existing and syn-magmatic updoming.

5.2 Introduction

As the largest known layered igneous intrusion in the world the Bushveld Complex (BC) has been the focus of intense study since its discovery in the late 1800s. Debates remain despite the immense amount of work done on the BC. Connectivity of the western and eastern lobes and emplacement mechanisms are two issues where geophysics can contribute meaningfully and have done so in the past. For instance geophysical models have been used in support of geological models seeking to explain the emplacement mechanism of the BC (e.g. Von Gruenewaldt, 1979; Sharpe et al., 1981; Cheney and Twist, 1991; Clarke et al., 2009).

Published gravity models of the BC show various configurations for the western and eastern lobes. Earlier models showed the two lobes as separate intrusions to account for low gravity values in the centre of the Complex (Cousins, 1959; Du Plessis and Kleywegt, 1987; Meyer and De Beer 1987). However, the low gravity values could also be explained by 5 – 6 km thicker crust underneath the BC compared to the surrounding Kaapvaal Craton as revealed by the Southern African Seismic Experiment (SASE, Fouch et al., 2004). The first 2.5D gravity model that included this information showed the western and eastern lobes of the Rustenburg Layered Suite (RLS) to be connected (Webb et al., 2004), supporting an earlier postulation that the RLS could be modelled as a continuous intrusion between the two lobes if isostatic compensation at the Moho was taken into consideration (Cawthorn et al., 1998). Full three dimensional gravity modelling that included three crustal thickness models (Nguuri et al., 2001, Nair et al., 2006; Kgaswane et al., 2009, 2012) corroborated this, showing a roughly 6 km thick RLS for most of the BC (Cole, Webb and Finn, 2014).

Combined (gravity and magnetic) three dimensional modelling that includes seismologically-derived crustal thicknesses for the northern lobe (Finn et al., 2015) provided evidence for the extension of the northern lobe to the west under generally less than 2 km of younger lithologies. The model showed an average thickness of 4 km for the RLS, but it reached 12 km at the Mokopane feeder. The thick high density feeder was originally modelled in 2D by Van Der Merwe (1976) using gravity data.

At present a similar model has not been published for the central and south-eastern BC. Very simple 3D gravity models testing the effect of different crustal thickness models on the gravity response (Cole, Webb and Finn, 2014) did not include magnetic data and also did not separate the mafic and ultramafic parts of the complex (the Rustenburg Layered Suite) into the recognised Upper, Main, Critical, Lower and Marginal Zones. The latter is important since the zones have different petrophysical and especially magnetic properties, and combining them into one unit is an oversimplification and prohibits magnetic modelling.

Here, we show for the first time full 3D gravity and magnetic modelling over the central and south-eastern BC with crustal thickness information included and the RLS separated into zones. Specific questions that we seek to address with this model are 1) what is the extent and connectivity of the RLS in the central and southeastern BC?.2) What are the thickness variations of the Upper, Main, and Lower Zones of the RLS? 3) Is there evidence for large feeders to the BC? 4) What does the model reveal about the 3-D geometry of Transvaal domes and Archaean basement ridges?

5.3 Geology

The BC sits in the northeast of South Africa where it intruded a thick succession of mostly sedimentary and some volcanic rocks constituting the Transvaal Supergroup (Figure 5.1). The intrusion comprises the mafic/ultramafic Rustenburg Layered Suite (RLS) that generally defines the outer rim of the BC, and the acidic Rashoop Granophyre and Lebowa Granite Suite that cover the centre. New high precision age dates suggest that the RLS could have been emplaced rapidly (< 1 Ma) ~2055-2057 Ma (e.g. Scoates and Wall, 2015; Zeh et al., 2015). However, inconsistencies between field evidence and the age dates suggest that the zircon ages may not reflect emplacement timing, but may represent a later phase of residual melt migration within a crystal mush (Karykowski and Maier, 2017).

The RLS is usually divided into five zones, but a layered section consisting of highly magnesian pyroxenites, harzburgites and dunites, the Basal Ultramafic Sequence, has been identified at the base of the RLS in the north-eastern part of the eastern lobe (Wilson, 2015). Above this base is the discontinuous Marginal Zone consisting of pyroxenite, peridotite, norite and gabbro (Harmer and Sharpe, 1985; Wilson, 2012). The Lower Zone is composed of pyroxenite and harzburgite with well-defined cyclic layering (Wilson, 2012). This is followed by the mineral-rich Critical Zone comprising repeated layers of chromitite, pyroxenite, norite and anorthosite (Cawthorn et al., 2006). The Main Zone is a thick succession of norite and gabbronorite (Cawthorn et al., 2006). Pyroxenite and anorthosite are rare, confined to the pyroxenite marker and the Main and Upper

Mottled Anorthosites respectively (Eales and Cawthorn, 1995). The Upper Zone consists of gabbronorites and anorthosites with cumulus Fe-rich pyroxenes and olivine, magnetite and apatite (Cawthorn et al., 2006).

Inliers of Transvaal Supergroup and older Archaean basement material occur in the eastern and western lobes where the BC rocks are at or close to the surface (Figure 5.1). The Crocodile River Fragment (CRF) in the western lobe is mapped as a domal structure with Pretoria Group rocks steeply dipping towards the surrounding Bushveld granites (Hartzer, 1989, 1995). The oldest units of the Transvaal Supergroup crop out in this dome. One hypothesis for the development of the CRF is that updoming started during the deposition of the Transvaal Supergroup as a result of interference folding (Hartzer, 1989). Three phases of folding deformed the CRF. The first resulted in NE striking folds in the north and NE striking folds in the south. The second phase refolded the already folded rock along a NW-SE axis and in the third phase folding was oriented ENE (Hartzer, 1989). Superimposing different phases of folding with different orientations results in an interference pattern resembling updoming (Ramsey, 1962). The CRF and the Rooiberg Fragment to its north have also been described as roof pendants (Dietvorst, 1991; Lenhardt and Eriksson, 2012). In contrast to the CRF, the Rooiberg Fragment is a synformal structure of upper Transvaal Supergroup rocks and lavas of the Rooiberg Group (Hartzer, 1995). The latter forms the roof to the BC in this area (Cawthorn et al., 2006).

A series of inliers of basement occurs in the eastern lobe, mostly between the Steelpoort and Wonderkop Faults (Figure 5.1). The Dennilton Dome comprises a core of Archaean gneisses, felsites and some greenstone remnants, flanked to the south by older Transvaal Supergroup. The Marble Hall Fragment to the north of the Dennilton Dome has a core of early Transvaal Supergroup rocks. Diorite sills in the north of this fragment was considered Main Zone to Upper Zone at one stage (De Waal, 1970). Geochemical studies now correlate them with the sill emplacements that immediately preceded the intrusion of the RLS (De Waal and Armstrong, 2000) and was derived from the same magma that was parental to the Lower Zone (De Waal et al., 2008).

The Dennilton Dome and Marble Hall Fragment, or dome, to the north has been considered a single entity that also formed as a result of interference folding (Hartzer, 1995; Clubley-Armstrong and Sharpe, 1979). In one model the domes formed prior to the intrusions of the BC (Hartzer, 1995) while in another the first phase of deformation started before or during the initial stages of the intrusion followed by a second deformation phase during the emplacement of the RLS (De Waal, 1970). A more recent model places the updoming during the emplacement of the Upper Zone (Kruger and Behr, 2002). This interpretation is based on differences in dips of the Main Zone and the Upper Zone along

the southern flank of the Dennilton Dome. The Stavoren Fragment comprises upper Transvaal Supergroup rocks, and overlies Bushveld granites and granophyres (Hartzer, 1995).

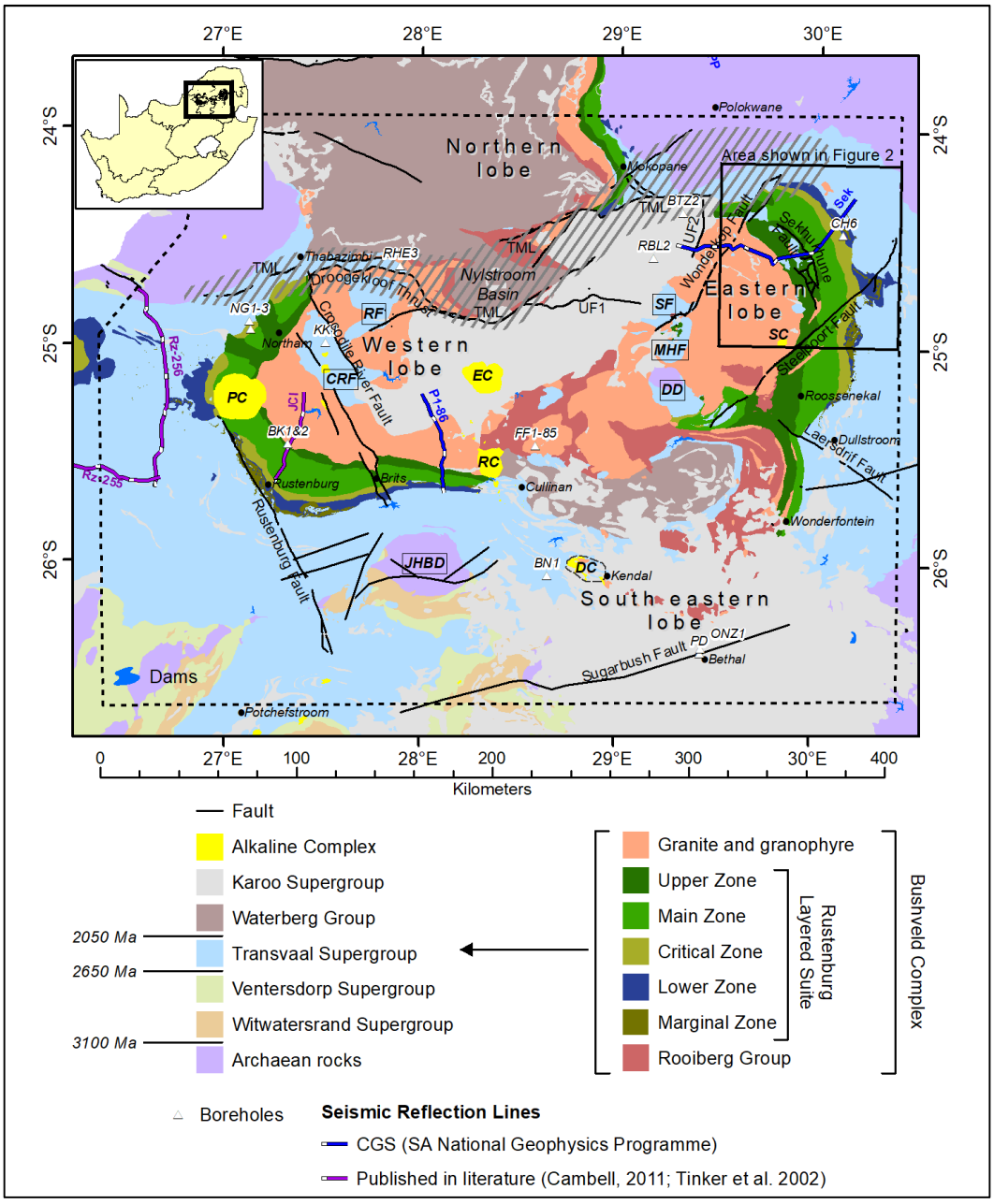


Figure 5.1. Geological map of the Bushveld Complex. The dashed line indicates the outline of the modelling area. CRF – Crocodile River Fragment; RF – Rooiberg Fragment; DD – Dennilton Dome; MHF – Marble Hall Fragment; SF – Stavoren Fragment; JHBD – Johannesburg Dome; DC – Dwarsfontein Complex; EC – Elandskraal Complex; PC – Pilanesberg Complex; RC – Roodeplaat Complex; SC – Spitskop Complex; TML – Thabazimbi-Murchison Lineament; UF1 and UF2 – unnamed faults. The hatched area indicates the TML zone

Numerous smaller Transvaal inliers occurs further to the northeast, mostly between the Wonderkop and Steelpoort Faults (Figure 5.2). These will not be discussed individually but many of these are considered to be diapirs that formed as a result of the intrusion of the RLS (Clarke et al., 2000; Scoon, 2002; Gerya et al., 2003).

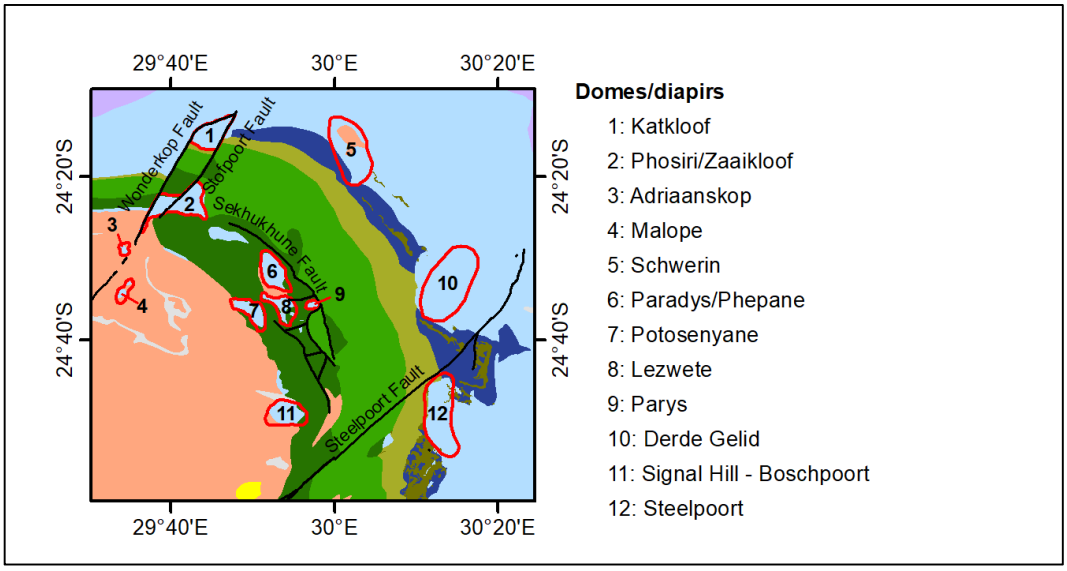


Figure 5.2. Diapirs in the northeastern Bushveld Complex (see Figure 5.1 for locality)

5.4 Data

5.4.1 Gravity Data

Regional gravity data with a resolution of roughly one measurement every 14 km^2 cover the BC (Figure 5.3a). Data were collected using LaCoste and Romberg gravimeters; elevations were determined using micro-barometers. Calculation of Bouguer anomaly values assumes a mean density of 2670 kg/m^3. The measurements were tied to the International Gravity Standardisation Net values (Morelli et al., 1974) and referred to the gravity formula based on the 1980 geodetic reference system (Moritz, 1992). The maximum error (including reading, positional and elevation inaccuracies) in the Bouguer anomaly value was estimated to be within 2 mgal (Stettler et al., 2000).

5.4.2 Magnetic Data

Regional magnetic data covering the whole Bushveld Complex were collected between 1969 and 1978 using a line spacing of 1 km, tie line spacing of 15 km and terrain clearance of 100 to 150 m (Ledwaba et al., 2009). The line direction was north-south for most surveys, but east-west over the northern lobe and the north-eastern part of the

eastern lobe. The surveys generally used a Geometrics G803 proton magnetometer, but a few surveys were done with a Gulf Fluxgate Mark III magnetometer. A sampling rate of 1 Hz resulted in a magnetic reading roughly every 63 m along a flight line. The appropriate IGRFs (in terms of locality, elevation and survey date) were removed from the data sets prior to merging them together (Figure 5.3b). On average the prevailing magnetic field at the time of data collections had a strength of 28500 nT, an inclination of -63º and a declination of -17º.

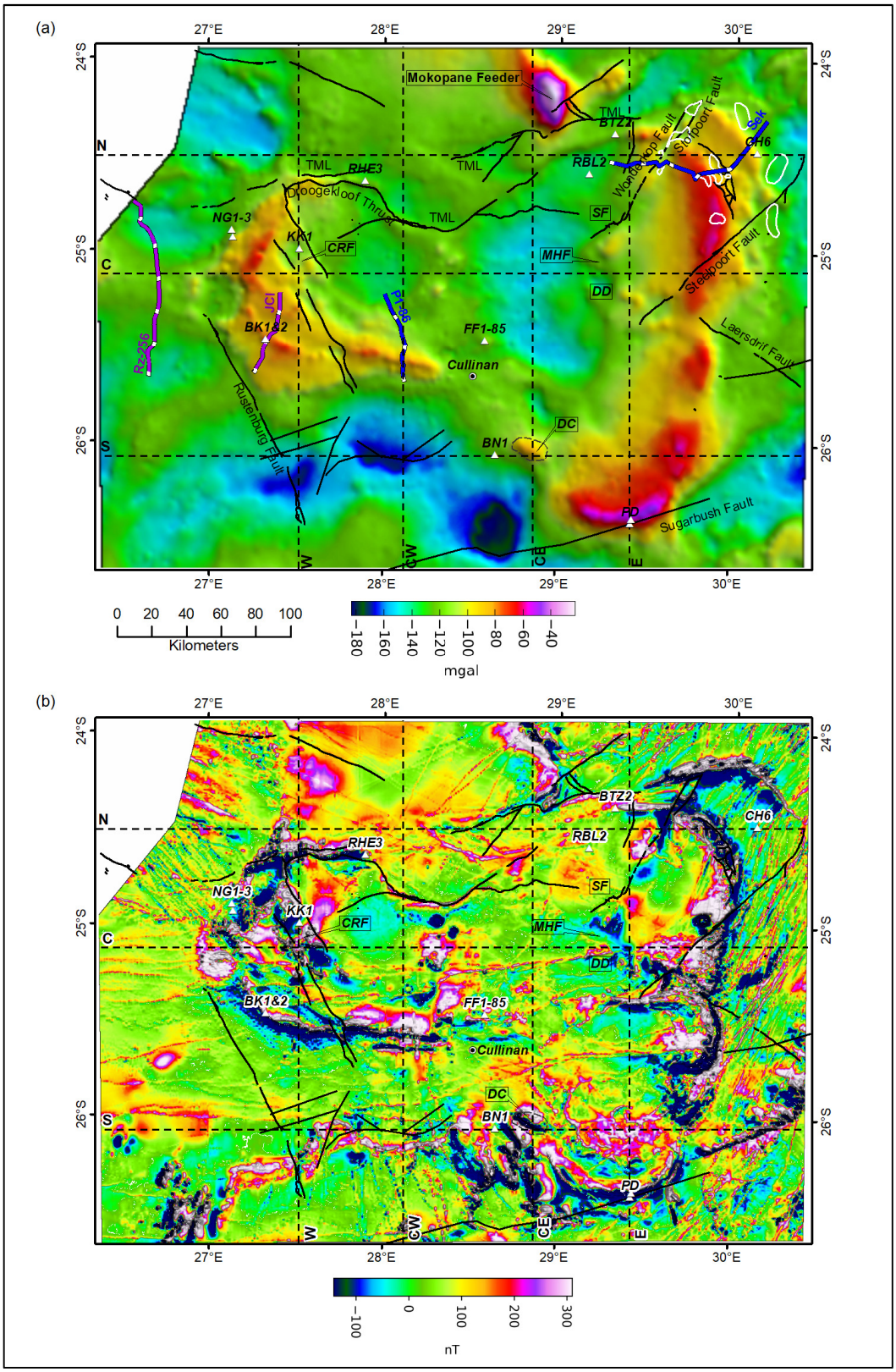


Figure 5.3. (a) Regional gravity and (b) magnetic data. Dashed lines indicate profiles extracted from the 3D model and shown in Figure 5.10, Figure 5.12, Figure 5.13 and Figure 5.15. Borehole localities, large faults and pre-BC inliers, and deep reflection seismic lines are shown. Diapirs from Figure 5.2 are outlined in white.

5.4.3 Crustal Thickness Models

Broadband seismic data collected during the Southern African Seismic Experiment (SASE) (Fouch et al., 2004) provided for the derivation of crustal thickness models underneath the Kaapvaal Craton. Five crustal thickness models that were derived from this data using different methods (Nguuri et al., 2001; Nair et al., 2006; Kgaswane et al., 2009, 2012; Youssof et al. 2013; Delph and Porter, 2015) all show thick crust underneath the central and northern parts of the Bushveld Complex, but substantial differences between the models under the eastern lobe (Figure 5.4a, c, e and Figure 5.5a,c). The studies revealed a diffuse crust-mantle transition under the BC which made it difficult to calculate accurate crustal thicknesses. Very low quality P to S conversions under the eastern lobe explains the large variation in crustal thicknesses in this area.

Undulations in the Moho add long wavelength anomalies to the gravity field calculated for a model of the Bushveld Complex in the upper crust. Variations in the crustal thickness will therefore affect the geometry of the model. This underpins the work of Cawthorn et al. (1998) and Webb et al. (2004) who showed that the RLS could be present in the central part of the Bushveld Complex if isostatic adjustment at the crust mantle boundary was taken into account. It follows therefore that differences between crustal thickness models will also cause differences in gravity models of the BC. However, profiles extracted from simple 3D gravity models using different crustal thickness models show that the geometry of the RLS remains similar, but the thickness of the RLS and surrounding geological units vary (Figure 5.6). For two models (Nair et al., 2006; Kgaswane et al., 2009, 2012) deep dense material was necessary under the eastern (Figure 5.6b) and western (Figure 5.6d) lobes to achieve the required gravity amplitudes. These bodies may be remnants of greenstone material in the crust or intrusions that may be related to the BC, although this is difficult to establish. Previous studies also illustrated the effect of variations in crustal thicknesses on gravity modelling of the central BC (Cole et al., 2014) and Northern Lobe (Finn et al., 2015).

It is not possible to rate any of the models above the others in terms of accuracy, and therefore the average of all the models were calculated and used in the gravity modelling (Figure 5.5e,f).

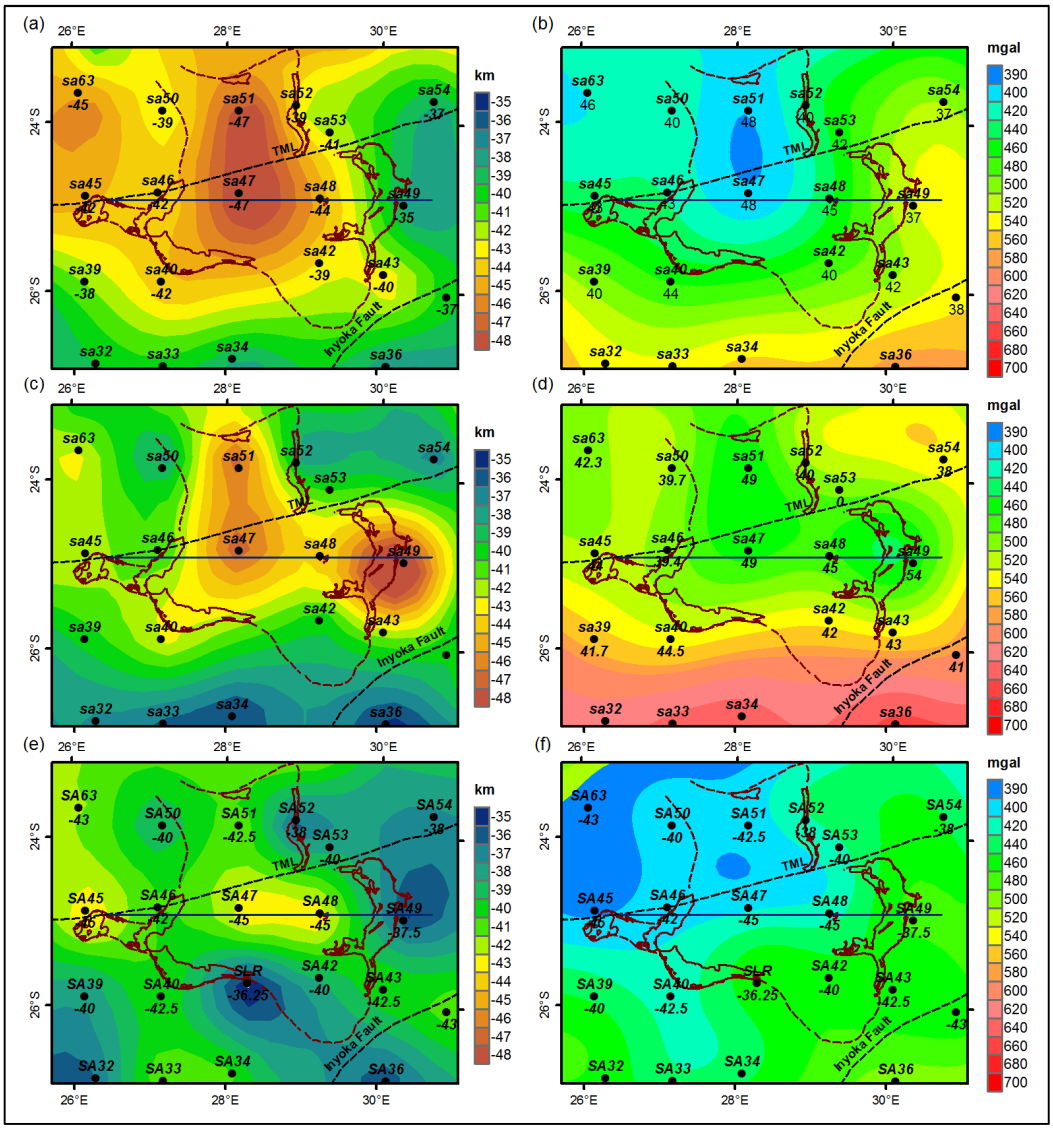


Figure 5.4. Depth to Moho derived by (a) Nguuri et al. 2001, (c) Nair et al. 2006, (e) Kgaswane et al. 2012 and gravity fields calculated for the models using a crustal density of 2700 kg/m^3 and an upper mantle density of 3380 kg/m^3 (b, d and f). Black dots are SASE stations with the station number above and Moho depth underneath the dot. Major structural features and the outline of the RLS are shown. Models extracted from simple 3D gravity models along the WE profile (blue line) are shown in Figure 5.6

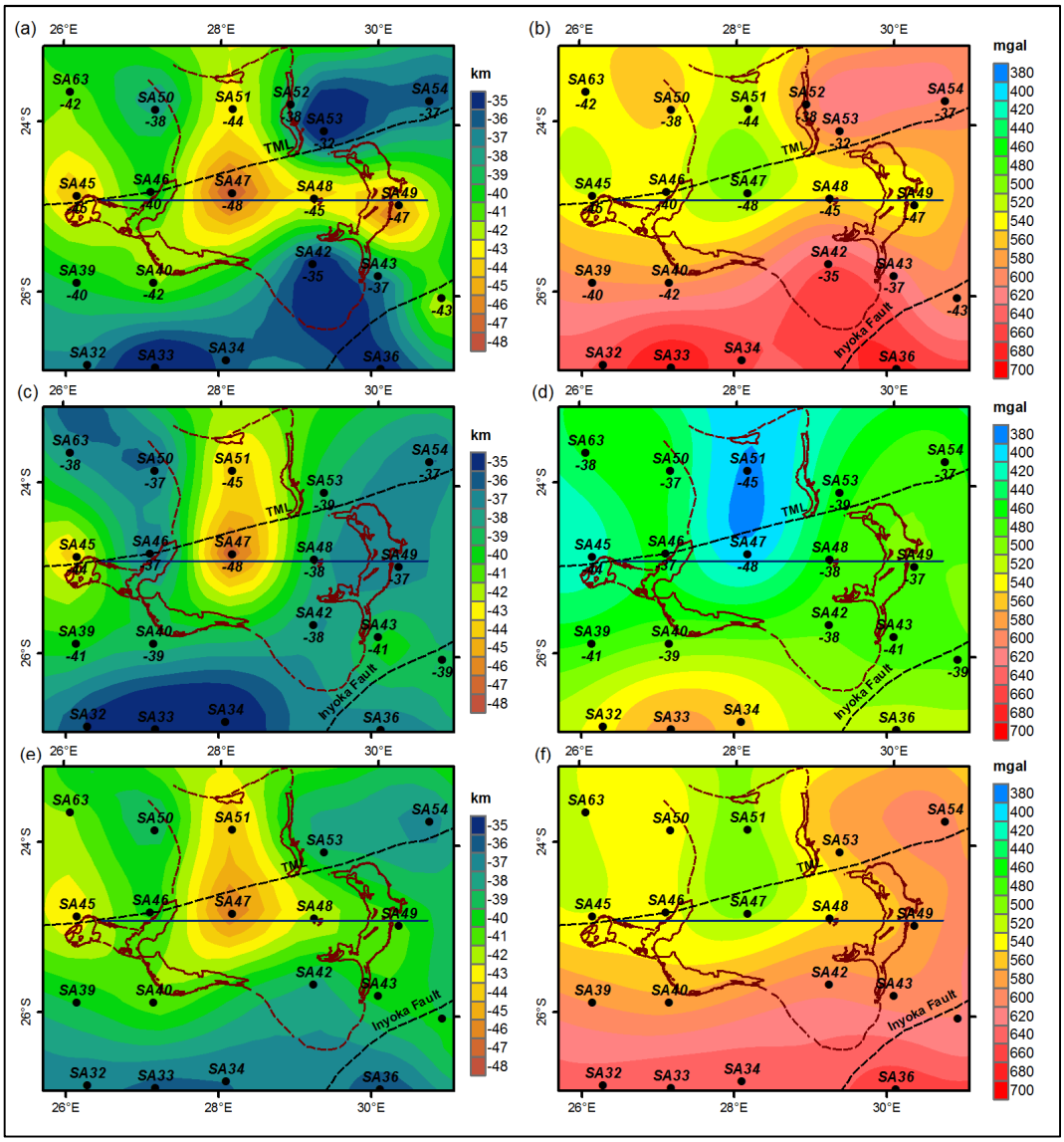
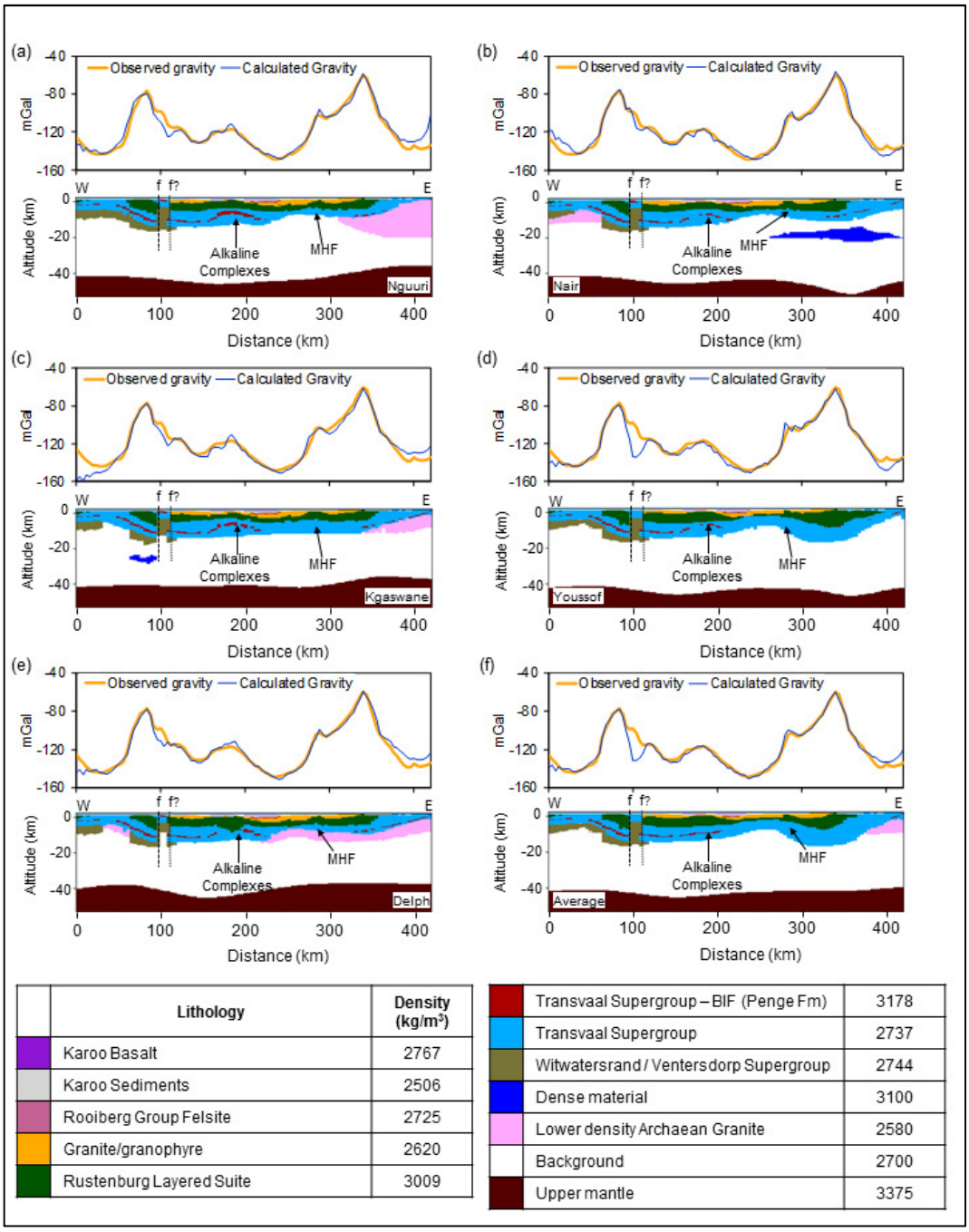


Figure 5.5. Depth to Moho derived by (a) Youssof et al. (2013), (c) Delph and Porter (2015), (e) average of the five crustal thickness models and gravity fields calculated for the models using a crustal density of 2700 kg/m^3 and an upper mantle density of 3380 kg/m^3 (b, d and f). Black dots are SASE stations with the station number above and Moho depth underneath the dot. Major structural features and the outline of the RLS are shown. Models extracted from simple 3D gravity models along the WE profile (blue line) are shown in Figure 5.6



	Lithology	Density (kg/m³)
	Karoo Basalt	2767
	Karoo Sediments	2506
	Rooiberg Group Felsite	2725
	Granite/granophyre	2620
	Rustenburg Layered Suite	3009

	Transvaal Supergroup – BIF (Penge Fm)	3178
	Transvaal Supergroup	2737
	Witwatersrand / Ventersdorp Supergroup	2744
	Dense material	3100
	Lower density Archaean Granite	2580
	Background	2700
	Upper mantle	3375

Figure 5.6. Models extracted from simple 3D gravity models along the profile shown in Figure 5.4 and Figure 5.5. The models include crustal thickness from different studies (a - Nguuri et al., 2001; b - Nair et al., 2006; c - Kgaswane et al., 2009, 2012; d - Youssof et al. 2013; e - Delph and Porter, 2015; f – the average crustal thickness model) and show that changes in the crustal thicknesses affect the RLS thickness, but the overall geometry remains relatively similar

5.5 Modelling constraints

Published geological maps, physical properties, published deep seismic reflection lines and boreholes constrained the model. Published information about generally expected thicknesses of the geological units, specifically the zones within the RLS, guided the modelling but could not be enforced too rigidly as they are generally averages.

5.5.1 Geological maps

Published 1:250 000 geological maps provided surface constraints for the modelling (Geological Survey of South Africa, 1974,1978a,b,1981,1986a,b,c,d). These were supplemented by more detailed published maps, e.g. a map of the northern lobe's southern section near Mokopane (Van der Merwe, 2008). Where dips were indicated on the maps they were used to constrain the model. The larger faults (Figure 5.1) from these maps were included in the modelling. Although the localities of the faults are known, their dips and depth extents are generally not as only the Wonderkop and Sekhukhune Faults appear on any of the published seismic reflection lines (Figure 5.7b).

5.5.2 Physical properties

Densities and magnetic properties were obtained from various sources (Table 5.1). Since the main focus of the model is the BC, stratigraphic units have been grouped together where possible to simplify the modelling process. For example, the Transvaal Supergroup is modelled as one unit, with only the banded ironformation separated out due to the high density and magnetic susceptibility of BIF. The Witwatersrand and Ventersdorp Supergroups were combined into a single unit in the model except in a few instances where magnetic shale of the Lower Witwatersrand was needed to model magnetic anomalies. In the BC itself, the Marginal, Lower and Critical Zones were grouped since they are all very dense but not magnetic, and it is not possible to reliably distinguish between them based on the regional gravity data. However, in certain instances the Lower Zone was separated out, e.g. to model feeders that consist of Lower Zone only. This may also include the Basal Ultramafic Sequence observed by Wilson (2015). Granites and granophyres of the Lebowa Granite Suite and Rashoop Granophyre Suite respectively were also modelled as one unit.

Table 5.1. Geological units with the petrophysical properties used in the modelling (Table 2.3, Table 2.4 and palaeomagnetic data from Letts et al., 2009).

Lithology	Density (kg/m^3)	Susceptibility (SI)	NRM (A/m)	Remanent Inclination (º)	Remanent Declination (º)
Dolerite	2800	0.08			
Karoo Basalt	2767	1508.2×10^{-5}	1.6050		
Karoo Sediments	2506	14.6×10^{-5}	0.0006		
Roodeplaat and related Complexes	2677	0.015*	5.0		
Pilanesberg Complex	2687	0.005*	0.1*		
Pyroxenite pipes	3200*	0.02*	5.443*	50*	-10*
Waterberg Group	2645	8.2×10^{-5}	0.1	-35.2	169.9
Granite/granophyre	2620	356.4×10^{-5}			
Upper Zone	3135	0.184	2	-61	174.8
Main Zone	2911	0.0017	1	63.8	14.7
Critical/Lower/Marginal Zone	3042				
Lower Zone	3142				
Rooiberg Group Felsite	2725	2986×10^{-5}	2.961		
Transvaal Supergroup – BIF	2900+	0.005	4.309+		
Transvaal Supergroup	2737				
Witwatersrand / Ventersdorp Supergroup	2744	0.03			
Dominion Supergroup	2970	0.01*			
Greenstone material	3100*	0.1*			
Lower density Archaean Granite	2550*				
Background	2700				
Deep dense material	3000				
Upper mantle	3375				

*Estimate; +Adapted to account for exaggerated thickness

5.5.3 Deep seismic reflection

Deep seismic reflection lines and boreholes helped to constrain the depth aspect of the modelling. Very few deep seismic reflection lines across the Bushveld Complex are publicly available. During the 1980s seismic surveys were done under the auspices of the South African National Geophysics Programme (SANGP) and two of these lines crossed parts of the Bushveld Complex (Figure 5.3a), namely *P1-86* in the southern part of the western lobe (Odgers, Hinds and Von Gruenewaldt, 1993) and *Sek* in the northern part of the eastern lobe (Odgers and Du Plessis, 1993). Published lines include the *JCI* line starting near Rustenburg in the western lobe (Campbell, 2011) and *RZ256 and RZ255* to the west of the Pilanesberg Complex (Tinker, De Wit and Grotzinger, 2002). If we assume an average velocity of 6 km/s in the upper crust, the RLS in the south is approximately 4.5 km thick and covered by almost 5 km of Bushveld granites and granophyres (Figure 5.7a). Along the published line further to the west, north of Rustenburg (Campbell, 2011) the RLS reaches a maximum thickness of about 6 km. In the northeast preliminary processing of the *Sek* line (Odgers and Du Plessis, 1993) also shows the RLS to be 6 km thick where it crops out, and thinning westward to roughly 4 km west of the Malope Dome (Figure 5.7b).

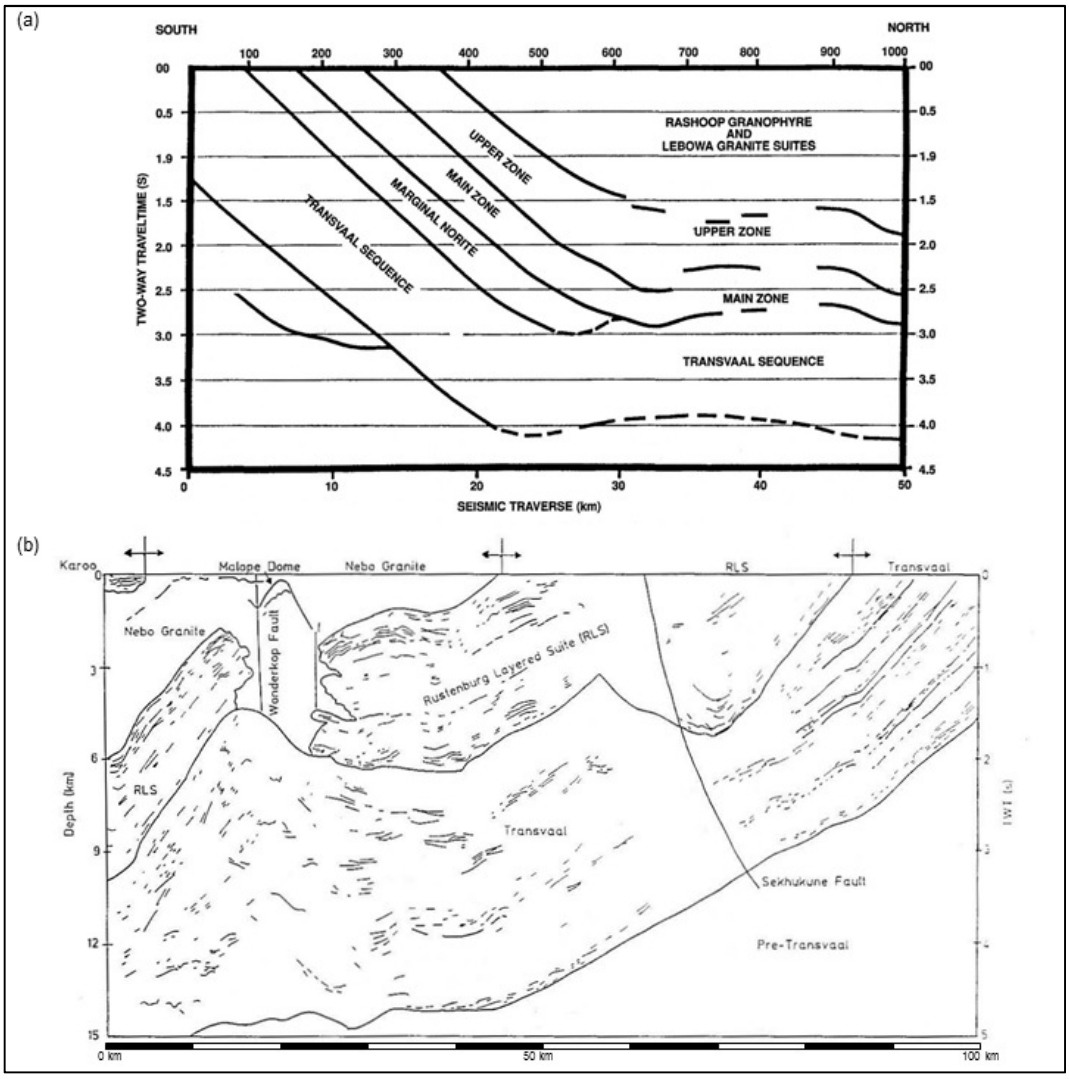


Figure 5.7. Deep seismic reflection lines with positions of profiles indicated. (a) P1-86 line (Odgers, Hinds and Von Gruenewaldt, 1993)**; (b) Sekukhuneland line (Odgers and Du Plessis 1993)**

5.5.4 Boreholes

Some deep borehole logs were available to the study, but very few penetrated through the whole RLS (localities shown in Figure 5.1 and logs in Figure 5.8). Together the Nooitgedacht boreholes (Figure 5.8a) in the western lobe (Teigler and Eales, 1996) and the Bierkraal boreholes (Figure 5.8b) near Rustenburg (Tegner, Cawthorn and Kruger, 2006) gave the most complete logs of the whole RLS.

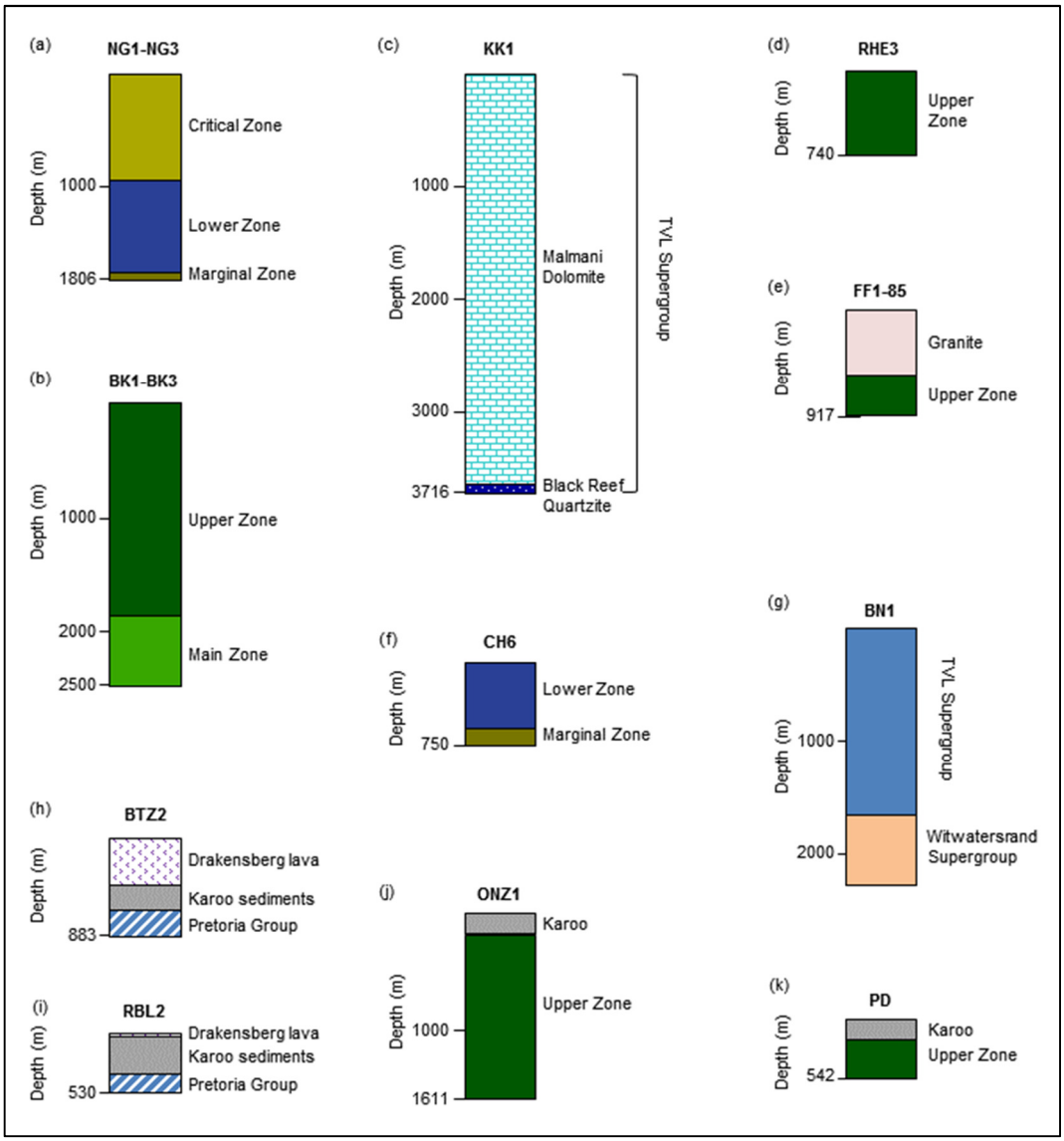


Figure 5.8. Logs for boreholes of which the localities are shown in Figure 5.1 and in the models in Figure 5.10, Figure 5.12and Figure 5.13. (a) (Teigler and Eales, 1996)**; (b) from** (Tegner, Cawthorn and Kruger, 2006)**; (c) from Hartzer (2000); (d) Donated to the Council for Geoscience by Goldfields (Pty) Ltd; (e) from Moen (1989) ; (f) from Wilson (2015); (g) Drilled by the Council for Geoscience in 1963 (h) Drilled by the Council for Geoscience in 2006; (i) Donated to the Council for Geoscience Transvaal Consolidated Land and Exploration Company (j) and (k) from Buchanan (1975)**

5.5.5 Combined gravity and magnetic modelling

Most published potential field models of the Bushveld Complex only use gravity data, but magnetic data provide additional constraints. Gravity and magnetic data reflect the distribution of density and magnetic properties respectively. While all rocks have a certain

density, not all rocks are magnetic. For example, the UZ is highly magnetic and very dense, but the other zones in the RLS are not very magnetic although still very dense. Combining the two data sets makes it possible to separate the UZ from the other zones.

The magnetic data resolution is higher than the gravity data resolution making it well suited to constraining the shallower aspects of bodies. This includes both the depth to the magnetic material and the horizontal extent.

5.5.6 Self-demagnetisation

Positive and negative magnetic charges develop on the surface of all magnetic bodies placed in an external magnetic field, and these charges induce a secondary magnetic field in the magnetic body (Guo et al., 2001). The secondary field always reduces the resultant magnetic field (hence the term self-demagnetisation) and in magnetically homogeneous and isotropic bodies the induced field is directly opposite to the external magnetic field (Guo et al., 1998). Although it affects all magnetic bodies, its effect is generally considered negligible for bodies with susceptibilities less than 0.1 SI (Guo et al., 2001; Lelièvre and Oldenburg, 2006; Wallace, 2007). Self-demagnetisation depends on body shape and is proportional to the induced magnetisation within the body. The constant of proportionality, called the demagnetisation factor (Purss and Cull, 2005), has been calculated for many simple body shapes (Guo et al., 2001 and references therein).

The magnetic susceptibility of the RLS Upper Zone is greater than 0.1 (Table 5.1) and self-demagnetisation may be important. To this end the effective magnetisation of a rectangular prism with dimensions of 50 x 5 x 1.5 km and susceptibility of 0.184 SI was calculated following the example of Clark and Emerson (1999). In the test the magnetic body is in a magnetic field with an intensity of 28 000 nT, inclination of -63º and declination of -17º (Figure 5.9a). The Upper Zone contains some remanent magnetisation, but the Q-ratio is only 0.5 and does not change the anomaly in a significant way. After taking self-demagnetisation into account, the effective magnetic field is just over 1000 nT lower and the inclination and declination changed by 2º (Figure 5.9b). The effect of self-demagnetisation is not significant.

Case studies reported in the literature generally consider bodies with susceptibilities greater than 1 SI (Schmidt and Brewer, 2007; Wallace, 2007; Austin et al., 2014) which is higher than the Upper Zone susceptibility of 0.184 SI. However, this is an average estimate of the whole Upper Zone, and is adequate for a regional scale magnetic model. For more detailed studies self-demagnetisation of the magnetite layers with sucseptibilities reaching 3- 4 SI (Ashwal et al., 2005) will become important.

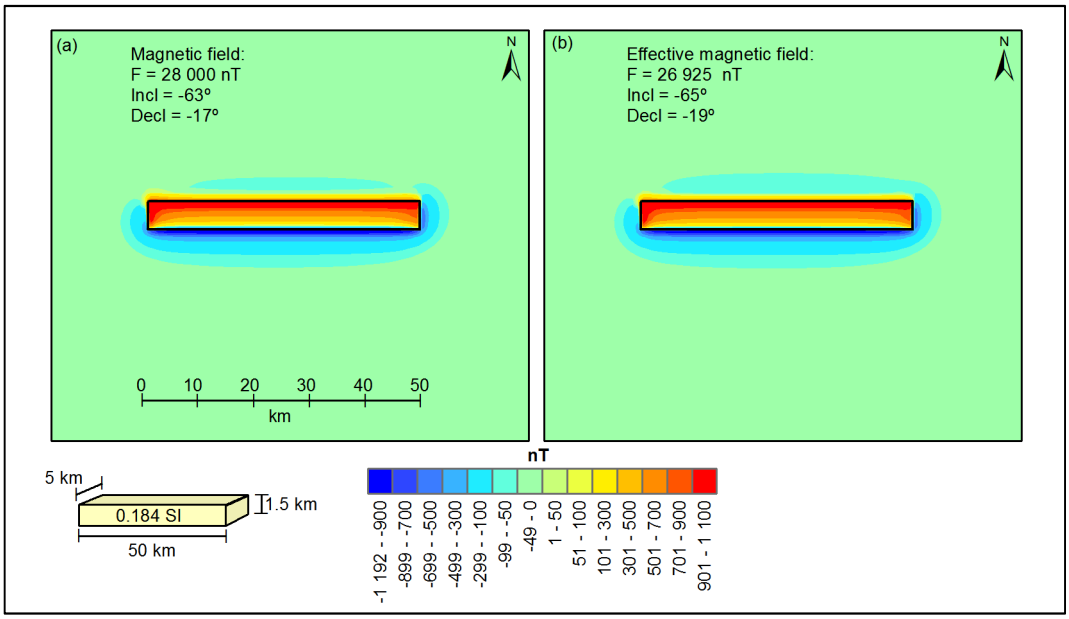


Figure 5.9(a) Magnetic field calculated for a tabular body representing the Upper Zone; (b) Magnetic field of the same tabular body after the effect of self-demagnetisation has been taken into account following the approach of Clark and Emerson (1999)

5.6 Modelling Results

3D forward modelling was done using PyGMI, an open source software package (http://patrick-cole.github.io/pygmi/). The software divides the modelling area into cuboids and calculates the contribution of each cuboid to the magnetic and gravity field. A cuboid is like a cube in that it has six faces that meet perpendicularly, but the faces do not have the same size. Rectangular cuboids of 1500 x 1500 x 200 m (X x Y x Z) were used in the BC model. Although the modelling software is fully 3D, i.e. it does not interpolate between parallel profiles but calculates the response at each point based on contributions from all the surrounding points, the model is generally created along E-W and N-S profiles, and/or along vertical layers or depth slices and the results are shown this way. Custom oriented profiles can also be used. The model includes the whole central and south-eastern BC, and the southern part of the northern lobe, an area of approximately 410 km by 300 km (Figure 5.1). Most of the more detailed modelling focussed on the upper 25 km of the crust, but the gravity effect of the crust-mantle interface and other deeper-seated material were included in the calculated field. Therefore, even if only the upper crustal model is shown, the deeper-seated density contrasts are accounted for.

5.6.1 Deeper-seated dense material

The density contrast between the crust and mantle causes a roughly 100 mgal long wavelength anomaly in the calculated field (Figure 5.5) on which the short wavelength anomalies of the upper crustal material are superimposed. The thickest crust and

therefore lowest gravity values underlie the western and northern lobes. As a result the RLS had to be more than 10 km thick to fit the calculated to the observed gravity field. An alternative way to achieve a good fit is to add deeper-seated dense material in this part of the BC. Material with a density of 3250 kg/m^3 was added at the Moho, but it can also be modelled shallower, although it will then have to be thinner or less dense. Changing the crustal thickness can also have a similar effect. The individual crustal thickness models have uncertainties of 2-3 km (Nair et al., 2006; Kgaswane et al., 2009, 2012; Youssof et al. 2013) but variations between the models can be more than 10 km. However, to limit the number of unknowns in our model, the average crustal thickness was not edited.

5.6.2 Thickness and depth

The RLS in the western lobe has a relatively consistent thickness in the order of 5 to 6 km (Figure 5.10), reaching more than 7 km in places (Figure 5.11). Along the edges where the gravity values are the highest, the RLS is at or close to the surface. It dips at angles of 8º to 15º towards the centre of the BC until it flattens out and stays at relatively constant depth up to the gravity high in the centre of the BC, except where it is interrupted by the Crocodile River Fragment (Figure 5.10a). The modelled dips are shallower than the mapped dips that range between 10º and 20º, but the resolution of the model makes it difficult to establish dips to better than a few degrees. Along the P1-86 seismic line, the modelled RLS is at the same depth as in the seismic interpretation, but almost double the thickness (Figure 5.7a, Figure 5.10d). This is not the case along the JCI seismic line roughly 75 km to the west, where the modelled RLS depth and thickness correspond well to the seismic interpretation. Odgers et al. (1993) observed poor signal quality north of CMP 600 on P1-86 (Figure 5.7a). CMP 600 corresponds to the area where the RLS flattens out and it is possible that the poor data quality compromised the seismic interpretation.

The amplitudes of the gravity highs over the eastern lobe are generally 10 to 20 mgal larger than those over the western lobe (Figure 5.3a). This is in part because the RLS crops out or is closer to the surface in the eastern lobe, but the thinner crust under the eastern lobe also contributes (Figure 5.6f). Along the eastern margin the modelled RLS thickness ranges between roughly 5 and 8 km (Figure 5.10a, Figure 5.11, Figure 5.12a), thinning gradually from north of the Steelpoort Fault southward. It dips towards the west at angles on average between 5º and 10º but west of the Stofpoort Fault in the north the dips are in excess of 70º to the south. These dips correspond well to dips shown on geological maps. Correlation with the depth to and thickness of the RLS interpreted on the *Sek* seismic line is good east of the Malope Dome, but the model does not show the drastic thinning indicated on the seismic line west of the dome (Figure 5.7b, Figure

5.12a). Another interpretation of the *Sek* seismic line shows the thickness of the RLS to remain relatively constant on either side of the Malope Dome (Sargeant, 2001).

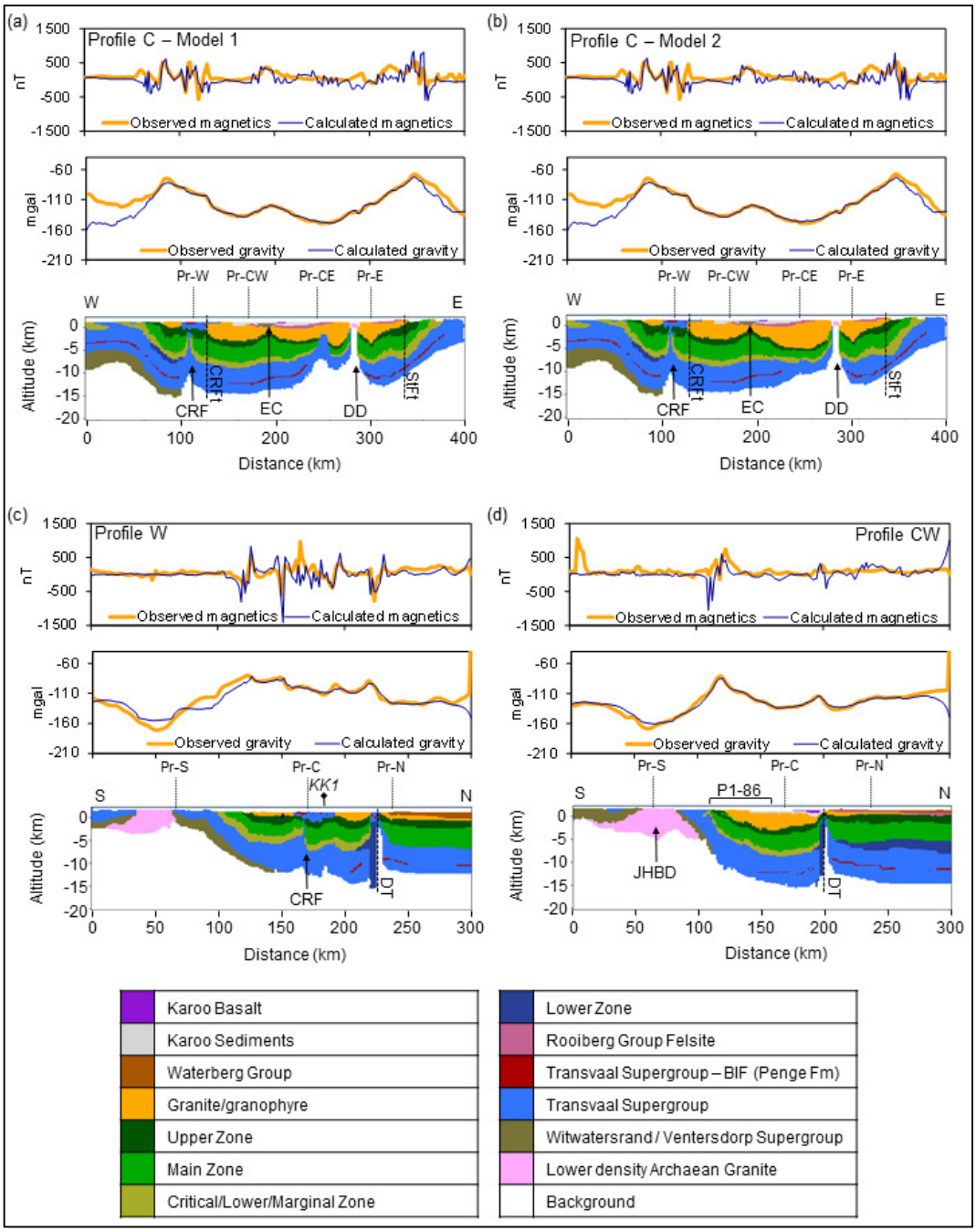


Figure 5.10. Models along profiles extracted from the 3D model. (a) and (b) Two different ways of modelling the eastern gravity low along Profile C; (c) Model along Profile W, with the locality of borehole KK1 shown (log in Figure 5.8c); (d) Profiles CW with the P1-86 deep seismic reflection line shown (Figure 5.7a). Figure 5.3 shows the profile localities. CRF – Crocodile River Fragment; CRFt – Crocodile River Fault; DD – Dennilton Dome; DT – Droogekloof Thrust; EC - Elandskraal Complex; JHBD – Johannesburg Dome; StFt – Steelpoort Fault. Localities of crossing profiles are indicated above the model (eg. Pr-W). Table 5.1 shows the densities and magnetic properties used in the model

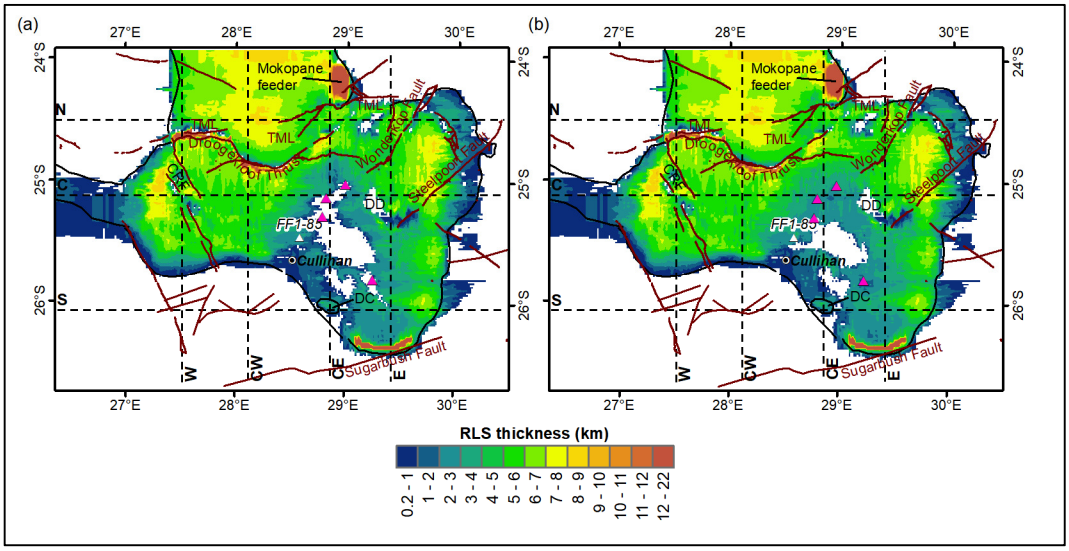


Figure 5.11. Thickness of the modelled RLS for two models. (a) Model with updoming in the east; (b) Model with thick granite-granophyre in the east. Pink triangles indicate areas where the two models differ the most. DC – Dwarsfontein Complex; DD – Dennilton Dome; FF1-85 is a borehole (log in Figure 5.8e)

In the area between the Dennilton Dome, Marble Hall and Stavoren Fragments in the west, and the outcropping RLS in the east, the RLS does not flatten out but rather continues gradually deeper until it encounters one of the numerous inliers of pre-BC rocks and moves up against its sides, giving it an almost synclinal form (Figure 5.10a,b). The Bushveld granite/granophyre is approximately 1.5 – 3 km thick here. In our models the RLS is generally thinner west of the Marble Hall and Dennilton Domes and in places are less than 3 km thick (Figure 5.11).

Lower Zone material was included separately from the Lower/Critical Zone material in the north-east (Figure 5.12a) due to the presence of very thick Lower Zone in this area (Cameron, 1978; Wilson 2015). Three boreholes drilled in the Clapham Compartment (CH1, CH6, CH7 in Figure 5.1) intersected 2.1 km of Lower Zone, Marginal Zone and the Basal Ultramafic Sequence (Wilson, 2015) (Figure 5.1).

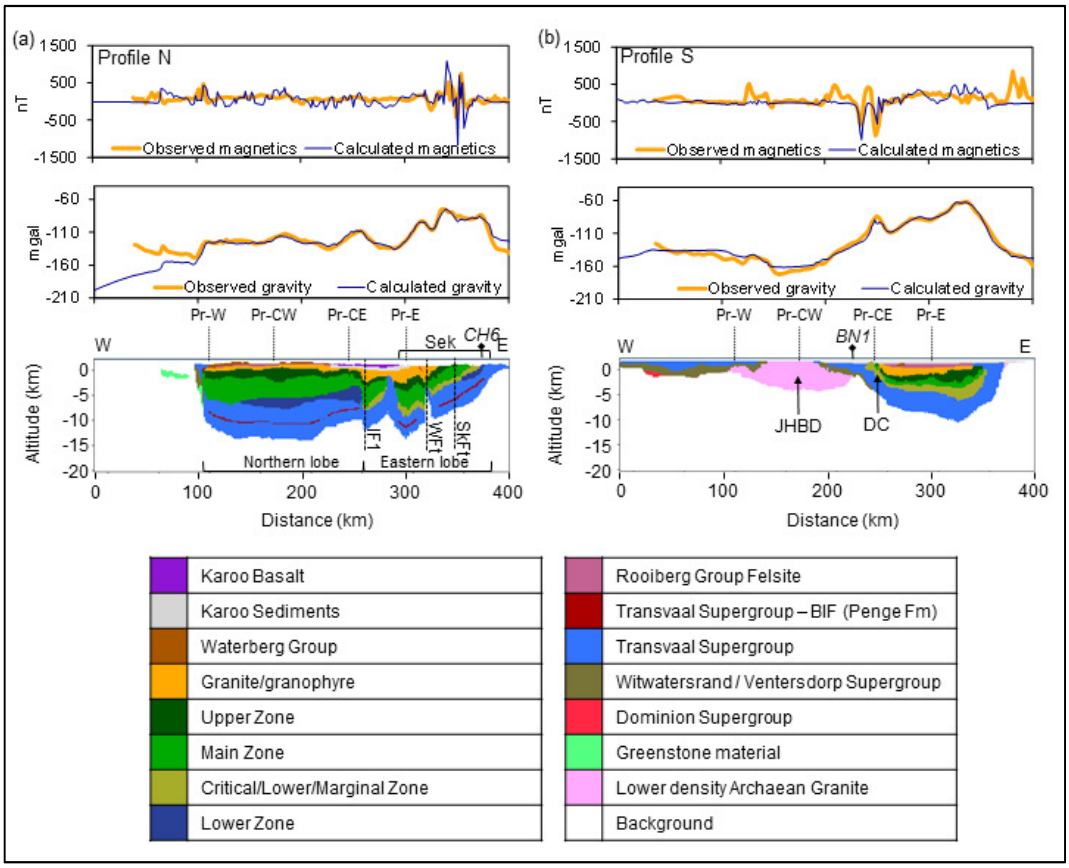


Figure 5.12. (a) Model extracted from the 3D model along profile N; (b) Model extracted from the 3D model along profile S. Figure 5.3 shows the profile localities. The position of the deep seismic reflection line Sek (Figure 5.7b) is indicated in (a). CH6 and BN1 are boreholes (logs in Figure 5.8f, g). DC – Dwarsfontein Complex; IF1 – Inferred Fault 1; JHBD – Johannesburg Dome; StFt – Steelpoort Fault; WFt – Wonderkop Fault. Localities of crossing profiles are indicated above the model (eg. Pr-W). Table 5.1 shows the densities and magnetic properties used in the model

Regional gravity and aeromagnetic data revealed the presence of Bushveld Complex rocks underneath younger cover material south of the eastern lobe. This has not been studied as extensively as the rest of the Complex with most work published in the late 1970s by Buchanan (1975, 1976, 1977, 1979). Boreholes drilled on the gravity high (Figure 5.3a, Figure 5.8j,k) revealed five petrographic zones, four of which were correlated with the Upper Zone and one which represents the Lower Zone of the Bushveld Complex (Buchanan 1975, 1976, 1977, 1979). The apparent absence of the Critical and Main Zones was cited as evidence that these rocks represented an injection centre separate from the main Bushveld basin.

The highest amplitude gravity values along the southern margin of the south-eastern lobe are roughly 5 - 10 mgal larger than the highest gravity values in the eastern lobe. Considering that the RLS is close to the surface in the eastern lobe but covered by a kilometre of lower density acidic BC rocks and younger sediments in the south-eastern lobe, much thicker RLS is required to model the gravity in the south-eastern lobe than in the eastern lobe. Also, since the thick Main Zone was not encountered in the boreholes drilled into this lobe, the Lower Zone had to be more than 10 km thick in places (Figure 5.13). The peak of the gravity anomaly that defines this lobe is approximately 10 km wide. North of this the gravity values decrease gradually and requires thinner dense mafic material to obtain a fit. The mafic material continues getting deeper for about 50 km north of the peak after which it flattens out at a depth 4 km below the surface. The lack of large amplitude magnetic anomalies requires the highly magnetic Upper Zone to be deep, with Rooiberg Felsite accounting for the shallow short wavelength anomalies. The RLS continues northwards up to the RLS outcrop south of the Dennilton Dome. Since the Main Zone crops out here, it is conceivable that it continues further to the south. In our model the Main Zone thins out where the dip of the RLS increases (Figure 5.13).

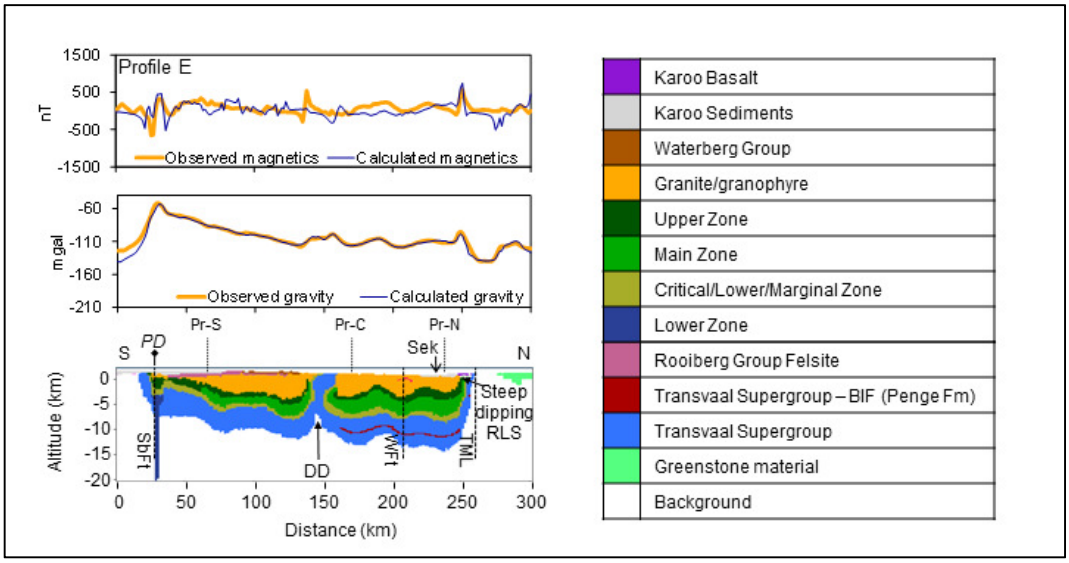


Figure 5.13. Model extracted from the 3D model along profile E. Figure 5.3 shows the profile locality. The position where the profile crosses the deep seismic reflection line Sek (Figure 5.7b) is indicated. ONZ1 and PD are boreholes (logs in Figure 5.8j, k). DD – Dennilton Dome; SbFt – Sugarbush Fault; TML – Thabazimbi-Murchison Lineament; WFt – Wonderkop Fault. Localities of crossing profiles are indicated above the model (eg. Pr-S). Table 5.1 shows the densities and magnetic properties used in the model

A gravity high and associated magnetic anomaly located to the northwest of the south-eastern lobe gravity anomaly is known as the Dwarsfontein Complex (Figure 5.1, Figure 5.3 and Figure 5.12b). This complex consists of mafic layered rocks with distinctive zoning that intruded into the Pretoria and Rooiberg Groups and Loskop Formation (Schutte, 1990). The zones correspond to the Critical, Main and Upper Zones. Pyroxenite and wehrlite (with PGE) make up the Critical Zone. The Main Zone consists of norite, gabbro, diorite and anorthosite and the Upper Zone contains magnetite gabbro, diorite and pyroxenite. In contrast, Anhaeusser (2006) mentioned that exploration drilling on the complex encountered analogues of the Upper, Main and Lower Zones but noted that the Critical Zone appeared to be absent. Sulphide mineralization is present in the Lower Zone. Although these authors differ on the presence of Critical and Lower Zone, it is important to note that they both refer to the presence of the Main Zone, confirming that the Main Zone is present in part of the south-eastern lobe. Schutte (1990) attributed the large magnetic anomaly to the magnetite gabbro of the Upper Zone, but the large amplitude negative anomaly may be partly due to magnetic shales of the Lower Witwatersrand Supergroup that is located in this area and cause the anomalies to the south.

In our model the northern part of the Dwarsfontein Complex is a continuation of the south-eastern lobe, but the southern part is separated by updomed TVL Supergroup (Figure 5.11). To obtain a high enough amplitude calculated gravity field the RLS has to be 2 to 3 km thick (Figure 5.11, Figure 5.12b). The magnetic data constrains the thickness of and depth to the Upper Zone, and the remanent magnetisation of the Main Zone also prohibits it from being too thick in the model. Therefore, the Critical and Lower Zones has to be very thick. It is also possible to model the deepest part as Lower Zone only.

5.6.3 Domes and diapirs

Mapped pre-BC inliers generally cause gravity lows (Figure 5.3a), and where magnetic anomalies occur they correlate with mapped iron-formation in the TVL Supergroup (Figure 5.3b). The northern part of the Marble Hall Fragment is different, showing a gravity high and reversely magnetised magnetic anomalies.

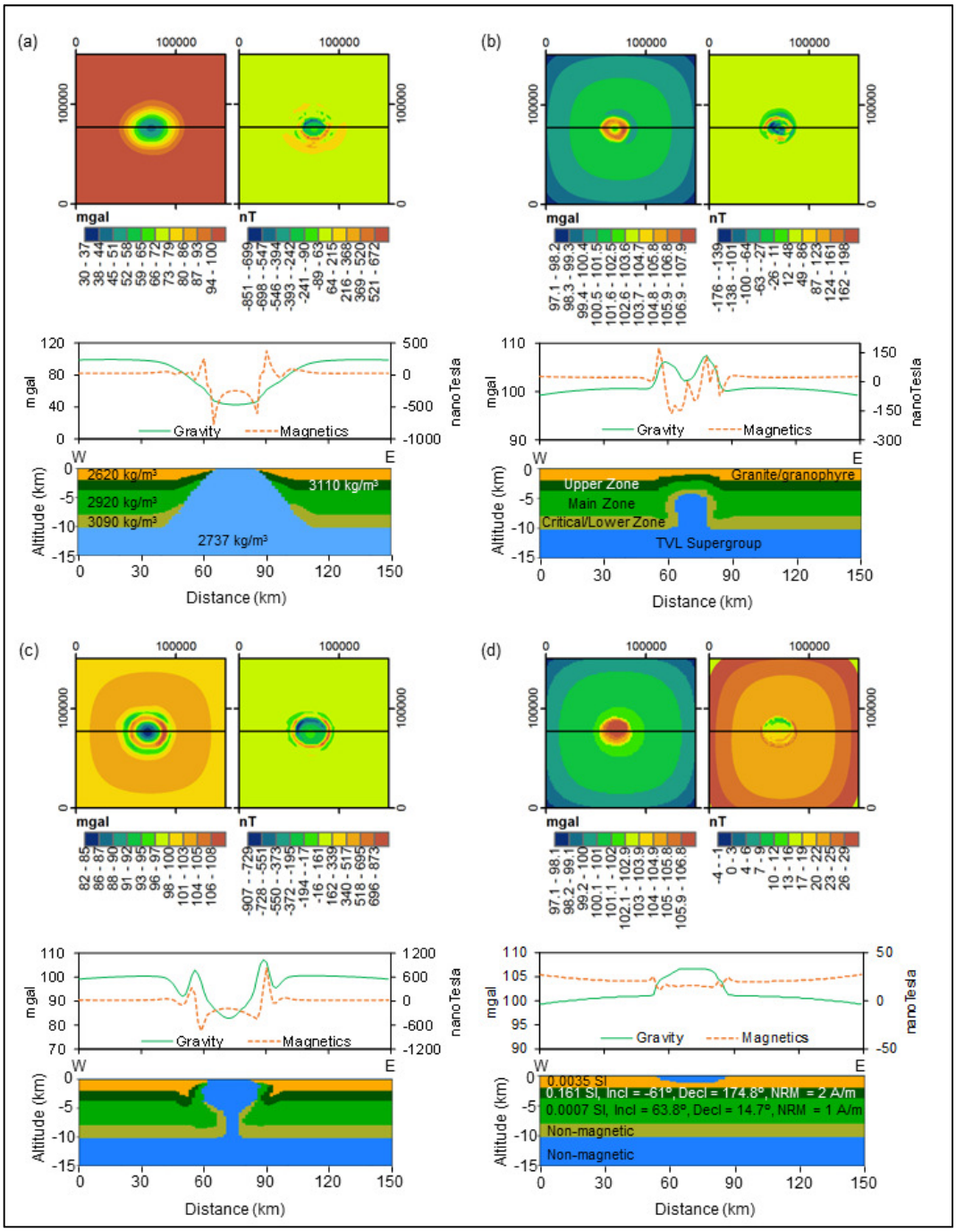


Figure 5.14. Synthetic potential field models of (a) a dome surrounded by dense material; (b) and (c) a diapir at different stages of development; (d) a diapir that has been completely disconnected from its base. Physical properties of the individual layers are indicated in the model. In (d) magnetic remanence properties are shown where applicable. The ambient magnetic field has an inclination of -63º, a declination of -17º, and an intensity of 28 500 nT

Synthetic models were created to investigate the magnetic and gravity responses of a dome and a diapir at different stages of development (Figure 5.14). The simple models

reflect the development of a diapir in the BC based on numerical modelling (Gerya et al., 2004). For a simple dome with onlapping RLS the gravity anomaly is a simple low over the dome (Figure 5.14a). The magnetic anomaly is also relatively simple with peaks over the magnetic Upper Zone where it is close to the surface. As a diapir starts to develop, the dense material over the diapir causes positive gravity anomalies, but the low density material at the core of the diapir causes a low at the centre of the gravity high (Figure 5.14b). At the same time the magnetic Upper Zone over the diapir causes an additional positive anomaly over the diapir. The next model (Figure 5.14c) shows the diapir at a more advanced stage where the dense RLS is not present over the diapir anymore but has been dragged underneath the bulbous part of the diapir. Gravity highs associated with the folded high density RLS surround the gravity low. These highs are surrounded in turn by lows caused by the down warping of the dense material around the diapir. The magnetic anomaly is similar to that for a simple dome (Figure 5.14a). In the final model (Figure 5.14d) the diapir has been disconnected from its base and the layers it pushed through have reconnected. The contrast between the low density granitic material (2620 kg/m^3) and the sediments forming the diapir (2737 kg/m^3) causes the gravity high.

Crocodile River Fragment

The CRF is considered to be updomed TVL Supergroup resulting from interference folding (Hartzer, 1989, 1995). However, even though the CRF correlates with low gravity values, the values are not low enough to be modelled by updomed TVL Supergroup only. Including dense material underneath the TVL rocks (Ventersdorp/Witwatersrand and Dominion Supergroups were tested) did not adequately lift the calculated gravity field. The easiest way to obtain a reasonable fit was to model the CRF as a diapir with RLS impinging underneath the mapped TVL rock (Figure 5.10a,b,c).

Dennilton Dome

The Dennilton Dome is a roughly 18 km wide outcrop of Archaean material surrounded by Bushveld granites in the west, north and east, and south-eastward dipping TVL Supergroup in the southeast (Figure 5.1). Further to the southeast the Lower and Critical Zones of the RLS overlay the TVL Supergroup. As expected, the outcropping granites cause a gravity low to coincide with this part of the dome and in order to model it very low density material (2550 kg/m^3) was needed (Figure 5.10a,b). It corresponds to the mapped extent of Vaalfontein Suite gneisses (Hartzer, 1995). The density is very low for gneissic material but is feasible since similar densities were measured for the Archaean Goudplaats - Hout River gneiss north of the TML. The gravity low coincides with the centre of the dome, but the diameter of the outcropping granite-gneiss is almost 10 km larger than the gravity low. Higher density material is therefore needed underneath the

outer part of the granite. Similarly, along the southern margin of the dome RLS had to be included underneath the TVL Supergroup in order to fit the gravity data (Figure 5.13) which indicates possible diapirism in this part of the dome.

Marble Hall Fragment

Archaean granite cropping out in the southern part of the Marble Hall Fragment correlates with low gravity values, but a gravity high coincides with the northern part of the Marble Hall Fragment. Here lower TVL Supergroup forms the core and increasingly younger TVL Supergroup rocks surround it. The geological map shows Upper Zone in the centre of the fragment, which explains the high gravity values, however, the absence of any substantial magnetic anomalies casts doubt that this is indeed Upper Zone. De Waal et al. (2008) describes the rocks as dioritic sills derived from a magma that formed during the same time as the magma considered to be parental to the Lower Zone with an age of 2055.6 ± 3.1 Ma. By replacing the Upper Zone with Lower Zone material in the model it was possible to model both the gravity and magnetic data. However, the northern part of the Marble Hall Fragment could not be modelled as a simple dome capped by Lower Zone. The ultramafics would have to be 3 km thick to fit the observed gravity data, whereas the diorite sills are generally 2 to 10 m thick (De Waal et al., 2008). They form stacks, but these also only reach a few hundred metres in thickness. A detailed study of pre- and syn-Bushveld sills in the Transvaal Supergroup rocks east of the BC showed and average thickness of 34 m for these sills, with one sill of 238 m encountered (Button and Cawthorn, 2015). It therefore seems unlikely to have a 3 km thick sill. A good fit could be obtained by including dense material underneath the TVL Supergroup rocks.

Smaller inliers

Lower gravity values coincide with the Stofpoort and Wonderkop faults and along the inferred southward extension of the latter. A series of domes or diapirs is situated along these faults all the way from the northernmost edge down to the Stavoren and Marble Hall Fragments (Button, 1978) (Figure 5.2). The Katkloof (Uken and Watkeys, 1997) and Zaaikloof (Phosiri) Domes (Scoon, 2002) have both been described as diapiric structures that mobilized during contact metamorphism of the Transvaal Supergroup by the emplacement of the RLS.

5.6.4 Gravity lows in the eastern lobe

A borehole drilled (RBL2, Figure 5.1, Figure 5.3a) into the gravity low in the north of the eastern lobe encountered sediment of the TVL Supergroup rocks at a depth of 380 m and stops in these sediments at 530 m (Figure 5.8i). The anomaly is typical of a dome (Figure 5.14a) and the gravity low was therefore modelled as simple updomed pre-BC material.

The large gravity lows over the western part of the eastern lobe, south of the EW trending unnamed fault (UF1 in Figure 5.1) could be modelled in two ways that can be considered as end members of the possible ways to achieve the observed gravity lows. The one model shows updomed pre-BC material over which the RLS is absent (Figure 5.10a, Figure 5.15a). It was impossible to model RLS covering the domes and still maintain low enough gravity values. These updomed areas correspond with outcropping Rooiberg Group and Bushveld granite-granophyre surrounded by younger sediments of the Waterberg Group and Karoo Supergroup. In places very low density (2500 kg/m^3) was needed under the domes to lower the calculated gravity field sufficiently.

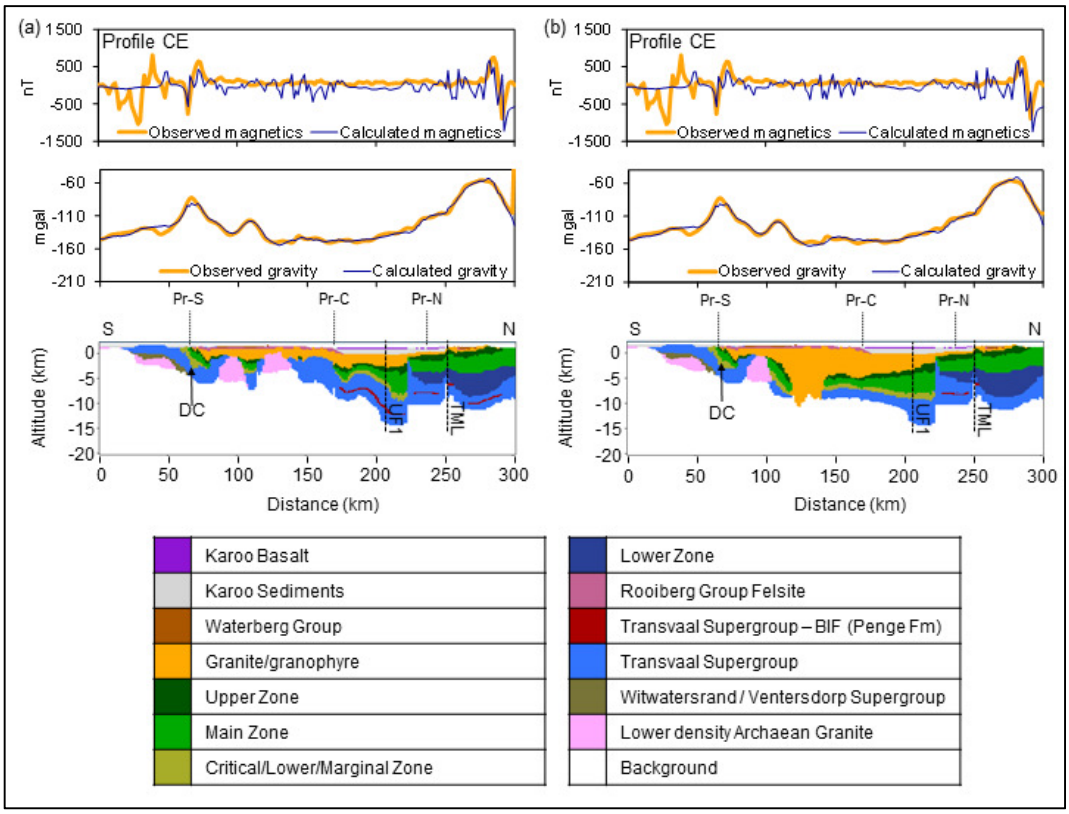


Figure 5.15. Two models along profile CE extracted from the 3D model. (a) Gravity lows in the southern half modelled as domes; (b) Gravity lows in the southern half modelled as a dome and thick granite-granophyre. Figure 5.3 shows the profile locality. DC – Dwarsfontein Complex; UF1 – Unnamed Fault 1; TML – Thabazimbi-Murchison Lineament. Localities of crossing profiles are indicated above the model (eg. Pr-S). Table 5.1 shows the densities and magnetic properties used in the model

In the second model the thickness of the BC granite-granophyres was increased, ranging between 5 and 10 km, and the RLS had to be very thin (2-3 km) (Figure 5.10b, Figure

5.15b). Where the gravity field reaches its lowest values, the RLS had to be completely absent with the granite-granophyre extending even deeper.

In both models the RLS is very thin in the eastern lobe between the updomed RLS in the centre of the BC and the Dennilton and Marble Hall structures.

5.6.5 Feeders

Over the years different feeders have been proposed for the RLS. Sharpe et al. (1981) interpreted a number of gravity highs as feeder sites, however, these highs can be modelled without feeders (Kruger, 2005). The Steelpoort Fault has also been considered a feeder in the eastern lobe (Kruger, 2005; Cawthorn et al., 2002; Kruger and Behr, 2002) and Buchanan (1975) suggested a separate feeder for the southeastern lobe. Most consensus is that the TML, which separates the northern lobe from the central BC, played an important role in the emplacement of the Bushveld Complex (e.g. Du Plessis and Walraven, 1990; Good and De Wit, 1997; Kruger, 2005; Clarke et al., 2009; Maier et al., 2013; Finn et al., 2015).

In this section, anomalies that may indicate possible feeders will be discussed. The absence of an anomaly does not preclude the possibility that a feeder was present at a certain locality, but the geophysics can only show preserved feeders with sufficient size and physical properties contrast with the surrounding material

Mokopane feeder

The 110 mgal gravity anomaly west of Mokopane (Figure 5.3a) was modelled in the past as a feeder consisting predominantly of Lower Zone material (Van Der Merwe, 1976; Du Plessis and Kleywegt, 1987; Finn et al., 2015) and we also found this to be the only way to obtain a reasonable fit between observed and calculated gravity fields (Figure 5.15). Similar to the previous geophysical models, in this study the feeder near Mokopane was taken to consist wholly of Lower Zone rocks. The surface geological map of Van der Merwe (2008) constrained the upper part of the model. Despite the high density of the Lower Zone (3200 kg/m^3) the body had to extend to a depth of 20 km to achieve high enough gravity values (Figure 5.11). At its widest the feeder is roughly 30 by 40 km. It narrows down to 1.5 km which is the resolution of the model. The difference in depth extent between this model and the model by Finn et al. (2015) shows the effect of different crustal thicknesses on the gravity models and density contrast. As discussed in Finn et al. (2015), the thickness of the proposed feeder is therefore not well constrained, but must be at least 10 km.

TML

Positive magnetic anomalies and high gravity values occur along the Droogekloof Thrust west of Mokopane and deeper-seated dense material was necessary to model the gravity anomaly (Figure 5.10c, d). The Droogekloof Thrust forms part of the Thabazimbi-Murchison Lineament (TML). BIF brought closer to the surface by the thrust accounted for the magnetic anomalies. One possible explanation for the deeper-seated dense material is RLS caught up in the TML (Figure 5.10c, d) as shown by the thick Rustenburg Layered Suite (RLS) along the TML previously modelled (Finn et al., 2015). The Droogekloof Thrust was active during the emplacement of the BC (Good and De Wit, 1997) and if the TML acted as a feeder zone, remnants of the RLS may be present in the TML. Very dense material was necessary to fit the gravity anomaly and modelling it as Lower Zone yielded the best fit. The Lower Zone in the TML was modelled down to depths of 15 km and it extends south from the TML underneath the western lobe for roughly 20 km. This differs from the previous model (Finn et al., 2015) that showed thickened (9 km) MZ along the south of the TML. Densities were only available for a few samples in the Lower Zone (Chapter 2) but based on its ultramafic composition it is expected to be denser than the Main Zone. Both models show that the gravity data requires dense material in the TML.

South-eastern lobe

For both the Dwarsfontein Complex and the rest of the south-eastern lobe thick Lower Zone was modelled underneath the gravity peaks, in places extending down to 8 km (Figure 5.12b, Figure 5.13, Figure 5.15). The shape of the Lower Zone along the southern margin of the south-eastern lobe resembles a feeder.

5.6.6 Faulting

South-north profiles across the southern, east-west striking part of the western lobe show stepwise decreases in the observed gravity field. This was best modelled with the RLS increasing in depth in a similarly stepwise fashion, resembling normal faulting with down-throw on the northern side (Figure 5.16).

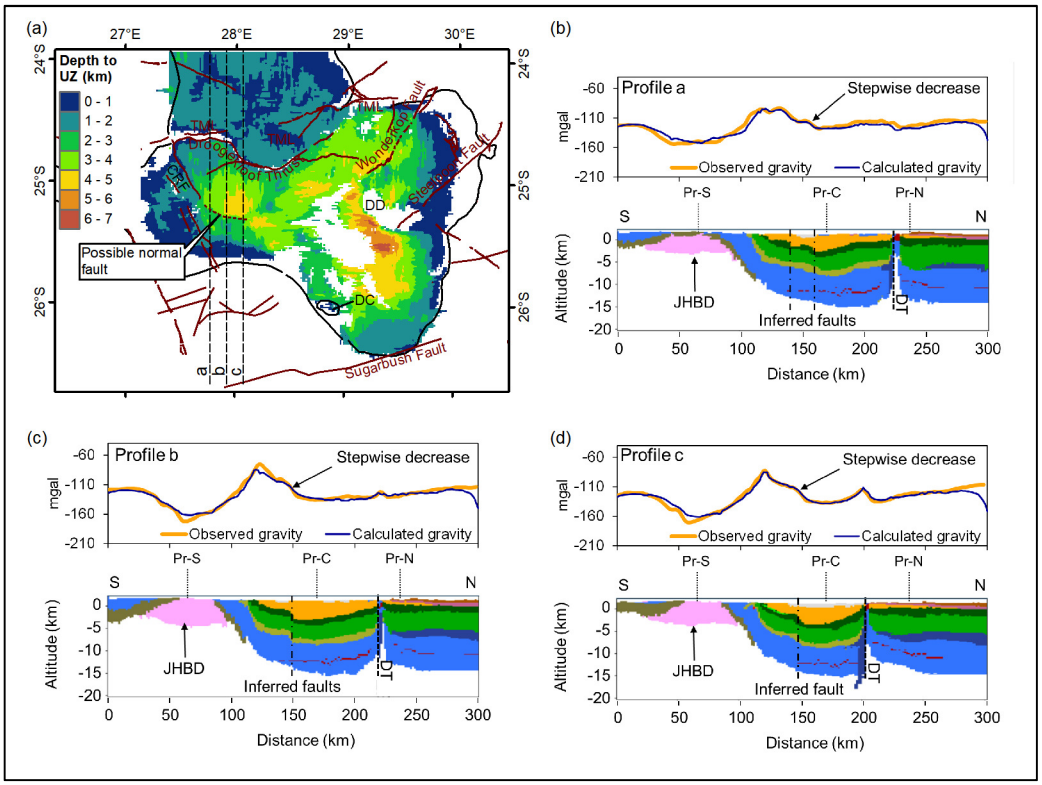


Figure 5.16. (a) Modelled depth to the Upper Zone; (b) to (d) Models extracted from the 3D model along three profiles where normal faults were modelled.; DC – Dwarsfontein Complex; DD – Dennilton Dome; DT – Droogekloof Thrust; JHBD – Johannesburg Dome. Localities of crossing profiles are indicated above the model (eg. Pr-S). Table 5.1 shows the densities and magnetic properties used in the model

Boreholes drilled to the west of the Upper Zone (e.g. BTZ2, Figure 5.8h, Figure 5.17) encountered Transvaal Supergroup rocks below the Karoo Supergroup. Decreased gravity values and no clear deep-seated magnetic anomalies indicate that the RLS is absent between the western edge of the Upper Zone magnetic anomaly and an inferred fault (IF1 in Figure 5.17). This inferred fault defines the southeastern edge of the northern lobe. Downward displaced rocks continue from the updomed TVL Supergroup rocks north of the TML.

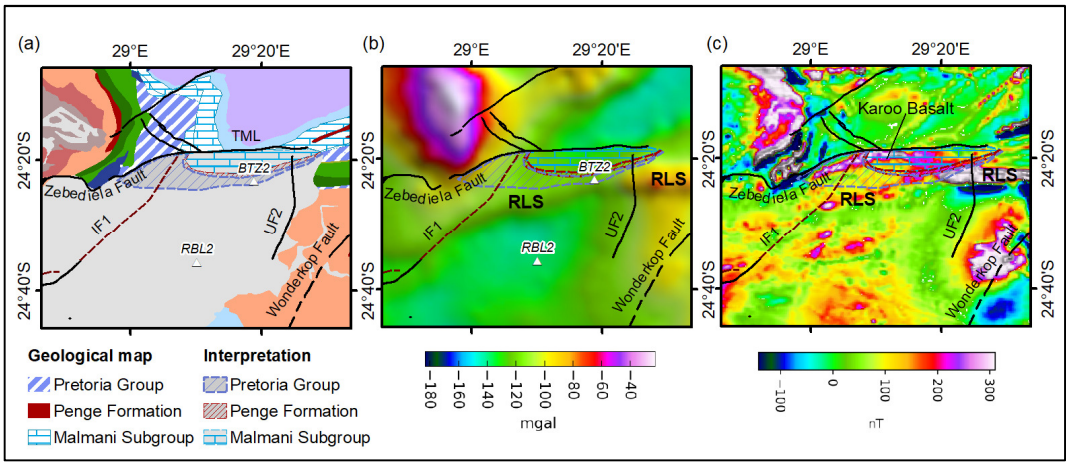


Figure 5.17. (a) Interpreted down-faulted TVL Supergroup rocks south of the TML in the northeast of the BC; (b) Gravity data with the interpretation overlain; (c) Magnetic data with the interpretation overlain. IF1 – Inferred fault 1; UF2 – Unnamed fault 2

5.7 Discussion

5.7.1 Deep-seated dense material

To fit long wavelength anomalies, dense material had to be added at depth underneath the northern lobe and around the western and eastern lobes (A1 to A4 in Figure 5.18). The exact depth and density of the deep-seated dense material is not important in this instance, but rather the fact that dense material can be included underneath parts of the BC. The dense material may be a remnant of a magma staging chamber or chambers proposed to be present by many researchers (e.g. Harris et al., 2005; Mondal and Mathez, 2006; Naldrett et al., 2009; Wilson, 2012). This interpretation is very tentative since the diffuse Moho introduces a degree of uncertainty in the crustal thickness model, specifically underneath the BC (Delph and Porter, 2015). Also, dense material lower in the crust does not necessarily have to be caused by a staging chamber but can point to magmatic underplating.

The difference between the models requiring additional deep dense material and the models showing the effects of different crustal thickness models (Figure 5.6) is due to the oversimplification of the latter. The RLS was modelled as one entity with a density of 3009 kg/m^3, whereas the more detailed models separated the RLS into zones. As the Main Zone is the thickest and has the lowest density of all the zones (2911 kg/m^3), it most affects the calculated field. Synthetic model shows a decrease of almost 10 mgal when dividing the RLS into zones.

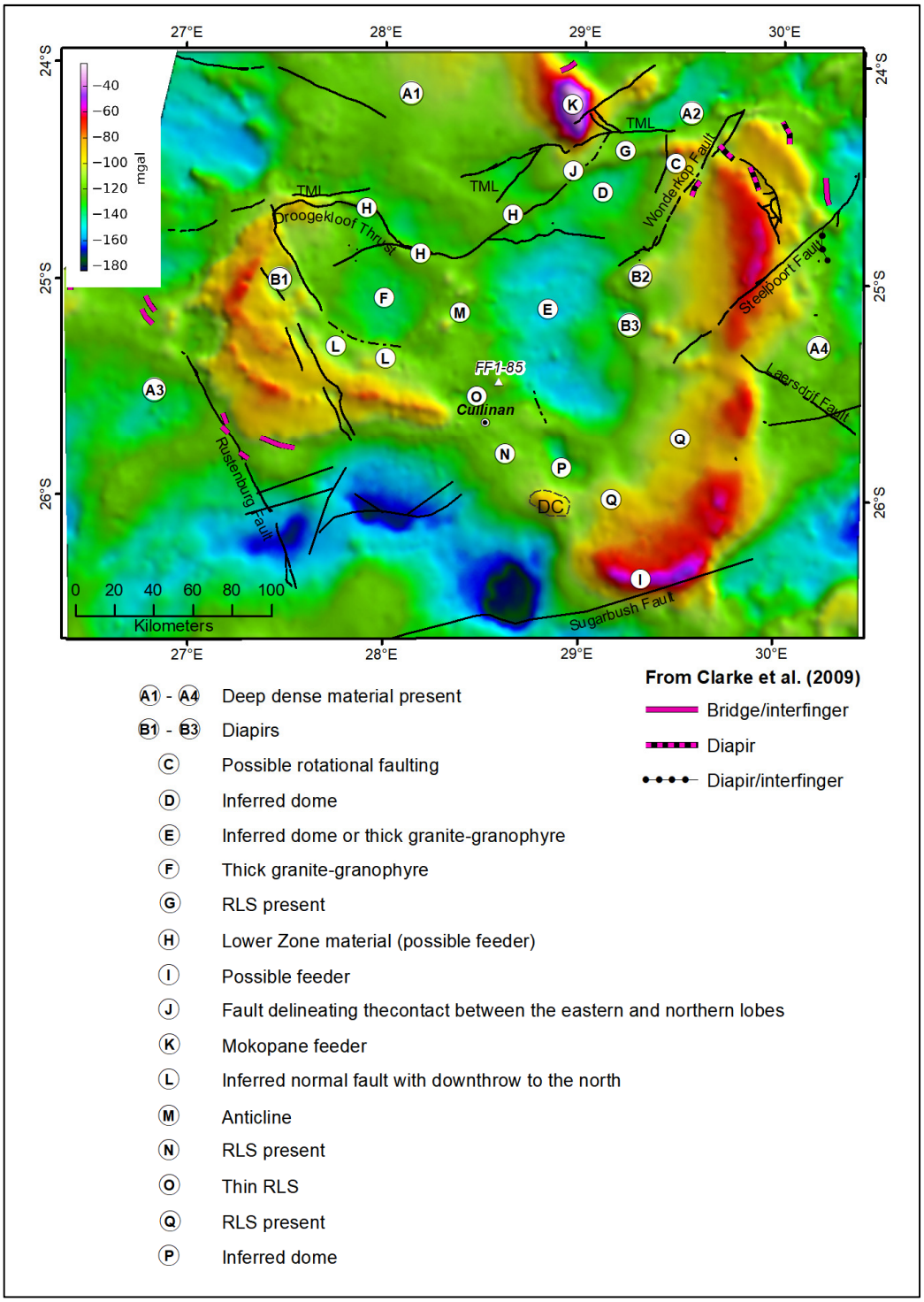


Figure 5.18. Some of the main findings shown on the observed gravity data set

5.7.2 Domes and diapirs

The potential field data clearly shows the presence of the numerous TVL Supergroup inliers throughout the central BC, and possible updomed areas under more recent cover

material. Many of these, specifically the smaller inliers in the northeast have been described as diapirs that formed due to the heating of the TVL Supergroup sediments by the RLS magmas (Clarke et al., 2000; Scoon, 2002; Gerya et al., 2003). The resolution of our model prohibited detailed modelling of these smaller features, but the concept of diapirism may extend to the other larger inliers. The CRF corresponds to a gravity low, but it could not be modelled as simply underlain by TVL Supergroup rocks (B1 in Figure 5.18). By modelling the RLS to impinge upon the TVL rocks underneath the CRF the fit was improved. The resulting model represents a diapir with the TVL rocks forming a relatively thin stem before mushrooming out at the top (Figure 5.19).

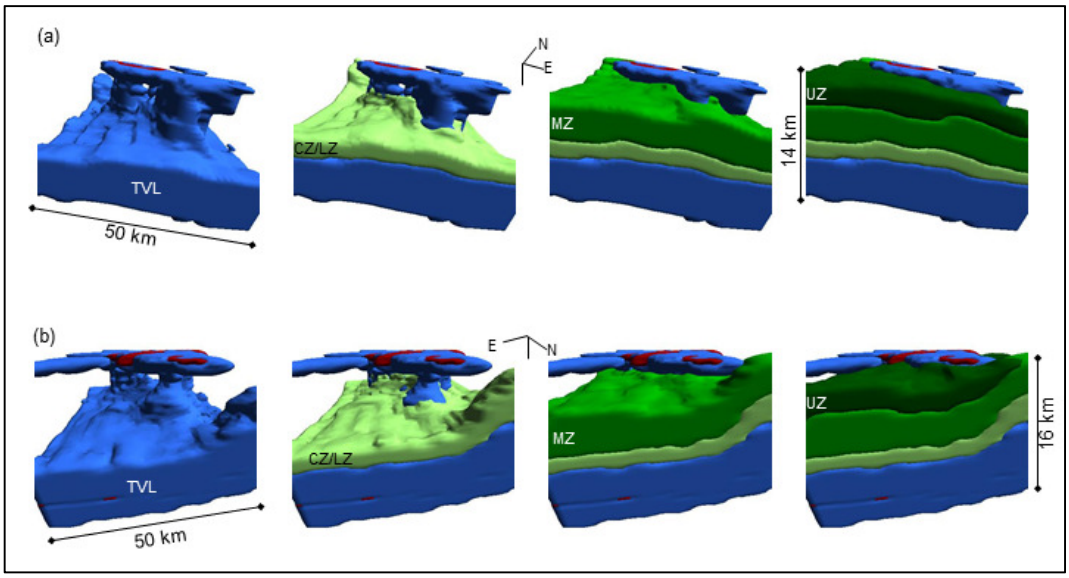


Figure 5.19. Perspective views of the CRF looking from the (a) south and (b) north showing the modelled diapiric shape. From left to right, images show additions of the various components of the model

The large inliers in the eastern lobe present a more complex situation (B2, B3 in Figure 5.18). Various authors proposed folding events before and during the intrusion of the BC. Bumby et al. (1998) described shortening events after the deposition of the Transvaal Supergroup but prior to the intrusion of the BC that resulted in interference folding in the western lobe. The D_1 shortening direction was NE-SW, followed by a NNW-SSE directed D_2 shortening event. Clarke et al. (2010) questioned the pre-Bushveld origin of these folds, preferring a model whereby the folds were interfinger deformation zones that formed during the intrusion of the BC. In yet another proposal a shortening event with σ_1 NE-SW started during emplacement of the Upper Zone and continued until after emplacement of the acid phase (Du Plessis and Walraven, 1990). Large transgressions

of Bushveld rocks into lower stratigraphic levels in the northern and southeastern lobes led Von Gruenewaldt (1979) to suggest the existence of anticlines in these areas during the emplacement of the layered sequence. He proposed that one of these, the Zebediela-Pretoria anticlinal warp defined by the Marble Hall, Dennilton and Malope Domes existed at the time of emplacement and that it was tectonically active during the emplacement of the Bushveld Complex.

Simple synthetic geophysical models show the gravity and magnetic responses of a dome with onlapping RLS, and diapirs at different stages of development (Figure 5.14). Our models show that the Dennilton and Marble Hall Fragments cannot be modelled as simple domes with onlapping younger material, even though this is what the mapped geology shows, but that dense material is present underneath the mapped pre-BC rocks. A possible explanation could be greenstone material in the Archaean basement brought closer to the surface during folding (or just as a pre-existing basement high). Greenstone complexes are present to the north and east of the BC and even in the core of the Dennilton Dome. Another explanation can be that the RLS intruded into lower stratigraphic levels and is present underneath the outcropping pre-BC lithologies. In both of these scenarios the domes pre-date the intrusion of the BC. Any RLS that may have covered the domes have been eroded away. A third way to explain the gravity anomalies over the domes is to invoke a complex situation of diapirism and domal ridges following the emplacement model of Clarke et al. (2009). In this version of the model the Dennilton Dome is a relatively advanced diapir, but it has not reached the late stage where the stem disconnects. The outcropping granite in the south of the Marble Hall Fragment may still form part of the Dennilton diapir while the TVL Supergroup rocks to the north presents a late stage diapir where the buoyant lower density material has been totally disconnected from its base and floats separately above RLS at depth (Figure 5.20).

The TVL Supergroup and RLS lapping onto the south of the Archaean granite in the Dennilton Dome present a compelling argument for a pre-Bushveld dome. However, the requirement of dense material underneath the mapped dome may indicate that the Dennilton Dome may have been a pre-existing dome that started to undergo diaiprism during the intrusion of the RLS, but diapirism ended at some point. Granite's melting temperature is roughly 990ºC at 5 kbar (Holland and Powell, 2001) and the RLS intruded the upper crust at a pressure of < 4 kbar and with a starting temperature of 1150ºC (Zeh et al., 2015), although 1320ºC has also been proposed (Cawthorn and Webb, 2013). The thermal effect of the hot magma would penetrate to the floor rocks, and will have to be above 990ºC for the diapiric model (Figure 5.20) to work. If we assume that this was the case, the upper part of the pre-existing dome would melt and become boyant, initiating

diapirism. Rapid cooling of the magma chamber to 900ºC within about 250 ka (Cawthorn and Webb, 2013) implies that diapirism happened during the early phase of the intrusion.

Many of the domes and/or diapirs correlate with large faults, namely the NW-trending Crocodile River and Brits Faults in the western lobe, and the NE-striking Wonderkop and Stofpoort Faults in the eastern lobe. The Crocodile River and Wonderkop Faults have been described as pre-existing faults that were reactivated by the BC intrusion (Hartzer, 1995) and they have the same orientations as pre-Bushveld extensional features (Du Plessis and Walraven, 1990). Diapirs also occur on the downthrown side of the Sekhukhune Fault. It has been shown that normal faults can control the distribution of salt diapirs (Kempler et al., 1996), but it is not clear whether the pre-existing normal faults in the BC represented zones of weakness where diapirs could form easier. Diapirism is not restricted to the fault zone since previous workers noted a correlation between anticlines and what they described as floor-attached domal structures in the eastern lobe (Du Plessis and Walraven, 1990).

The dip of the RLS suddenly increases west of the Wonderkop and Stofpoort Faults indicating rotational faulting (C in Figure 5.18). Diapirism is a ductile process that took place during the intrusion of the RLS, but the rotational faulting would have taken place after crystallisation of the magma. No age has been published for these faults but it is considered to postdate the RLS (Brandl and Baglow, 2007). The coincidence between the linear zone of ductile deformation and later faulting shows that a zone of weakness existed during the intrusion of the RLS that controlled the locality of a series of diapirs, and which remained a zone of weakness after the emplacement and crystallisation of the RLS.

A gravity low of roughly 10 mgal separates the gravity anomalies at the Cullinan Diamond Mine (CDM) and borehole FF1-85 (Figure 5.18) and was modelled as a dome covered by 1 – 2 km thick RLS (Figure 5.11, O in Figure 5.18). A larger gravity low north of the Dwarsfontein Complex was also modelled as updomed material but in this case very low density basement material has to be included to lower the calculated gravity field sufficiently (Figure 5.15, P in Figure 5.18). The density of 2500 kg/m^3 is the same as that of the Vaalfontein Suite gneiss in the Dennilton Dome.

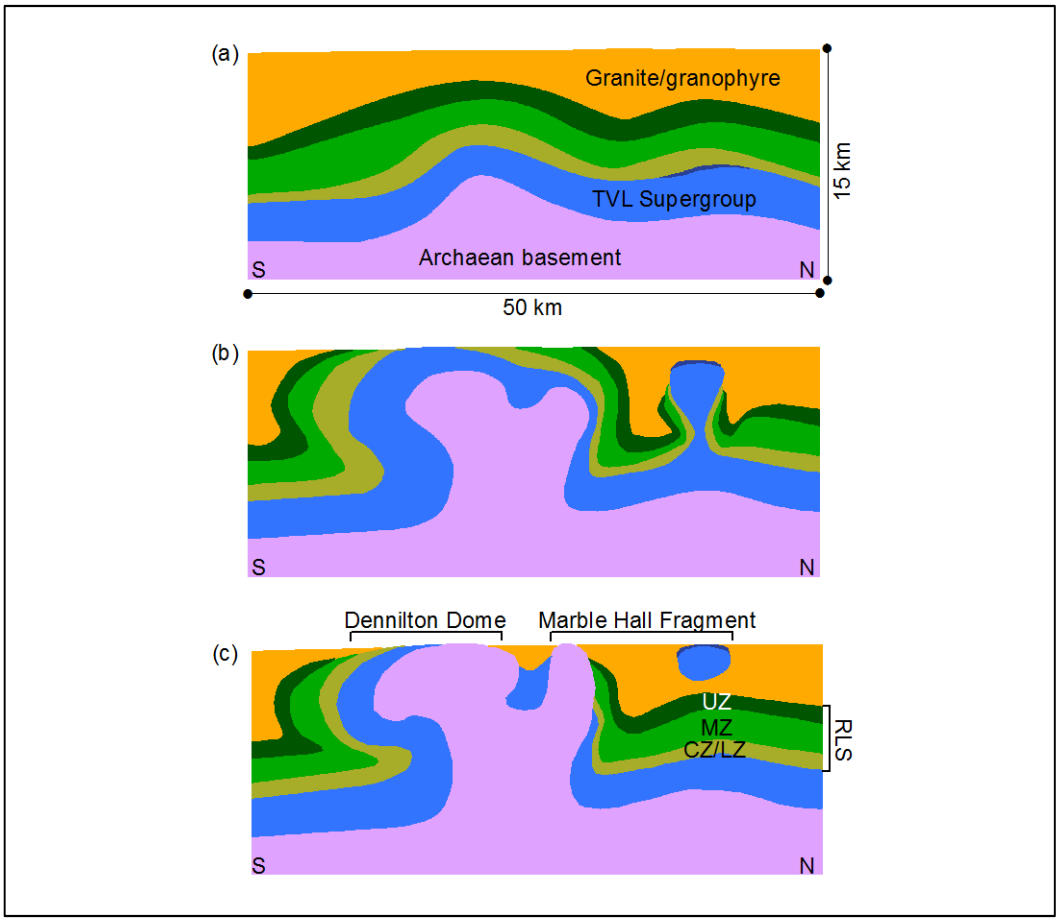


Figure 5.20. One possible development sequence for the Dennilton and Marble Hall pre-BC inliers. (a) Updoming starts due to the heat of the RLS. The floor may have been already undulating prior to the intrusion; (b) Diaprism brings deeper material closer to the surface; (c) Current situation

5.7.3 Gravity low in the eastern lobe

Gravity values for the eastern half of the BC (D, E in Figure 5.18) is 12 to 15 mgal lower than the gravity low over the western half (Figure 5.3a, Figure 5.10a,b, F in Figure 5.18). Lower gravity values result from lower densities and the gravity data therefore shows thinner or lower density material under the eastern lobe compared to the western lobe. The northernmost gravity low (D in Figure 5.18) was modelled as updomed TVL Supergroup rocks based on the fact that these lithologies were encountered in borehole RBL2 (Figure 5.3a, Figure 5.8i, Figure 5.12a). The anomaly resembles that of a simple dome with no diapirism (Figure 5.14a). This dome may be a continuation of the basement dome north of the TML and if so it would have existed prior to the intrusion of the BC. Our model shows RLS between this dome and the TML to the north (G in Figure 5.18) and continuing south of the dome. RLS that conceivably covered the dome have been eroded

in the almost 2 Ga between the intrusion of the BC and the deposition of the Karoo Supergroup.

Gravity lows to the south of UF1 (E in Figure 5.18) was modelled in two ways, namely as thin RLS covering updomed pre-Bushveld Complex rocks and as very thick granite and granophyre overlaying the RLS (Figure 5.10a,b, Figure 5.15). In the first option the RLS thins on the sides of the dome and laps onto the dome (Figure 5.10a, Figure 5.15a). Granite-granophyre covers the dome. Bushveld granites have been dated at 2054.4 ± 1.8 Ma (Walraven and Hattingh, 1993) which is very close to the age of the RLS (around 2055.91 Ma, Mungall et al., 2016; Zeh et al., 2015). This leaves almost no time for RLS to be eroded if it covered the domes, suggesting that the domes existed prior to the intrusion of the RLS and that the RLS did not cover it. If the dome formed during the emplacement of the RLS it may be a domal ridge that developed from an interfinger deformation zone as proposed in Clarke et al.'s (2009) emplacement model. In their model the magma intruded from the TML in the north and formed fingers of magma that moved southward in the TVL Supergroup rocks. Sedimentary rocks in the zones between magma fingers underwent compressive deformation and lead to the development of domal ridges and in some instances, diapirs. Whether a domal ridge can be as wide as in our model (30-40 km) is unclear. The mafic rocks are present to the west and south of this dome showing that it did not impede the intrusion of the RLS. Clarke et al.'s (2009) emplacement model shows diapirs, interfinger zones and bridges mostly in the northeastern and western lobes, not in the areas around our inferred Dennilton and Crocodile River diapirs (Figure 5.18).

In the second model 5 to 10 km thick granite-granophyre overlies thin RLS (Figure 5.10b, Figure 5.15b). Where the gravity field is lowest, the RLS is absent and the acidic rocks continue even deeper, resembling a feeder. The Lebowa Granite Suite is considered to be a composite tabular intrusion that forced the roof (Rooiberg Group) and floor (RLS) apart, causing vertical displacement of the host rocks via normal faults and flexural slip (Wilson, Ferré and Lespinasse, 2000). The potential field model shows one main feeder, but other work suggests numerous feeders. Large vertical displacement of the RLS is inferred to be normal faults that formed during the intrusion of the granite (Figure 5.21).

The common factor in both of the 3D models is the thinness and even absence of RLS in large parts of the eastern BC. The average crustal thickness model also shows thinner crust under the eastern gravity low than under the western gravity low (Figure 5.6f). This may indicate less isostatic adjustment and by implication less subsidence due to thick RLS in contrast to the centre, corroborating the modelled thin RLS.

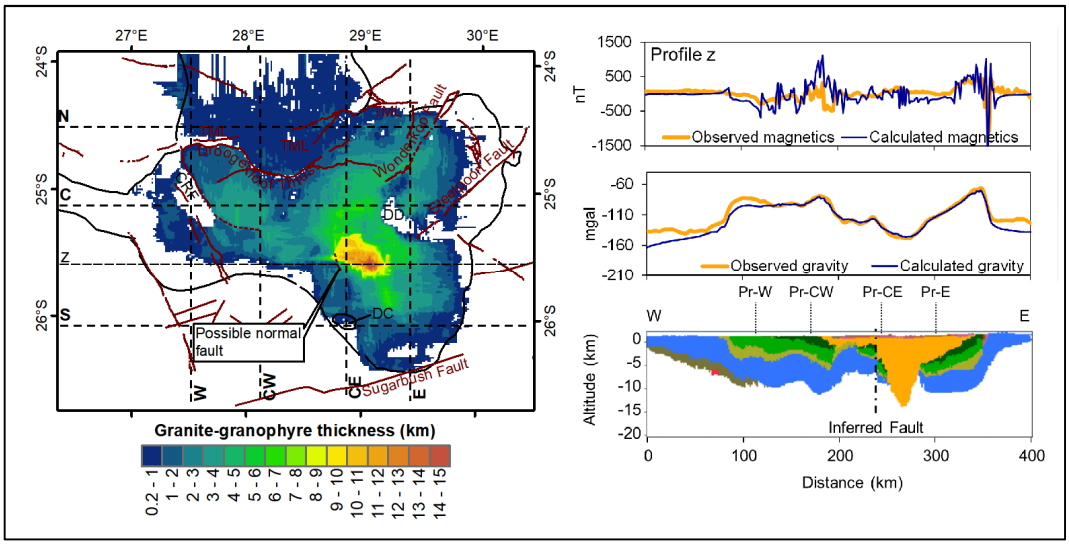


Figure 5.21. Modelled thickness of the granite-granophyre for the model with a possible feeder for these rocks in the east. DC – Dwarsfontein Complex; DD – Dennilton Dome. Localities of crossing profiles are indicated above the model (eg. Pr-W)

5.7.4 Feeders

Positive magnetic anomalies and high gravity values occur all along the TML in the western lobe (H in Figure 5.18). In most instances banded iron formation (BIF) of the Penge Formation that was brought close to the surface along the Droogekloof Thrust can explain the magnetic highs, and since BIF is very dense (3178 kg/m^3) it can cause the gravity highs. The gravity anomalies are broad which usually suggests that the causative dense material is found at depth. However, the spatial resolution of the gravity data is very low and the anomaly may be due to shallow material, but appears broad due to the low sampling interval. This was tested with a simple synthetic model consisting of a single dipping BIF layer (Figure 5.22a). The layer was about 300 m wide, similar to the width of the BIF on the 1:250 000 geological map, and the gravity field was calculated on a 100 m by 100 m grid (Figure 5.22b). Assigning a density of 3178 kg/m^3 to the BIF resulted in a 12 mgal anomaly. The calculated field values were then extracted at actual gravity station points and regridded using a 1 km by 1 km cell size (Figure 5.22c). The amplitude of the anomaly decreased significantly to about 6 to 8 mgal, except where gravity stations coincided with the gravity high in the high resolution data set. The anomaly width did not increase on the lower resolution image but remained at roughly 6 km. As a second test a deeper seated 2 km wide body with a density of 3200 kg/m^3 was added (Figure 5.22d) resulting in a 21 mgal anomaly (Figure 5.22e). Following the same procedure, a 1 km by 1 km data set was created (Figure 5.22f). The anomaly is 4 to 6 mgal lower than in the high resolution data set, a decrease of roughly 20 to 30%. The anomaly width again

remained the same on both images, approximately 10 km. The important factor is therefore the gravity anomaly amplitudes rather than the anomaly widths, and the amplitude is a function of the width and density of the causative body. The observed gravity anomalies have amplitudes of 10 to 20 mgal and are roughly 5 to 10 km wide. Since the BIF is generally not thicker than 300 m in the western lobe, the amplitudes of gravity anomalies are too high to be caused by BIF alone.

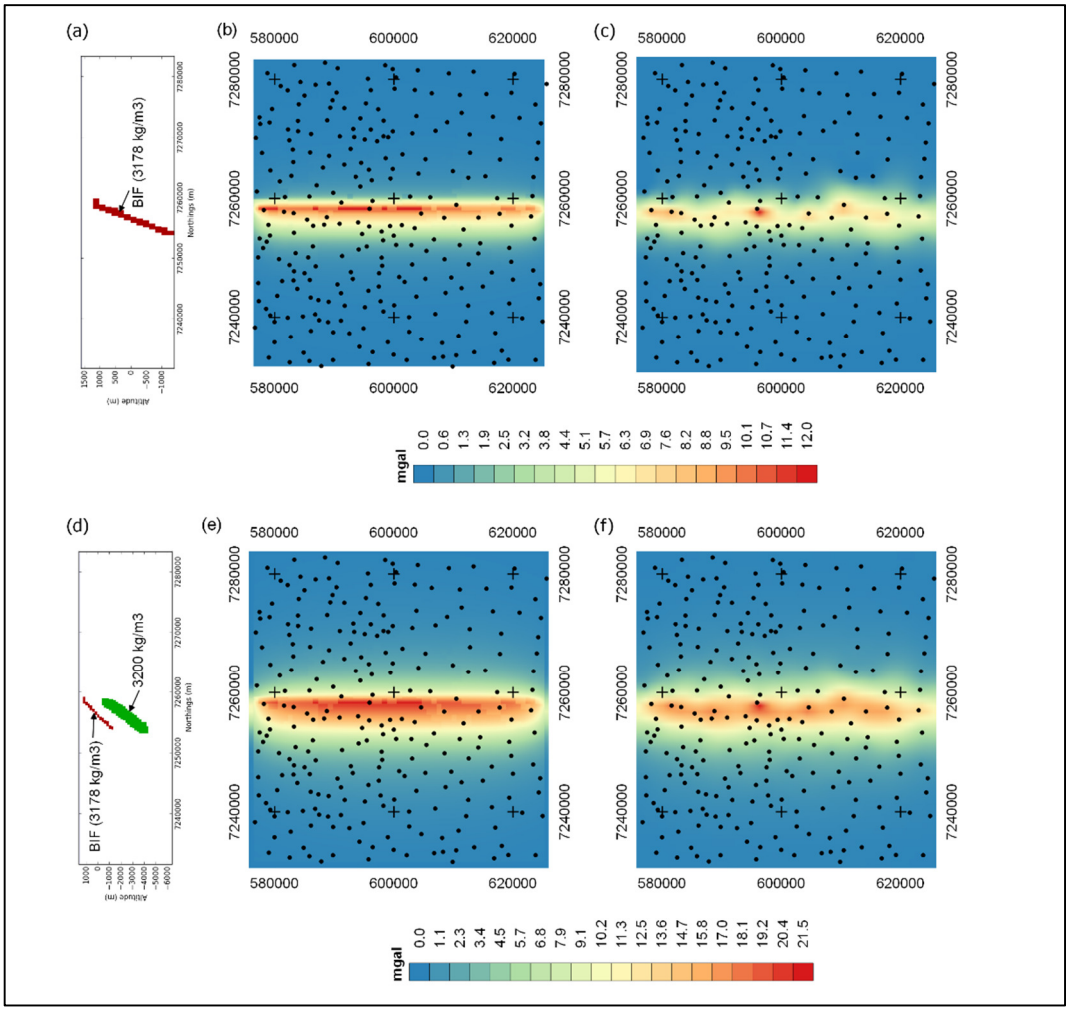


Figure 5.22. (a) Synthetic model with a single BIF layer; (b) Calculated gravity field (100 m cell size) for model in (a). Black dots are gravity stations; (c) Regridded gravity field of data extracted at gravity stations (1 km cell size); (d) Synthetic model with a BIF layer and a deeper seated dense body; (e) Calculated gravity field (100 m cell size) for model in (d); (f) Regridded gravity field of data extracted at gravity stations (1 km cell size).

The very thick Lower Zone along the southern margin of the south-eastern lobe (Figure 5.13, I in Figure 5.18) resembles a feeder zone. The dense material can be modelled to

extend down to more than 20 km if it narrows with depth (Figure 5.13). It coincides with a section of the Sugarbush Fault which parallels the TML along the southern margin of the south-eastern lobe (Du Plessis and Walraven, 1990). This fault developed during Central Rand Group time (~2.8 Ga, Koglin et al., 2010) and became inactive prior to the Transvaal Supergroup (Myers, Myers and McCarthy, 1987). It does not have an expression on the magnetic or gravity data and it is not possible to see any splays from this fault which could explain the curve of the south-eastern lobe away from the fault. The interpretation of a feeder in the south-eastern lobe concurs with Buchanan's (1975) proposal that the south-eastern lobe was emplaced from a separate injection centre than the rest of the BC.

5.7.5 Faulting

The Droogekloof Thrust which forms part of the Thabazimbi-Murchison Lineament (TML) defines the northern margin of the western lobe. Lower Transvaal Supergroup lithologies were moved up by this fault and crop out at the present day erosional surface. An age of 2061 Ma has been reported for this fault (Good and De Wit, 1997) which puts it within the timeframe of the BC emplacement, however, the accuracy of the dating was not given. In our model the RLS exploited the thrust fault.

In our model the north-eastern extension of an unnamed fault east of the Droogekloof Thrust (IF1 in Figure 5.12a, Figure 5.17, J in Figure 5.18)), not the Zebediela Fault, defines the southern extent of the northern lobe. This follows from the observation that the Droogekloof Thrust separates the western and northern lobes further to the west (H in Figure 5.18). The Mokopane gravity high (K in Figure 5.18) does not end against the Zebediela Fault but decreases in amplitude south of the fault. The southern limit of the Mokopane feeder lines up with an inferred continuation of the unnamed fault. This is in agreement with Van der Merwe (2008) who inferred from gravity that the RLS continued south of the Zebediela fault for about 10 km.

Strike-slip faulting, reactivated in places to normal faulting prior to the intrusion of the RLS characterises the TML in the eastern lobe (Good and De Wit, 1997). Long after the intrusion of the Bushveld Complex, a half graben formed along the south of the TML in which the Karoo Supergroup was deposited. The RLS extends westward for roughly 13 km underneath the Karoo Supergroup (Figure 5.17). A north-south striking inferred fault (UF2 in Figure 5.1) displaces the Upper Zone magnetic anomaly roughly 1 km southward on the western side of the fault. This fault also displaces the Karoo Supergroup and in the south juxtaposes the Lebowa Granite Suite against the Karoo sediments. It therefore appears to be a normal fault with down-throw to the west in the south, and a strike slip fault in the north. However, it may have changed from strike-slip after the crystallisation of

the RLS to a normal fault before the deposition of the Karoo Supergroup. In the north it displaces the Karoo basalt suggesting it was still active after Karoo times.

Step-like gravity anomalies along the southern part of the western lobe (Figure 5.16, L in Figure 5.18) were modelled as down-faulting of the RLS. This points to subsidence after crystallisation of the magma. However, considering the size and density of the magma chamber, it is conceivable that subsidence would have started during the emplacement of the magma prior to crystallisation. Indeed, Carr et al. (1994) and Maier et al. (2013) observed field evidence (e.g. slumping structures, potholes with steep up-dip margins) suggesting that subsidence of the intrusion was synmagmatic but these features are often small and could not be discerned on the regional geophysical data.

5.7.6 Connectivity between the different lobes

Our 3D model supports connected eastern and western lobes (Webb et al., 2004) but reveals a more complex picture. The RLS in the western lobe has a typical saucer shape as described by Kruger (2005), with steeper dips along the edges and flattening out in the centre (F in Figure 5.18). Similar to the 2.5D model of Webb et al. (2004) the gravity high over the centre of the BC (M in Figure 5.18) was modelled as a subtle anticline. A series of Mokolian-aged intrusions on this gravity high may have exploited weak zones in the anticline.

Our model shows that the south-eastern lobe is probably connected to the western and eastern lobes (Figure 5.11, Figure 5.13, Q in Figure 5.18). This is contrary to Buchanan's (1975, 1977) view that the south-eastern lobe is completely separate from the main BC and more in line with Kruger's (2005) proposal that the Upper Zone flowed into the whole Bushveld chamber from both the south-eastern lobe and the TML.

The mapped RLS in the western lobe stops at the Roodeplaat Complex, but Upper Critical Zone was recorded in the Cullinan Diamond Mine (CDM) 15 km further to the east (Cawthorn and McKenna, 2006).Twenty kilometres NNE of the Cullinan Mine and 30 km NE of the mapped limit of the RLS, a borehole (FF1 -85) drilled into Upper Zone at a depth of almost 600 m (Moen, 1989) over which are gravity and slight magnetic highs. (Figure 5.1). The amplitude of the gravity field remains relatively constant between the CDM and the Dwarsfontein Complex 50 km to the southeast (Figure 5.3, N in Figure 5.18). The low amplitude of the magnetic field in this area shows that the Upper Zone is thin, deep or absent between the CDM and Dwarsfontein Complex. Lower and Critical Zone were modelled here at a depth of about 2 km below the surface (Figure 5.11). Only Upper Critical Zone was encountered in the CDM (Cawthorn and McKenna, 2006). Thin Upper Zone was added to the east to account for a subtle long wavelength anomaly on the magnetic data.

5.8 Summary and Conclusions

Three dimensional magnetic and gravity modelling of the BC yielded new interpretations of some aspects of the BC. For example, gravity lows coinciding with the large pre-BC inliers in the western and eastern lobes have in the past been qualitatively used to support the notion that they are domes. However, neither the Crocodile River Fragment in the western lobe nor the Dennilton Dome in the eastern lobe could be modelled as simple domes. Modelling them as diapirs yielded better fits between the observed and modelled potential field data. In fact, the whole Dennilton Dome – Marble Hall Fragment in the eastern lobe was modelled as connected diapirs at different stages of maturity. This interpretation fits in well the emplacement model of Clarke et al.(2009) where host rocks form domal ridges and diapirs between finger of hot magma flowing from the TML in the north.

The model revealed significant changes in thickness in the eastern half of the BC. The RLS in the western lobe has a relatively constant thickness of 6 - 7 km stretching from the mapped occurrence in the west to the centre of the complex. In the eastern lobe the RLS has similar thicknesses between the outcrop in the east and the pre-BC inliers, but between the inliers and the centre of the complex, our model shows the RLS to be only 2 - 3 km thick and even absent in places. Low gravity values in this area were best modelled by either updomed Transvaal Supergroup material, or very thick granite-granophyre with a possible feeder. In the case of the former, the domes are considered to be pre-existing as they are covered by the acidic rocks of the BC and it is doubtful that there would have been enough time for the RLS to be eroded prior to the intrusion of granites. The domes only cause local interruptions in the continuity of the RLS between the eastern and western lobes, and on a large scale our models still support the view of the RLS as interconnected between the eastern and western lobes. Large domes can influence the composition of the RLS zones, e.g. a dome underneath the Steelpoort fault may have caused changes in Cr content across the fault (Clarke, Uken and Reinhardt, 2009).

Three proposed feeder sites are the Mokopane feeder in the northern lobe, the TML where possible remnants of a feeder were preserved in the western lobe and the southern margin of the south-eastern lobe. In our model the south-eastern lobe is connected to both the eastern and western lobes. The Main and Critical Zones continues southward from the eastern lobe but peters out. The absence of geophysical evidence for other feeders does not preclude the possibility that they existed, but no evidence of them remained.

In terms of the modelling process, the importance of full three-dimensional modelling that includes magnetic data and crustal thickness information for this size model became clear. The magnetic data constrained the depth to and thickness of the highly magnetic Upper Zone, and also the remanenty magnetised Main Zone in places. Crustal thickness variations caused long wavelength anomalies on the gravity field that had a large impact on the modelling results. Three-dimensional modelling can better account for the complexity of real-life geology than 2D models.

CHAPTER 6 A POSSIBLE MAGMA STAGING CHAMBER UNDER THE BUSHVELD COMPLEX

This chapter will be submitted as a paper to a high impact publication. The manuscript was constructed by me with editing and suggestions for improvements by my co-authors.

Cole – 70% (conducted the research and constructed the manuscript)

Finn – 25% (reviewed the manuscript and suggested improvements)

Webb - 5% (reviewed the manuscript and suggested improvements)

Magmatic staging chambers for the Bushveld Complex in South Africa imaged with Geophysical data

Janine Cole

Geophysics Unit, Council for Geoscience, Private Bag X112, Pretoria, 0001, South Africa
School of Geosciences, University of the Witwatersrand, Private Bag 3, WITS, 2050, South Africa
email: jcole@geoscience.org.za

Carol A. Finn

US Geological Survey, Denver, Colorado 80225, USA
email: cfinn@usgs.gov

Susan J. Webb

School of Geosciences, University of the Witwatersrand, Private Bag 3, WITS, 2050, South Africa
email: susan.webb@wits.ac.za

6.1 Abstract

The mafic magmatic staging chambers of the Bushveld Complex, the world's largest and most economically important layered mafic intrusion, have been conjectured but not imaged. Their existence has long been postulated from geochemical models which require multiple magma injections from staging chambers to account for the multi-scale layering. Seismic receiver function data identify a diffuse crust-mantle transition underneath the Bushveld Complex that suggests high velocity lower crust and perhaps underplating. Here we present 3D gravity modelling of the Bushveld Complex that includes dense material at the crust mantle boundary, imaging for the first time, remnants of magma staging chambers. The chambers, constrained by the extent of the diffuse crust-mantle transition, underlie the northern, south-eastern and western parts of the complex. Feeders correlate with the northern and south-eastern chambers.

6.2 Introduction

Magmatic systems consisting of interconnected crustal magma chambers effectively explain the formation of layered igneous intrusions (Marsh, 2015). In fact, based on geochemical evidence, deeper-seated crustal magma chambers have been used to explain compositional changes in layered intrusions in various parts of the world (Hanski

et al., 2001; Owen-Smith and Ashwal, 2015), not least of which is the Bushveld Complex, the world's largest known layered igneous intrusion (Ashwal et al., 2005; Eales and Costin, 2012; Maier et al., 2013 McDonald and Holwell; 2007; Prevec et al., 2005; Roelofse and Ashwal, 2012; Wilson, 2012). Geochemical evidence supports the existence of such deeper-seated chambers (normally referred to as staging chambers), but such chambers have not been previously imaged. We combined seismic, geologic and gravity data into a model that shows, for the first time, a staging chamber beneath the Bushveld Complex.

The Bushveld Complex (BC) crops out in four lobes in the north of South Africa, with a covered fifth lobe in the southeast (Figure 6.1). It consists of the mafic/ultramafic Rustenburg Layered Suite (RLS, dated at 2055.91 ± 0.26 Ma (Zeh et al., 2015)) and the acidic Rashoop Granophyre and Lebowa Granite Suite. The RLS is usually divided into five zones, each of which displays substantial cyclic layering. The exception to this is a thick succession of norite and gabbronorite that constitutes the Main Zone. An extra layered unit, the Basal Ultramafic Sequence, was recently identified at the base of the RLS in the eastern lobe (Wilson, 2015). There appears to be consensus that multiple magma injections account for most of the layering, although the number of magma pulses and compositions of parental magmas are still hotly debated (Cawthorn, 2007; Eales, 2002; Eales and Costin, 2012; Kruger, 2005; Tegner et al., 2006; Wilson, 2012, 2015).

Large ENE-striking faults coincide with boundaries in the BC (Figure 6.1). RLS rocks of the northern lobe crop out south of the Palala Shear Zone which forms the boundary between the Kaapvaal Craton to the south and the Limpopo Mobile Belt to the north. The latter separates the Kaapvaal and Zimbabwe Cratons that collided roughly 2.6 Ga (Geng et al., 2014). The Palala Shear Zone underwent a phase of strike-slip faulting between the time of the BC intrusion and later sedimentary deposition between 1.95 and 1.85 Ga (Schaller, 1999). The Thabazimbi-Murchison Lineament (TML) forms the boundary between the western and northern lobes, and the northern boundary of the eastern lobe. It is a crustal feature that may extend down to the mantle and which has seen episodic reactivation since at least 2.96 Ga (Good and De Wit, 1997). Since the TML represents a zone of weakness, it has been considered important in the emplacement of the Bushveld Complex (Clarke et al., 2009; Du Plessis and Walraven, 1990; Finn et al., 2015; Good and De Wit, 1997; Kruger, 2005). The Sugarbush Fault runs along the southern margin of the south-eastern lobe. Its tectonic history is not well understood and it has been described as a left-lateral wrench fault, a normal fault and a combination of normal and sinistral faulting, and although it is not fully understood it is considered to be of pre-Bushveld age (Dankert and Hein, 2010). The Inyoka Fault represents a suture zone between Archaean blocks that amalgamated ~ 3 Ga (De Wit et al., 1992). It crops out in

the Barberton Greenstone Belt roughly 100 km to the east but its locality in the study area is approximate as younger lithologies cover it.

Despite the lobate appearance of the intrusion, gravity modelling shows that the lobes are interconnected below the younger cover material if isostatic adjustment at the crust-mantle boundary is accounted for (Cole et al., 2014; Finn et al., 2015; Webb et al., 2004). Seismic receiver function data collected during the Southern African Seismic Experiment (SASE) (Fouch et al., 2004) confirmed thicker crust underneath the BC. The data also showed the crust-mantle transition underneath the BC to be less defined than under the surrounding undisturbed Kaapvaal Craton (Delph and Porter, 2015; Kgaswane et al., 2009, 2012; Nair et al., 2006; Nguuri et al., 2001; Youssof et al., 2013). Here (Delph and Porter, 2015; Nair et al., 2006; Nguuri et al., 2001) and in other parts of Southern Africa (e.g. under the Central Zone of the Limpopo Mobile Belt (Gore et al., 2009; Stankiewicz and Wit, 2013), under the Okwa/Magondi terranes to the west of the Limpopo Mobile Belt and Zimbabwe Craton (Mapeo and Kampunzu, 2004; Nguuri et al., 2001) (see inset in Figure 6.1) and under the Namaqua Metamorphic Province (Durrheim and Green, 1992; Stankiewicz and De Wit, 2013)), diffuse Moho has generally been attributed to mafic underplating of indeterminate age, not as staging chambers. Our modelling reveals a connection between underplating and feeder zones to the BC, supporting a staging chamber over underplating.

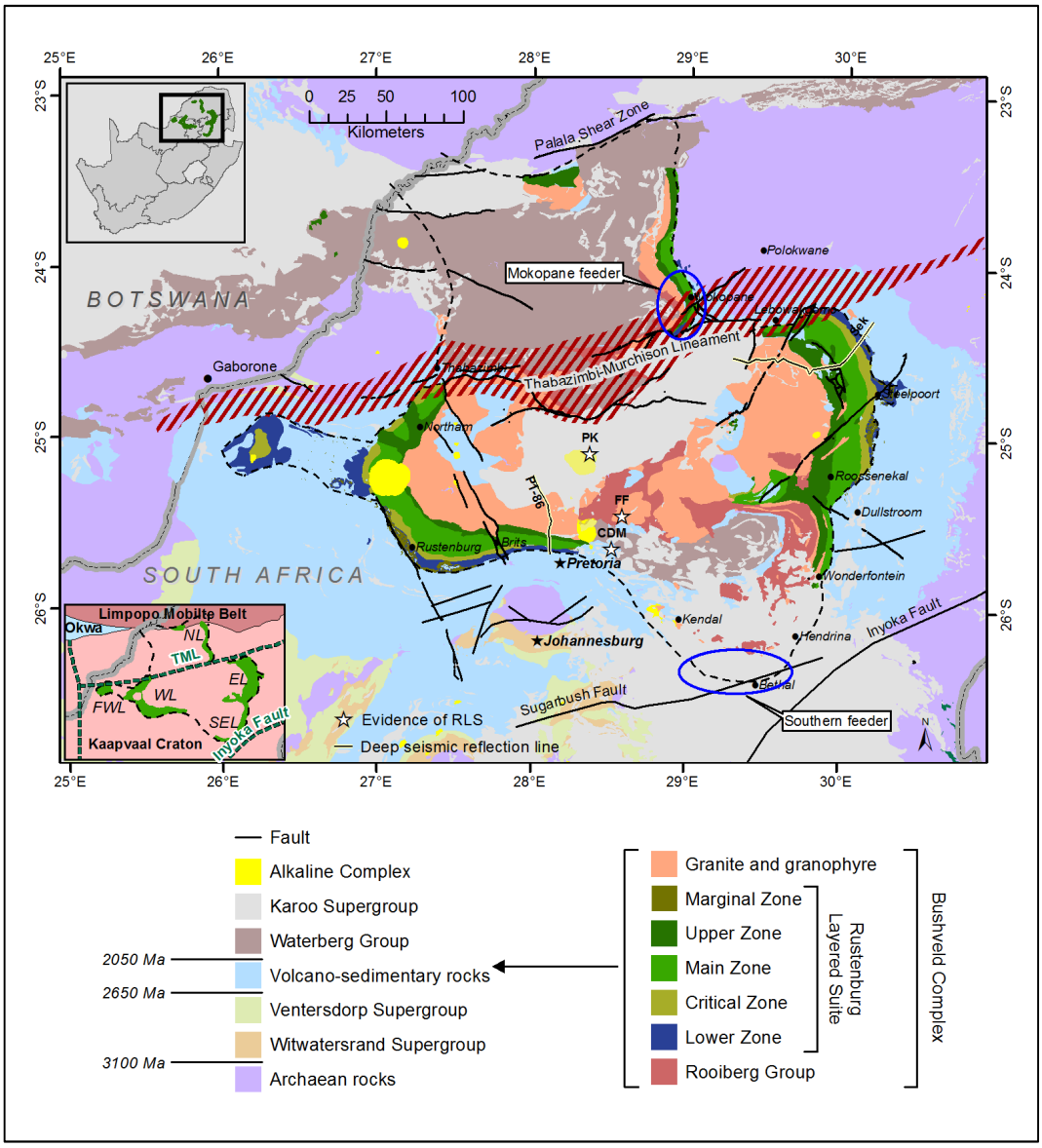


Figure 6.1. Simplified geological map of the Bushveld Complex. The dashed black line shows the extent inferred from geophysical data. Blue ellipses indicate feeders inferred from gravity data. The hachured area is the Thabazimbi Murchison Lineament. PK – Palmietgat kimberlite; FF – Fairfield borehole; CDM – Cullinan diamond mine. Lower left inset: NL – Northern lobe, EL – Eastern lobe, SEL – South-eastern lobe, WL – Western lobe, FWL – Far western lobe

6.3 Methods

6.3.1 Gravity data

Regional gravity data with a resolution of roughly one measurement every 14 km^2 cover the BC. Data were collected using LaCoste and Romberg gravimeters and elevations were determined using micro-barometers. Bouguer anomaly values were calculated

assuming a mean density of 2670 kg/m³. The measurements were tied to the International Gravity Standardisation Net values (Morelli et al., 1974) and referred to the gravity formula based on the 1980 geodetic reference system (Moritz, 1992). The maximum error (including reading, positional and elevation inaccuracies) in the Bouguer anomaly value was estimated to be within 2 mgal (Stettler et al., 2000).

6.3.2 Broadband Seismic Data (SASE)

Between 1997 and 1999 an array of three-component seismometers were deployed across Southern Africa to form the Southern African Seismic Experiment (SASE). Data were recorded at a total of 79 temporary stations and supplemented by data from three permanent broadband stations (Fouch et al., 2004). Sixteen of the stations were located on or in the vicinity of the Bushveld Complex.

6.3.3 Gravity modelling

All the forward geophysical modelling was done in three dimensions using the open source software package PyGMI (http://patrick-cole.github.io/pygmi/). The software divides the modelling area into cubes and calculates the contribution of each cube (or more correctly, rectangular cuboid) to the gravity field using the algorithm developed by Blakely (Blakely, 1996: 186-187). The cell size was 2 km in the x and y directions, and 1 km in the z direction.

6.4 Crust-mantle transition

Seismic receiver function data measure the arrival times of longitudinal (P) and shear (S) waves that travel through the Earth. A significant seismic velocity contrast exists across the Mohorovičić discontinuity (Moho) which forms the boundary between the crust and mantle, and this causes some of the P-wave energy to be converted to S waves (Zhu and Kanamori, 2000). Differences in arrival times of the two phases are used to estimate the crustal thickness.

Seismic receiver function studies by various authors using the SASE data show weak P to S wave conversions at the crust-mantle interface underneath the BC (Delph and Porter, 2015; Nair et al., 2006; Nguuri et al., 2001; Youssof et al., 2013). These studies used H-k stacking (Zhu and Kanamori, 2000) to determine the crustal thickness (H) and V_p/V_s (k), providing valuable information regarding crustal composition (for example, a high ratio reflects decreasing silica content as for mafic rocks) (Zandt and Ammon, 1995). V_p/V_s higher than 1.77 (the average crustal ratio) generally indicates more mafic material (Christensen, 1996; Delph and Porter, 2015) (Figure 6.2a). Diffuse crust-mantle transitions can explain the weak conversions. Magmatic underplating can cause these

diffuse transitions or, in the case of the Limpopo Belt, high metamorphic grade/velocity crust related to shortening and crustal thickening during the collision of the Kaapvaal and Zimbabwe cratons in the Archaean (James, Niu and Rokosky, 2003) (Figure 6.2a). Another explanation may be the lower velocity contrast between the lower crust and mantle beneath the BC. The SASE data revealed lower seismic velocities in the mantle under the BC that may result from an increase in Fe content due to the depletion of Mg during magmatic emplacement (James et al., 2001) or metasomatism (Webb, 2009). The Moho sharpness factor (equation 6.1) is generally low (< 1.5) over the BC also indicating a diffuse Moho (Youssof et al., 2013) (Figure 6.2b).

$$\frac{[Pds_i]_{amplitude}}{\frac{1}{N}\sum_{i=1}^{N}[Pds_i]_{amplitude}} \tag{6.1}$$

Where N is the total number of stations in the array and Pds is the P to S conversion at a depth d.

Application of a Gaussian-weighting common conversion point stacking for each receiver function to obtain better resolution variations in spatial amplitude also encountered weak conversions for most of the BC (Delph and Porter, 2015) (Figure 6.2c). In these instances H and k values that gave the best stacking amplitudes were selected manually and not through an automated iterative process. A shear wave velocity study also using the SASE data (Kgaswane et al., 2009) revealed a high shear wave velocity (V_s) layer of varying thickness and depth in the lower crust over much of the region (Figure 6.2d). Notably high velocity lower crust to the north corresponds to the Limpopo Belt (De Beer and Stettler, 1992). In the undisturbed part of the Kaapvaal Craton southwest of the BC, this layer is generally less than 3 km thick. Given an uncertainty of 2 – 3 km in the thickness (Kgaswane et al., 2009) the results correspond well to results from a dense seismic array near Kimberley (Figure 6.2f) that showed intermediate velocity (Vp = 6.46 km/s, Vs = 3.71 km/s) lower crust underneath the Kaapvaal Craton (Niu and James, 2002). On the craton the high Vs lower crust is therefore restricted to the area underneath and around the BC.

Combining information from the seismic studies into a single ternary image highlights locations of diffuse Moho (Figure 6.2e). The image uses the thickness of the high Vs layer in the lower crust (Kgaswane et al., 2009), the inverse of the Moho sharpness (Youssof et al., 2013) (more diffuse Moho will correlate to brighter green colours), and the inverse of the P to S conversion quality (Delph and Porter, 2015) (lower quality will translate to brighter blues). These three elements relate to the same aspect, namely diffuse crust-mantle transitions, but were determined by independent investigators using different methods. The most diffuse crust-mantle transitions lie under the centre of the BC, extending to the far western lobe, and under the northern lobe (Figure 6.2e). The

stations south of the western and south-eastern lobes (SA 39 to SA 42) generally record high amplitude P to S conversions. Low amplitude P-S conversions south of the south-eastern lobe correlate with diffuse Moho and a thick high Vs layer around station SA35, and a thick high Vs layer around station SA36.

The gradational transition underneath the BC is generally attributed to mafic underplating (Nguuri et al., 2001; Youssof et al., 2013) and mafic lower crust (Delph and Porter, 2015; Kgaswane et al., 2009, 2012). A possible explanation for underplating may relate to the Karoo magmatic event that saw the extrusion of basaltic lava and the intrusion of dolerite sills throughout southern Africa and Antarctica during the break-up of Gondwana around 180 Ma (Jourdan et al., 2005). A simple comparison between the current distribution of these rocks and the ternary map shows no clear correlation (Figure 6.2f). Another possibility is that the Archean lower crust was mafic prior to the intrusion of the BC, but results from a dense seismic array near Kimberley shows a lower crust of intermediate composition (Niu and James, 2002). Seismic refraction studies over the Witwatersrand Basin south of the BC produced V_p of 6.5-6.8 km/s for the lower crust, described as felsic granulite (Durrheim and Green, 1992).

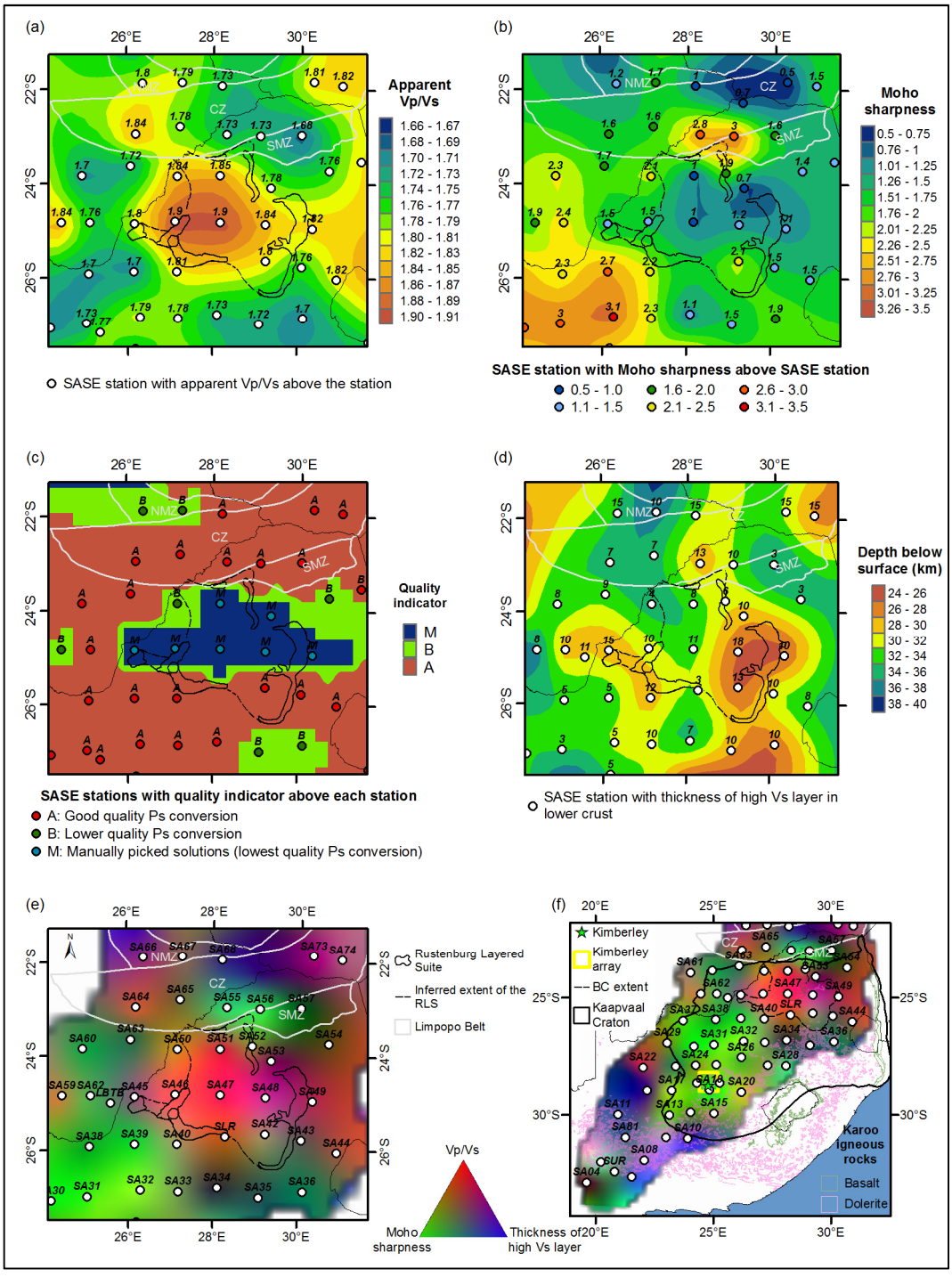


Figure 6.2. Results from seismic receiver function studies. The Northern Marginal Zone (NMZ), Central Zone (CZ) and Southern Marginal Zone (SMZ) of the Limpopo Belt are outlined (Kgaswane et al., 2009)**. (a) Apparent V_P/V_S (Delph and Porter, 2015); (b) Moho sharpness (Youssof et al., 2013). The Moho sharpness quantifies the quality of the P to S conversions. Higher values indicate sharper Moho; (c) Quality of P to S conversions (Delph and Porter, 2015). (d) Thickness of the high Vs layer in the lower crust overlain on the depth to this layer (Kgaswane et al., 2009, 2012); (e) Ternary image combining normalised values of Vp/Vs** (Delph and Porter, 2015)**, Moho sharpness** (Youssof et al., 2013) **and the thickness of**

the high Vs lower crustal layer (Kgaswane et al., 2009, 2012); (f) Distribution of the Karoo Large Igneous Province in South Africa overlain on the ternary image

6.5 Gravity model with staging chamber

The lack of a sharp velocity contrast at the Moho suggests high velocity and therefore high density material at the base of the crust. To test whether dense material can be modelled underneath the BC, we averaged four different crustal thickness models (Delph and Porter, 2015; Kgaswane et al., 2009, 2012; Nair et al., 2006; Youssof et al., 2013) as done for the Northern Lobe (Finn et al., 2015).The thicknesses vary in places but uncertainties in crustal thicknesses in areas with diffuse Moho can be in the order of 5 km (Kgaswane et al., 2009). The maximum RLS thickness was conservatively limited to 10 km, although geologic outcrop, drilling (Ashwal et al., 2005; Roelofse and Ashwal, 2012; Teigler and Eales, 1996) and seismic reflection data (Campbell, 2011; Odgers et al., 1993; Odgers and Du Plessis, 1993) show the intrusion to be roughly 7 km thick. These geological, borehole and seismic data sets constrained the model of the BC and surrounding geological units. For example, in the northeastern corner (SA55 and SA57), the high density granulitic Southern Marginal Zone of the Limpopo Mobile Belt accounts for the thick high Vs layer (Kgaswane et al., 2009). Also, dense material is evident between depths of 20 and 30 km on shear wave velocity models (Kgaswane et al., 2009) to the west of the BC. This layer can be a remnant of high grade metamorphism related to the 2.72 Ga Ventersdorp rifting event that affected the Kaapvaal Craton as far north as the Limpopo Mobile Belt (Stankiewicz and De Wit, 2013). Granulite xenoliths brought to the surface by kimberlites carried evidence of ultrahigh-temperature metamorphism in the middle to lower crust (Schmitz and Bowring, 2003). Seismic velocities for these specific xenoliths are unknown, but high pressure high temperature granulite xenoliths of metapellitic origin in New Mexico had P-wave velocities 7.23 and 7.93 km/s (Reid et al., 1989). This exceeds the 6.5-6.8 km/s for the lower crust of the Kaapvaal Craton (Durrheim and Green, 1992). Shallower and thick high velocity zones occur east of the Bushveld (Figure 6.2d).

Densities for the proposed staging chamber were derived from shear wave velocities (Kgaswane et al., 2009, 2012) observed at the crust mantle boundary underneath the Bushveld Complex. The velocities (4.0 to 4.3 km/s) translate to densities between 3145 kg/m^3 and 3360 kg/m^3 (using the empirical equation of Christensen and Stanley (2003)), with an average of 3250 kg/m^3. SASE results also guided the densities used for the lower crust and mantle. Detailed seismic tomography work on an undisturbed part of the Kaapvaal Craton in South Africa revealed a lower crust with a density of 2860 kg/m^3

overlying a dense mantle (3300 kg/m^3) (Niu and James, 2002). However, seismic velocities for the mantle underneath the Bushveld Complex are lower than for the surrounding area, possibly due to iron enrichment accompanying the Bushveld event (Fouch et al., 2004). The higher iron content will result in higher densities, and therefore the mantle density underneath the BC was increased to 3330 kg/m^3.

A staging chamber with a density of 3250 kg/m^3 was added to the gravity model in areas where the RLS had to be unreasonably thick to obtain a fit. We used a forward modelling algorithm based on the 'gbox' routine of Blakely (1996:377) to calculate the gravity field. SASE stations with diffuse crust-mantle transitions helped to constrain the extent of the modelled chamber. The proposed staging chamber underlies the whole northern part of the BC and extends to the east and west of the complex (Figure 6.3a). It thins towards the south and is absent under a large part of the central BC. Dense material was also required underneath the south-eastern lobe. Under the northern and western lobes it is 4-8 km thick, while it is 8-12 km thick west and east of the northern lobe. It continues westward into Botswana. Near Mokopane where a feeder has been modelled (Finn et al., 2015) the modelled chamber is around 10 km thick.

Profiles extracted from the 3D gravity model show that the differences between the calculated gravity field with and without the magma staging chambers are substantial (Figure 6.3b to e). Changing the density of the chamber will affect its thickness and the horizontal extent to a degree, but it is clear that dense material is definitely required under much of the BC to obtain a geologically reasonable model.

The proposed staging chamber remnant does not underlie the whole BC and is not restricted to the present-day extent of the complex. The bulk of the chamber lies beneath the northern part of the BC and extends to the east and west of the BC, but a chamber is also present under the south-eastern lobe (Figure 6.3a). This chamber underlies the feeders required by the gravity data (Figure 6.3c, e).

As a test, we constructed a second model where the high Vs lower crust (Kgaswane et al., 2009, 2012) with a density of 3250 kg/m^3 formed the staging chamber. The high Vs layer east of the eastern lobe is up to 10 km thicker than under the BC (Figure 6.2d). This increased the gravity field in the east substantially making it impossible to fit the calculated field to the observed field with the RLS constrained by the deep seismic reflection lines P-186 and Sek (Figure 6.1). Constraining the result to the P1-86 seismic line in the western lobe required the complete absence of RLS in the eastern lobe, which is clearly not the case. Alternatively, keeping the high Vs layer thickness under the eastern lobe meant the RLS in the western lobe had to be 12 to 18 km thick, but the reflection seismic data and boreholes do not support this. The RLS in the southern parts

of the eastern lobe (around Roossenekal) was also completely absent, and still the calculated field was too high. This suggests substantial overestimation of the high Vs layer's thickness in the east. This can be due to uncertainty in earthquake location, origin time and moment tensor (Gao and Shen, 2015). If we remove the staging chamber east of the southeastern lobe, dense material is required in the crust to fit the gravity data (Figure 6.3d).

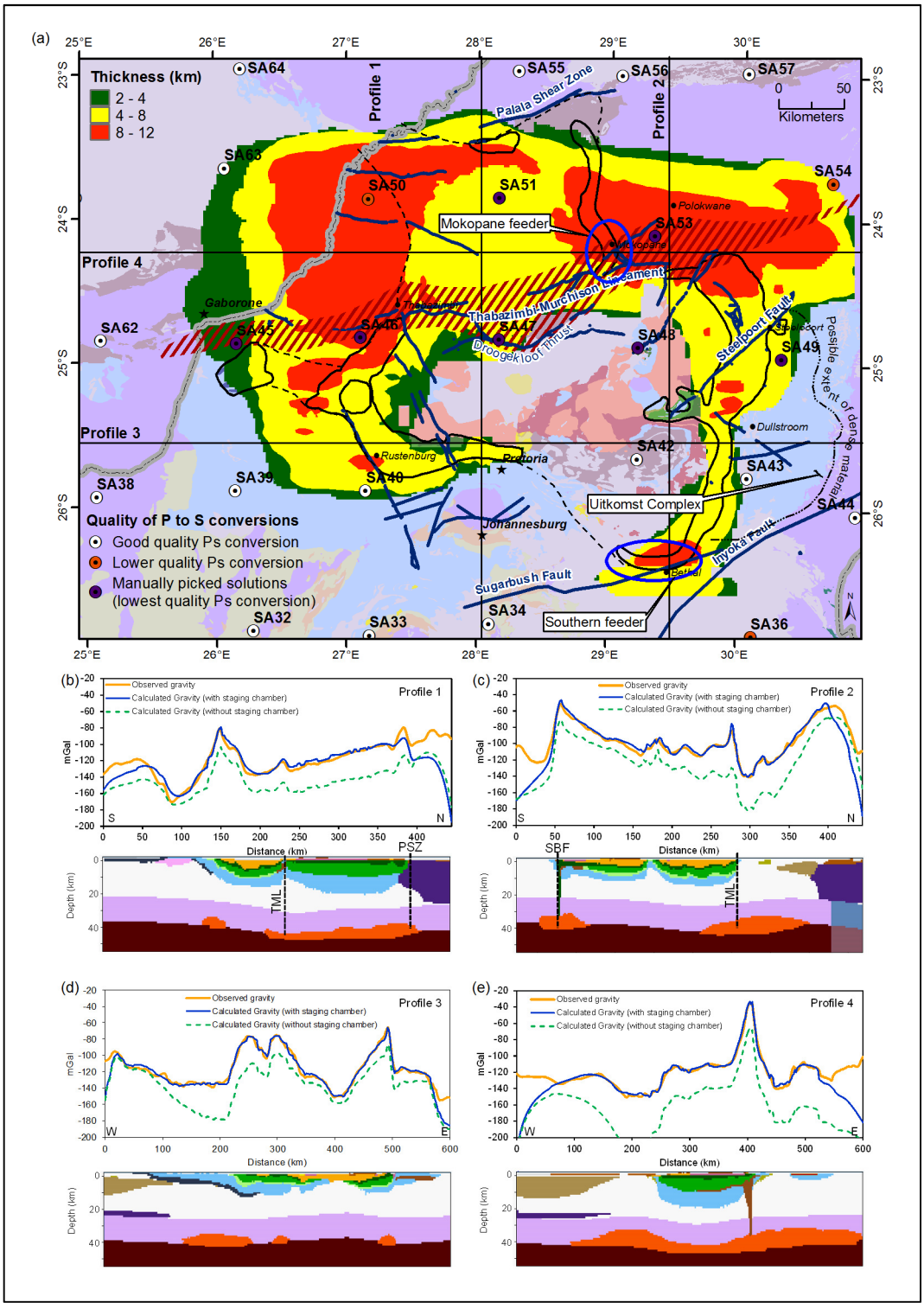


Figure 6.3. (a) Inferred extent and thickness estimates for a magma staging chamber with a density of 3250 kg/m^3 underneath the BC. Thick blue lines are known faults. The cross-hatched area indicates the TML; (b) to (e) Profiles extracted from the 3D gravity model along the profiles indicated in (a). PSZ – Palala Shear Zone; SBF – Sugarbush Fault; TML – Thabazimbi-Murchison Lineament; Table 6.1 lists the densities used in the model

Table 6.1. Densities used in the gravity model

Lithology	Density (kg/m^3)
Karoo Sediments	2506
Pilanesberg Complex	2687
Pyroxenite pipes	3200
Waterberg Group	2645
Granite/granophyre	2620
Upper Zone	3110
Main Zone	2920
Critical/Lower/Marginal Zone	3090
Lower Zone	3200
Rooiberg Group Felsite	2725
Transvaal Supergroup (Volcano-sedimentary rocks)	2737
Witwatersrand / Ventersdorp Supergroup	2744
Greenstone material	3100
Dense crust (mixture of granite-gneiss and greenstone material)	2900
Granulite terrane (Southern Marginal Zone of the Limpopo Mobile Belt)	2920
Lower density Archaean Granite	2550
Background	2700
Magma staging chamber	3250
Lower crust under Southern Marginal Zone (Limpopo Mobile Belt)	2960
Lower crust under Kaapvaal Craton	2860
Upper mantle under BC	3330
Upper mantle under Kaapvaal Craton and Southern Marginal Zone (Limpopo Mobile Belt)	3300

6.6 Discussion

There appears to be a spatial correlation between the modelled chamber and most of the large ENE-striking faults, the exception being the Palala Shear Zone in the north (Figure 6.3a). Although co-location does not imply interaction between the faults and the staging chamber, it does present the possibility of at least some faults tapping the proposed staging chamber. Correlation between two modelled feeders and two of the faults makes this possibility more enticing.

The proposed Mokopane feeder in the north was identified on the basis of a 110 mgal gravity anomaly that has been modelled as a funnel-shaped body coinciding with the intersection of northerly trending faults in the northern lobe, and NE and ENE striking faults that form part of the TML (Finn et al., 2015). The 110 mgal anomaly requires very dense material and typically Lower Zone densities were used (Finn et al., 2015; Van Der Merwe, 1976). However, the feeder may consist of a mixture of different magmas that passed through it. Lowering the density to 3010 kg/m^3 to reflect a combination of Lower, Main and Upper Zone material resulted in a wider feeder. In both cases, the feeder was modelled all the way down to the staging chamber.

The proposed feeder in the south-eastern lobe (Buchanan, 1975) is best modelled with a conduit extending down to the staging chamber. The conduit ensures a good fit for the narrow gravity high at 50 km in Profile 2 (Figure 6.3c). Boreholes drilled into the gravity high intersected only Upper and Lower Zone rocks and on the basis of this it was interpreted as a separate lobe with its own feeder (Buchanan, 1975). Later Sr-isotope studies of magma compositions suggested that a feeder at the south-eastern lobe was the source of the Upper Zone in the south-eastern, western and eastern lobes (Kruger, 2005). The feeder was therefore modelled using the Upper Zone density of 3010 kg/m^3. The Sugarbush Fault has never been explicitly mentioned as a possible feeder zone for the BC. It was active prior to the intrusion of the BC, but its tectonic history has not been studied (Dankert and Hein, 2010) and it is also unknown whether the fault extends down to the mantle. The fault's position along the southern margin of the south-eastern lobe where both a feeder and staging chamber have been modelled makes it a candidate for being a feeder conduit. The Inyoka Fault further to the south represents a suture zone of two Archaean blocks and likely extends to the mantle. However, its exact position is uncertain and the correlation with the modelled staging chamber may be fortuitous.

The staging chamber underlies the whole TML. The TML has been described as a large-scale relay structure at the time of the BC intrusion (Good and De Wit, 1997) and may represent a lithospheric boundary (Silver et al., 2004). The structural complexity of relay structures makes them ideal pathways for fluids, including magmas (Dankert and Hein,

2010). Although our model is too regional to show complexity in the TML, it can be modelled with dense material potentially related to feeders (Finn et al., 2015) caught up in it. Both the Mokopane and proposed southern feeder extend down to the staging chamber. The feeder remnants in the TML are mostly modelled in the Droogekloof Thrust along the southern margin of the TML in the western lobe. Previous geophysical modelling showed 9 km thick Main Zone on the southern side of the TML (Finn et al., 2015). If it extends deeper it is too thin to impact significantly the calculated gravity field.

The thickest part of the modelled staging chamber generally corresponds relatively well with the pink area on the ternary image that highlights where the Moho is diffuse (Youssof et al., 2013), Vp/Vs is high indicating mafic material (Delph and Porter, 2015) and the high Vs layer is thick (Kgaswane et al., 2009) (Figure 6.2e). The biggest differences between the modelled chamber and the ternary image are in the central part of the BC. The absence of a staging chamber remnant in the central part of the BC does not mean that the proposed chamber did not exist here. The high Vs layer in the lower crust is relatively thick at stations SA42, SA47 and SA48 (Kgaswane et al., 2009) (Figure 6.2d). However, the thickness of this layer depends the specific processing parameters used to generate the Vs models (Kgaswane et al., 2012). The thickness should therefore not be considered exact, but rather as an indication that a high Vs layer is present. It is therefore even feasible that a thin staging chamber remnant is present underneath the Central BC. Alternatively, the high Vp/Vs values in this area (Figure 6.2a) may reflect the mafic rocks of the BC in the upper crust, and the diffuse Moho and low quality P to S conversions may result from undulations in the Moho topography (Delph and Porter, 2015).

The very thick high Vs layer east of the south-eastern lobe (SA43, Figure 6.2d) corresponds to lower Vp/Vs values (Figure 6.2a), good P to S conversions (Figure 6.2c) and somewhat sharper Moho (Figure 6.2b). If such thick mafic material existed here, the Vp/Vs value should be much higher and the P to S conversions would be lower. The gravity data requires some dense material in this area, but the nature of the anomaly suggests shallower causative material. Of interest in the first area is the presence of the Uitkomst Complex (Figure 6.3a). This is a mafic-ultramafic intrusion contemporaneous with the RLS, originated from a magma that gave rise to sub-Rustenburg Layered Suite mafic intrusions (De Waal et al., 2001). These intrusions are thin with the similarly-aged Marble Hall diorite sills in the eastern lobe only a few tens of meters thick (De Waal and Armstrong, 2000), and the Uitkomst Complex 800 m thick (Gauert, De Waal and Wallmach, 1995). The Uitkomst Complex had a parental magma similar to the parental magma that gave rise to the Lower and Critical Zones of the Rustenburg Layered Suite (De Waal et al., 2001). It is situated almost 65 km east of the eastern lobe in the carbonates of the lower Transvaal Supergroup and shows that the RLS extended further

than the present-day expression. We included Lower Zone material in the TVL Supergroup rocks extending up to 80 km east of the eastern lobe (extent indicated in Figure 6.3a, d). Alternatively greenstone material may be present in the Archaean basement. This is feasible as greenstone are ubiquitous in the Kaapvaal Craton and occur all around the BC. If the thick high Vs layer is real, it may be the remnant of a wide conduit that linked chambers at different depths. For example, it is possible that a mid-crustal staging chamber existed here.

One could argue that removing the RLS from the central area between the eastern and western lobes will limit the requirement for deep dense material around the BC. However, there is compelling evidence that the RLS is continuous, for example Critical Zone material was found in a waste rock dump at the Palmietgat kimberlite (Webb, Ashwal and Cawthorn, 2011) (PK in Figure 6.1), the Fairfield borehole was drilled into Upper Zone rocks (Moen, 1989) (FF in Figure 6.1), Upper Critical Zone was encountered at the Cullinan diamond mine (Cawthorn and McKenna, 2006) (CDM in Figure 6.1) and the RLS does not taper out on seismic lines in the northeast (Odgers and Du Plessis, 1993) (Sek in Figure 6.1) and southwest (Odgers, Hinds and Von Gruenewaldt, 1993) (P1-86 in Figure 6.1). Gravity modelling taking into account crustal flexure resulting from the intrusion of the dense, thick RLS also imaged RLS in the centre if the whole crustal structure down to the Moho is taken into account (Webb et al., 2004). The RLS can therefore not simply be removed from the centre of the BC but the density deficits underneath and surrounding parts of the complex need to be explained.

We have shown that it is possible to model the gravity field with a staging chamber at depth below the BC, and in fact that deep, dense material is required under parts of the BC to obtain the correct gravity amplitudes while restricting the RLS to a reasonable thickness. A shear wave velocity model (Kgaswane et al., 2009) shows the presence of mafic material in the lower crust, but its thickness and extent is not well constrained. The well constrained upper crustal structure in the gravity model resulted in a better estimation of the locality and lateral extent of the staging chamber. Large faults that predate the intrusion of the BC and coincide with the modelled staging chamber, present zones of weakness ideally located to tap a magma staging chamber that formed at the Moho (Figure 6.4).

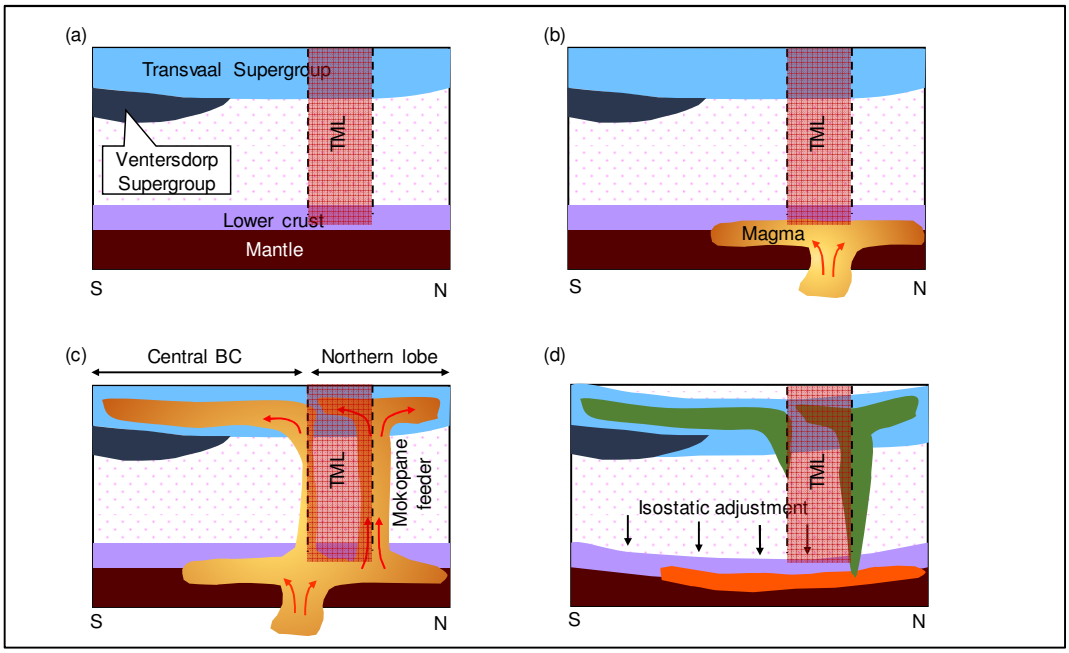


Figure 6.4. Simple diagram showing the possible stages of development of a staging chamber remnant under parts of the BC. (a) Situation prior to the intrusion of the RLS. The TML was already present at this time (Good and De Wit, 1997)**; (b) A magma chamber forms at the lower curst-mantle interface; (c) Magma flows upwards in the TML and Mokopane feeder and intrudes into the volcano-sedimentary Transvaal Supergroup; (d) The RLS and magma chamber solidifies and isostatic adjustment due to the dense thick RLS in the upper crust results in thicker crust underneath the BC**

CHAPTER 7 CONCLUSIONS AND FUTURE WORK

This study contributed to different aspects of our geophysical understanding of the Bushveld Complex. It firstly provided a summary of the densities and magnetic susceptibilities of different lithologies in the Bushveld Complex, a resource that can be used in conjunction with the palaeomagnetic work of Letts et al. (2009) by any scientist working on potential field studies of the Bushveld Complex. It also shows that the value of combining petrophysical and petrographic data improves our understanding of petrophysical data distributions.

The inclusion of isostatic adjustment at the crust-mantle boundary underneath the dense and thick Bushveld Complex (Cawthorn et al., 1998, Cawthorn and Webb, 2001 and Webb et al, 2004) changed our approach to modelling the Bushveld Complex, and indeed any large, dense intrusion. However, there is uncertainty in the crustal thickness models, and the effect of different models on the gravity field has a large impact on the calculated gravity field for the Bushveld Complex. This in turn substantially affects the inferred thickness of and depth to the Rustenburg Layered Suite. Most of these uncertainties affected the derived crustal thickness under the eastern lobe, while the thicknesses under the western and central parts of the BC were less variable. The important conclusion though is that potential field modelling shows that the western and eastern lobes are not separate intrusions, but it continuous underneath the Bushveld Complex.

The final three dimensional model and its variations provide new insight into the geometry of the BC. It shows continuity of the RLS throughout all the lobes of the BC, even though there are some instances where the RLS may be thinner and even absent. These interruptions in the RLS do not negate the continuous nature of the mafics and ultramafics, but are simply localised disruptions. The model shows areas of pre- and syn Bushveld Complex updoming and diapirism, as well as post-crystallisation faulting. The faulting suggests that subsidence continued even after crystallisation.

In some areas large gravity highs could only be modelled by very thick dense material resembling feeders. Three feeders in the model occurs in the north near Mokopane, in the western lobe along the Thabazimbi Murchison Lineaments, and along the southern margin of the south-eastern lobe. The feeders coincide with large faults that could have tapped a deep seated magma staging chamber or chambers included in the model. Based on geochemical evidence, deeper-seated crustal magma chambers have been used to explain compositional changes in layered intrusions in various parts of the world and in the Bushveld Complex, and for the first time a geophysical model showed that it is

possible to model such a staging chamber under the Bushveld Complex. In fact deep, dense material is required under parts of the BC to obtain the correct gravity amplitudes while restricting the RLS to a reasonable thickness.

This study emphasises that to avoid flawed conclusions, modelling should be done in three dimensions, and that for models the size of the Bushveld Complex it is extremely important to take into account deep seated features and their varying lithological properties. For regional scale models, density variations in the lower crust and upper mantle cause long wavelength gravity anomalies that cannot be modelled by shallow crustal features alone.

7.1 Future work

One area where there is much scope for future work is the improvement of the crustal thickness model to the east of the Bushveld Complex. The seismic tomography studies produced low quality data in this area which resulted in large uncertainty in the crustal thickness models under the eastern lobe. Ideally more broadband seismometers should be deployed to collect more data and investigate the cause of the data uncertainty.

The two deep seismic reflection lines in the western and northeastern lobes should be reprocessed and properly interpreted to improve the constraints on the potential field modelling.

More detailed modelling can now be conducted on smaller areas of interest using the regional model as a basis. The model can thus be refined, thereby further improving our understanding of the Bushveld Complex.

CHAPTER 8 REFERENCES

Anhaeusser, C.R., 2006. Ultramafic and mafic intrusions of the Kaapvaal Craton. In: M.R. Johnson, C.R. Anhaeusser and R.J. Thomas, eds., *The Geology of South Africa*. Geological Society of South Africa (Johannesburg) and Council for Geoscience (Pretoria), pp.95–134.

Ashwal, L.D., Webb, S.J. and Knoper, M.W., 2005. Magmatic stratigraphy in the Bushveld Northern Lobe: Continuous geophysical and mineralogical data from the 2950 m Bellevue drillcore. *South African Journal of Geology*, 108(2), pp.199–232.

Austin, J., Geuna, S., Clark, D. and Hillan, D., 2014. Remanence, self-demagnetization and their ramifications for magnetic modelling of iron oxide copper-gold deposits: An example from Candelaria, Chile. *Journal of Applied Geophysics*, 109, pp.242–255.

Blakely, R.J., 1996. *Potential Theory in Gravity and Magnetic Applications*. 1st ed. Cambridge University Press, Cambridge, UK, 441 pp.

Braitenberg, C., Wienecke, S., Ebbing, J., Bom, W. and Redfield, T., 2007. Joint gravity and isostatic analysis for basement studies – a novel tool. In: *Extended Abstracts, EGM 2007 International Workshop, Innovation in EM, Grav and Mag Methods: A New Perspective for Exploration, Villa Orlandi, Capri – Italy, 15–18 April 2007*.

Brandl, G. and Baglow, N., 2007. *The geology of the country between Chuniespoort and the Downs, Explanation to sheets 2429BA Ga-Maja, 2429BB Bewaarkloof and 2430 Serala*. Council for Geoscience.

Buchanan, D.L., 1975. The petrography of the Bushveld Complex intersected by boreholes in the Bethal area. *Transactions of the Geological Society of South Africa*, 78, pp.335–348.

Buchanan, D.L., 1976. The sulphide and oxide assemblages in the Bushveld Complex rocks of the Bethal area. *Transactions of the Geological Society of South Africa*, 79, pp.76–80.

Buchanan, D.L., 1977. Cryptic variation in minerals from the Bushveld Complex rocks of the Bethal area. *Transactions of the Geological Society of South Africa*, 80, pp.49–52.

Buchanan, D.L., 1979. A combined transmission electron microscope and electron

microprobe study of Bushveld pyroxenes from the Bethal area. *Journal of Petrology*, 20, pp.327–354.

Buick, I.S., Maas, R. and Gibson, R.L., 2001. Precise U-Pb titanite age constraints on the emplacement of the Bushveld Complex, South Africa. *Journal of the Geological Society*, 158(1), pp.3–6.

Bumby, A.J., Eriksson, P.G. and Van der Merwe, R., 1998. Compressive deformation in the floor rocks to the Bushveld Complex (South Africa): evidence from the Rustenburg Fault Zone. *Journal of African Earth Sciences*, 27(3–4), pp.307–330.

Button, A., 1978. *Diapiric structures in the Bushveld, Northeastern Transvaal*. Economic Geology Research Unit, University of the Witwatersrand, Information Circular 123, 10 pp.

Button, A. and Cawthorn, R.G., 2015. Distribution of mafic sills in the Transvaal Supergroup, northeastern South Africa. *Journal of the Geological Society*, 172(3), pp.357–367.

Cameron, E.N., 1978. The Lower Zone of the eastern Bushveld Complex in the Olifants River trough. *Journal of Petrology*, 19(3), pp.437–462.

Cameron, E.N., 1980. Evolution of the Lower Critical Zone, central sector, eastern Bushveld Complex, and its chromite deposits. *Economic Geology*, 75(6), pp.845–871.

Cameron, E.N., 1982. The Upper Critical Zone of the eastern Bushveld Complex - precursor of the Merensky Reef. *Economic Geology*, 77(6), pp.1307–1327.

Campbell, G., 2011. Exploration geophysics of the Bushveld Complex in South Africa. *The Leading Edge*, (June), pp.622–638.

Carr, H.W., Groves, D.I. and Cawthorn, R.G., 1994. The importance of synmagmatic deformation in the formation of Merensky Reef potholes in the Bushveld Complex. *Economic Geology*, 89, pp.1398–1410.

Cawthorn, R.G., 2006. The centenary of the discovery of platinum in the Bushveld Complex (10th November , 1906). In: *International Platinum Conference*. pp.1–4.

Cawthorn, R.G., 2007. Cr and Sr : Keys to parental magmas and processes in the Bushveld Complex , South Africa. *Lithos*, 95, pp.381–398.

Cawthorn, R.G., Cooper, G.R.J. and Webb, S.J., 1998. Connectivity between the western and eastern limbs of the Bushveld Complex. *South African Journal of Geology*, 101,

pp.291–298.

Cawthorn, R.G., Eales, H. V, Walraven, F., Uken, R. and Watkeys, M.K., 2006. The Bushveld Complex. In: M.R. Johnson, C.R. Anhaeusser and R.J. Thomas, eds., *The Geology of South Africa*. Geological Society of South Africa, Johannesburg, and Council for Geoscience, Pretoria, pp.261–281.

Cawthorn, R.G. and McKenna, N., 2006. The extension of the western limb, Bushveld Complex (South Africa), at Cullinan Diamond Mine. *Mineralogical Magazine*, 70(3), pp.241–256.

Cawthorn, R.G., Merkle, R.K.W. and Viljoen, M.J., 2002. Platinum-Group Element deposits in the Bushveld Complex, South Africa. In: L.J. Cabri, ed., *The geology, geochemistry, mineralogy and mineral beneficiation of platinum-group elements*. Canadian Institute of Mining and Metallurgy, Special Volume 54, pp.389–429.

Cawthorn, R.G. and Spies, L., 2003. Plagioclase content of cyclic units in the Bushveld Complex, South Africa. *Contributions to Mineralogy and Petrology*, 145(1), pp.47–60.

Cawthorn, R.G. and Webb, S.J., 2001. Connectivity between the western and eastern limbs of the Bushveld Complex. *Tectonophysics*, 330, pp.195–209.

Chatfield, M., 2009. *Wire-line Course*. 26-27 February 2009, Johannesburg, South Africa.

Cheney, E.S. and Twist, D., 1991. The conformable emplacement of the Bushveld mafic rocks along a regional unconformity in the Transvaal succession of South Africa. *Precambrian Research*, 52(1–2), pp.115–132.

Christensen, N.I., 1996. Poisson's ratio and crustal seismology. *Journal of Geophysical Research*, 101(B2), pp.3139–3156.

Christensen, N.I. and Stanley, D., 2003. Seismic velocities and Densities of Rocks. In: *International Handbook of Earthquake and Engineering Seismology, 81B*. pp.1587–1593.

Clark, D.A. and Emerson, D.W., 1999. Self-demagnetisation. *Preview*, April, pp.22–25.

Clarke, B.M., Uken, R. and Reinhardt, J., 2009. Structural and compositional constraints on the emplacement of the Bushveld Complex , South Africa. *LITHOS*, 111(1–2), pp.21–36.

Clarke, B.M., Uken, R. and Reinhardt, J., 2010. Reply to Rigby , M . J ., Eriksson , P . G . and Mavimbela , P . K . Comments on " Structural and compositional constraints on the

emplacement of the. *LITHOS*, 115(1–4), pp.276–278.

Clarke, B.M., Uken, R. and Watkeys, M.K., 2000. Intrusion mechanisms of the southwestern Rustenburg Layered Suite as deduced from the Spruitfontein inlier. *South African Journal of Geology*, 103(2), pp.120–127.

Clubley-Armstrong, A. and Sharpe, M.R., 1979. The structural evolution of the Dennilton Dome and its relationship to the intrusion of the Busveld Complex. *Transactions of the Geological Society of South Africa*, 82, pp.23–36.

Cole, J., Webb, S.J. and Finn, C.A., 2014. Gravity models of the Bushveld Complex – Have we come full circle ? *Journal of African Earth Sciences*, 92, pp.97–118.

Corriveau, L. and Morin, D., 2000. Modelling 3D architecture of western Grenville from surface geology, xenoliths, styles of magma emplacement, and Lithoprobe reflectors. *Canadian Journal of Earth Sciences*, 37(1), pp.235–251.

Council for Geoscience, 1997. *Gravity Map of South Africa, 1:1,000,000 Map Series*.

Cousins, C.A., 1959. The structure of the mafic portion of the Bushveld Igneous Complex. *Transactions of the Geological Society of South Africa*, 62, pp.179–189.

Dankert, B.T. and Hein, K.A.A., 2010. Evaluating the structural character and tectonic history of the Witwatersrand Basin. *Precambrian Research*, 177(1–2), pp.1–22.

De Beer, J.H. and Stettler, E.H., 1992. The deep structure of the Limpopo Belt from geophysical studies. *Precambrian Research*, 55(1–4), pp.173–186.

De Waal, S.A., 1970. Interference folding of Bushveld Igneous Complex age in the Transvaal System north of Marble Hall, Transvaal. *The Geological Society of South Africa, Special Publication 1: Symposium on the Bushveld Igneous Complex and other layered intrusions*, pp.283–298.

De Waal, S.A. and Armstrong, R.A., 2000. The age of the Marble Hall diorite, its relationship to the Uitkomst Complex, and evidence for a new magma type associated with the Bushveld igneous event. *South African Journal of Geology*, 103(2), pp.128–140.

De Waal, S.A., Maier, W.D., Armstrong, R.A. and Gauert, C.D.K., 2001. Parental magma and emplacement of the stratiform Uitkomst Complex, South Africa. *Canadian Mineralogist*, 39(2), pp.557–571.

De Waal, S., Schweitzer, J.K., Graham, I., Gauert, C. and Ripley, E., 2008. A Bushveld-

related high-Ti igneous suite (HITIS) derived from an alkali to transitional basaltic magma, South Africa. *South African Journal of Geology*, 111(2–3), pp.201–224.

Deemer, S.J. and Hurich, C.A., 1997. Seismic image of the basal portion of the Bjerkreim-Sokndal layered intrusion. *Geology*, 25(12), pp.1107–1110.

Delph, J.R. and Porter, R.C., 2015. Crustal structure beneath southern Africa : insight into how tectonic events affect the Mohorovi˘ c discontinuity. *Geophysical Journal International*, 200, pp.254–264.

Dietvorst, E.J.L., 1991. Instability and basin formation on the Kaapvaal Craton, southern Africa. *Journal of African Earth Sciences*, 13(3–4), pp.359–365.

Du Plessis, A. and Kleywegt, R.J., 1987. A dipping sheet model for the mafic lobes of the Bushveld Complex. *South African Journal of Geology*, 90, pp.1–6.

Du Plessis, C.P. and Walraven, F., 1990. The tectonic setting of the Bushveld Complex in Southern Africa, Part 1. Structural deformation and distribution. *Tectonophysics*, 179(3–4), pp.305–319.

Durrheim, R.J. and Green, R.W.E., 1992. A seismic refraction investigation of the Archaean Kaapvaal Craton, South Africa, using mine tremors as the energy source. *Geophysical Journal International*, 108(3), pp.812–832.

Eales, H. V., 2002. Caveats in defining the magmas parental to the mafic rocks of the Bushveld Complex, and the manner of their emplacement: review and commentary. *Mineralogical Magazine*, 66(6), pp.815–832.

Eales, H. V. and Costin, G., 2012. Crustally contaminated komatiite: Primary source of the chromitites and marginal, Lower, and Critical Zone magmas in a staging chamber beneath the Bushveld Complex. *Economic Geology*, 107(4), pp.645–665.

Eales, H.V. and Cawthorn, R.G., 1995. The Bushveld Complex. In: R.G. Cawthorn, ed., *Layered Intrusions*. Elsevier Science, Amsterdam, pp.181–230.

Filmalter, G.F., 1986. *Geotegniese ondersoeke op monsters verkry vanaf die Fairfield boorgat te Moloto*. Geological Survey of South Africa unpublished report, 1986-0081, 11 pp.

Finn, C.A., Bedrosian, P.A., Cole, J., Khoza, T.D. and Webb, S.J., 2015. Mapping the 3D extent of the Northern Lobe of the Bushveld layered mafic intrusion from geophysical data. *Precambrian Research*, 268, pp.279–294.

Fouch, M.J., James, D.E., Vandecar, J.C., Van Der Lee, S. and Kaapvaal Seismic Group, 2004. Mantle seismic structure beneath the Kaapvaal and Zimbabwe Cratons. *South African Journal of Geology*, 107, pp.33–44.

Frick, C. and Walraven, F., 1985. The petrology and geochemitry of the pre-Karoo Elandskraal Volcano, South Africa. *Transactions of the Geological Society of South Africa*, 88, pp.225–243.

Gao, H. and Shen, Y., 2015. Validation of Recent Shear Wave Velocity Models in the United States with Full-Wave Simulation. *Journal of Geophysical Research: Solid Earth*, 120, pp.344–358.

Gauert, C.D.K., De Waal, S.A. and Wallmach, T., 1995. Geology of the ultrabasic to basic Uitkomst complex , eastern Transvaal , South Africa : an overview. *Journal of African Earth Sciences*, 21(4), pp.553–570.

Geng, H., Brandl, G., Sun, M., Wong, J. and Kröner, A., 2014. Zircon ages defining deposition of the palaeoproterozoic soutpansberg group and further evidence for eoarchaean crust in South Africa. *Precambrian Research*, 249, pp.247–262.

Geological Survey of South Africa, 1958. *Geological Map of the Union of South Africa 1:1,000,000, second Gravity ed. Special Publication 17*.

Geological Survey of South Africa, 1974. *1:250 000 Geological Series, Thabazimbi (2426)*.

Geological Survey of South Africa, 1978a. *1:250 000 Geological Series, Nylstroom (2428)*.

Geological Survey of South Africa, 1978b. *1:250 000 Geological Series, Pretoria (2528)*.

Geological Survey of South Africa, 1981. *1:250 000 Geological Series, Rustenburg (2526)*.

Geological Survey of South Africa, 1986a. *1:250 000 Geological Series, Barberton (2530)*.

Geological Survey of South Africa, 1986b. *1:250 000 Geological Series, East Rand (2628)*.

Geological Survey of South Africa, 1986c. *1:250 000 Geological Series, Pilgrim's Rest (2430)*.

Geological Survey of South Africa, 1986d. *1:250 000 Geological Series, West Rand (2626)*.

Gerya, T. V, Uken, R., Reinhardt, J., Watkeys, M.K., Maresch, W. V and Clarke, B.M., 2004. 'Cold' diapirs triggered by intrusion of the Bushveld Complex: Insight from two-dimensional numerical modeling. In: D.L. Whitney, C. Teyssier and C.S. Siddoway, eds., *Gneiss domes in orogeny*. Geological Society of America Special Paper 380, pp.117–127.

Gerya, T. V, Uken, R., Watkeys, M.K., Maresch, W. V and Clarke, B.M., 2003. Cold fingers in a hot magma : Numerical modeling of country-rock diapirs in the Bushveld Complex, South Africa. *Geology*, 31(9), pp.753–756.

Good, N. and De Wit, M.J., 1997. The Thabazimbi-Murchison Lineament of the Kaapvaal Craton, South Africa: 2700 Ma of episodic deformation. *Journal of the Geological Society*, 154(1), pp.93–97.

Gore, J., James, D.E., Zengeni, T.G. and Gwavava, O., 2009. Crustal structure of the Zimbabwe Craton and the Limpopo Belt of Southern Africa: New constraints from seismic data and implications for its evolution. *South African Journal of Geology*, 112, pp.213–228.

Guo, W., Dentith, M.C., Bird, R.T. and Clark, D.A., 2001. Systematic error analysis of demagnetization and implications for magnetic interpretation. *Geophysics*, 66(2), p.562.

Guo, W., Dentith, M.C., Zhengxiang, L. and Powell, C.M., 1998. Self demagnetisation corrections in magnetic modelling: some examples. *Exploration Geophysics*, 29, pp.396–401.

Gupta, V.K. and Sutcliffe, R.H., 1990. Mafic-ultramafic intrusives and their gravity field: Lac des Iles area, northern Ontario. *Geological Society of America Bulletin*, 102, pp.1471–1483.

Hall, A.L., 1932. *The Bushveld Igneous Complex of the central Transvaal*. Geological Survey of South Africa Memoir 28, 560 pp.

Hanski, E., Walker, R.J., Huhma, H. and Suominen, I., 2001. The Os and Nd isotopic systematics of c. 2.44 Ga Akanvaara and Koitelainen mafic layered intrusions in northern Finland. *Precambrian Research*, 109(1–2), pp.73–102.

Harmer, R.E. and Sharpe, M.R., 1985. Field relations and strontium isotope systematics of the marginal rocks of the eastern Bushveld Complex. *Economic Geology*, 80(4),

pp.813–837.

Harris, C., Pronost, J.M., Ashwal, L.D. and Cawthorn, R.G., 2005. Oxygen and hydrogen isotope stratigraphy of the Rustenburg Layered Suite, Bushveld Complex: Constraints on crustal contamination. *Journal of Petrology*, 46(3), pp.579–601.

Hartzer, F.J., 1989. Stratigraphy, structure, and tectonic evolution of the Crocodile River Fragment. *South African Journal of Geology*, 92, pp.110–124.

Hartzer, F.J., 1995. Transvaal Supergroup inliers : geology , tectonic development and relationship with the Bushveld complex , South Africa. *Journal of African Earth Sciences*, 21(4), pp.521–547.

Hartzer, F.J., 2000. *Geology of Transvaal inliers in the Bushveld Complex*. Council for Geoscience, Memoir 88, 222 pp.

Hattingh, P.J., 1980. The structure of the Bushveld Complex in the Groblersdal-Lydenburg-Belfast area of the Eastern Transvaal as interpreted from a regional gravity survey. *Transactions of the Geological Society of South Africa*, 83, pp.125–133.

Hattingh, P.J., 1986a. The palaeomagnetism of the main zone in the western Bushveld Complex. *Earth and Planetary Science Letters*, 79, pp.441–452.

Hattingh, P.J., 1986b. The palaeomagnetism of the main zone of the eastern Bushveld Complex. *Tectonophysics*, 124(3–4), pp.271–295.

Hattingh, P.J., 1989. Palaeomagnetism of the upper zone of the Bushveld Complex. *Tectonophysics*, 165, pp.131–142.

Hattingh, P.J., 1990. Palaeomagnetism of granites in the Bushveld Complex. *South African Journal of Geology*, 93(3), pp.519–524.

Hattingh, P.J., 1991. The magnetic susceptibility of the mafic rocks of the Bushveld Complex. *South African Journal of Geology*.

Hattingh, P.J. and Pauls, N.D., 1994. New Palaeomagnetic results from the northern Bushveld Complex of South Africa. *Precambrian Research*, 69, pp.229–240.

Hatton, C.J. and Schweitzer, J.K., 1995. Evidence for synchronous extrusive and intrusive Bushveld magmatism. *Journal of African Earth Sciences*, 21, pp.579–594.

Holland, T. and Powell, R., 2001. Calculation of Phase Relations Involving Haplogranitic Melts Using an Internally Consistent Thermodynamic Dataset. *Journal of Petrology*,

42(4), pp.673–683.

James, D.E., Fouch, M.J., VanDecar, J.C. and Van der Lee, S., 2001. Tectospheric structure beneath southern Africa. *Geophysical Research Letters*, 28(13), pp.2485–2488.

James, D.E., Niu, F. and Rokosky, J., 2003. Crustal structure of the Kaapvaal craton and its significance for early crustal evolution. *Lithos*, 71(2–4), pp.413–429.

Jourdan, F., Féraud, G., Bertrand, H., Kampunzu, A.B., Tshoso, G., Watkeys, M.K. and Le Gall, B., 2005. Karoo large igneous province: Brevity, origin, and relation to mass extinction questioned by new 40Ar/39Ar age data. *Geology*, 33(9), pp.745–748.

Karinen, T., 2010. *The Koillismaa Intrusion, Northeastern Finland – Evidence for PGE Reef Forming Processes in the Layered Series*. Geological Survey of Finland, Bulletin 404, 178 pp.

Karykowski, B.T. and Maier, W.D., 2017. Microtextural characterisation of the Lower Zone in the western limb of the Bushveld Complex, South Africa: evidence for extensive melt migration within a sill complex. *Contributions to Mineralogy and Petrology*, 172(8), pp.1–18.

Kempler, D., Mart, Y., Herut, B. and McCoy, F.W., 1996. Diapiric features in the southeastern Mediterranean sea: Possible indication of extension in a zone of incipient continental collision. *Marine Geology*, 134(3–4), pp.237–248.

Kgaswane, E.M., Nyblade, A.A., Durrheim, R.J., Julià, J., Dirks, P.H.G.M. and Webb, S.J., 2012. Shear wave velocity structure of the Bushveld Complex, South Africa. *Tectonophysics*, 554–557, pp.83–104.

Kgaswane, E.M., Nyblade, A.A., Julià, J., Dirks, P.H.G.M., Durrheim, R.J. and Pasyanos, M.E., 2009. Shear wave velocity structure of the lower crust in southern Africa: Evidence for compositional heterogeneity within Archaean and Proterozoic terrains. *Journal of Geophysical Research: Solid Earth*, 114(12), pp.1–19.

Koglin, N., Zeh, A., Frimmel, H.E. and Gerdes, A., 2010. New constraints on the auriferous Witwatersrand sediment provenance from combined detrital zircon U-Pb and Lu-Hf isotope data for the Eldorado Reef (Central Rand Group, South Africa). *Precambrian Research*, 183(4), pp.817–824.

Kruger, F.J., 2005. Filling the Bushveld Complex magma chamber: lateral expansion, roof and floor interaction, magmatic unconformities, and the formation of giant chromitite, PGE and Ti-V-magnetitite deposits. *Mineralium Deposita*, 40(5), pp.451–472.

Kruger, F.J. and Behr, S.H., 2002. The Henderson Reef in the Dennilton Dome and Mineral Range Areas - A Homologue of the Platreef. In: *9th International Platinum Symposium*. Billings, Montana, USA.

Ledwaba, L., Dingoko, O., Cole, P. and Havenga, M., 2009. *Compilation of Survey Specifications for all the old regional airborne geophysical surveys conducted over South Africa*. Council for Geoscience, Unpublished report 2009-0130, 40 pp.

Lelièvre, P.G. and Oldenburg, D.W., 2006. Magnetic forward modelling and inversion for high susceptibility. *Geophysical Journal International*, 166(1), pp.76–90.

Lenhardt, N. and Eriksson, P.G., 2012. Volcanism of the Palaeoproterozoic Bushveld Large Igneous Province: The Rooiberg Group, Kaapvaal Craton, South Africa. *Precambrian Research*, 214–215, pp.82–94.

Letts, S., Torsvik, T.H., Webb, S.J. and Ashwal, L.D., 2009. Palaeomagnetism of the 2054 Ma Bushveld Complex (South Africa): implications for emplacement and cooling. *Geophysical Journal International*, 179, pp.850–872.

Loncarevic, B.D., Feininger, T. and Lefebvre, D., 1990. The Sept-Iles layered mafic intrusion: geophysical expression. *Canadian Journal of Earth Sciences*, 27, pp.501–512.

Maier, W.D., Barnes, S. and Groves, D.I., 2013. The Bushveld Complex, South Africa: formation of platinum – palladium, chrome- and vanadium-rich layers via hydrodynamic sorting of a mobilized cumulate slurry in a large, relatively slowly cooling, subsiding magma chamber. *Mineralium Deposita*, 48, pp.1–56.

Mapeo, R.B.M. and Kampunzu, A.B., 2004. Bushveld-age magmatism in southeastern Botswana : evidence from U-Pb zircon and titanite geochronology of the Moshaneng Complex. *South African Journal of Geology*, 107, pp.219–232.

Maré, L.P., 2010. *Comparison of results from different magnetic susceptibility instruments*. Council for Geoscience unpublished report 2010-0233, 75 pp.

Maré, L.P., 2011. *Petrophysical Laboratory, Density Results*. [online] Petrophysical Laboratory, Density Results. Available at: <http://www.geoscience.org.za/index.php/geophysics/35-more-on-geophysics/118-petrophysical-laboratory.>.

Maré, L.P. and Loots, L., 2007. *Physical property analysis on core samples from Moordkopje in the Northern Limb of the Bushveld Complex*. Council for Geoscience unpublished report, 2007-0067, 44 pp.

Marsh, B.D., 2015. Magmatism, Magma, and Magma Chambers. In: G. Schubert, ed., *Treatise on Geophysics, Volume 1*, 2nd Editio. Elsevier, pp.275–333.

McDonald, I. and Holwell, D.A., 2007. Did lower zone magma conduits store PGE-rich sulphides that were later supplied to the Platreef? *South African Journal of Geology*, 110(4), pp.611–616.

Meyer, R. and De Beer, J.H., 1987. Structure of the Bushveld Complex from resistivity measurements. *Nature*, 325, pp.610–612.

Moen, H.F.G., 1989. A petrographical study of Bushveld-type rocks from boreholes on the Moloto geophysical anomaly, northeast of Pretoria. *South African Journal of Geology*, 92, pp.84–94.

Molengraaff, G.A.F., 1901. Géologie de la République Sud Africaine du Transvaal. In: *Bulletin de la Société Géologique de France, 4 série Tome*. English Translation by J.H. Ronaldson published in 1904 by Esson and Perkins, Johannesburg, with addition and alterations by the author., pp.13–92.

Molyneux, T.G. and Klinkert, P.S., 1978. A structural interpretation of part of the eastern mafic lobe of the Bushveld Complex and its surrounds. *Transactions of the Geological Society of South Africa*, 81, pp.359–368.

Mondal, S.K. and Mathez, E.A., 2007. Origin of the UG2 chromitite layer, Bushveld Complex. *Journal of Petrology*, 48(3), pp.495–510.

Morelli, C., Gantar, C., Honkasalo, T., McConnel, R.K., Tanner, J.G., Szabo, B., Uotila, U. and Whalen, C.T., 1974. *The International Gravity Standardisation Net 1971 (IGSN71)*. *Special Publication No. 4.*, International Association of Geodesy, Paris.

Moritz, H., 1992. Geodetic Reference System 1980. *Journal of Geodesy*, 66(2), pp.128–133.

Mungall, J.E., Kamo, S.L. and Mcquade, S., 2016. U-Pb geochronology documents out-of-sequence emplacement of ultramafic layers in the Bushveld Igneous Complex of South Africa. *Nature Communications*, 7, pp.1–13.

Myers, M., Myers, R.E. and McCarthy, T.S., 1987. Re-examination of the Sugarbush Fault and associated structures. *South African Journal of Geology*, 90, pp.270–281.

Nair, S.K., Gao, S.S., Liu, K.H. and Silver, P.G., 2006. Southern African crustal evolution and composition: Constraints from receiver function studies. *Journal of Geophysical*

Research, 111(B2), p.B02304.

Naldrett, A.J., Wilson, A., Kinnaird, J. and Chunnett, G., 2009. PGE tenor and metal ratios within and below the Merensky Reef, Bushveld Complex: Implications for its genesis. *Journal of Petrology*, 50(4), pp.625–659.

Nguuri, T.K., Gore, J., James, D.E., Webb, S.J., Wright, C., Zengeni, T.G., Gwavava, O., Snoke, J.A. and Group, K.S., 2001. Crustal structure beneath southern Africa and its implications for the formation and evolution of the Kaapvaal and Zimbabwe cratons. *Geophysical Research Letters*, 28(13), pp.2501–2504.

Niu, F. and James, D.E., 2002. Fine structure of the lowermost crust beneath the Kaapvaal craton and its implications for crustal formation and evolution. *Earth and Planetary Science Letters*, 200(1–2), pp.121–130.

Odgers, A.T.R., Hinds, R.C. and Von Gruenewaldt, G., 1993. Interpretation of a seismic reflection survey across the southern Bushveld Complex. *South African Journal of Geology*, 96, pp.205–212.

Odgers, A.T.R. and Du Plessis, A., 1993. Interpretation of a regional reflection seismic survey in the north-eastern Bushveld Complex. In: *3rd Biennial Technical Meeting of the South African Geophysical Association*. Cape Town, pp.125–129.

Owen-Smith, T.M. and Ashwal, L.D., 2015. Evidence for multiple pulses of crystal-bearing magma during emplacement of the Doros layered intrusion, Namibia. *Lithos*, 238, pp.120–139.

Prevec, S.A., Ashwal, L.D. and Mkaza, M.S., 2005. Mineral disequilibrium in the Merensky Reef, western Bushveld Complex, South Africa: New Sm-Nd isotopic evidence. *Contributions to Mineralogy and Petrology*, 149(3), pp.306–315.

Purss, M.B.J. and Cull, J.P., 2005. A new iterative method for computing the magnetic field at high magnetic susceptibilities. *Geophysics*, 70(5), pp.53–62.

Ramsey, J.G., 1962. Interference Patterns Produced by the Superposition of Folds of Similar Type. *Journal of Geology*, 70(4), pp.466–481.

Reid, M.R., Hart, S.R., Padovani, E.R. and Wandless, G.A., 1989. Contribution of metapelitic sediments to the composition, heat production, and seismic velocity of the lower crust of southern New Mexico, U.S.A. *Earth and Planetary Science Letters*, 95(3–4), pp.367–381.

Roelofse, F., 2012. *Mineralogical, geochemical and isotopic constraints on the evolution of the Lower Main Zone and Platreef on the Northern Limb of the Bushveld Complex*. Council for Geoscience, Bulletin 141, 131 pp.

Roelofse, F. and Ashwal, L.D., 2012. The Lower Main Zone in the northern limb of the Bushveld Complex - a >1.3 km thick sequence of intruded and variably contaminated crystal mushes. *Journal of Petrology*, 53(7), pp.1449–1476.

SACS (South African Committee for Stratigraphy), 1980. *Stratigraphy of South Africa. Part 1: Geological Survey of South Africa, Handbook, v. 8, 690 pp*.

Sargeant, F., 2001. *The seismic stratigraphy of the Bushveld Igneous Complex, South Africa*. The University of Liverpool, PhD Thesis (Unpublished), 425 pp.

Schaller, M., 1999. Exhumation of Limpopo Central Zone granulites and dextral continent-scale transcurrent movement at 2.0 Ga along the Palala Shear Zone, Northern Province, South Africa. *Precambrian Research*, 96(3–4), pp.263–288.

Schmidt, P. and Brewer, A., 2007. Magnetic Anomaly of the Bramfield Iron Formation, South Australia. In: *ASEG 2007*. Perth, Western Australia. 18-22 November 2007.

Schmitz, M.D. and Bowring, S.A., 2003. Ultrahigh-temperature metamorphism in the lower crust during Neoarchean Ventersdorp rifting and magmatism, Kaapvaal craton, southern Africa. *Bulletin of the Geological Society of America*, 115(5), pp.533–548.

Schutte, I.C., 1990. Die petrografie an geochemie van die Dwarsfontein Kompleks (The petrography and geochemistry of the Dwarsfontein Complex). In: *Annual Technical Report of the Council for Geoscience*. Council for Geoscience, Pretoria, pp.42–44.

Scoates, J.S. and Wall, C.J., 2015. Geochronology of Layered Intrusions. In: B. Charlier, O. Namur, R. Latypov and C. Tegener, eds., *Layered Intrusions*. Springer Geology, pp.3–74.

Scoon, R.N., 2002. A new occurrence of Merensky reef on the flanks of the Zaaikloof Dome, Northeastern Bushveld complex: Relationship between diapirism and magma replenishment. *Economic Geology*, 97(5), pp.1037–1049.

Serra, O., 1984. *Fundamentals of Well-log Interpretation: The Acquisition of Logging Data v. 1 (Developments in Petroleum Science)*. Developments in Petroleum Science, 15A, Elsevier, Amsterdam, 423 pp.

Sharpe, M.R., Bahat, D. and Von Gruenewaldt, G., 1981. The concentric elliptical

structure of feeder sites to the Bushveld Complex and possible economic implications. *Transactions of the Geological Society of South Africa*, 84, pp.239–244.

Silver, P.G., Fouch, M.J., Gao, S.S. and Schmitz, M., 2004. Seismic anisotropy , mantle fabric , and the magmatic evolution of Precambrian southern Africa. *South African Journal of Geology*, 107, pp.45–58.

Stankiewicz, J. and De Wit, M., 2013. 3.5 billion years of reshaped Moho, southern Africa. *Tectonophysics*, 609, pp.675–689.

Stettler, R.H., Du Plessis, J.G., Hattingh, P.J., Venter, C.P. and Hattingh, E., 2000. *Regional gravity survey of the 2528 (Pretoria) 1:250 000 sheet.* Council for Geoscience, Unpublished Report 2000-0043, 66 pp.

Talwani, M., Worzel, J.L. and Landisman, M., 1959. Rapid gravity computations for two-dimensional bodies with application to the Mendocino submarine fracture zone. *Journal of Geophysical Research*, 64, pp.49–59.

Tegner, C., Cawthorn, R.G. and Kruger, F.J., 2006. Cyclicity in the Main and Upper Zones of the Bushveld Complex, South Africa: Crystallization from a Zoned Magma Sheet. *Journal of Petrology*, 47(11), pp.2257–2279.

Teigler, B. and Eales, H. V, 1996. *The Lower and Critical Zones of the western limb of the Bushveld Complex as intersected by the Nooitgedacht boreholes*. Council for Geoscience, Bulletin 111, 126 pp.

Teigler, B., Eales, H. V. and Scoon, R.N., 1992. The cumulate succession in the Critical Zone of the Rustenburg Layered Suite at Brits, western Bushveld Complex. *South African Journal of Geology*, 95(1–2), pp.17–28.

Telford, W.M., Geldart, L.P., Sheriff, R.E. and Keys, D.A., 1976. *Applied Geophysics*. Cambridge University Press, 860 pp.

Temple, A.K., 1966. Alteration of ilmenite. *Economic Geology*, 61(4), pp.695–714.

Tinker, J., De Wit, M. and Grotzinger, J., 2002. Seismic Stratigraphic Constraints on Neoarchean - Paleoproterozoic Evolution of the Western Margin of the Kaapvaal. *South African Journal of Geology*, 105, pp.107–134.

Uken, R. and Watkeys, M.K., 1997. Diapirism initiated by the Bushveld Complex , South Africa. *Geology*, 25(8), pp.723–726.

Van der Merwe, M.J., 1976. The layered sequence of the Potgietersrus limb of the Bushveld Complex. *Economic Geology*, 71(7), pp.1337–1351.

Van der Merwe, M.J., 2008. The geology and structure of the Rustenburg Layered Suite in the Potgietersrus/Mokopane area of the Bushveld Complex, South Africa. *Mineralium Deposita*, 43(4), pp.405–419.

Von Gruenewaldt, G., 1976. Sulfides in the Upper Zone of the eastern Bushveld Complex. *Economic Geology*, 71(7), pp.1324–1336.

Von Gruenewaldt, G., 1979. A review of some recent concepts of the Bushveld Complex with particular reference to sulfide mineralization. *Canadian Mineralogist*, 17, pp.233–256.

Wallace, Y., 2007. 3D Modelling of Banded Iron Formation incorporating demagnetisation – a case study at the Musselwhite Mine , Ontario, Canada. *Exploration Geophysics*, 38(July 2006), pp.254–259.

Walraven, F., 1987. Geochronological studies of Bushveld Complex rocks from the Fairfield borehole at Moloto, northeast of Pretoria. *South African Journal of Geology*, 90, pp.352–360.

Walraven, F. and Hattingh, E., 1993. Geochronology of the Nebo Granite, Bushveld Complex. *South African Journal of Geology*, 96, pp.31–41.

Webb, S.J., 2009. *The use of potential field and seismological data to analyze the structure of the lithosphere beneath southern Africa*. PhD Thesis (unplublished), University of the Witwatersrand, 377 pp.

Webb, S.J., Ashwal, L.D. and Cawthorn, R.G., 2011. Continuity between eastern and western Bushveld Complex , South Africa , confirmed by xenoliths from kimberlite. *Contributions to Mineralogy and Petrology*, 162, pp.102–107.

Webb, S.J., Cawthorn, R.G., Nguuri, T. and James, D., 2004. Gravity modeling of Bushveld Complex connectivity supported by Southern African Seismic Experiment results. *South African Journal of Geology*, 107, pp.207–218.

Wilson, A.H., 2012. A Chill Sequence to the Bushveld Complex: Insight into the First Stage of Emplacement and Implications for the Parental Magmas. *Journal of Petrology*, 53(6), pp.1123–1168.

Wilson, A.H., 2015. The earliest stages of emplacement of the eastern Bushveld

Complex: Development of the Lower Zone, Marginal Zone and Basal Ultramafic Sequence. *Journal of Petrology*, 56(2), pp.347–388.

Wilson, J., Ferré, E.C. and Lespinasse, P., 2000. Repeated tabular injection of high-level alkaline granites in the eastern Bushveld, South Africa. *Joural of the Geological Society, London*, 157, pp.1077–1088.

Winchell, H., 1961. Regressions of physical properties on the compositions of clinopyroxenes II. Optical properties and specific gravity. *American Journal of Science*, 259, pp.295–319.

De Wit, M.J., Roering, C., Hart, R.J., Armstrong, R.A., De Ronde, C.E.J., Green, R.W.E., Tredoux, M., Peberdy, E. and Hart, R.A., 1992. Formation of an Archaean continent. *Nature*, 357(6379), pp.553–562.

Youssof, M., Thybo, H., Artemieva, I.M. and Levander, A., 2013. Moho depth and crustal composition in Southern Africa. *Tectonophysics*, 609, pp.267–287.

Yudovskaya, M.A., Kinnaird, J.A., Sobolev, A. V., Kuzmin, D. V., McDonald, I. and Wilson, A.H., 2013. Petrogenesis of the Lower Zone olivine-rich cumulates beneath the Platreef and their correlation with recognized occurrences in the Bushveld Complex. *Economic Geology*, 108(8), pp.1923–1952.

Zandt, G. and Ammon, C.J., 1995. Continental crust composition constrained by measurements of crustal Poisson's ratio. *Nature*, 374, pp.152–154.

Zeh, A., Ovtcharova, M., Wilson, A.H. and Schaltegger, U., 2015. The Bushveld Complex was emplaced and cooled in less than one million years – results of zirconology, and geotectonic implications. *Earth and Planetary Science Letters*, 418, pp.103–114.

Zhu, L. and Kanamori, H., 2000. Moho depth variation in southern California from teleseismic receiver functions. *Journal of Geophysical Research*, 105(B2), pp.2969–2980.

APPENDIX ADDITIONAL PAPER

I contributed to this paper for which my co-supervisor Dr. CA Finn was the main author.

Finn, C.A., Bedrosian, P.A., Cole, J., Khoza, D.T., Webb, S.J. 2015. Mapping the 3D extent of the Northern Lobe of the Bushveld layered mafic intrusion from geophysical data. Precambrian Research, 268, 279-294.